R-12-12

Prototype repository

Hydromechanical measurements during operation phase 2003-05-01 to 2010-02-01

Ingvar Rhén, Torbjörn Forsmark
Sweco Environment

June 2014

Svensk Kärnbränslehantering AB
Swedish Nuclear Fuel
and Waste Management Co

Box 250, SE-101 24 Stockholm
Phone +46 8 459 84 00

ISSN 1402-3091
SKB R-12-12
ID 1354554
June 2015

Prototype repository

Hydromechanical measurements during operation phase 2003-05-01 to 2010-02-01

Ingvar Rhén, Torbjörn Forsmark
Sweco Environment

Förord

Prototype repository project är ett internationellt, EU-stött projekt (fram till april 2004), med syfte att i full skala undersöka den integrerade funktionen hos ingenjörers barriärer och närfältsberg i ett simulerat slutförvar i kristallint berg med hänsyn till värmeutveckling, bergmekanik, vattengenomströmning, vattenkemi, gasbildning och mikrobiologi under naturliga och realistiska förhållanden på ca 450 m djup.

Försöksplatsen är en 65 m lång TBM-borrad ort från vilken sex vertikala deponeringshål med 1,75 m diameter och 8 m djup borrats i enlighet med KBS-3 konceptet. Testplatsen är delad i två delar; en inre 40 m lång sektion (sektion I) med 4 deponeringshål och en yttre del (sektion II) med två deponeringshål. Stela och täta pluggar separerar sektionerna och sektion II från resten av Äspölaboratoriet (ÄHRL).

Ett stort antal borrhål har borrats för att karakterisera berget. Dessa borrhål användes för långtidsmoniteringen av prototypförvaret. En av frågeställningarna som studerades var hur sprickorna i berget påverkades hydromekaniskt av den ökade temperaturen i bergmassan. Denna rapport beskriver dessa mätningar.

Summary

The Prototype repository is an international, EC-supported activity (up to April 2004), with the objective to investigate, on a full-scale, the integrated performance of engineered barriers and near-field rock of simulated deep repository. This is done in crystalline rock with respect to heat evolution, rock mechanics, water flow, water chemistry, gas evolution and microbial processes under natural and realistic conditions at approximately 450 m depth below the ground surface.

The test site is a 65 m long TBM-bored drift with diameter of 5 m from which six 1.75 m diameter deposition holes are extended downwards to 8.37 m depth in accordance with the KBS-3 concept. The test site is divided in two parts, an inner 40 m long section (section I) with 4 deposition holes and an outer section (section II) with 2 deposition holes. Stiff and tight plugs separate section I and section II from the rest of the Äspö Hard Rock Laboratory (ÄHRL).

A large number of boreholes have been drilled in order to characterize the rock mass. These boreholes are used for the long-term monitoring of the Prototype repository. One of the issues that are investigated is the hydromechanical behaviour of fractures in crystalline rock as a result of increased temperature due to the electrical heaters.

The objective of the hydromechanical tests is to measure if the temperature increase affects the rock mass stress in such way that fracture width or/and fracture transmissivity, changes.

The hydromechanical tests started in May 2003 with 11 boreholes with a section equipped with deformation measurement equipment.

Comments and conclusions made from the deformation measurements within the prototype project are divided into the following:

- Hydromechanical sensor performance.
- Temperature measurements.
- Long-term deformation measurements.
- Short-term measurements (hydraulic test campaigns).
- Hydraulic head changes.
- Flow into the deposition holes.
- Main conclusions.

Hydromechanical sensor performance

In the summer months of 2003 most of the measurement sensors were still working. During that period when there are valid measurement data, there is increasing temperature in the rock and the rock expands while the measured fractures are generally being compressed. The best hydromechanical sensor performances are the ones in KA3554G01:2. Both sensors have mostly been functional since 2003 with the exception of the total breakdown in 2005, which occurred in all holes, see Chapter 5. Otherwise the equipment, one or both sensors, see Table S-1, the remaining 10 boreholes have stopped functioning.

Out of 22 temperature sensors within the hydromechanical equipment only 13 are still working 2006-10-01.

By 2010-01-01 only 4 out of the 22 temperature sensors were working and of the HM sensors only the rock and fracture sensor in KA3542G02:2 was in operation.

- The measurements indicate sudden “jumps” which could be caused by either expansion or compression of a fracture. This is the general pattern for both the sections with intact rock only and for the sections one or several fractures. The reason can either be that the anchor itself has slipped which is the plausible explanation for sections with intact rock only, or that a movement in a fracture suddenly occurs, which may be the explanation for fracture sections.

- When the backfilling of section II in the Prototype repository was in progress of vibrations were generated in the process of packing the backfill during the period 2003-04-29–2003-06-27. It is an open question whether the energy from this vibration could have been large enough to cause the observed fast "deformations" that could possibly be micro slips of the anchors or micro-movements in fractures. The first explanation, slips of the anchor, is the most probable reason as there are sudden movements later in the project, see below.
- Due to the fact that many sections with intact rock show sudden displacements, it appears that the anchor construction is not optimal to the current conditions. There are very small displacements involved and perhaps the anchors would have performed better with a larger area (and softer) in contact with the rock surface compared to the steel pin and steel edge collar on the anchor that were in contact with the borehole wall in this experiment. cf. Figure 4-1 and Figures 2-6 and 2-7 in Rhén et al. (2003). The original design with expandable copper bladders on the anchors, as delivered from Geokon Inc., was tested in laboratory and was found to not work properly for measuring small deformations. The anchors was therefore modified and tested in the laboratory, but as indicated above, the new design did not perform satisfactory and should probably be developed further if new tests are to be made.

Table S-1. Status of the long-term measurements 2010-01-01. An OK means that it has been possible to evaluate the measurement data. To evaluate the fracture properties it is necessary to have good data from both the intact rock and the rock and fracture sensor. The measurements started 2003-05-06.

Borehole	Intact rock sensor	rock and fracture sensor	Fracture def. calc.	Comments
KG0010B01	–	–		The temperature is affected of the air temperature in the tunnel. The borehole is a reference hole for undisturbed conditions (i.e. undisturbed by the heaters). The rock and fracture deformation is not evaluated. Measurements failed 2006-09-30.
KA3539G:2	–	–		The rock and fracture measurements failed in February 2005 and the intact rock sensor in mid-2008.
KA3542G01:3	–	–		The rock and fracture measurements failed in February 2005.
KA3542G02:4	–	OK		The rock measurements failed in February 2005 and only one sensor operates October 2006.
KA3544G01:2	–	–		The rock and fracture measurements failed in November 2003.
KA3546G01:2	–	–		The rock and fracture measurements failed in November 2003.
KA3548A01:3	–	–		The rock and fracture measurements failed in November 2003.
KA3550G01:2	–	–		Expansion of intact rock observed. The "rock and fracture"-sensor failed at July 2003. The "intact rock"-sensor failed in January 2004.
KA3552G01:2	–	–		The temperature data is replaced with data from KA3550G01:2. Both sensors failed in September 2003.
KA3554G01:2	–	–		The rock and fracture measurements failed in October 2006.
KA3554G02:4	–	–		The rock and fracture measurements failed in February 2005.

Temperature measurements

The temperature increases to more than 40°C in the test sections closest to a canister hole, while the increase is more modest in holes more distant to the heating source. The tested sections can be divided into classes with "thermal" distances, where the distance is the closest distance to a heating canister, see Figure S-1:

- approx. 1 m : KA3550G01:2 and KA3552G01:2,
- approx. 1.5 m : KA3544G01:2 and KA3546G01:2,
- approx. 10 m : KA3539G:2 and KA3554G02:4,
- approx. 15 m : KA3542G01:3 and KA3548A01:3,
- approx. 20 m : KA3542G02:2 and KA3554G01:2.

The temperature increase is rather small in most sections except for KA3544G01:2, KA3546G01:2, KA3550G01:2 and KA3552G01:2.

The temperature correction of the measured deformation over a long time period with significant temperature increase is essential for an experiment like the Prototype experiment. As many temperature sensors, mounted within the deformation sensor equipment, failed, one could possibly in a future experiment install one extra temperature sensor near the anchors for the deformation measurement.

For the long term observations the temperature corrections are important. As an example the applied temperature corrections on the deformation for 5, 10 and 30°C increase are 20 µm, 40 µm and 120 µm, compare with Figure S-1. The observed long term deformations, although irregular (which is discussed in the next section), are generally larger than the temperature corrections indicated above, thus indicating that incorrect temperature corrections generally should not be expected to produce artificial deformations. However, if the observed deformation small and the temperature change large, the uncertainty in the small observed deformation can be large if there is a significant uncertainty in the correction of the deformation related to the temperature change.

During the short term tests it was possible to observe small temperature changes in some cases, up to c. 0.4°C during a test. In some case the change was observed in a section with fractures, the change was probably caused by the flowing water. Other causes were probably related to that one heater was stopped for a period, and that caused a temperature pulse in the rock mass. The temperature corrections of the deformations during the short term tests are small compared to the deformations observed. So, even though the temperature correction should be accurate considering how the equipment is constructed, the observed deformations during the short term tests is not considered to be an artefact of just temperature corrections, assuming that it is time delay between when the temperature pulse affects the strain gauge and the sensor for the temperature measurements. However, as there have been a large number of failures of temperature gauges it cannot be excluded that in some cases where data is missing that there is a noticeable effect of the temperature correction on the measured deformation, but still it seems from the available results that the effect may be relatively small.

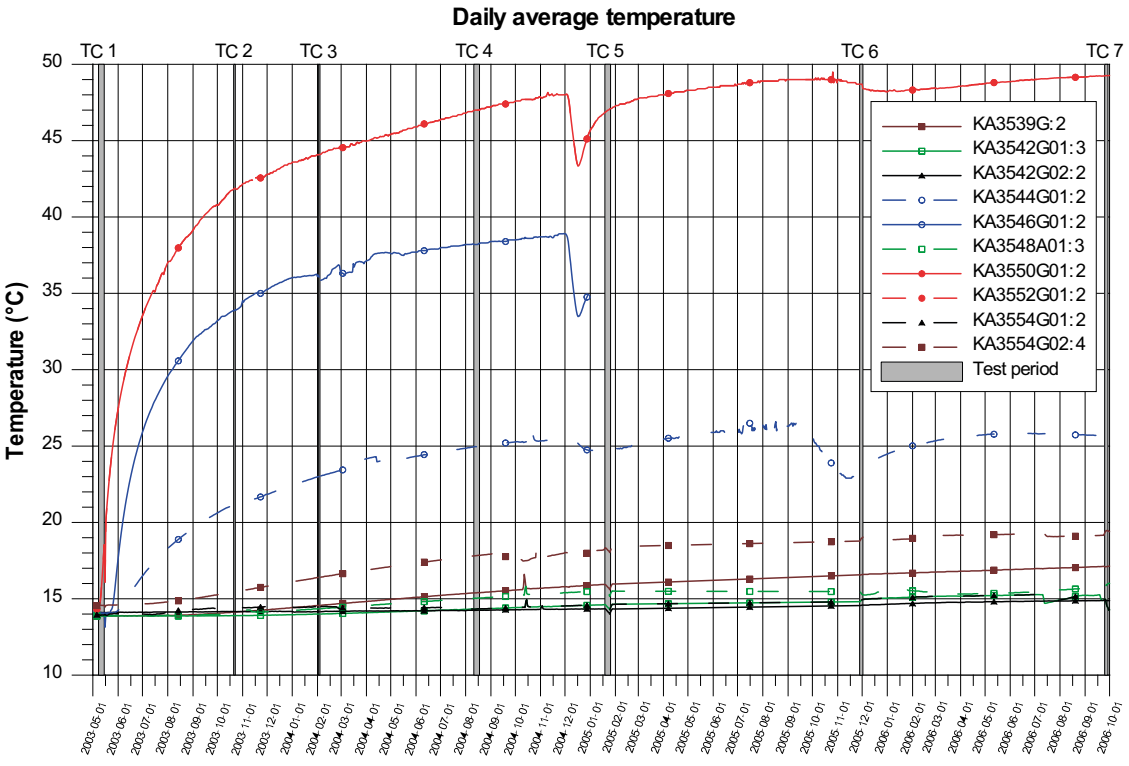

Figure S-1. *Temperature development in the boreholes. The temperature drop is due to that the heaters were shut down for a period. The figure also shows the time when the first 7 hydraulic test campaigns were made.*

The temperature sensor, thermistor, with measurement range –80 to +150°C has an accuracy ±0.5°C. The measured temperatures, as shown in Figure S-1, should be accurate.

Evaluated transmissivities

The evaluated transmissivities (T) are based on two evaluation methods:

1 The method suggested by Moye (1967) assumes a steady state radial flow near the tested section and spherical flow at some distance.

2 For the transient evaluation the measured flow rate for the flowing phase is used (multirate approach) and the pressure from the pressure build-up period is used for the evaluation. Evaluating the transient data, the pressure change, Δp, is plotted versus the equivalent time, dt_e, in minutes. The solution used in the analysis is the Dougherty-Babu model for a pumping test in a confined aquifer (Dougherty and Babu 1984).

For method 1 only borehole geometry, test section length, flow rate and pressure difference are and no subjective judgment of the data is needed to calculate the T. Geometrical factors do not change between the tests and the pressure measurements can be considered very accurate. The flow rate, however, can change if the test duration changes, as some test section may not reach fully steady state. To avoid major problem with this the chosen test duration was generally rather long; 60–180 minutes. These individual test-section flow times were used for the repeated tests, with the purpose that the measured last flow rate would be close to steady state flow rate and if not fully developed steady state the same flow times should provide comparable conditions for evaluation of changes of T.

The benefits with method 2 are that near-borehole effects (skin factor) can be filtered out and the evaluated T can be considered to better represent the transmissivity of the fracture. The negative side is that the method demands more from the monitoring of the tests (high frequency of sampling of flow rate and pressure) and that there is some subjectivity in the evaluation process of fitting models to the measured data. In our case the monitoring has been made with a high frequency sampling rate, so data quality is good in that sense. Some tests show complicated flow regime developments and in such cases one can easily get differences in estimated T due to different judgments of what is a reasonable fit for parameter estimation. To minimise the problems of subjectivity in the evaluation, the flow regimes were carefully studied and all previous made tests for a specific test section were checked before the evaluation of a new test; in order to perform the evaluation in a similar manner. With this methodology it was believed that the relative changes of T could be described accurately.

In general one can say that evaluated transmissivities for a test section is dependent of test time, evaluations methods as well as effects from boundary conditions (some may be transient or constant head). As described above, the attempt has been to avoid major problems in order to get relative changes that should be accurate, the relative changes which were considered important for the project. The changes observed for T can generally be considered small and within an estimated uncertainty for an absolute value of T. There are a few greater changes of T and one can be certain that there exist a change of the absolute T. On the other hand, the frequent observation of small changes of T is also an important result as it tells us that no major changes occurred when the rock was heated. These small changes can probably be within expected uncertainties for an absolute estimate of T and observed small trends of the relative changes are uncertain. In a few cases where there are several observations showing a trend one can probably be more certain that there is a trend although small relative changes. However, this assumes that the major changes are due to compression or extension of fractures related to a slow change of stresses. If there is a fracture slip one can have a sudden increase or a decrease of the fracture transmissivity. There are a few observations that possibly can be related to slips but it has not been possible to confirm this cause to the change.

Long-term deformation measurements

The accuracy based on individual calibration that were performed of the sensors were; Measurement range 0.76–2.1 mm, Resolution (logger) 0.10–0.28 µm, Accuracy 0.76–2.1 µm a, which can be considered as a sufficient accuracy for the test.

In borehole KA3552G01:2, which is c. 1.2 m from the centre line of the heater (c. 0.6 m outside the deposition hole wall) with temperature increase from c. 14 to 49°C, there is a clear deformation and transmissivity decrease from c. $5 \cdot 10^{-9}$ m^2/s to c. $6 \cdot 10^{-10}$ m^2/s in the section with a fracture with orientation 193/44. KA3550G01:2 which is in a similar position as KA3552G01:2 but due to packer failure no data are available.

KA3544G01:2 and KA3546G01:2 are fairly close to the heaters, which are c. 1.2 m from the centre line of the heater (c. 0.6 m outside the deposition hole) but located near the bottom of the heater. The temperature increase is c. from c. 14 to 25°C (KA3544G01:2) and 38°C (KA3546G01:2) and the monitored sections have 3–4 fractures with different orientations. In KA3544G01:2 the transmissivity decreases from c. c. $1 \cdot 10^{-8}$ m^2/s to c. $7 \cdot 10^{-9}$ m^2/s (only two measurements) but in KA3544G01:2 there seem to be no decrease in transmissivity.

There are a few observations that indicate a sudden transmissivity increase, e.g. KA3542G02:2, which possibly can indicate a fracture slip; a few months after the heater were started. After this sudden increase, the transmissivity decreases. In other borehole sections the transmissivity changes are small and not possible to judge if they are due to the decreasing water pressure or increasing load due to temperature increase.

The long-term deformation measurements are very difficult to evaluate due to a number of rapid changes that have not been possible to couple to a known cause, or the deformations seem unrealistic in some cases.

Short-term measurements (hydraulic test campaigns)

During the seven hydraulic test campaigns (TC1–TC7) several of the test sections reacts as expected. During flow phase the fracture located within the tested section reacts with decreased fracture width in response to the lower hydrostatic pressure in the section. When the flow phase ends the fracture width increases once again. The best results are from KA3542G01:3 (TC2–TC4) and KA3554G01:2 (TC3–TC7). There is a more or less linear relationship between hydrostatic water pressure loss and fracture width in the data from the two boreholes. The magnitude of the pressure response in the third hole, KA3539G:2, is minor. In the rest of the Hydromechanical monitored holes there are no complete test series with data of both fracture deformation and different pressure changes during hydraulic tests.

The fracture transmissivity decreases slightly when the fracture or set of fractures are being compressed during the hydraulic tests, see Figure S-2.

It seems that in some cases the deformation during a short test does not come back to initial values before the sudden pressure decrease. This may indicate a permanent deformation of the fracture but it cannot be excluded that it is small anchor slips that is observed.

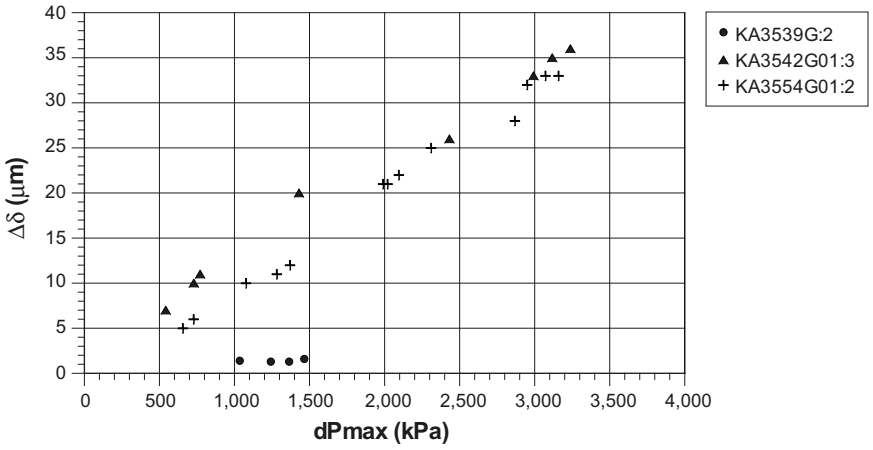

Figure S-2. *dPmax versus maximum fracture width decrease during the flow period of a test.*

One of the questions considered is:

- If fracture transmissivities have changed, can it be correlated to measured deformations of fractures?

The transmissivity change is minor but clear in all four tests presented in Figures S-3 and S-4. In these figures the transmissivity is plotted against maximum change in fracture width, Δδ, and hydrostatic water pressure loss, dPmax. The Figures show that there is a correlation as expected between the fracture width and transmissivity but the deformations are small and the transmissivity changes are small. At the depth that the experiments were performed one can expect that all fractures are under a high stress from the outset and a stress increase due to temperature load or decrease in water pressure should just cause small deformations of the fractures, as also can be seen in the figures.

Hydraulic head changes

There seem to be a slowly decreasing trend over the years in the water pressure by time in boreholes near the Prototype repository. At least partly, this cannot be explained as effects from the Prototype repository itself or nearby tunnels, as one can observe a decreasing trend en several of the boreholes in the Äspö HRL. During the same period the total inflow of water to the tunnels has also decreased. The mechanism for this behaviour cannot be explained at present with concepts earlier presented (as; stress changes due to the excavation, chemical precipitation and/or gas release near the tunnel due to pressure decrease of the inflowing water) but possibly can successive fault gauge movements and/or small and slow creep deformation of the rock cause very small changes of the permeability of the fracture system within long distances from the tunnels creating a slightly lower mean permeability.

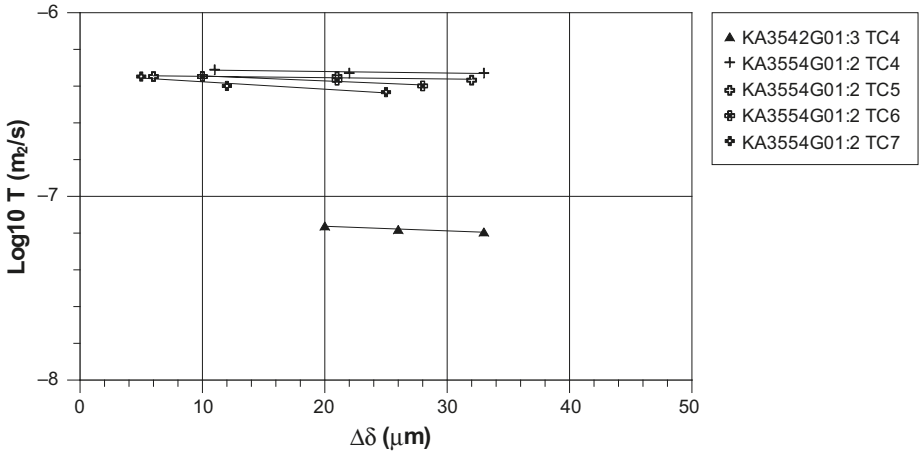

Figure S-3. *Maximum change in fracture widths (Δδ) during flowing of section versus corresponding T (data from test campaigns 4, 5, 6 and 7).*

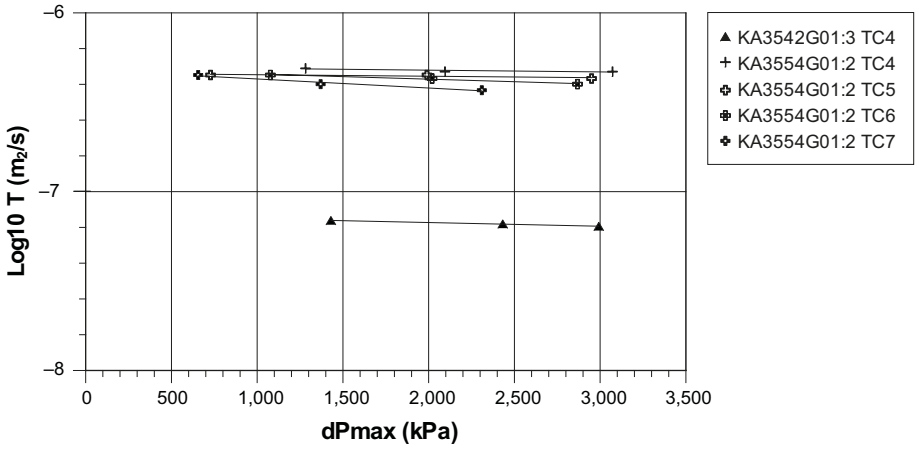

Figure S-4. *dPmax during flowing of section versus corresponding T (data from test campaigns 4, 5, 6 and 7).*

Flow into the deposition holes

The inflow to the deposition holes DA3551G01 and DA3545G01 were measured 1999-12 to 2000-06 three times (Rhén and Forsmark 2001). In the winter 2012–2013, after the backfill and the buffer had been removed in tunnel section II, the flow measurements were repeated for two of the depositions holes. The measured flow rates for the two occasions are shown in Table S-2. As can be seen the inflow rates has decreased.

Table S-2. Result of inflow measurements to deposition boreholes DA3551G01 and DA3545G01.

Borehole	Q 2000-03-28–2000-03-31 (L/min)	Q 2012-12-20–2013-02-07 (L/min)
DA3551G01	0.00155	0
DA3545G01	0.00270	0.00045

Main conclusions

- The observed deformations and transmissivity changes during the measurement period are small. This was expected as the initial rock stress before the heating is rather high at the depth for the Prototype repository. The transmissivity decrease is c. 0.1 of the initial transmissivity value for one observation just outside a deposition hole but all other observations near or distant from the deposition holes show less changes.
- Hydraulic tests with different water pressure decreases show that the evaluated transmissivity is dependent of the applied water pressure decrease. However, the transmissivity changes are small relative the pressure change. This is expected as the tests are performed at such large depth with relatively high initial rock stresses.
- Although the measurements in some respect have been successful (according to the point above) one can conclude that the deformation measurements are difficult. The deformations are small and one has to be very sure that the anchor does not slip on the rock wall. The sensors (strain gauge and temperature) in the deformation measurement equipment should also withstand the environment (temperature, water pressure, vibration (e.g. from packing the backfill in the tunnels)) in the borehole better than the equipment used. It is presently not known the reason for the deformation measurement-equipment failure.
- The methodology for performing hydraulic tests has worked well but in any future similar investigations one should perform several tests with different pressure drawdowns (e.g 200 kPa (or at least somewhat lower than used in the present study) as start value and then increase the differential pressure in a number of steps suitable for the project) during each test campaign in each test section already from the outset. Data will be useful for evaluating fracture compressibility and one can use the test with the lowest differential pressure when comparing long term behaviour, which would be preferable. To show permeability changes qualitative one can probably also use a third test (besides evaluation of T using stationary and transient methods) by plotting the specific drawdown versus time for all tests made in a specific test section.
- The characterisation of the Prototype tunnel before the tunnel was backfilled and the experiment started, was extensive and it was possible to do several types of geological and hydrogeological investigations that provided a good basis for planning the experiment. However, one method was excluded; the flow logging with Posiva flow log aiming to detect individual flowing fractures and estimate their transmissivity. Investigations in other projects later made by SKB using this tool has proven valuable as a compliment to geological characterisation and orientation of fractures and hydraulic tests with small and large test-section lengths.
- The installed hydraulic packers in tunnel section II have functioned well but unfortunately there have been a few packer failures that have spoiled the possibilities to perform hydraulic tests in those boreholes.
- The water pressure around the deposition tunnels did not increase as expected. First of all, section I was drained most of test period due to electrical problems with one canister heater when the water pressure increased, which also affect the pressure around section II. There also exists a

general pressure decrease near the Prototype repository, but also in Äspö HRL in general. It does not have a main influence of the evaluation of the short-term deformations (other than it limits to use high differential pressures), but it can affect the long-term deformation measurements in that respect that the effective stress in the fractures changes. If the deformation due to the thermal load is limited, the observed small deformations may just be due to long term pressure changes.

- The nearby experiment in tunnel TASS has significantly disturbed the Prototype experiment. The drilling and the grouting for the Fine Sealing project (year 2007) as well as excavation of the TASS tunnel, disturbed the pressures and probably has grout affected at least one of the observation boreholes drilled from the Prototype tunnel. The drilling, the grouting and tunnel excavation have however not had an impact of most result related to hydraulic tests and deformation measurements, as the main part of the result are from the period before 2007. The boundary conditions for the Prototype project significantly changed after 2007 due to the TASS tunnel. Pressure levels and pressure trends have changed in several cases comparing data before drill start and after excavation.

Contents

1 Background

1.1 Äspö Hard Rock Laboratory

In order to prepare for the siting and licensing of a spent fuel repository SKB has constructed an underground research laboratory.

In the autumn of 1990, SKB began the construction of Äspö Hard Rock Laboratory (Äspö HRL), see Figure 1-1 and 1-2, near Oskarshamn in the south eastern part of Sweden. A 3.6 km long tunnel was excavated in crystalline rock down to a depth of approximately 460 m.

The laboratory was completed in 1995 and research concerning the disposal of nuclear waste in crystalline rock has since then been carried out.

Figure 1-3 shows the Prototype tunnel and other tunnels in the deepest part of the Äspö laboratory.

1.2 Prototype repository

The Äspö Hard Rock Laboratory is an essential part of the research, development, and demonstration work performed by SKB in preparation for construction and operation of the deep repository for spent fuel. Within the scope of the SKB program for RD&D 1995, SKB has decided to carry out a project with the designation “Prototype repository test“. The aim of the project is to test important components in the SKB deep repository system in full scale and in a realistic environment.

The Prototype repository Test is focused on testing and demonstrating the function of the SKB deep repository system. Activities aimed at contributing to development and testing of the practical, engineering measures required to rationally perform the steps of a deposition sequence are also included. However, efforts in this direction are limited, since these matters are addressed in the Demonstration of Repository Technology project and to some extent in the Backfill and Plug Test.

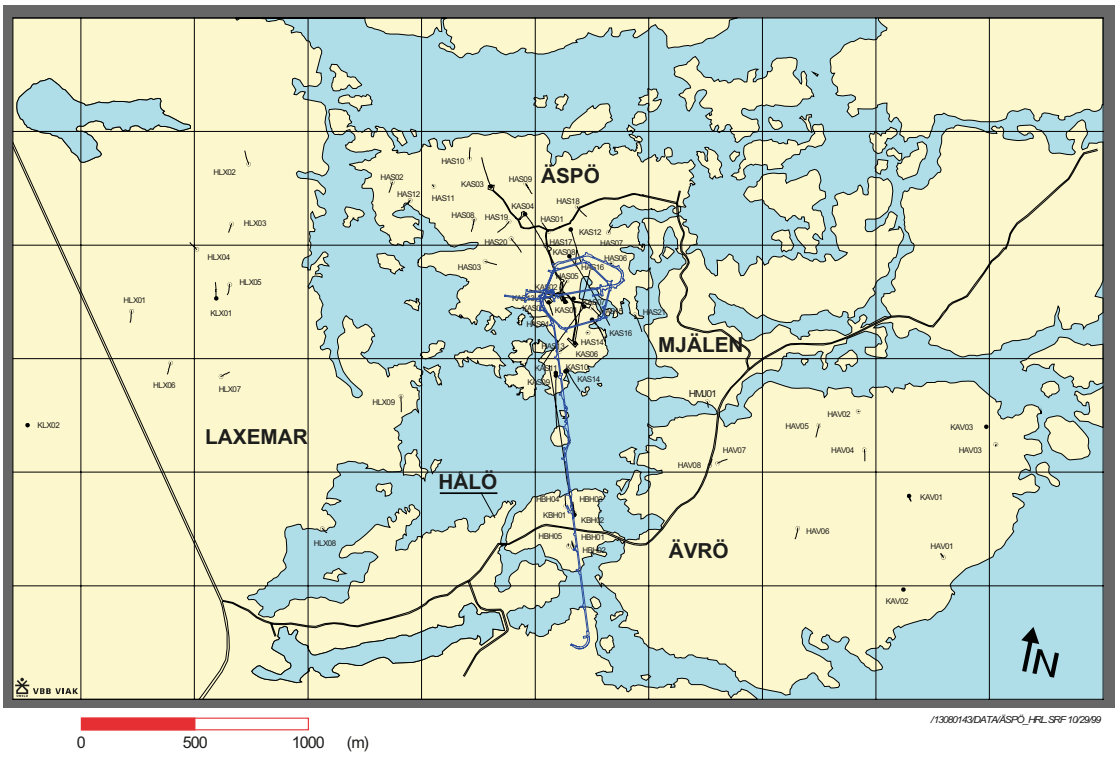

Figure 1-1. *Location of Äspö Hard Rock Laboratory.*

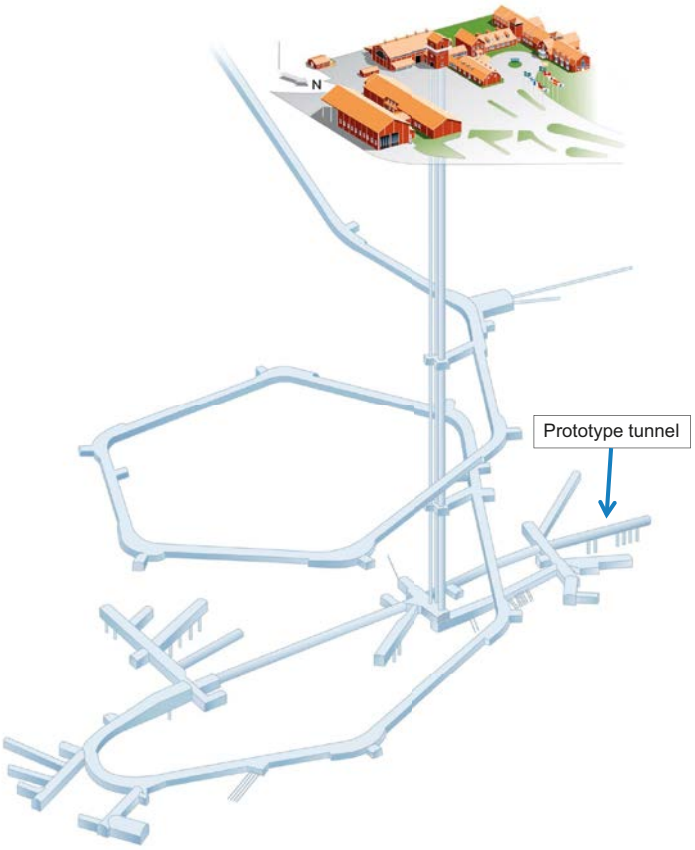

Figure 1-2. *Tunnel system at Äspö HRL. The prototype repository is located after section 3/500 m at the end of the tunnel system.*

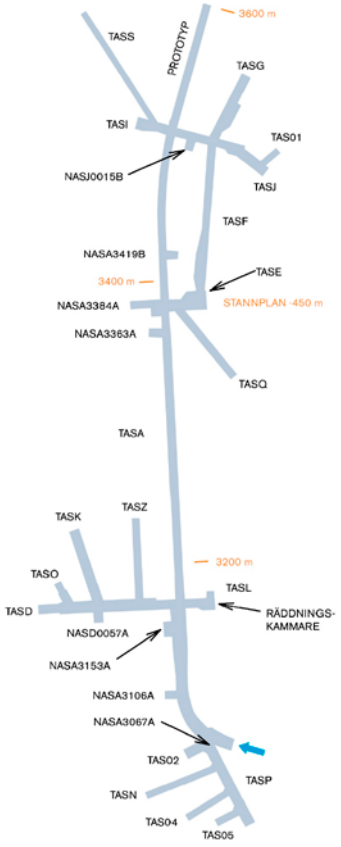

Figure 1-3. *The prototype repository and nearby tunnels.*

Investigations started 1997 and September 2001 the backfilling of the inner tunnel section (tunnel section I) started and late June 2003 the backfilling of tunnel section II was finalized. The casting of the outer plug was finalized 2003-09-11. Nearby experiments have been carried out in the TASS tunnel, see Figure 1-3. Drilling and grouting for the Fine Sealing project (at location of the TASS tunnel) was carried out between 2007-03-12 and 2007-11-19 and the excavation of the TASS tunnel was made 2007-12-11 to 2008-12-18. These activities have affected the Prototype measurements and will be commented in the report.

1.2.1 General objectives

The Prototype repository should simulate as many aspects as possible of a real repository, for example regarding geometry, materials, and rock environment. The Prototype repository is a demonstration of the integrated function of the repository components. Results are compared with models and assumptions to their validity.

The major objectives for the Prototype repository are:

- To test and demonstrate the integrated function of the repository components under realistic conditions in full scale and to compare results with models and assumptions.
- To develop, test and demonstrate appropriate engineering standards and quality assurance methods.
- To simulate appropriate parts of the repository design and construction process.

The objective for the operation phase program is:

- To monitor processes and properties in the canister, buffer material, backfill and near-field rock mass.

1.2.2 Background

During storage of nuclear waste in the rock mass the temperature will increase due to the heat loss from the canisters with spent fuel. This will increase the rock stresses and the fractures will generally close, but may locally open due to the stress situation (Hökmark et al. 2006. Fälth and Hökmark 2006, Alm et al. 2005, Rhén and Alm 2004).

As stated in Section 15.5.13 of SR-Site (SKB 2011), fractures with high flow rates intersecting deposition holes affect many identified safety related issues including piping. colloid release, inflow of corrodants potentially leading to canister failure and outflow of radionuclides. High flow rates in deposition holes are also generally associated with low F-values in the geosphere for both recharge and discharge flow paths. It is therefore of great interest to investigate the thermal effect on fracture transmissivity. Before the experiment started, scoping calculations were made of the expected behaviour of the fractures, see Rhén and Alm (2004). The conclusions, which will be discussed in Chapter 9 were:

- The hydraulic response will in general be decreased transmissivity. The decrease will be larger the closer the fractures are to the canisters.
- The transmissivity will be reduced to something between 10 and 80 percent of the in situ values.
- The fracture closure will be in the range of 5–70 micrometre.
- The hydraulic and mechanical responses on the fracture depend on the orientation of the fracture relative the stress field.
- Major part (~80%) of the increase in stress and temperature is reached within two years.

In order to investigate the hydromechanical response of the fractures as a result of the increased thermal load, two different approaches are considered.

The first approach is to measure the change of the fracture width as function of temperature and time. The displacement is both measured for the intact rock as for a section with one or more fractures. Displacement and temperature measurements are registered continuously every hour.

The second approach implies that the mechanical response is evaluated indirect by using the results from hydraulic tests. Hydro tests are performed in the same sections as the mechanical measurements are made. Hydraulic tests are made a number of times during the operation period for the ten measurement sections. Most tests are made during the first years of operation when the largest displacements are expected to be measured.

This report copes mainly with the first approach. The detailed results of the second approach are reported in Forsmark et al. (2004), Forsmark and Rhén (2004a, b, c, 2005a, b, c) and Forsmark (2006, 2007a, b, 2008, 2010). However, some main results from these hydraulic tests are also presented in this report. The hydrogeological instrumentation of the Prototype repository is shown in Rhén et al. (2001, 2003).

1.2.3 Objectives of hydromechanical tests

The objective of the hydromechanical tests is to measure if the temperature increase will affect the rock mass stress in such way that fracture width or/and fracture transmissivity, changes.

The following questions are considered:

- Is there any deformation observed on the intact rock that can be correlated to temperature?
- Is there any deformation of open fractures that can be correlated to temperature?
- Are there any changes of fracture transmissivities that can be correlated to temperature?
- If fracture transmissivities have changed, can it be correlated to measured deformations of fractures?

1.2.4 Contents of this report

- The background to the project is briefly described in Chapter 1.
- The scope of the performed measurements is briefly described in Chapter 2.
- The equipment used is briefly described in Chapter 3.
- The collection and preparation of data is described in Chapter 4.
- The geology of the prototype repository and the hydromechanical equipped borehole sections is described in brief in Chapter 5.
- In Chapter 6 an overview of the functionality of the measurement equipment and the canister heating performance is given.
- The results of the temperature and deformation measurements are detailed in Chapter 7.
- The transmissivity changes up to 2010-02-01 are summarized in Chapter 8.
- Conclusions are given in Chapter 9.

2 Scope of measurements

Temperature and mechanical measurements are done in 11 boreholes. The tested intervals are listed in Table 2-1 and shown in Figure 3-1. KG0010B01 in the table is a reference hole located some distance from the prototype repository in the nearby G-tunnel.

Table 2-1. Single hole tests sections. "X" indicates that section is equipped with HM sensors. (No tests were performed in KG0010B01, it was just a control hole in rock, for temperature and deformations, not affected by the heating from the canisters.)

Borehole	Section (m)	HM section
KG0010B01	2.80–4.35	X
KA3539G:2	15.85–17.6	X
KA3542G01:3	18.60–20.30	X
KA3542G02:2	25.60–27.20	X
KA3544G01:2	8.90–10.65	X
KA3546G01:2	6.75–8.30	X
KA3548A01:3	8.80–10.75	X
KA3550G01:2	5.20–7.30	X
KA3552G01:2	4.35–6.05	X
KA3554G01:2	22.60–24.15	X
KA3554G02:4	10.50–12.20	X

For the long-term study the following is done:

- Continuous measurement of deformation and temperature every hour in prototype section II (see Figure 3-1).
- The measurements started 2003-05-06. In this report results from May 2003 until October 2006 are reported as temperature plots and deformation plots.

During the operation phase a number of hydraulic test campaigns are conducted. Until October 2006 seven test campaigns were carried out.

- Campaign 1, May 8–11, 2003.
- Campaign 2, October 21–23, 2003.
- Campaign 3, February 2–4, 2004.
- Campaign 4, August 11–18, 2004.
- Campaign 5, January 19–25, 2005.
- Campaign 6, November 28–December 2, 2005.
- Campaign 7, September 25–29, 2006.

The objective with the hydraulic test campaigns is to estimate the transmissivity of each Hydro Mechanical (HM) test section. During these campaigns it is possible to measure and evaluate the deformation response on single fractures and intact rock of a sudden drop of the hydrostatic pressure. The results from these campaigns are reported in Forsmark et al. (2004), Forsmark and Rhén (2004a, b, c), Forsmark and Rhén (2005a, b, c) and Forsmark (2006, 2007a). In this report results from the test periods are reported as deformation plots.

A further three test campaigns (Forsmark 2007b, 2009, 2010) were carried out after September 2006. Since the mechanical sensors didn't work properly during the period after campaign 7, the results are only mentioned briefly in the plots of Chapter 8.

- Campaign 8, October 15–19, 2007.
- Campaign 9, October 20–24, 2008.
- Campaign 10, November 10–19, 2009.

3 Equipment

In Figure 3-1, the boreholes with monitoring sections in Prototype repository section II are shown. In Appendix 4 all boreholes in section I and II are shown. The colours along the boreholes indicate a packer or the type of measurement section:

- GREY, wide cylinder: Packer.
- NO COLOUR: Pressure section (P).
- RED: Hydro Chemical section (HC) + P.
- YELLOW: Flow section (F) + P.
- BLUE: Hydro Mechanical section (HM) + C + P + Temperature (T).

In this report the results from the hydromechanical sections are evaluated (BLUE sections in Figure 3-1). (Tunnel section I is not described in this report as no HM-measurements is made there.)

3.1 Measurement equipment

In order to measure the fracture deformation (and to separate the fracture deformation from the deformation of the intact rock) due to the increased temperature, new measurement equipment has been developed (Rhén et al. 2003).

The equipment consists of two hydraulic packers, which hydraulically isolate the test section. Between the packers three anchors are placed. These anchors are fixed to the borehole wall with fixed steel pins and are fully disconnected to the centre rod. Between the anchors sensors (strain gage) are mounted. The section between the fixed steel pins is called mechanical measurement sections. The sensors will register any relative movement between the anchors, i.e. the fixed steel pins, see Figure 3-2 and Figure 3-3. The temperature is also measured in each sensor by a thermistor. It is the temperature of the water surrounding the sensor that is measured, as the sensor is not in direct contact with the rock.

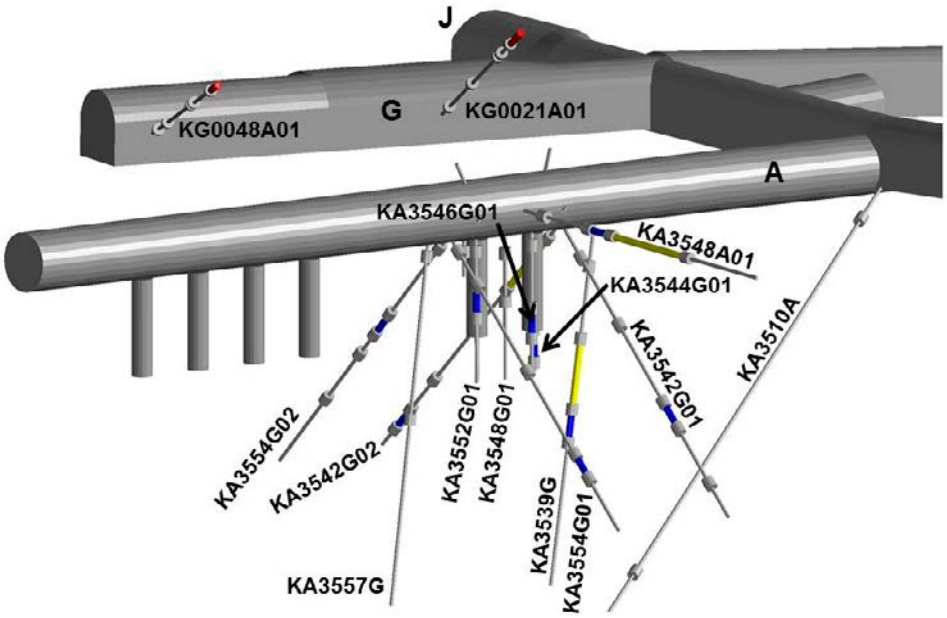

Figure 3-1. *Boreholes with monitoring sections in Prototype repository section II in tunnel A with two deposition holes. Section I in tunnel A includes the other four deposition holes. Tunnels A, G and J marked in the figure.*

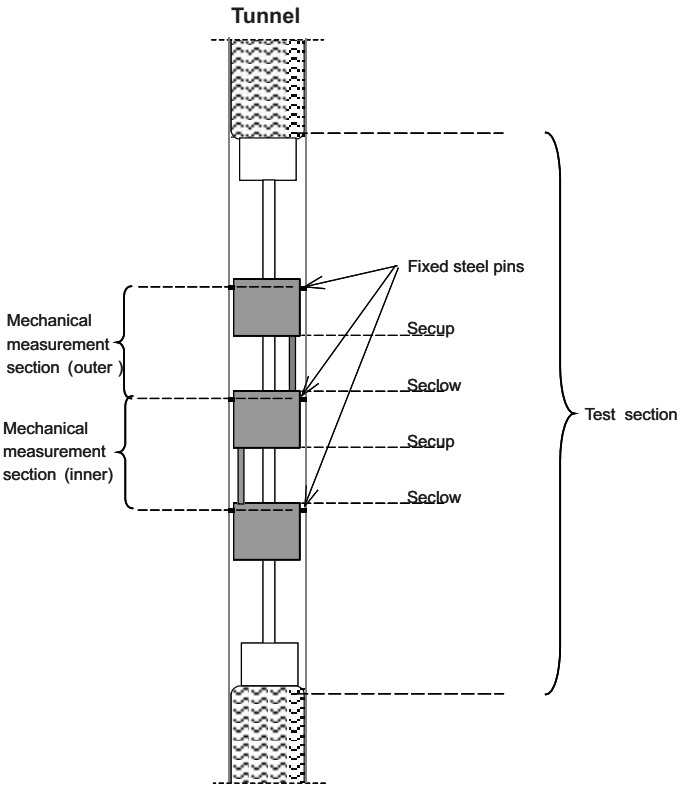

Figure 3-2. *A schematic figure, that shows the different parts of the test equipment and also the definitions of the terms outer and inner relative the tunnel.*

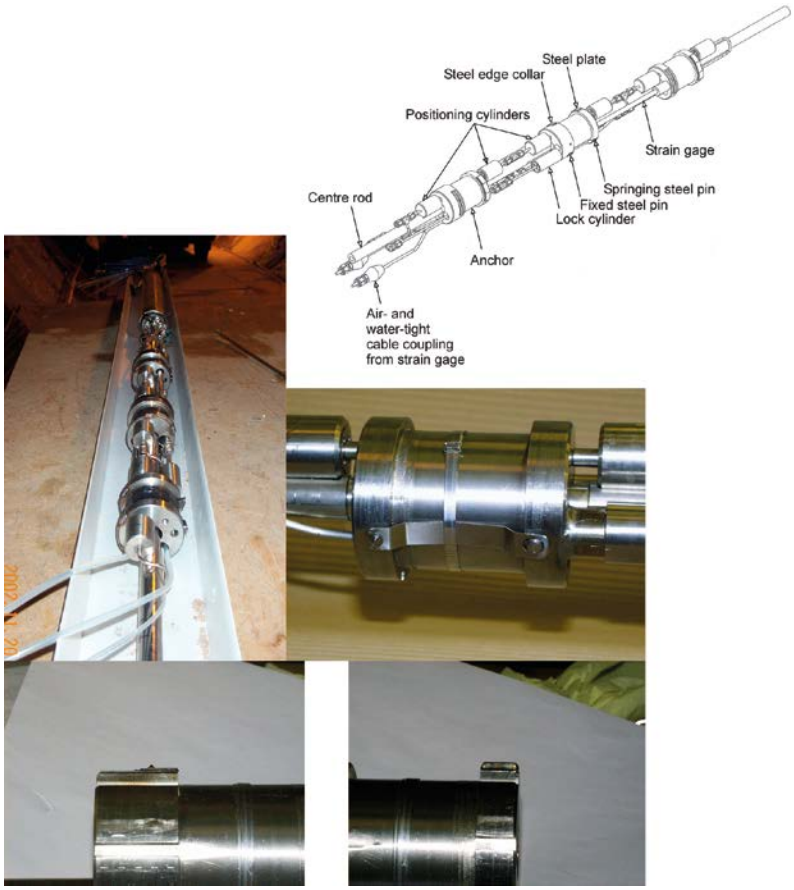

Figure 3-3. *A detailed figure of the three anchors, sensors (strain gage), positioning cylinder etc. (Rhén et al. 2003).*

The deformation is measured in two sections (inner and outer) in each borehole. One of the mechanical measurement sections is placed over a fracture (or fractures) and the other mechanical measurement section is placed over intact rock. That makes it possible to separate the fracture deformation from the deformation of the intact rock.

Of all boreholes in the prototype tunnel, ten are equipped as described above. In four of the boreholes the measurement sections are placed over a single fracture. In rest of the boreholes the measurement sections are placed over two to six fractures, see Figure 3-4 and Table 3-1.

Since hydraulic packers isolate the test sections from rest of the borehole and the test sections have contact with the tunnel (atmospheric pressure) via tubes and valves it is possible to perform hydraulic tests in the test sections.

In order to see if the sensors are affected of long-term running a reference hole was drilled in the G-tunnel. The reference hole is equipped in the same way as the other ten boreholes. The position of the reference hole is chosen so that the rock mass is undisturbed of the temperature increase due to the electrical heaters in the prototype repository.

3.1.1 Logger

In the hydromechanical tests all data is registered and saved by a Model 8020 Micro-10 Data logger. The Micro-10 Data logger is based on a Campbell Scientific CR10X MCU. The number of channels is expanded by a multiplexer (Model 8032 Multiplexer (MUX)). The logger as well as the multiplexer is delivered by Geokon Inc. (Lebanon, USA).

The data logger for the hydromechanical tests is placed in tunnel G, see Figure 3-5.

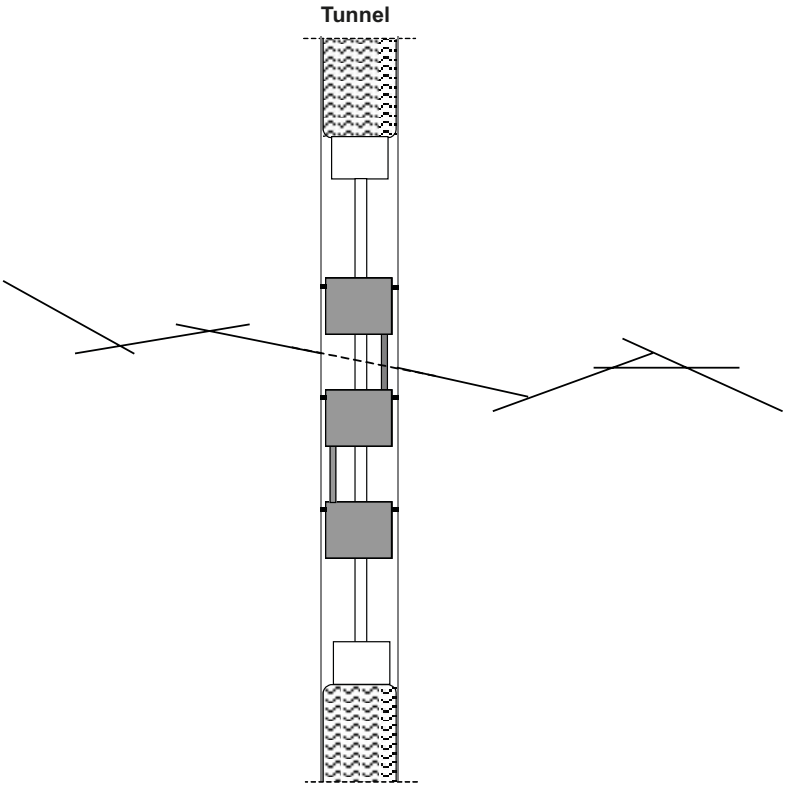

Figure 3-4. *Schematic figure that shows how the anchors are placed on each side of a single fracture and one mechanical measurement section is placed over intact rock.*

Figure 3-5. Data loggers for the hydromechanical equipment, located in Tunnel G.

Table 3-1. Data of the hydromechanical measurement sections (sensor ID, length, number of fractures etc).

Label	Cable mark	Sensor ID	Position	Secup (m)	Seclow (m)	Length of mech. measurement section (L_{fr}/L_{ir})[1] (mm)	Number of fractures
KA3539G-2-1	HRA 1121	3511	Inner	16.77	16.97	311	2
KA3539G-2-2	HRA 1122	3510	Outer	16.47	16.67	323.5	0
KA3542G01-3-1	HRA 1231	3513	Inner	19.47	19.67	311	0
KA3542G01-3-2	HRA 1232	3512	Outer	19.17	19.37	323.5	1
KA3542G02-2-1	HRA 1321	3515	Inner	26.50	26.70	311	1
KA3542G02-2-2	HRA 1322	3514	Outer	26.20	26.40	323.5	0
KA3544G01-2-1	HRA 1621	3509	Inner	9.82	10.02	311	2
KA3544G01-2-2	HRA 1622	3508	Outer	9.52	9.72	323.5	0
KA3546G01-2-1	HRA 1721	3517	Inner	7.67	7.87	311	1
KA3546G01-2-2	HRA 1722	3516	Outer	7.37	7.57	323.5	0
KA3548A01-3-1	HRA 1831	3526	Inner	9.70	10.15	561	2
KA3548A01-3-2	HRA 1832	3518	Outer	9.40	9.60	323.5	0
KA3550G01-2-1	HRA 2121	3527	Inner	6.10	6.70	711	6
KA3550G01-2-2	HRA 2122	3519	Outer	5.80	6.00	323.5	0
KA3552G01-2-1	HRA 2521	3521	Inner	5.25	5.45	311	0
KA3552G01-2-2	HRA 2522	3520	Outer	4.95	5.15	323.5	2
KA3554G01-2-1	HRA 2821	3525	Inner	23.54	23.80	371	2
KA3554G01-2-2	HRA 2822	3522	Outer	23.24	23.44	323.5	0
KA3554G02-4-1	HRA 2941	3524	Inner	11.40	11.60	311	0
KA3554G02-4-2	HRA 2942	3523	Outer	11.10	11.30	323.5	1
KG0010B01-1-1	–	3238	Inner	3.66	3.86	265	
KG0010B01-1-2	–	3507	Outer	3.36	3.56	323.5	

[1] see Figures 3-2 and 4-2.

3.1.2 Sensors

The sensors are manufactured by Geokon Inc. The strains are measured using the vibrating wire technique: A length of steel wire is tensioned between two end blocks. Deformations (i.e. strain changes) will cause the two end blocks to move relative each other, thus altering the tension in the wire. The tension is measured by plucking the wire and measuring its resonant frequency of vibration using an electromagnetic coil.

The advantage of the vibrating wire technique lies mainly in the use of a frequency as the output signal from the strain gage. Frequencies may be transmitted over long cable lengths without appreciable degradation caused by variation in cable resistance, or leakage to ground.

The sensor model used in the hydromechanical tests is type 4210X; specifications are listed in Table 3-2 and Table 3-3. Temperature sensor, thermistor with measurement range –80 to +150°C and accuracy ±0.5°C, is located near the electromagnetic coil. The strain gage temperature range is –20 to +80°C.

Table 3-2. Measurement range and accuracy for each length of the sensors. (Geokon type 4210X).

Length of sensor	Measurement range	Resolution (logger)	Accuracy (0.1% F.S.)
300 mm	0.90 mm	0.12 µm	0.90 µm
550 mm	1.65 mm	0.22 µm	1.65 µm
700 mm	2.10 mm	0.28 µm	2.10 µm
360 mm	1.08 mm	0.14 µm	1.08 µm
254 mm	0.76 mm	0.10 µm	0.76 µm

The normal accuracy for the hole measuring system including hysteresis, non-linearity, misalignment, batch factor variations etc is 1% F.S. according to Geokon. Table 3-2 shows the accuracy based on individual calibration of the sensors.

Table 3-3. Data of the sensors (sensor ID, gage factor, thermal coefficient etc).

Label	Cable mark	Sensor ID	Sensor length (L_s)[1], [mm]	Thermal expansion coefficient for the sensor (α_s) [ppm/°C]	Thermal expansion (therm coeff x sensor length) [mm/°C]	Gage factor [inch/digit]	Thermal expansion coefficient of anchor body (α_{ss}) [ppm/°C]
KA3539G-2-1	HRA 1121	3511	300	12.2	0.003582	0.000004121	17.3
KA3539G-2-2	HRA 1122	3510	300	12.2	0.003582	0.000004098	17.3
KA3542G01-3-1	HRA 1231	3513	300	12.2	0.003582	0.000004101	17.3
KA3542G01-3-2	HRA 1232	3512	300	12.2	0.003582	0.000004133	17.3
KA3542G02-2-1	HRA 1321	3515	300	12.2	0.003582	0.000004107	17.3
KA3542G02-2-2	HRA 1322	3514	300	12.2	0.003582	0.000004132	17.3
KA3544G01-2-1	HRA 1621	3509	300	12.2	0.003582	0.000004087	17.3
KA3544G01-2-2	HRA 1622	3508	300	12.2	0.003582	0.000004081	17.3
KA3546G01-2-1	HRA 1721	3517	300	12.2	0.003582	0.000004109	17.3
KA3546G01-2-2	HRA 1722	3516	300	12.2	0.003582	0.000004090	17.3
KA3548A01-3-1	HRA 1831	3526	550	12.2	0.006633	0.000007793	17.3
KA3548A01-3-2	HRA 1832	3518	300	12.2	0.003582	0.000004122	17.3
KA3550G01-2-1	HRA 2121	3527	700	12.2	0.008462	0.000010005	17.3
KA3550G01-2-2	HRA 2122	3519	300	12.2	0.003582	0.000004110	17.3
KA3552G01-2-1	HRA 2521	3521	300	12.2	0.003582	0.000004121	17.3
KA3552G01-2-2	HRA 2522	3520	300	12.2	0.003582	0.000004125	17.3
KA3554G01-2-1	HRA 2821	3525	360	12.2	0.004314	0.000004982	17.3
KA3554G01-2-2	HRA 2822	3522	300	12.2	0.003582	0.000004117	17.3
KA3554G02-4-1	HRA 2941	3524	300	12.2	0.003582	0.000004119	17.3
KA3554G02-4-2	HRA 2942	3523	300	12.2	0.003582	0.000004128	17.3
KG0010B01-1-1	–	3238	254	12.2	0.003070	0.000003368	17.3
KG0010B01-1-2	–	3507	300	12.2	0.003582	0.000004158	17.3

[1] see Figure 4-1.

4 Measurement and data analysis procedures

4.1 Deformation measurements principles

Measuring the deformation of fractures and intact rock during the operation phase is a continuous activity that is ongoing independent of other activities in the prototype area.

Beside the installation of the equipment the activities is limited to:

- Downloading data from the logger on a regular basis.
- Control of data in order to see if the sensors are working.
- Visual control of the logger equipment at certain intervals.

The main purpose of the measurements is to register both temperature change and deformation in the rock mass. The logger registers both temperature and strain (from each sensor) every hour.

If hydraulic tests are done, the measurement sampling rate is increased to twice every minute and downloading of data from logger has to be done at least after the test campaign is finished or earlier if the capacity of the storage of data is not enough.

4.2 Data handling of hydromechanical measurements

The data is down loaded and transferred (via telephone modem) to a server by Berg Bygg Konsult AB and then delivered to SWECO Environment AB. The raw data is evaluated and analysed and presented in this report.

All the referred activity plans for this report has been checked and all are reported and stored in SKB's database SICADA under project number F63.1.

4.3 Analyses and interpretation of hydromechanical measurements

The analyses and interpretation has to be done in four steps, namely:

1. Control and compare the temperature data from the inner and outer sensors and finally chose the data set that is used.
2. Calculate and evaluate the sensor deformation by using the gage factor and temperature data.
   – The sensor deformation is adjusted due to the temperature by using the thermal coefficient of the sensor (α_{sensor}) and thermal coefficient of the anchor body ($\alpha_{stainless\ steal}$).
3. Calculate the rock and fracture deformation.
   – In order to separate the fracture deformation from the deformation of the rock mass it is necessary to evaluate the strain of the intact rock.
4. Interpretation of the results.

4.3.1 Temperature data

In each test section there are two sensors and each of them contains thermistors that measure the temperature. Theoretically these two thermistors deliver the same data since they are close to each other and the ground water flow easily between the sensors. However, it has turned out that the zero-level is not the same between the thermistors. Some of the thermistors have failed as well or just delivers incorrect data.

The temperature data is controlled in three steps:

1. The raw data from inner and outer thermistor is plotted versus time.
2. Visual control,
   a. extreme values, such as temperature below zero, and over 100°C are removed,
   b. (occasionally) values that stand out from the rest are removed,
   c. data from failed thermistors are removed.
3. Chose temperature,
   a. if the raw data from both thermistors are good the average of them is chosen (In Appendix 1 temperature is shown for inner and outer sections),
   b. if just one of them is good that one is chosen,
   c. if none of the thermistors works, data from another section (with the same distance to the heater) is chosen.

4.3.2 Deformation data

The signal from the sensor is registered or presented as digits. Each sensor is calibrated and one digit represents a certain movement, i.e. gage factor. Since the sensor also is affected of the change in temperature the result must be compensated for the change in length due to the temperature increase or decrease.

Furthermore, there is a distance, $L_{anchor\ body}$, between the fixed steel pin (i.e. the contact point between the anchor and the borehole wall) and the attach point of the sensor. The readout from the sensor must be corrected due to the thermal expansion of this part of the anchor body, see Figure 4-1.

The correction due to the thermal expansion of sensor and the anchor bodies is done as follows, see Figure 4-1 and Table 3-3:

$$\Delta x^{corrected} = \Delta(number\ of\ digits) \times gage\ factor + (\alpha_{sensor} \times L_{sensor} \times \Delta T) + (\alpha_{stainless\ steel} \times L_{anchor\ body} \times \Delta T) \quad (4\text{-}1)$$

where:

$\alpha_{sensor} = \alpha_s$ = thermal coefficient for sensor = $12.2 \cdot 10^{-6}$/°C

$L_{sensor} = L_s$= length of the sensor

ΔT = change in temperature from reference temperature at time t0 =T(time t)–T(time t0)

$\alpha_{stainless\ steel} = a_{ss}$= thermal coefficient for anchor body = $17.3 \cdot 10^{-6}$/°C

$L_{anchor\ body} = L_a$ = length of the part between the fixed steel pin and the attach point of the sensor
L_a= c. 11 mm

Δ(number of digits) = digits(time t)–digits(reference position at time t0)

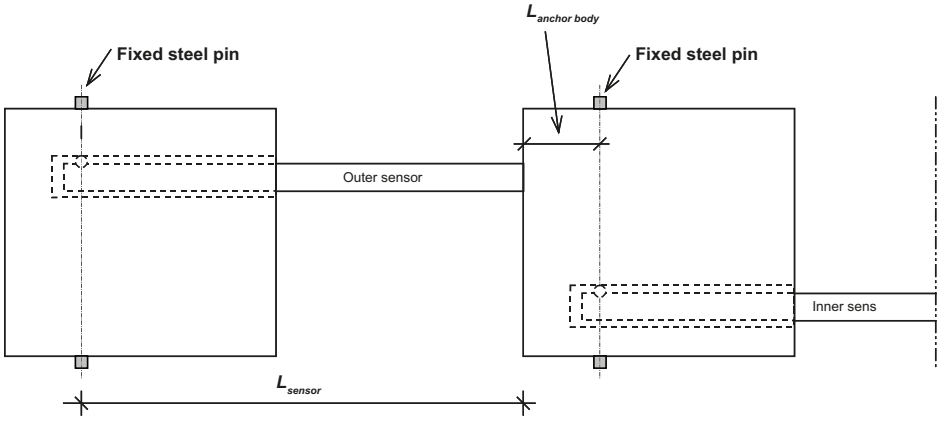

Figure 4-1. *The figure shows how the sensor is mounted to the anchor body as well as the fixed contact point (fixed steel pin) between the anchor and the borehole wall.*

Assuming the change in temperature is 1°C the correction for a 300 mm long sensor is 3.7E-6 m and the correction for the anchor body 2E-7 m. The correction for the anchor body is c. 10 to 20 smaller than the temperature correction related to the sensor for equipment used, and could in principle for this experiment be neglected. In Section 7.4 a few examples of the temperature change during short-term tests of the water in the test sections are shown. The examples indicate that the changes may be 0.1 to 0.2°C. This means that the applied correction to the short term deformation measurements may be up to c. 1E-6 m and the observed corrected deformations are up to c. 4E-5 m. The temperature corrections applied on the data for short term tests are thus generally significantly smaller than the deformation measurements made, see Section 7.4 for more details and comments.

The deformation data is controlled as well. The deformation data is controlled in two steps:

1. The raw data from inner and outer sensor is plotted versus time.
2. Visual control,
   a. extreme values, such as deformation larger than the measurement range are removed,
   b. exceptional values that stand out from the rest are removed,
   c. a failed sensor is removed. Eventually the data before breakdown can be used.

4.3.3 Results / Fracture deformation

Fracture deformation

Results from the measurement sections include deformation of intact rock as well as fractures and therefore need to be evaluated in order to separate the fracture deformation, $\Delta\delta_{fracture}$:

$$\Delta\delta_{fracture} = \Delta x_{fractured\ rock} - \Delta x_{intact\ rock}$$

However, since the length of the mechanical measurement sections varies with the change in fracture deformation, must be estimated by following calculation, see Figure 4-2 and Table 3-3.

$$\Delta\delta_{fracture} = \Delta x_{fr}^{corr} - \left(\frac{\Delta x_{ir}^{corr}}{L_{ir}} \times L_{fr} \right) \qquad (4\text{-}2)$$

where:

$\Delta x_{fr}^{corr} = \Delta x_{fractured\ rock}^{corrected}$ = corrected change in length of sensor placed in fractured rock

$\Delta x_{ir}^{corr} = \Delta x_{intact\ rock}^{corrected}$ = corrected change in length of sensor placed in intact rock

$L_{fr} = L_{fractured\ rock}$ = length of the mechanical measurement section (in fractured rock)

$L_{ir} = L_{intact\ rock}$ = length of the mechanical measurement section (in intact rock)

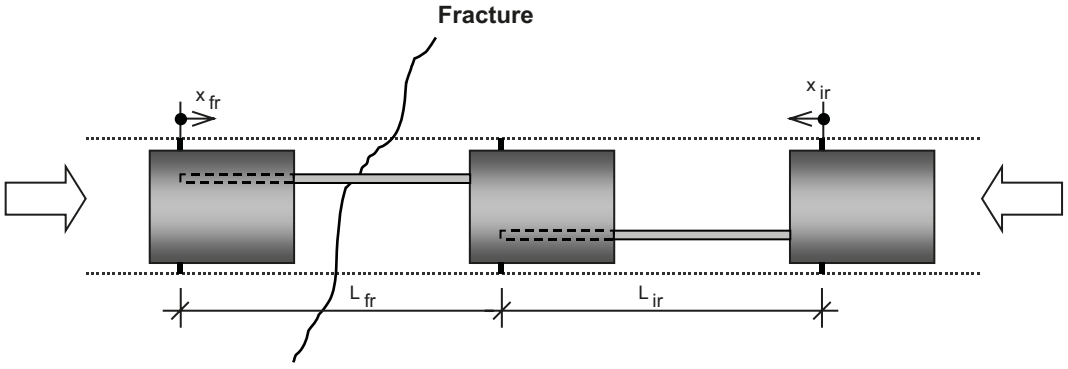

Figure 4-2. *Denominations used when calculating the fracture deformation.*

4.3.4 Hydraulic test campaigns

Test procedure

A selected borehole section is tested with a single hole pressure build-up test. A pressure build-up test roughly include following steps:

- Initialising of the HMS system 30 minutes before flow start with logging interval of 5 minutes.
- A couple of minutes before flow start and until 5 minutes after flow start the highest logging interval of 3 seconds are used for measuring the pressure changes. Thereafter the logging interval is 30 seconds which is used until 30 minutes after flow start and a logging interval of 5 minutes is then used once again.
- The flow is measured with a flow metre. The flow is also measured manually 2–3 times the first 5 minutes after flow start, 2–3 times the following 60 minutes and 3 times shortly before flow stop.
- From shortly before flow stop until 5 minutes after flow stop the highest logging interval of 3 seconds are used for measuring the pressure changes. Thereafter the logging frequency is 30 seconds which is used until 30 minutes after flow start and a logging frequency of 5 minutes is then used.
- The valve shutting is done as swiftly as possible.

The test procedure and the results are described in detail in Forsmark and Rhén (2004a, b, c, 2005a, b, c) and Forsmark (2006, 2007a, b, 2008, 2010) and in Appendix 3 there is an overview of the test campaigns.

Analyses and interpretation of the hydraulic test

Two methods are used; a stationary method (T_{Moye}) and a transient method applied on the recovery phase.

The Moye formula can be used for interpretation of steady state tests in order to get an estimate of the transmissivity (Moye 1967):

$T_{Moye} = Q \cdot (1 + \ln(L/(2 \cdot r_w))) / (2 \cdot \pi \cdot \Delta h)$ where

Q = average water flow before shutting the valve after the flowing phase [m^3/s]

$\Delta h = (p_0 - p_p) / (r_w \cdot g)$ [m]

L = test section length [m]

r_w = borehole radius [m]

p_0 = absolute pressure in test section before start of flow period [Pa]

p_p = absolute pressure in test section before stop of flow period [Pa]

r_w = water density [kg/m^3]

g = acceleration of gravity [m/s^2]

The method suggested by Moye (1967) assumes a steady state radial flow near the tested section and spherical flow at some distance.

For the transient evaluation the measured flow rate for the flowing phase is used (multirate approach) and the pressure from the pressure build-up period is used for the evaluation. Evaluating the transient data, the pressure change, Δp, is plotted versus the equivalent time, dt_e, in minutes. The equivalent time, dt_e, (Spane and Wurstner 1993) is defined as:

$dt_e = (t_p \cdot dt) / (t_p + dt)$ where

t_p = the flowing time of the borehole before shutting the valve

dt = the time after shutting the valve

The pressure change Δp is calculated as:

$\Delta p = p(dt) - p(tp)$

p(dt) = measured pressure at time dt after shutting the valve

p(tp) = measured pressure just before shutting the valve

The tests are evaluated using the software AQTESOLV ver. 4.50. AQTESOLV is the all-in-one software package for the design and analysis of aquifer tests including pumping tests, step-drawdown tests, variable-rate tests, recovery tests, single-well tests, slug tests and constant-head tests. The software is developed by HydroSOLVE, Inc., USA. General approach for transient analysis is presented in Horne (1995).

The solution used in the analysis is the Dougherty-Babu model for a pumping test in a confined aquifer (Dougherty and Babu 1984). The model assumes radial flow in a porous medium. AQTESOLV uses the principle of superposition in time to simulate variable-rate tests including recovery with the solution. The result consist of:

Transmissivity, T (m^2/s)

Skinfactor, Sw (-)

Both methods outlines above, the steady state and the transient methods, assume radial flow. However, Moye (1967) ads a spherical part and using a transient method one can evaluate the flow dimension to check if there is radial flow. Radial flow may not always be present but the evaluation of the flow dimension indicate that radial flow is approximately present in many cases with hydraulic transient tests in crystalline rock, which also has been seen in other SKB projects, see e.g. Rhén et al. (2008). It is there for judged that the evaluation methods used are appropriate for evaluating transmissivity changes during the experiment, even though it is a fractured medium and not a porous medium. Details of the observed flow regimes can be found in the reports for the individual tests, see References in the end of this report.

The effective stress in the fracture system will increase when the flowing period starts and will go back to its initial conditions during the pressure build-up period. T_{Moye} is based on the minimum flow rate and the maximum drawdown during the flow period and represents then a situation with lowest effective stress in the fracture/s. T from the transient evaluation will mainly depend on a match of pressures in the fracture(s that have effective stress close to the effective stress at the initial conditions. The transient evaluation can also take into account a skin factor, assumed to be a hydraulic resistance near the borehole wall. In general one would then expect that the transient evaluated T based on the pressure build-up period should be more relevant for evaluation of the actual transmissivity of a fracture.

To gain more information, the test campaigns were modified from test campaign 4. Applied Δp were c. 100 kPa, 200 kPa and maximum drawdown (open valves in the G-tunnel). In some test campaigns only c. 100 kPa and maximum drawdown could be applied. In test campaigns 1–3 only maximum drawdown was applied.

In Section 7-3 where the long-time evolution of the deformation and transmissivity are shown, it is the T-values from maximum drawdown that is plotted.

It is of uttermost importance when evaluation the hydraulic tests within the scope of this report that all tests are evaluated using the same approach between the test campaigns. This is important to be able to evaluate the relative difference of the transmissivity from one test campaign to another.

Fracture deformation

The fracture and rock deformation is evaluated as described in Section 4.3.2 and 4.3.3.

4.3.5 Pressure head in borehole sections

In Appendix 2 the long-term development of the pressure head in boreholes with HM – measurements are shown.

5 Geology of hydromechanical sections

In this chapter the geology is described in brief for each of the hydromechanical sections. The exact positioning of the hydromechanical equipment is detailed in Table 3-1. All tested sections are detailed in Appendix 5. An example is shown below.

5.1 Geology of Äspö Prototype repository area

The mapping (see Rhén and Forsmark 2001) of the TBM tunnel between chainage 3,500 and 3,600 metre shows that the main rock type is Äspö diorite with veins and xenolits of fine-grained granite, greenstone and pegmatite, see Figure 5-1.

The dominating fracture fillings at Äspö are chlorite and calcite. Epidote, hematite fluorite and quartz are also common. Clay minerals have been detected in some fracture zones and single fractures.

The mapped fractures in the area consist of two sets, one that is sub-horizontal and one that is a steep north-west set. There are also indications of a third set with steep fractures in the north-east direction.

In Figure 5-2 an example of the BIPS image of a section is shown. The fractures in this case that are monitored are at sections 16.86 and 16.87 m.

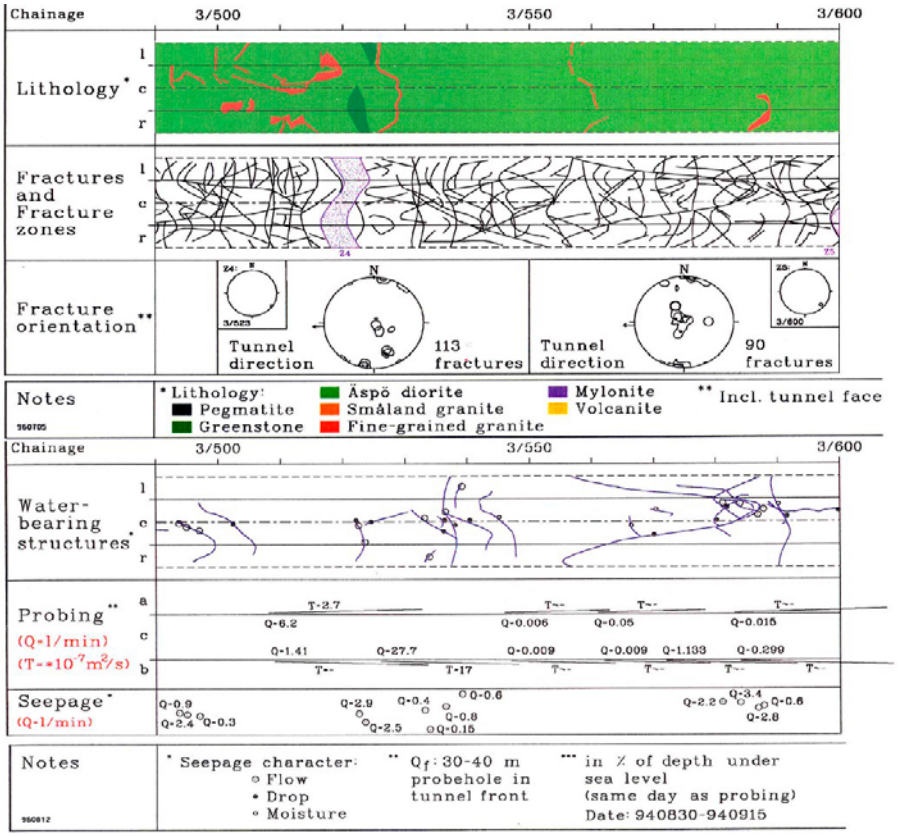

Figure 5-1. *Mapping of the TBM tunnel (Prototype repository area).*

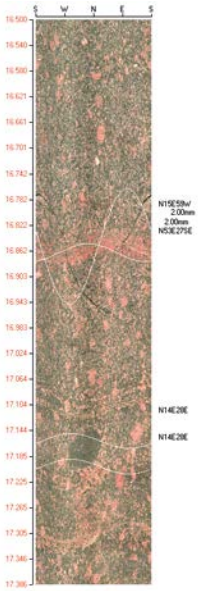

The rocktype of the section is granodiorite. There are xenoliths of mafic igneous rock between 16.15–16.20 m and 17.16–17.20 m.

Figure 5-2. *BIPS image of KA3539G (16.5–17.4 m).*

Table 5-1. Fractures in KA3539G, 15.85–17.60 m. (Aperture: Estimated from BIPS and should not be interpreted as hydraulic aperture but rather as an indication of difference of openness between observed (interpreted) open fracture.)

Borehole	Section (m)	Strike (°)	Dip (°)	Aperture (mm)	Mineral	Comments
KA3539G	16.86	195	59	2	Calcite	Monitored
KA3539G	16.87	53	27	2	Calcite	Monitored

6 Overview of hydromechanical performance, canister heating and hydraulic tests

6.1 Hydromechanical sensor performance

Several of the sensors failed due to different technical reasons during the period up to 2006-10-01. Below are shown in two diagrams the operational periods of each sensor.

The reason for the long non-operational period starting in February 2005 is due to the probable cause that increased water pressure, occurring when the drainage of Prototype section 1 was closed down 2004-11-01. This caused water entering the signal cables and finally the data logger equipment. The drainage-system was re-opened 2004-12-06 due to electrical problems with the canister heaters. Several sensors have unfortunately failed to operate after the replacement of logger and connecting equipment. They were permanently lost. The temperature measurements were however on-going for most sections.

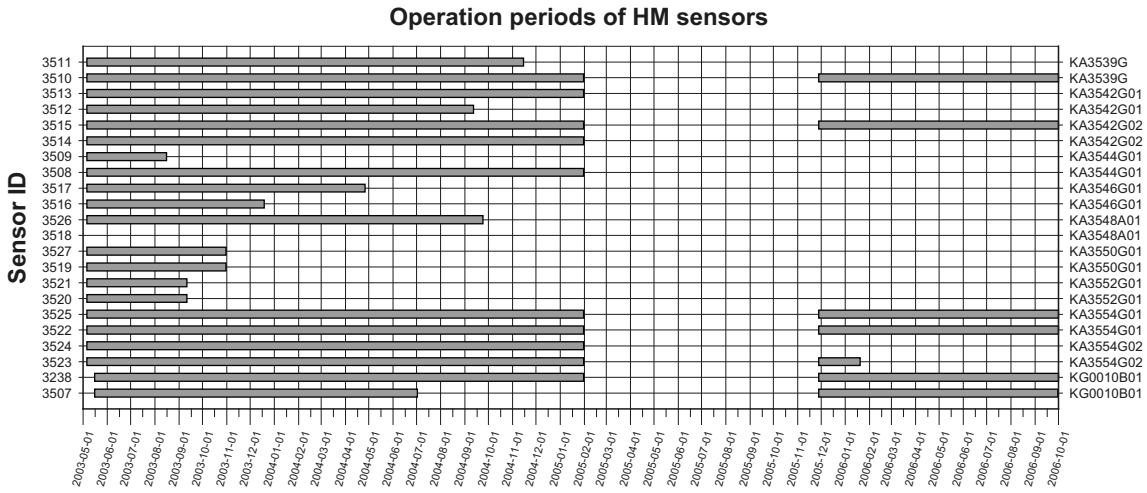

Figure 6-1. *Operational periods of hydromechanical sensors (Sensor ID, see Table 3-1).*

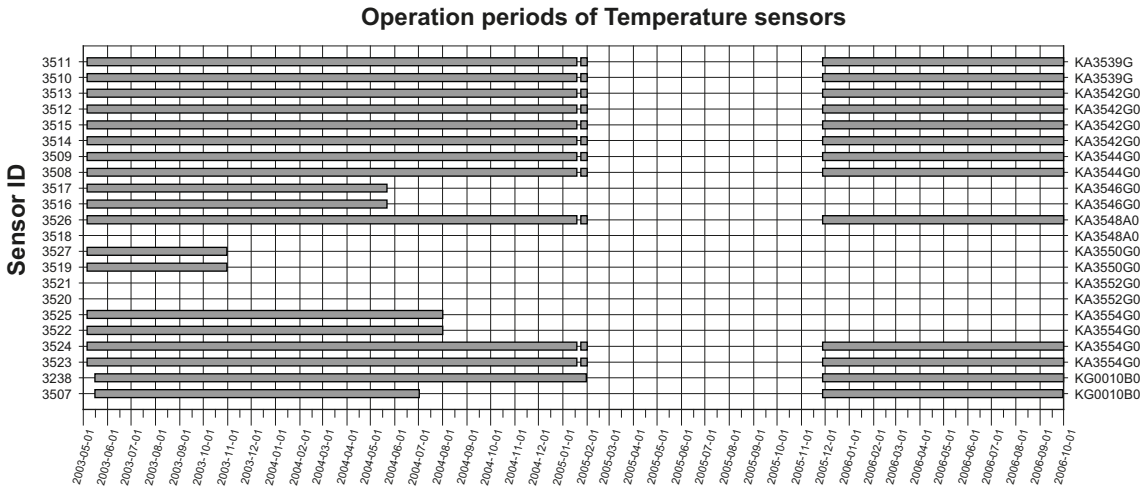

Figure 6-2. *Operational periods of temperature sensors in HM-equipment (Sensor ID, see Table 3-1).*

6.2 Canister heating performance

In the following figures the canister heating variations are shown for deposition hole 1 to 6. The starting dates for the heaters are shown in Table 6-1.

Table 6-1. Starting of heaters in canisters.

Canister in deposition hole	Date	Tunnel section
1 (DA3587G)	2001-09-17	I
2 (DA3581G)	2001-09-24	I
3 (DA3575G)	2001-11-10	I
4 (DA3569G)	2001-11-24	I
5 (DA3551G)	2003-05-08	II
6 (DA3545G)	2003-05-23	II

All heaters were closed down after electrical short-cut problem occurred when the drainage of Prototype section 1 was stopped in 2004-11-01. All heaters were re-started 2004-12-06 with the exception of DBH 2 which was closed down permanently.

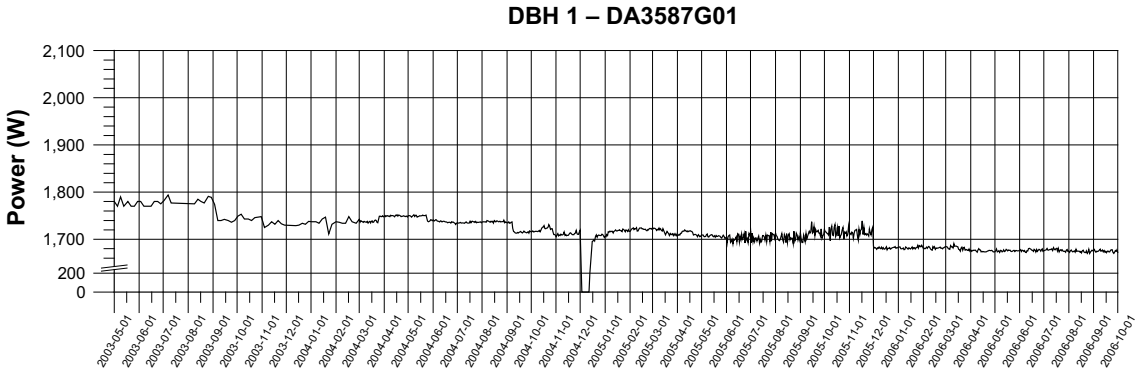

Figure 6-3. *Canister heating in deposition hole 1 (DA3587G01).*

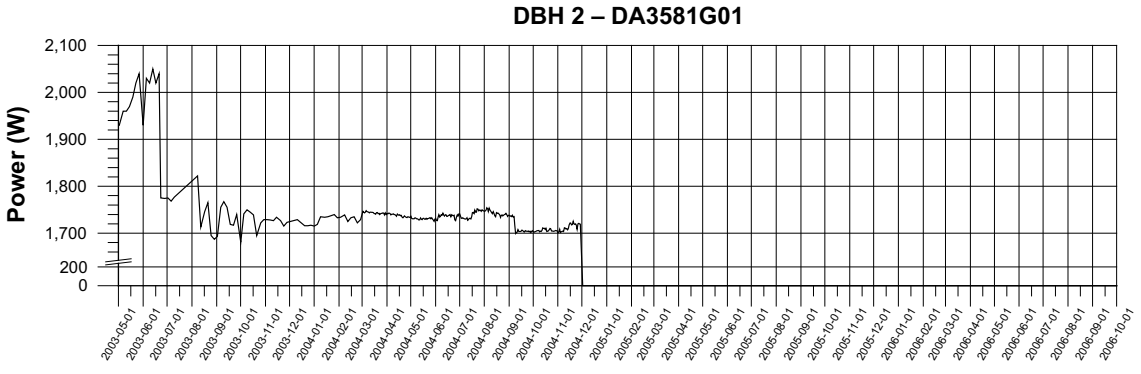

Figure 6-4. *Canister heating in deposition hole 2 (DA3581G01).*

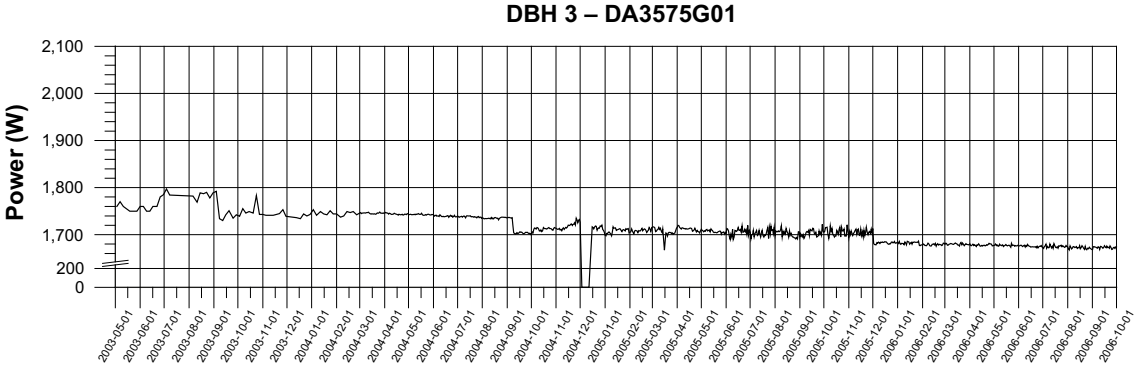

Figure 6-5. *Canister heating in deposition hole 3 (DA3575G01).*

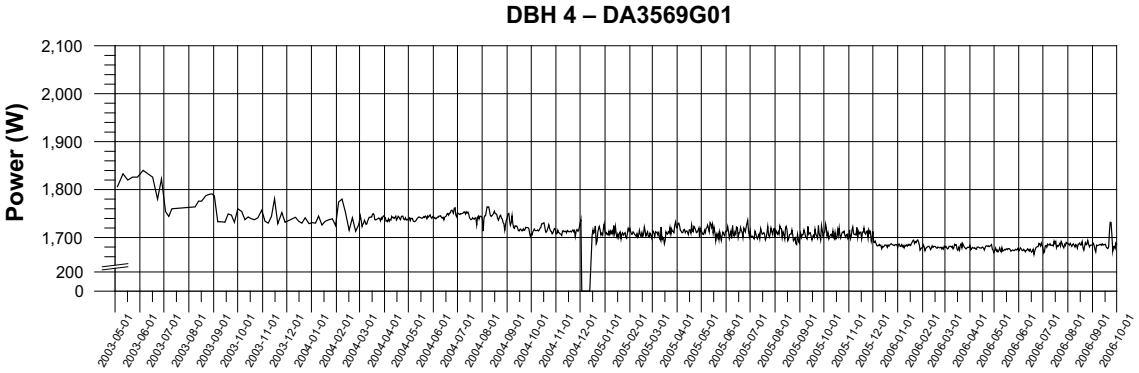

Figure 6-6. *Canister heating in deposition hole 4 (DA3569G01).*

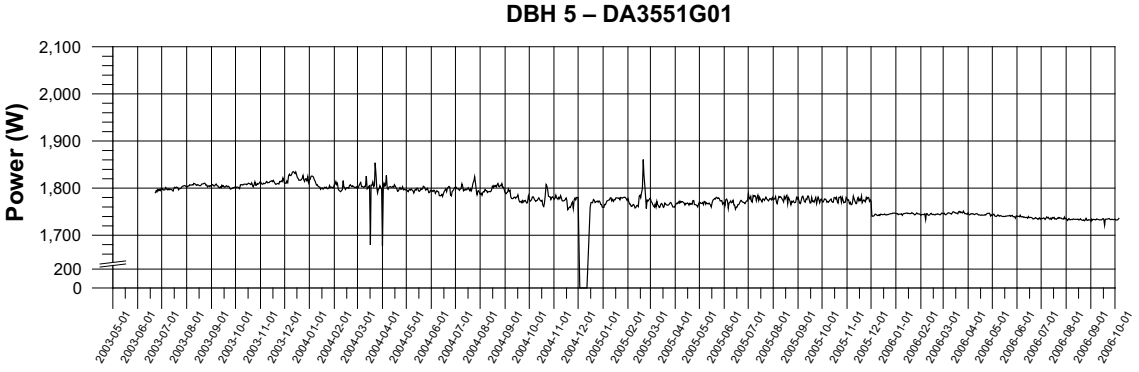

Figure 6-7. *Canister heating in deposition hole 5 (DA3551G01).*

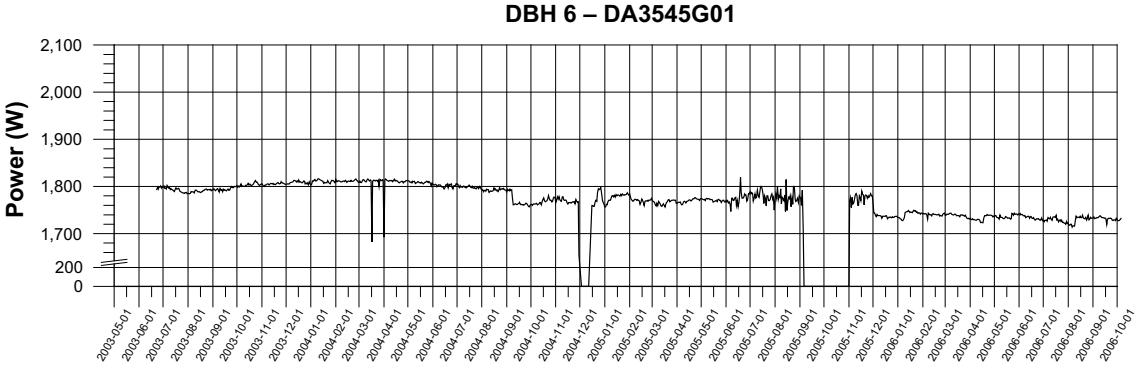

Figure 6-8. *Canister heating in deposition hole 6 (DA3545G01).*

6.3 Overview of temperature increase in prototype section II

The tested sections can be divided into classes with “thermal” distances, where the distance is the closest distance to a heating canister:

- approx. 1 m : KA3550G01:2 and KA3552G01:2,
- approx. 1.5 m : KA3544G01:2 and KA3546G01:2,
- approx. 10 m : KA3539G:2 and KA3554G02:4,
- approx. 15 m : KA3542G01:3 and KA3548A01:3,
- approx. 20 m : KA3542G02:2 and KA3554G01:2.

In Table 6-2 the reference temperature for each test section equipped with hydromechanical equipment is shown.

Table 6-2. Reference temperature in test sections.

Borehole section	Date	Temperature (°C)
KG0010B01	2003-05-16	12.62
KA3539G:2	2003-05-06	13.88
KA3542G01:3	2003-05-06	13.87
KA3542G02:2	2003-05-06	14.10
KA3544G01:2	2003-05-06	14.06
KA3546G01:2	2003-05-06	14.01
KA3548A01:3	2003-05-06	13.90
KA3550G01:2	2003-05-06	14.32
KA3552G01:2	2003-05-06	14.32
KA3554G01:2	2003-05-06	13.95
KA3554G02:4	2003-05-06	14.56

In the figure below the hydraulic test periods are shown as vertical lines.

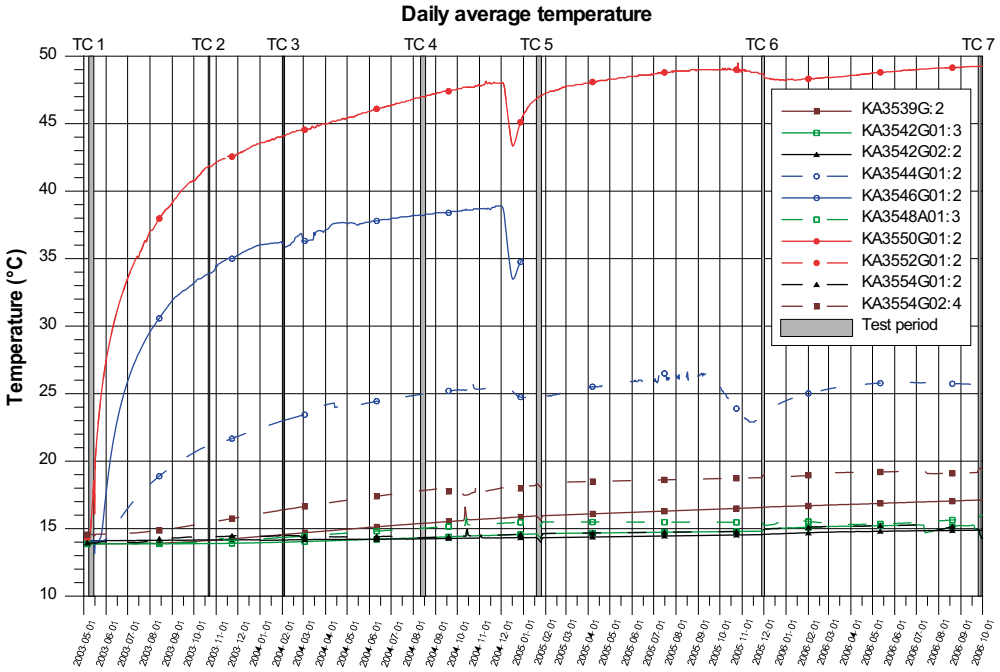

Figure 6-9. *Temperature development in the boreholes. Overview of hydraulic test periods until test campaign 7.*

6.4 Backfilling of section II and construction of plug

The backfilling of section II started 2003-04-29 and work continued until 2003-06-27. The casting of the outer plug was finalized 2003-09-11.

6.5 Operation period of section II

Measurements were made up to late 2010. Demolition work of the outer plug of section II started during December 2010 and was finalized during February 2011. The work was done by drilling several boreholes into the concrete plug continued by mechanical impact with a hydraulic hammer and a hydraulic breaker.

The backfill material was then carefully excavated with a lot of material samples taken every 2 metre to determine amongst other parameters water content and density. The heating canister in deposition hole 6 was retrieved 2011-07-14 and the same was done with the canister in deposition hole 5 2011-12-07. All demolition work in the tunnel section II was finalized by 2011-12-15.

7 Temperature and deformation measurements

In this chapter the following is presented:

- Deposition hole and canister size, see Section 7.1.
- The configuration of each borehole measurement section is presented in figures, see Section 7.2. In Appendix 4 alternative views of the boreholes are shown.
- The result from the long-term study of temperature and fracture deformation, see Section 7.3 – Pressure head in borehole section in this chapter are based on Appendix 2.
- The short term study of fracture deformation during hydraulic test campaigns 1–6, see Section 7.4.

Convention of signs

The convention of signs in the following deformation figures is as follows:

- Positive deformation is equal to expansion.
- Negative deformation is equal to compression.

(Figure 7-1).

7.1 Deposition hole size

The diameter of the deposition holes is 1.75 metres while the depth is 8.37 metres.

The canister size is 4.83 m long with a diameter of 1.05 m. Bentonite rings is placed around the canister, so it is centred in the deposition hole and its bottom approximately 0.5 m above the deposition hole bottom.

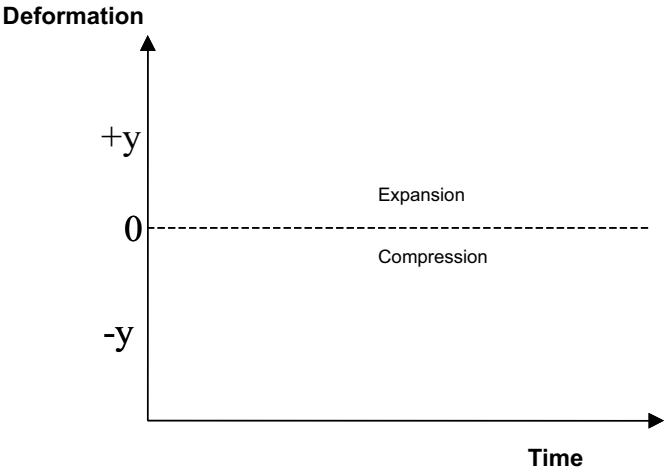

Figure 7-1. *Convention of signs.*

7.2 Test section data

7.2.1 KG0010B01

This borehole is 6.10 m long. The hydromechanical test section is between 2.80 m and 4.35 m. This hole is used as a reference hole not influenced by the increased temperature around the prototype repository itself.

Test section data

- Length of the hydromechanical measurement section (located below level of canister holes):
  - Inner: 0.265 m.
  - Outer: 0.3235 m.
- Spherical distance to centre of nearest heater: 47 m.
- Number of fractures:
  - Inner: – .
  - Outer: – .

(Figure 7-2).

7.2.2 KA3539G

This borehole is 30.01 m long. The hydromechanical test section is between 15.85 m and 17.60 m.

Test section data

- Length of the hydromechanical measurement section (located below level of canister hole bottom):
  - Inner: 0.311 m.
  - Outer: 0.3235 m.
- Distances:
  - Spherical distance to centre of nearest heater: 13.1 m.
  - Spherical distance to centre of the bottom of nearest heater: 9.2 m.
  - (Radial distance to centre line of nearest heater: 4.0 m).
- Number of fractures:
  - Inner: 2.
  - Outer: – .

(Figure 7-3).

7.2.3 KA3542G01

This borehole is 30.01 m long. The hydromechanical test section is between 18.60 m and 20.30 m.

Test section data

- Length of the hydromechanical measurement section (located below level of canister hole bottom):
  - Inner: 0.311 m.
  - Outer: 0.3235 m.
- Distances:
  - Spherical distance to centre of nearest heater: 17.4 m.
  - Spherical distance to centre of the bottom of nearest heater: 15.5 m.
  - (Radial distance to centre line of nearest heater: 14.6 m).
- Number of fractures:
  - Inner: – .
  - Outer: 1.

(Figure 7-4).

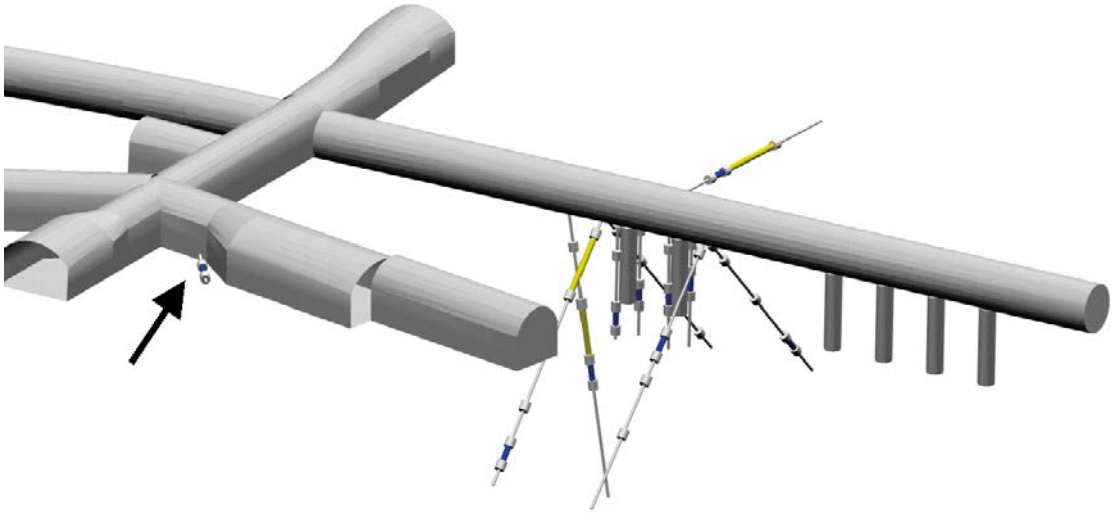

Figure 7-2. *Reference hole (KG0010B01) in G-tunnel.*

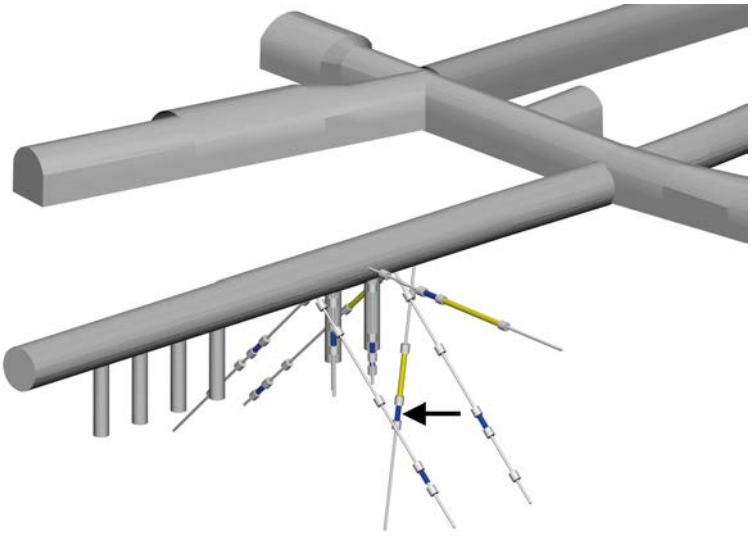

Figure 7-3. *Test section (KA3539G:2) relative the prototype tunnel.*

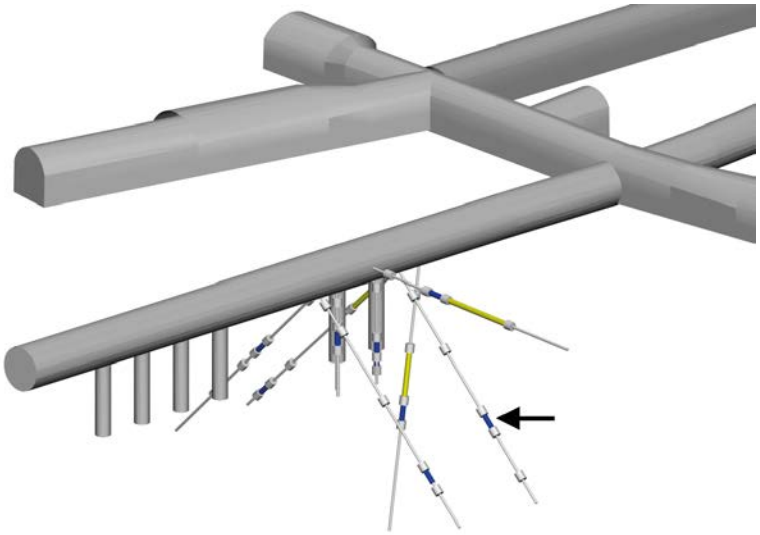

Figure 7-4. *Test section (KA3542G01:3) relative the prototype tunnel.*

7.2.4 KA3542G02

This borehole is 30.01 m long. The hydromechanical test section is between 25.60 m and 27.20 m.

Test section data

- Length of the hydromechanical measurement section (located below level of canister hole bottom):
  - Inner: 0.311 m.
  - Outer: 0.3235 m.
- Distances:
  - Spherical distance to centre of nearest heater: 24.2 m.
  - Spherical distance to centre of the bottom of nearest heater: 22.0 m.
  - (Radial distance to centre line of nearest heater: 19.6 m).
- Number of fractures:
  - Inner: 1.
  - Outer: – .

(Figure 7-5).

7.2.5 KA3544G01

This borehole is 12.00 m long. The hydromechanical test section is between 8.90 m and 10.65 m.

Test section data

- Length of the hydromechanical measurement section (located below level of canister hole bottom):
  - Inner: 0.311 m.
  - Outer: 0.3235 m.
- Distances:
  - (Spherical distance to centre of nearest heater: 5.6 m).
  - Spherical distance to centre of the bottom of nearest heater: 1.8 m.
  - Radial distance to centre line of nearest heater: 1.2 m.
- Number of fractures:
  - Inner: 1.
  - Outer: – .

(Figure 7-6).

7.2.6 KA3546G01

This borehole is 12.00 m long. The hydromechanical test section is between 6.75 m and 8.30 m.

Test section data

- Length of the hydromechanical measurement section (located above level of canister hole bottom):
  - Inner: 0.311 m.
  - Outer: 0.3235 m.
- Distances:
  - (Spherical distance to centre of nearest heater: 3.4 m).
  - Spherical distance to bottom of nearest heater: 1.6 m.
  - Radial distance to centre line of nearest heater: 1.2 m.
- Number of fractures:
  - Inner: 1.
  - Outer: – .

(Figure 7-7).

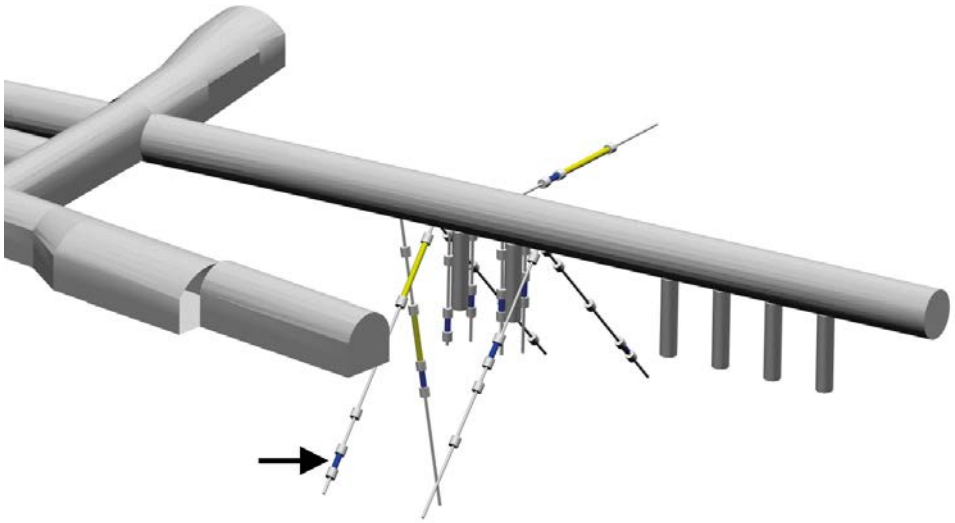

Figure 7-5. *Test section (KA3542G02:2) relative the prototype tunnel.*

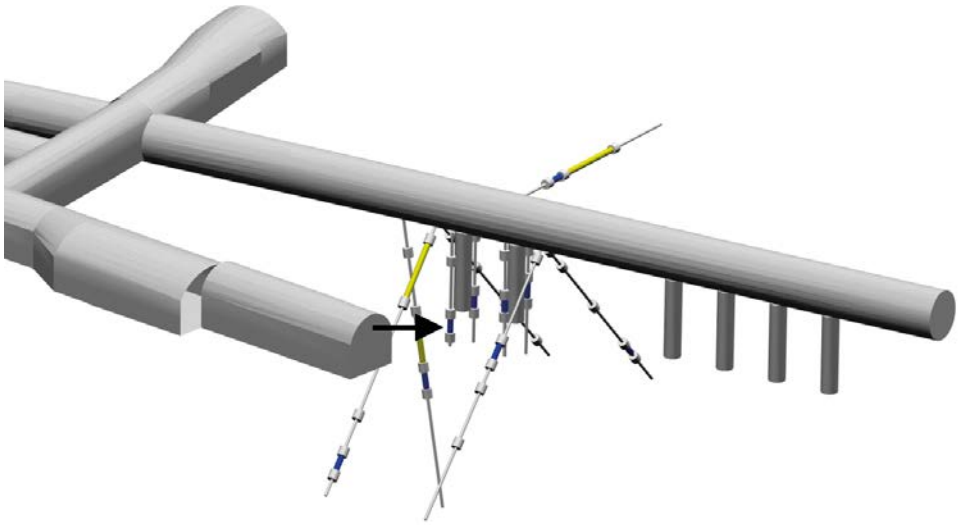

Figure 7-6. *Test section (KA3544G01:2) relative the prototype tunnel.*

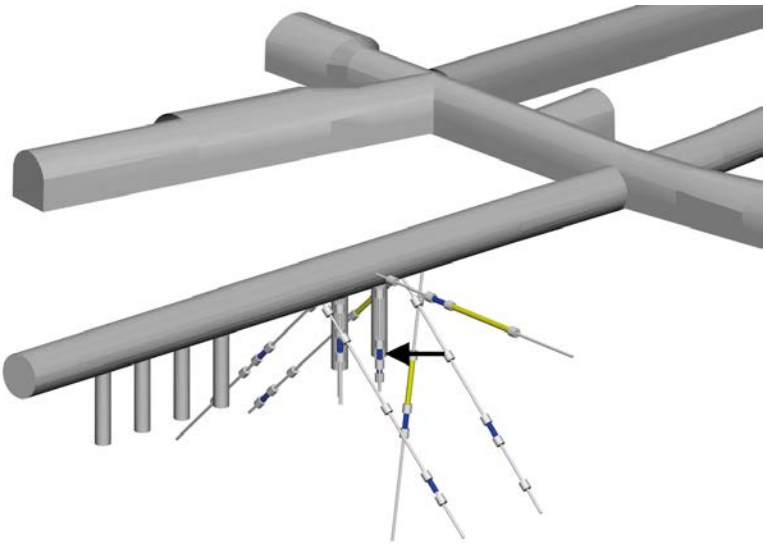

Figure 7-7. *Test section (KA3546G01:2) relative the prototype tunnel.*

7.2.7 KA3548A01

This borehole is 30.00 m long. The hydromechanical test section is between 8.80 m and 10.75 m.

Test section data

- Length of the hydromechanical measurement section (located above level of canister hole bottom):
  - Inner: 0.561 m.
  - Outer: 0.3235 m.
- Distances:
  - Spherical distance to centre of nearest heater: 14.0 m.
  - Spherical distance to centre of the bottom of nearest heater: 12.8 m.
  - Radial distance to centre line of nearest heater: 12.6 m.
- Number of fractures:
  - Inner: 2.
  - Outer: – .

(Figure 7-8).

7.2.8 KA3550G01

This borehole is 12.03 m long. The hydromechanical test section is between 5.20 m and 7.30 m.

Test section data

- Length of the hydromechanical measurement section (located above level of canister hole):
  - Inner: 0.711 m.
  - Outer: 0.3235 m.
- Distances:
  - (Spherical distance to centre of nearest heater: 2.2 m).
  - (Spherical distance to centre of the bottom of nearest heater: 2.5 m).
  - Radial distance to centre line of nearest heater: 1.1 m.
- Number of fractures:
  - Inner: 6.
  - Outer: – .

(Figure 7-9).

7.2.9 KA3552G01

This borehole is 12.00 m long. The hydromechanical test section is between 4.35 m and 6.05 m.

Test section data

- Length of the hydromechanical measurement section (located above level of canister hole):
  - Inner: 0.311 m.
  - Outer: 0.3235 m.
- Distances:
  - Spherical distance to centre of nearest heater: 1.5 m.
  - (Spherical distance to centre of the bottom of nearest heater: 3.5 m).
  - Radial distance to centre line of nearest heater: 1.2 m.
- Number of fractures:
  - Inner: – .
  - Outer: 2.

(Figure 7-10).

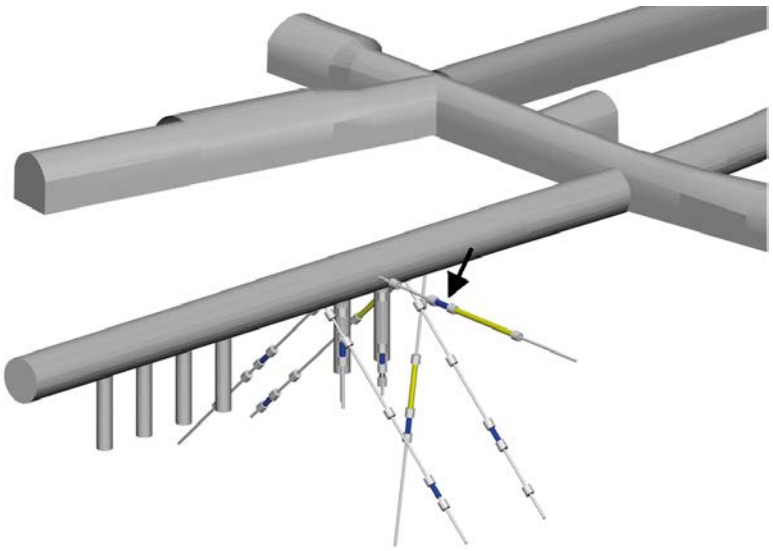

Figure 7-8. *Test section (KA3548A01:3) relative the prototype tunnel.*

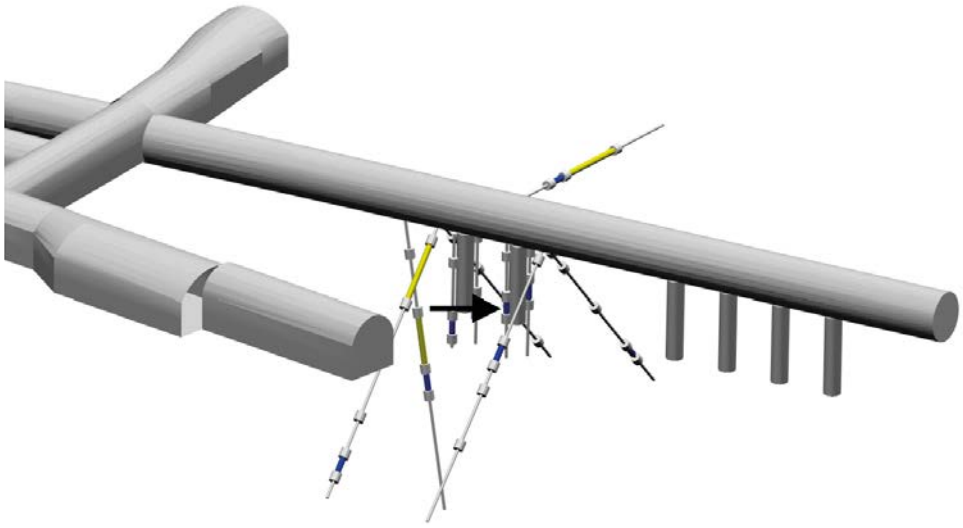

Figure 7-9. *Test section (KA3550G01:2) relative the prototype tunnel.*

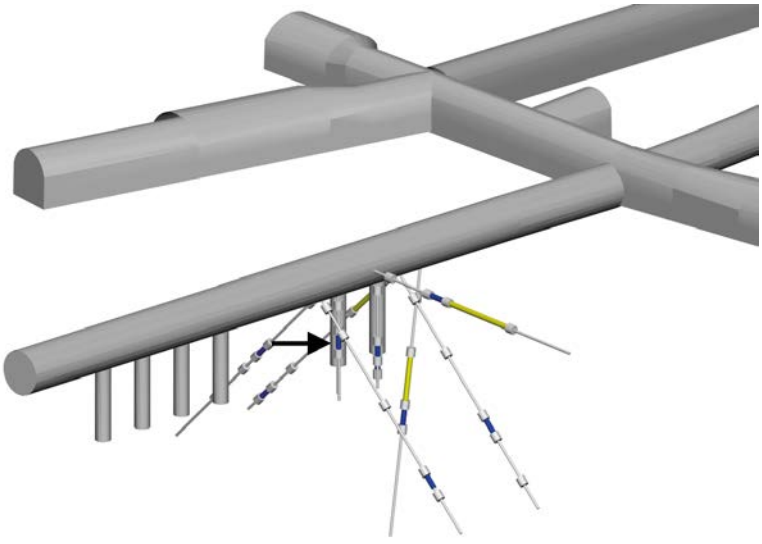

Figure 7-10. *Test section (KA3552G01:2) relative the prototype tunnel.*

7.2.10 KA3554G01

This borehole is 30.01 m long. The hydromechanical test section is between 22.60 m and 24.15 m.

Test section data

- Length of the hydromechanical measurement section (located below level of canister hole):
  - Inner: 0.371 m.
  - Outer: 0.3235 m.
- Distances:
  - Spherical distance to centre of nearest heater: 21.2 m.
  - Spherical distance to centre of the bottom of nearest heater: 19.1 m.
  - (Radial distance to centre line of nearest heater: 17.3 m).
- Number of fractures:
  - Inner: 2.
  - Outer: – .

(Figure 7-11).

7.2.11 KA3554G02

This borehole is 30.01 m long. The hydromechanical test section is between 10.50 m and 12.20 m.

Test section data

- Length of the hydromechanical measurement section (located above level of canister hole):
  - Inner: 0.311 m.
  - Outer: 0.3235 m.
- Distances:
  - Spherical distance to centre of nearest heater: 9.8 m.
  - Spherical distance to centre of the bottom of nearest heater: 9.1 m.
  - (Radial distance to centre line of nearest heater: 9.0 m).
- Number of fractures:

– Inner: – .
  - Outer: 1.

(Figure 7-12).

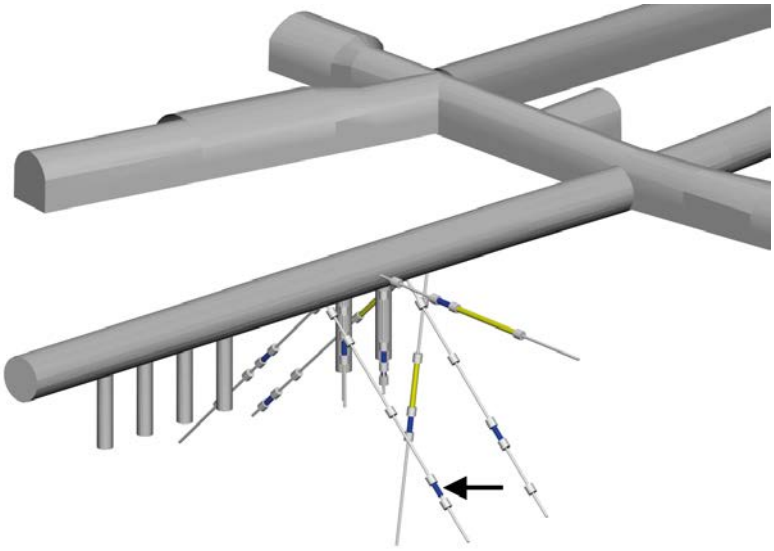

Figure 7-11. *Test section (KA3554G01:2) relative the prototype tunnel.*

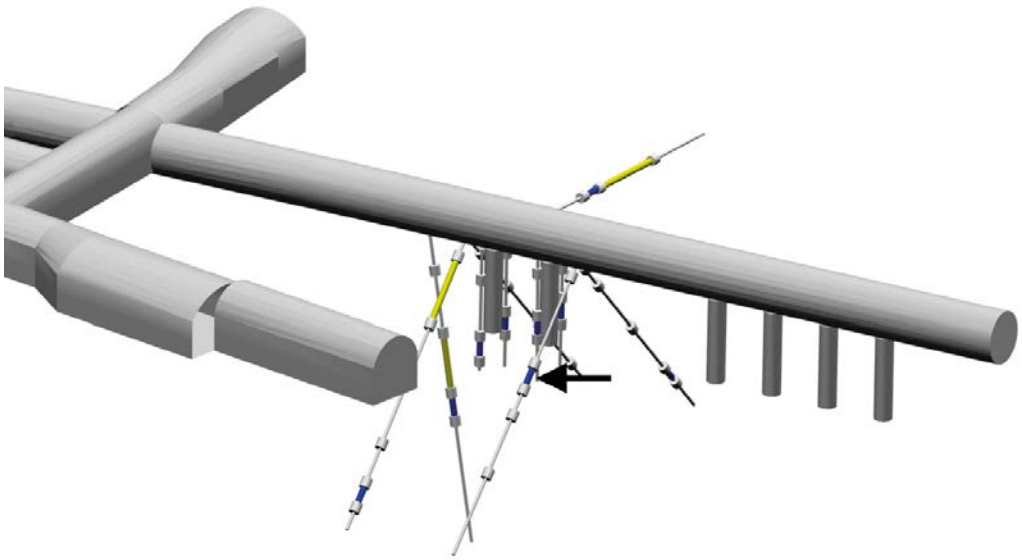

Figure 7-12. *Test section (KA3554G02:4) relative the prototype tunnel.*

7.3 Long term study

The expected behaviour of long term study is that:

- the intact rock expands during increase in temperature,
- the fracture is compressed during increase in temperature.

7.3.1 KG0010B01

Temperature

- The outer temperature sensor fails 2004-07-03 and after that date only the temperature from the inner sensor is used. It works again from December 2005.
- The temperature in KG0010B01 is affected by the air temperature in tunnel G.

(Figure 7-13, Figure 7-14).

Long-term deformation

- The deformation in KG0010B01 is a result of the change in air temperature. The rock both expands and shrinks.

(Figure 7-15).

7.3.2 KA3539G:2 (15.85–17.60 m)

Temperature

- Data between 2005-01-20 and 2005-01-24 is replaced by interpolated data.
- Data between 2005-02-01 and 2005-11-28 is replaced by interpolated data.

(Figure 7-16).

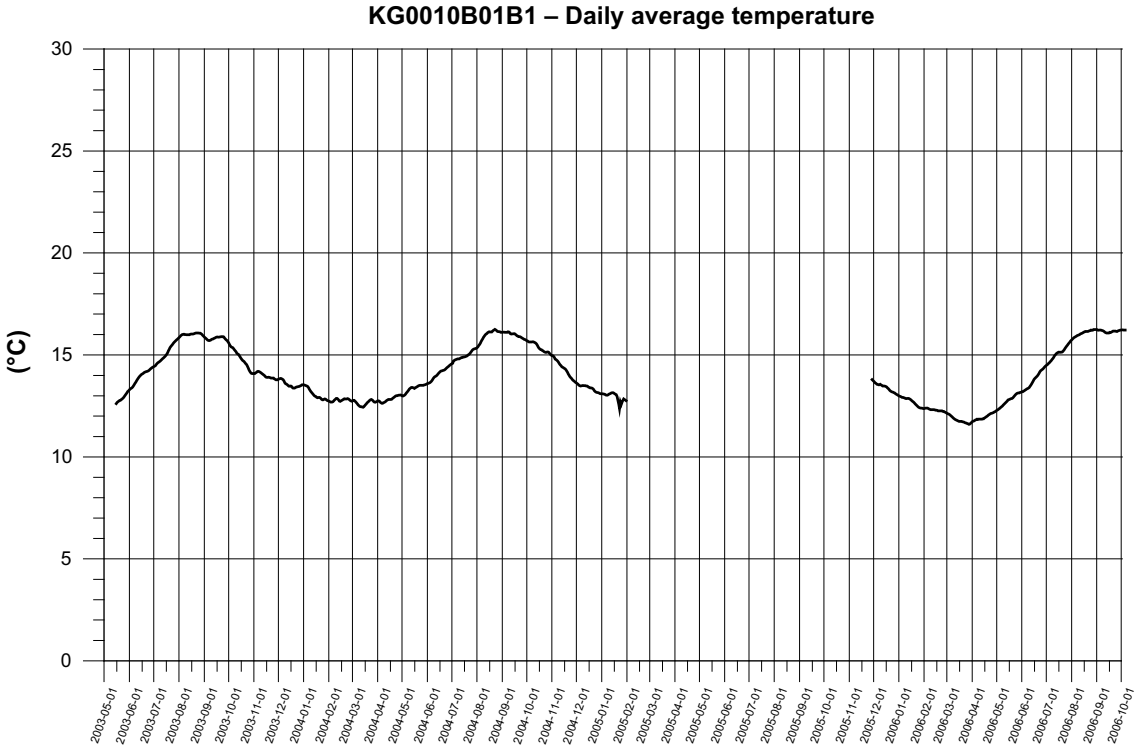

Figure 7-13. *Average temperature in KG0010B01.*

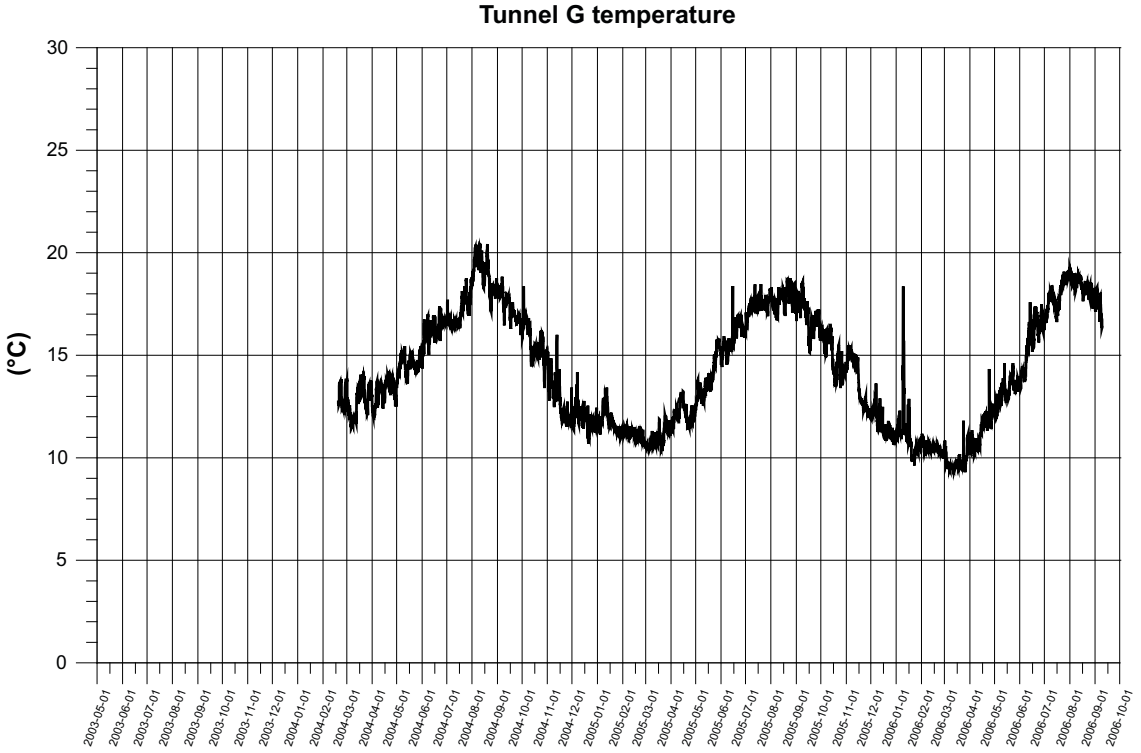

Figure 7-14. *Temperature in tunnel G (data is available from February 2004).*

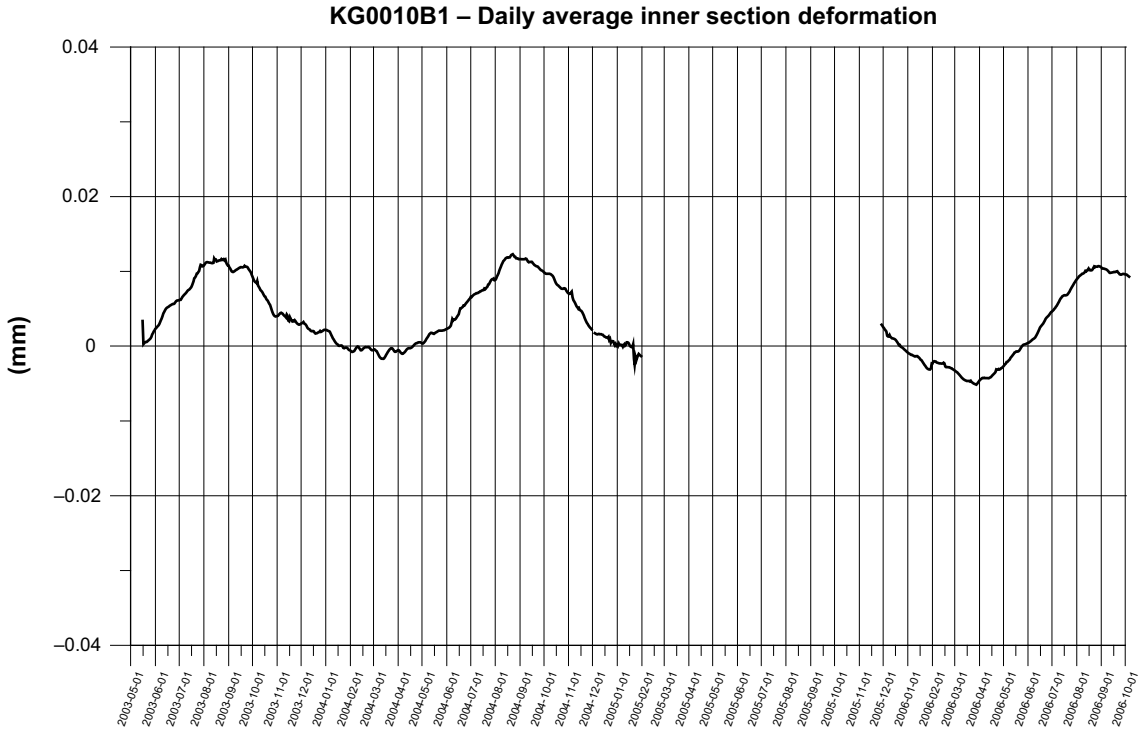

Figure 7-15. *Long-term deformation of the rock mass in KG0010B01.*

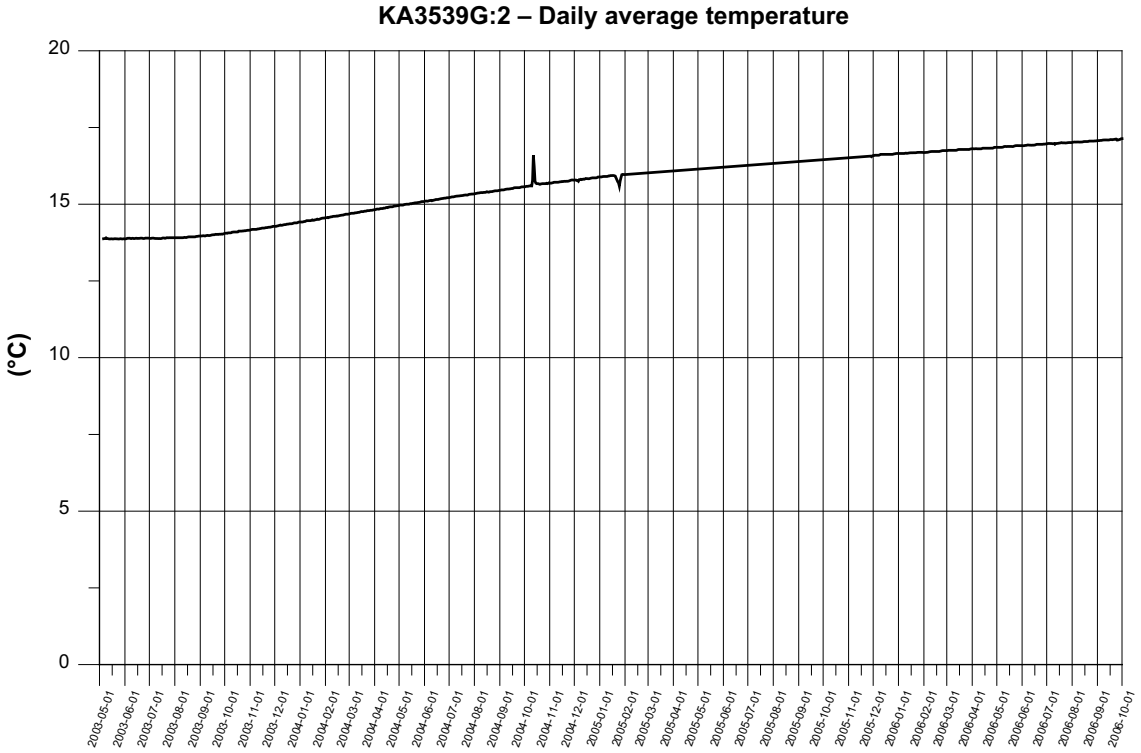

Figure 7-16. *KA3539G:2. Average temperature.*

Long-term deformation

- The analysis shows that the fracture expands, roughly 3.5 µm (until April 2004). This is contrary to the expected behaviour.
- The large fracture expansion cannot be explained by natural causes.
- The sensors fail in November 2004.

(Figure 7-17, Figure 7-18, Figure 7-19).

Transmissivity

The change of the transmissivity during the period is shown below (Forsmark and Rhén 2004a, b, c, 2005a, b, c, 2006, 2007a). (T-Moye: stationary assumption, T: evaluation based on transient data). Undisturbed pressure 2003-05 c. 2,400 kPa and 2006-10 c. 1,500 kPa, see Appendix 2.

- Chapter 7.5, Figure 7-104 indicates that log10 T may decrease up to c. 0.05 for a pressure drop of c. 1,000 kPa. The figure above includes effect from stress changes due to temperature and effective stress changes due to water pressure changes in the fracture and the effect of the temperature seem to dominate in this case. Both T and T_Moye decreases when the temperature increases.
- An earlier packer test for section 15–18 m gives $T = 2.5 \cdot 10^{-6}$ m^2/s (in log10 format: –5.60) (Rhén and Forsmark 2001).

(Figure 7-20, Figure 7-21).

7.3.3 KA3542G01:3 (18.60–20.30 m)

Temperature

- Data between 2005-01-20 and 2005-01-24 is replaced by interpolated data.
- Data between 2005-02-01 and 2005-11-28 is replaced by interpolated data.

(Figure 7-22).

Long-term deformation

- The long-term deformation shows that the fracture has been compressed after 16 months when the sensor fails.
- The large compression of the fracture at the beginning of November 2003 is due to the release of hydrostatic pressure when the packer fails.

(Figure 7-23, Figure 7-24, Figure 7-25).

Transmissivit

The change of the transmissivity during the period is shown below (Forsmark and Rhén 2004a, b, c, 2005a, b, c, Forsmark 2006, 2007a). (T-Moye: stationary assumption, T: evaluation based on transient data). Undisturbed pressure 2003-05 c. 3,500 kPa and 2006-10 c. 2,500 kPa, see Appendix 2.

- T_Moye and possibly T decreases when the temperature increases. However, Chapter 7.5, Figure 7-104 indicates that log10 T may decrease up to c. 0.05 for a pressure drop of c. 1,000 kPa and it is possible that the pressure decrease also influence the possible transmissivity change.
- An earlier packer test for section 18–21 m gives $T = 3.0 \cdot 10^{-7}$ m^2/s (in log10 format: –6.52) (Rhén and Forsmark 2001).

(Figure 7-26, Figure 7-27).

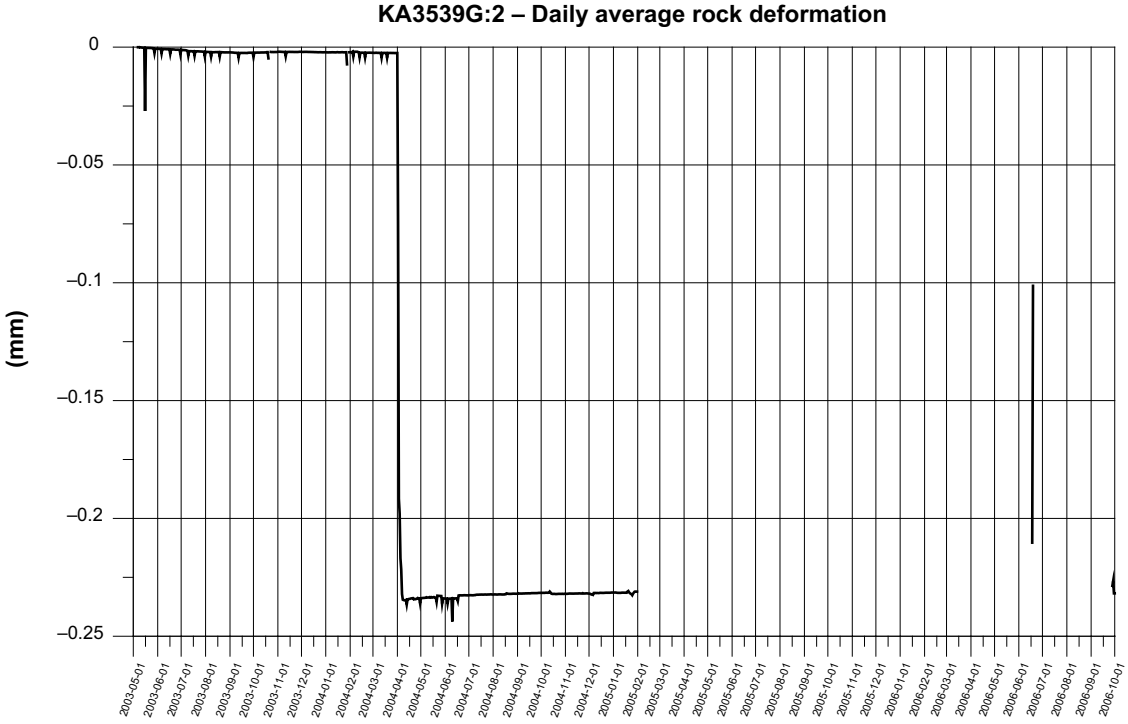

Figure 7-17. *KA3539G:2. Rock deformation – intact rock section.*

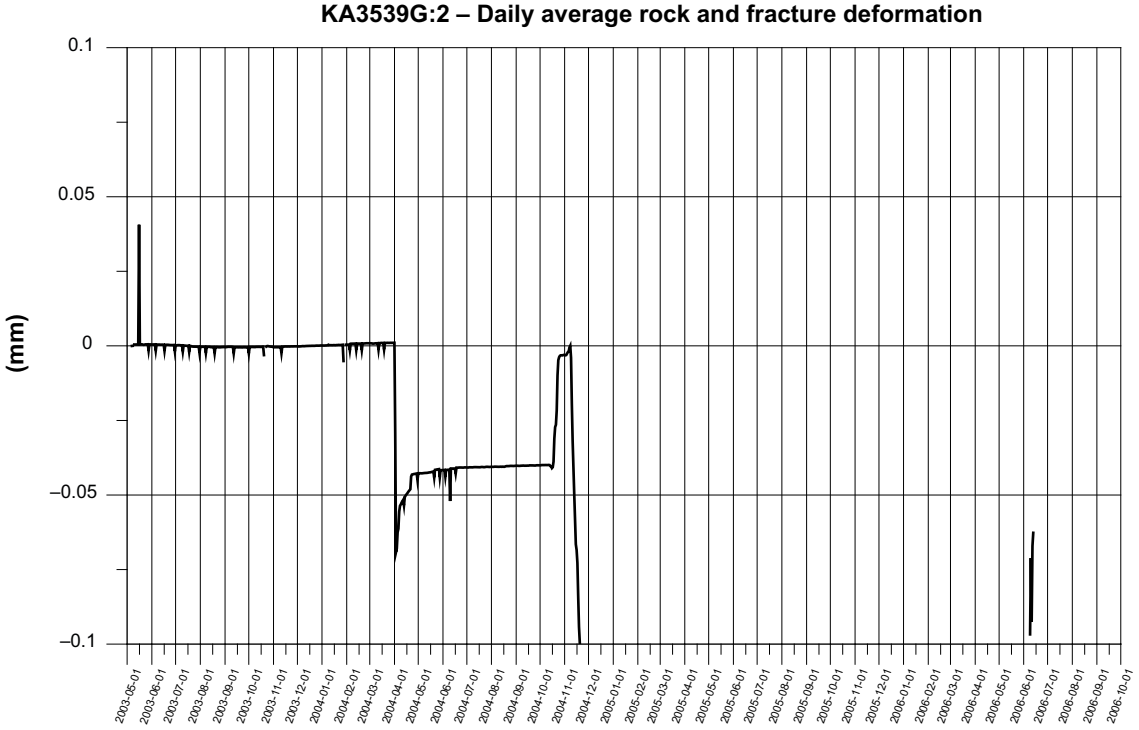

Figure 7-18. *KA3539G:2. Rock and fracture deformation.*

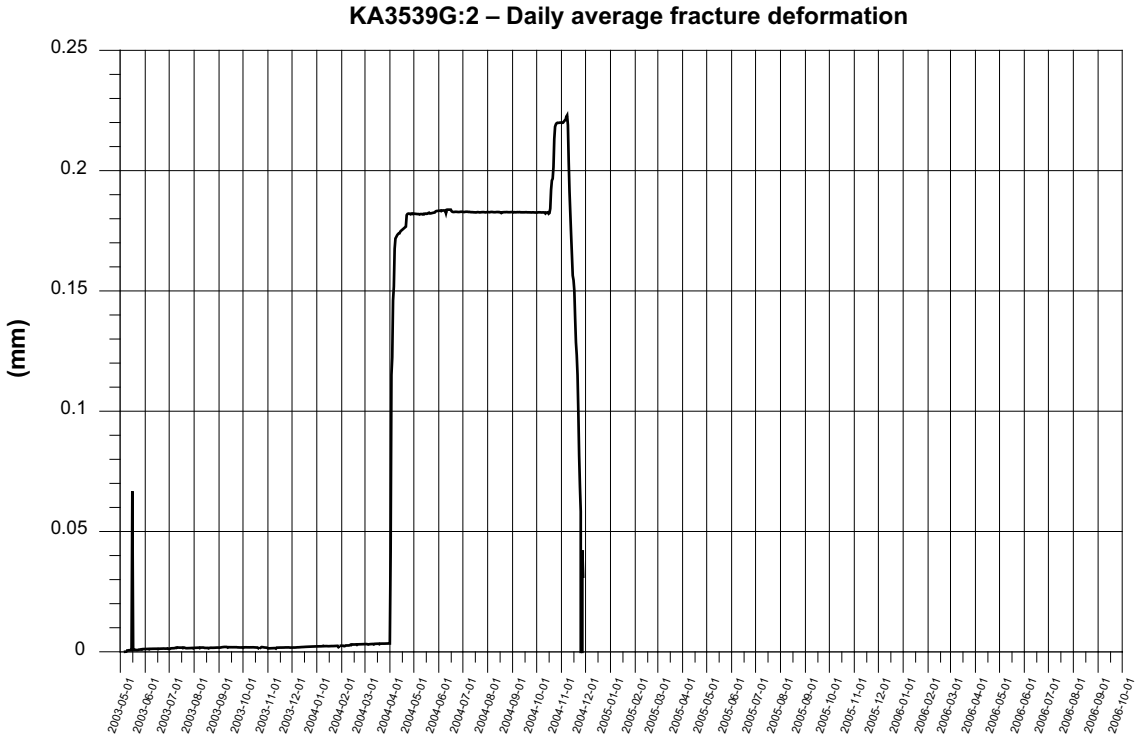

Figure 7-19. *KA3539G:2. Single fracture deformation.*

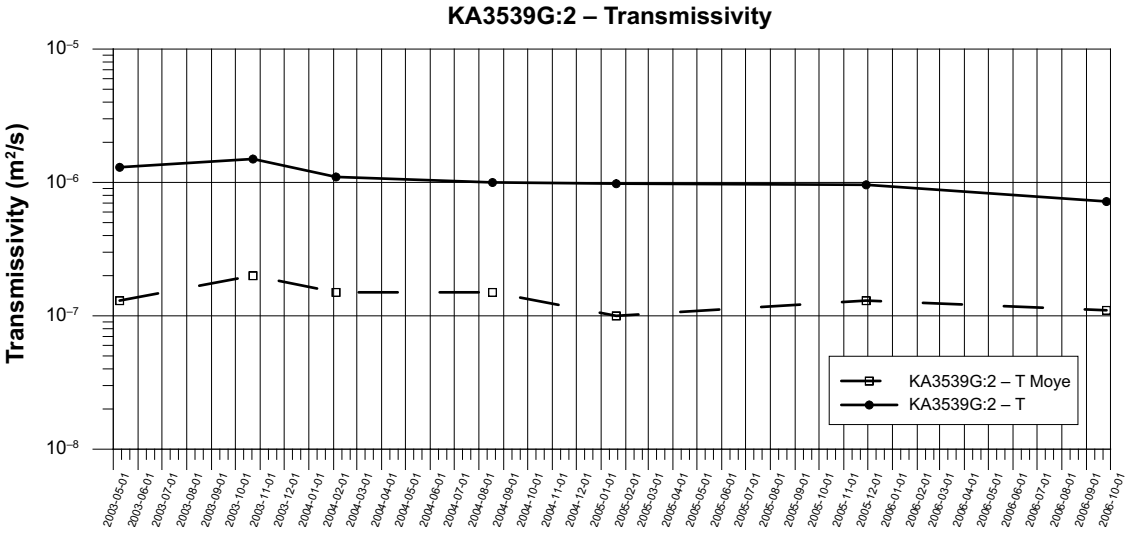

Figure 7-20. *Transmissivity change during the period 2003-05-01 to 2006-10-01.*

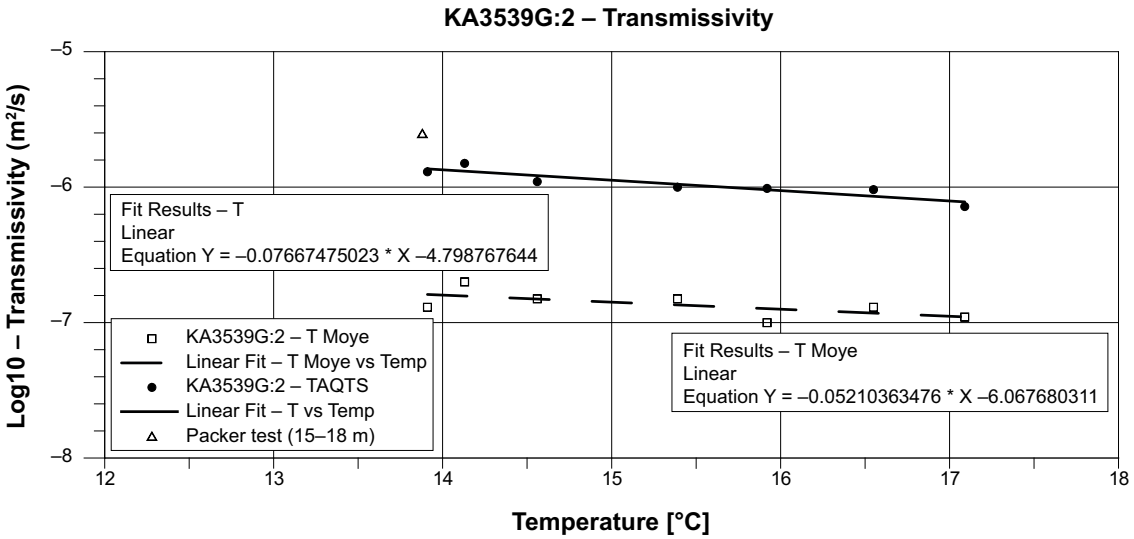

Figure 7-21. *Transmissivity versus temperature in KA3539G:2 (15.85–17.60 m).*

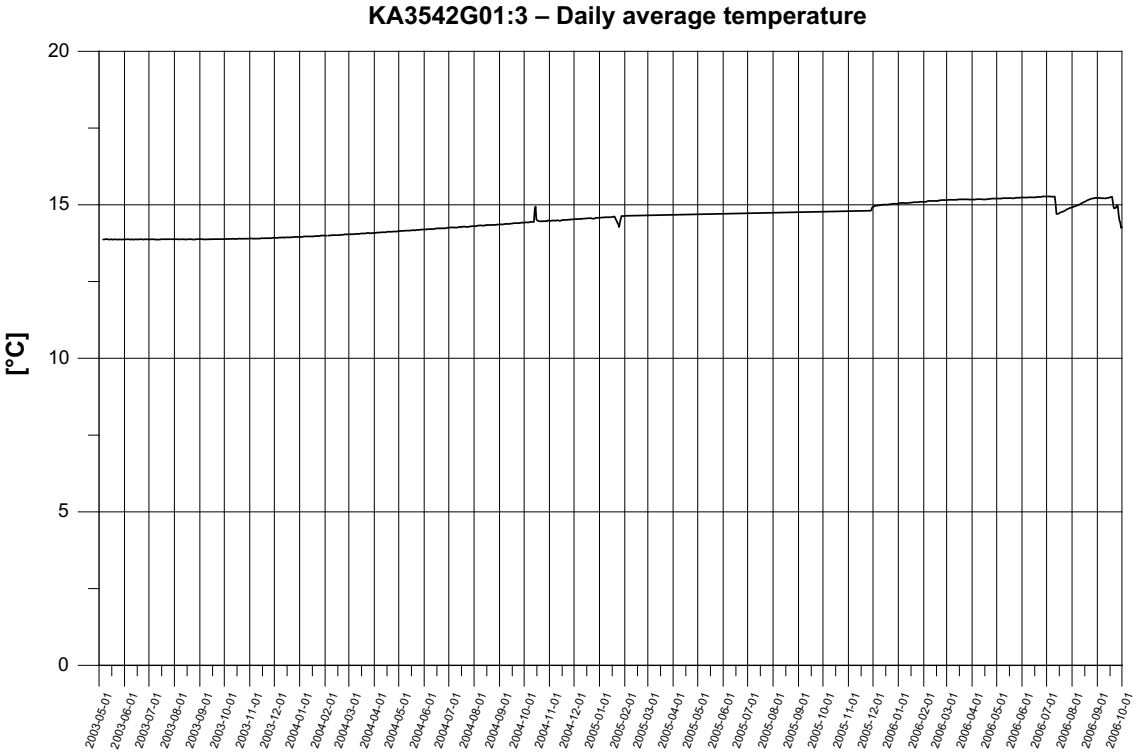

Figure 7-22. *KA3542G01:3. Average temperature.*

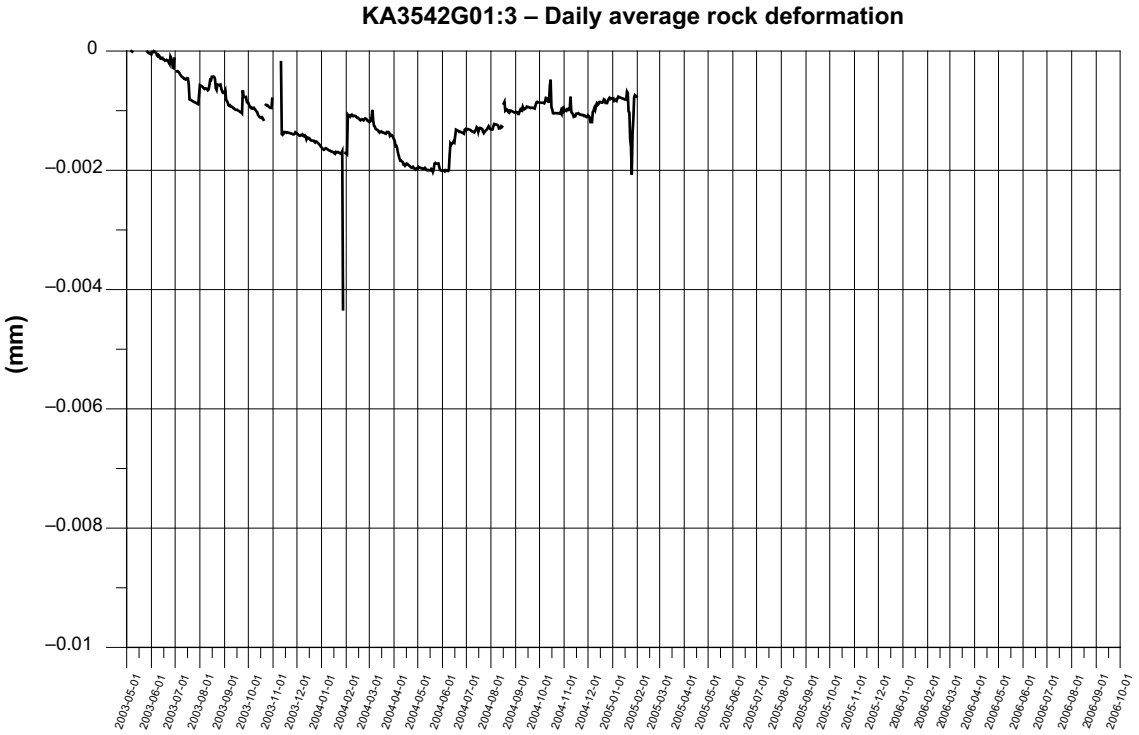

Figure 7-23. *KA3542G01:3. Rock deformation – intact rock section.*

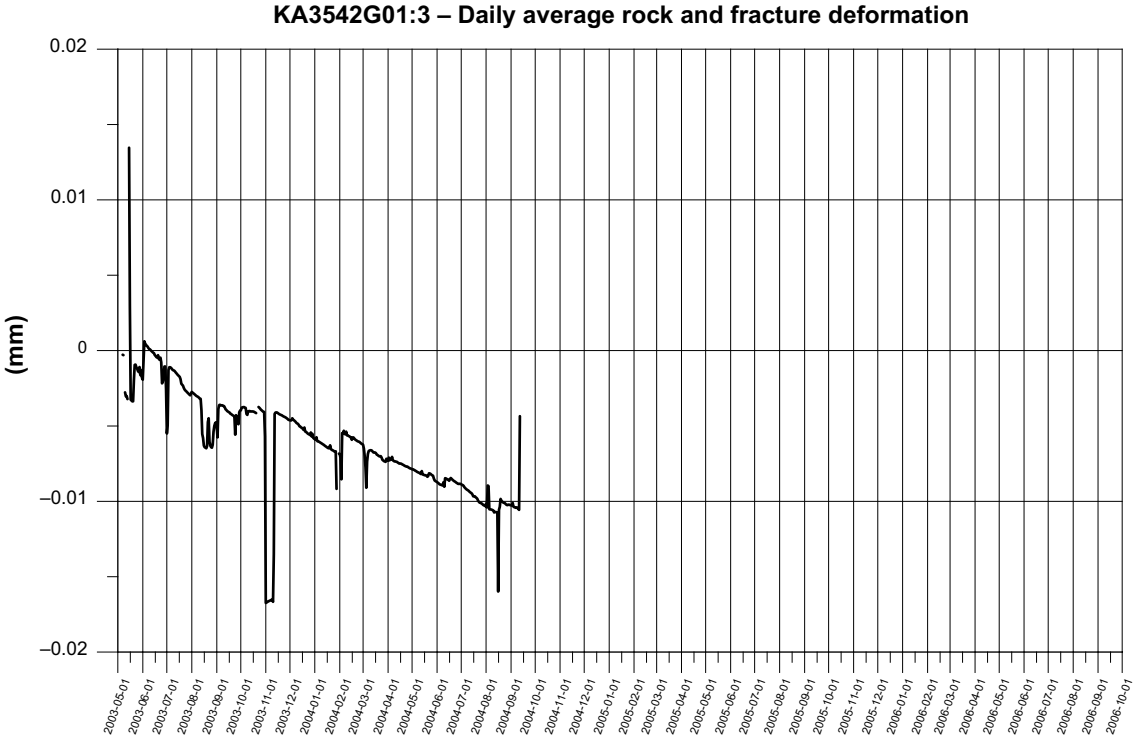

Figure 7-24. *KA3542G01:3. Rock and fracture deformation.*

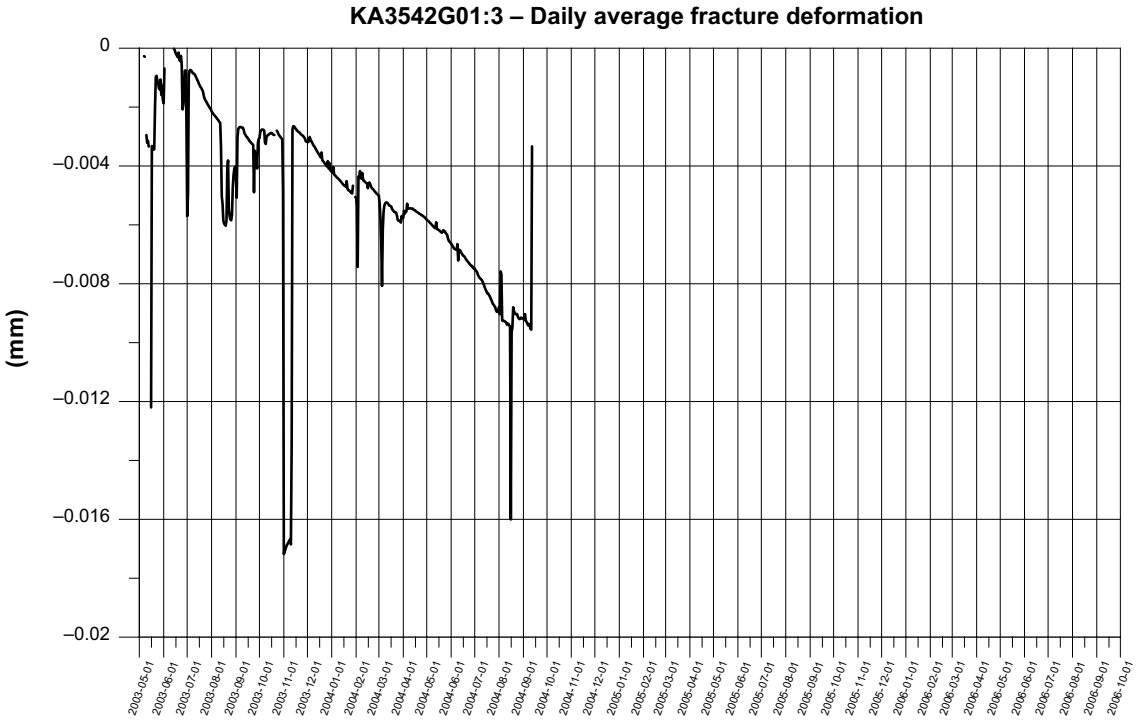

Figure 7-25. *KA3542G01:3. Single fracture deformation.*

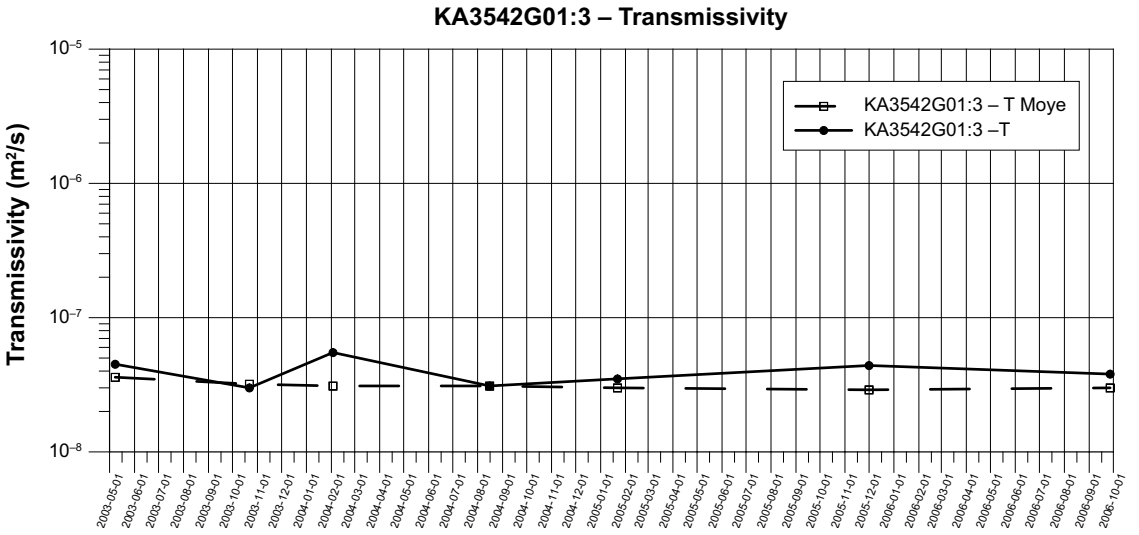

Figure 7-26. *Transmissivity change during the period 2003-05-01 to 2006-10-01.*

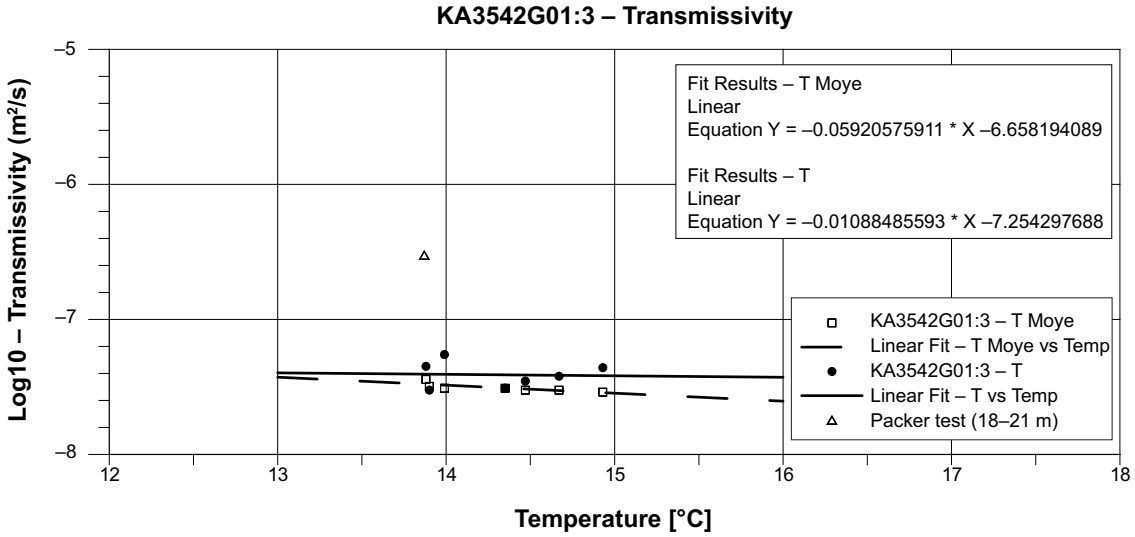

Figure 7-27. *Transmissivity versus temperature in KA3542G01:3 (18.60–20.30 m).*

7.3.4 KA3542G02:2 (25.6–27.2 m)

Temperature

- Data between 2005-01-20 and 2005-01-24 is replaced by interpolated data.
- Data between 2005-02-01 and 2005-11-28 is replaced by interpolated data.

(Figure 7-28).

Long-term deformation

- The data are good until the packer deflation and inflation around November 2003 when the hydraulic packers were deflated by accident. The sensors have a permanent displacement after the packers were re-inflated.
- The initial deformation is relatively small and that is in accordance with the small temperature increase. There may be a slip of the measurement equipment or by a fracture itself. There is an increase of the transmissivity after the "slip" at the end of October 2003.

(Figure 7-29, Figure 7-30, Figure 7-31).

Transmissivity

The change of the transmissivity during the period is shown below (Forsmark and Rhén 2004a, b, c, 2005a, b, c, Forsmark 2006, 2007a). (T-Moye: stationary assumption, T: evaluation based on transient data). Undisturbed pressure 2003-05 c. 2,500 kPa and 2006-10 c. 1,900 kPa, see Appendix 2.

- The increase of transmissivity due to temperature is probably not relevant. Possibly there is a slip in the fracture causing an increased transmissivity after November 2003.
- T_Moye increases when the temperature increases. This is contrary to what is expected. The temperature interval is however very narrow, only approximately 0.5°C. The transient transmissivity decreases however. If the first two points in time are discarded assuming a transmissivity before a slip of the fracture, T is clearly decreasing and T-Moye is slightly decreasing. However, Chapter 7.5, Figure 7-104 indicates that log10 T may decrease up to c. 0.05 for a pressure drop of c. 1,000 kPa and it is possible that the pressure decrease also influence the possible transmissivity change even though the tranmissivity change seem to be larger that can be expected just from the pressure changes.

- The “sudden” change in transmissivity between second and third test campaigns may be due to a fracture slip, see Figure 7-31.
- An earlier packer test for section 24–27 m gives $T = 9.4 \cdot 10^{-9}$ m^2/s (in log10 format: –8.03) (Rhén and Forsmark 2001).

(Figure 7-32, Figure 7-33).

7.3.5 KA3544G01:2 (8.90–12.65 m)

Temperature

- Data between 2005-01-20 and 2005-01-24 is replaced by interpolated data.
- Data between 2005-02-01 and 2005-11-28 is replaced by data calculated as the temperature data in TR6014 (Ghoudarzi and Johannesson 2006) (which is a temperature sensor in a hole drilled from inside the deposition hole DA3545G01 located 1.9 m from the HM section in KA3544G01) minus 3.7 degrees which was the temperature difference 2005-02-01.

(Figure 7-34).

Long-term deformation

- The data is not good enough to evaluate due to deflated hydraulic packers in the beginning of November 2003, which have not been possible to re-inflate since then.
- Until November 2003 the rock is expanding. The magnitude however is rather large.
- The sensor failed in mid-August 2003.

(Figure 7-35, Figure 7-36).

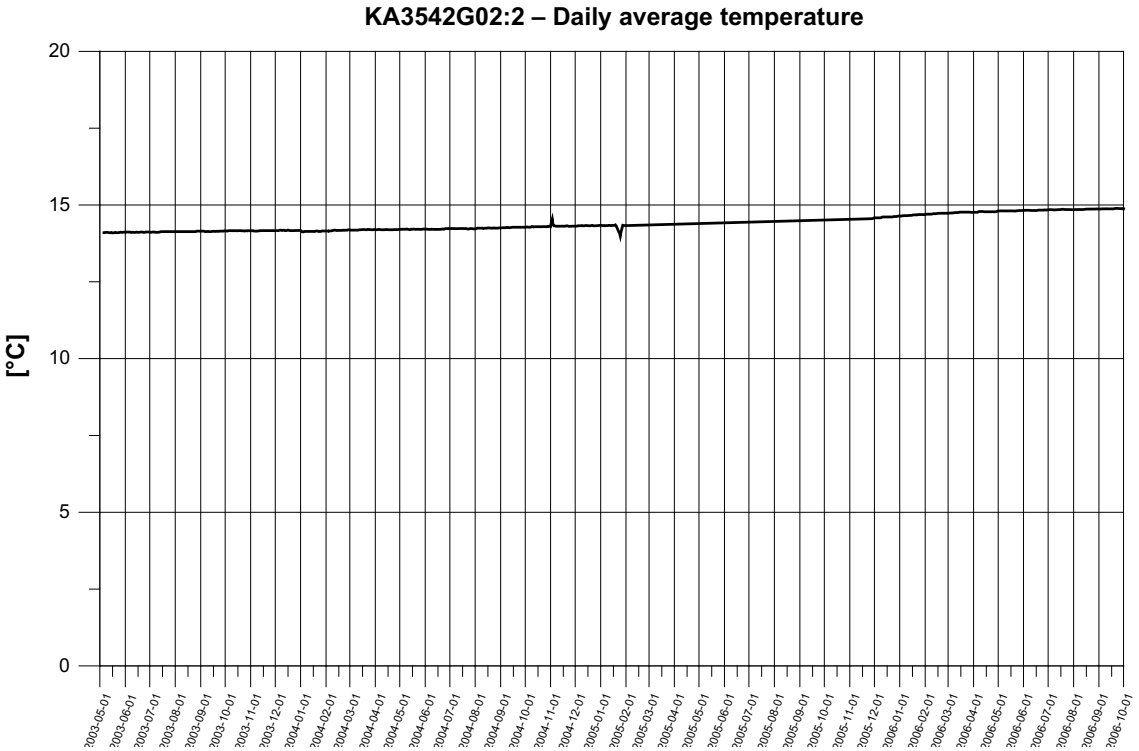

Figure 7-28. *KA3542G02:2. Average temperature.*

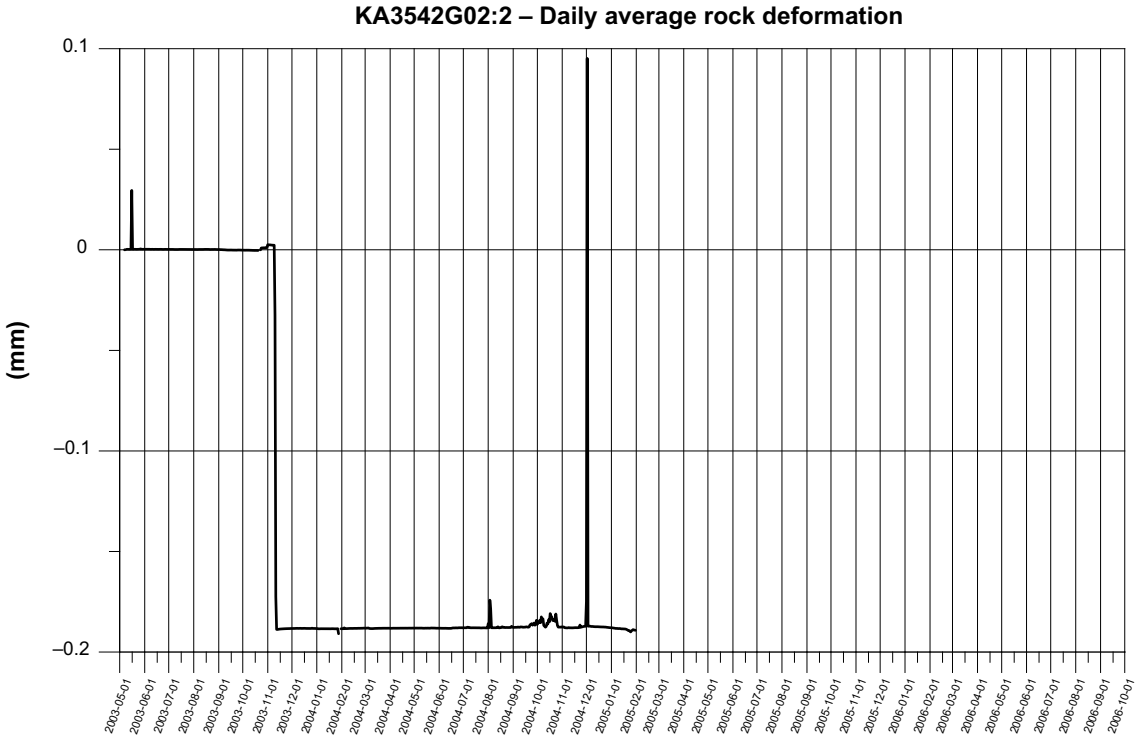

Figure 7-29. *KA3542G02:2. Rock deformation – intact rock section.*

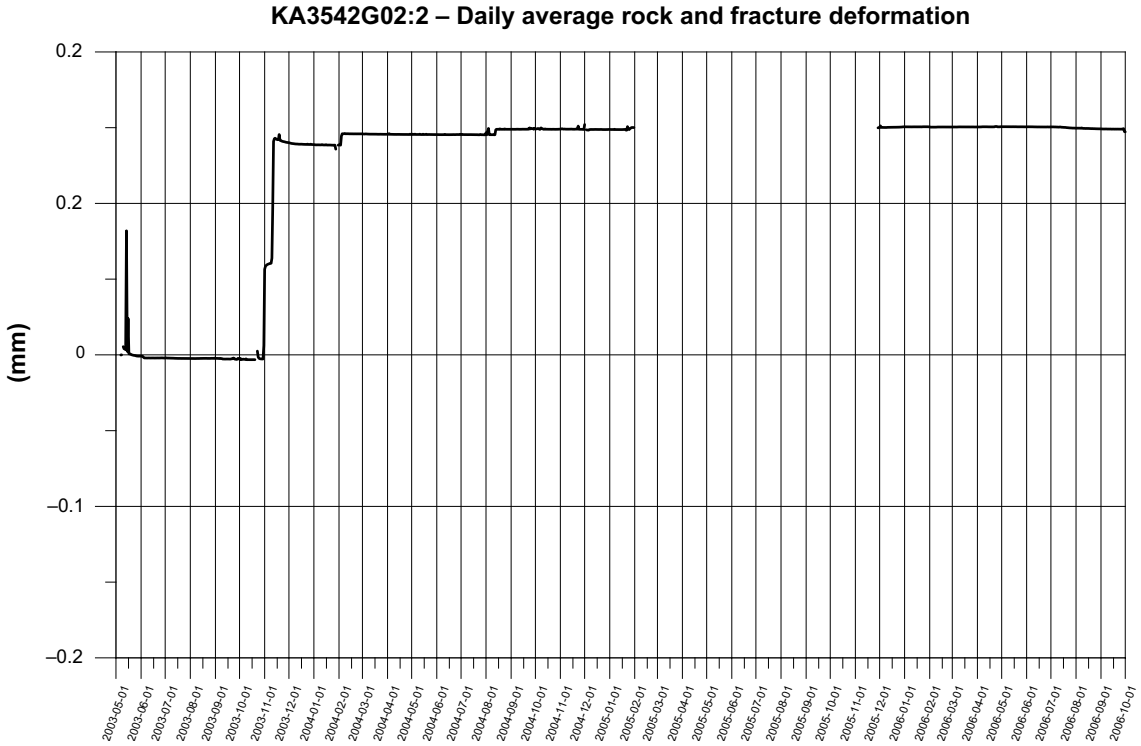

Figure 7-30. *KA3542G02:2. Rock and fracture deformation.*

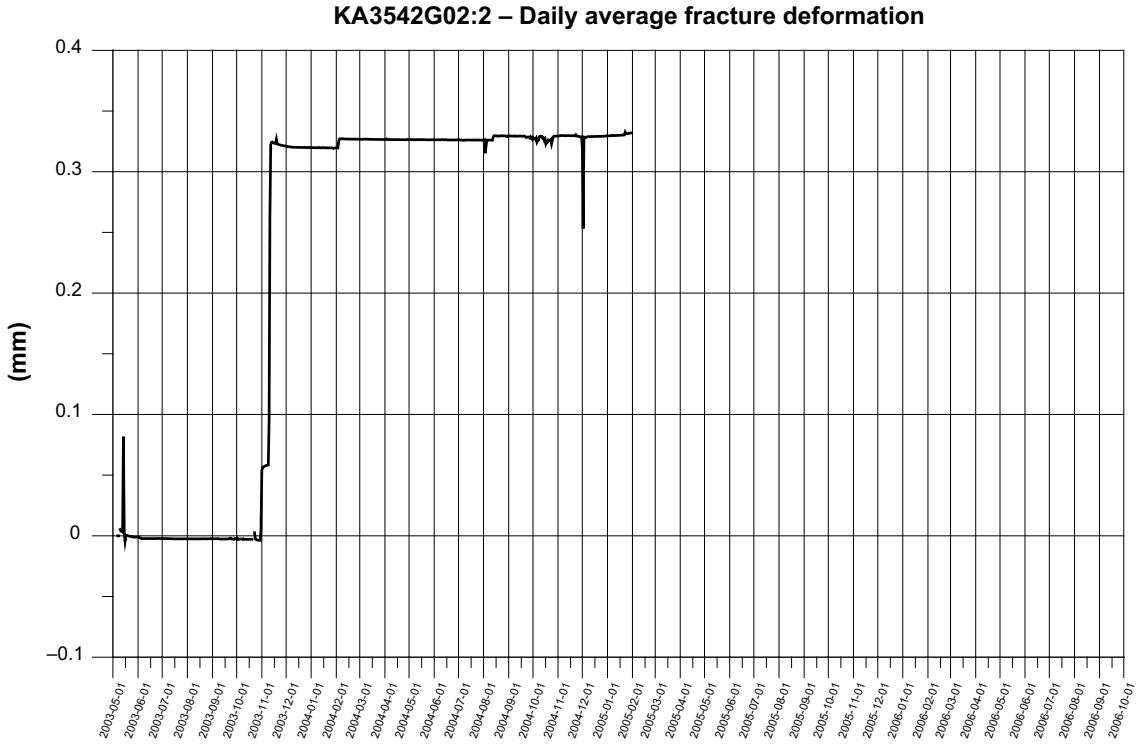

Figure 7-31. *KA3542G02:2. Single fracture deformation.*

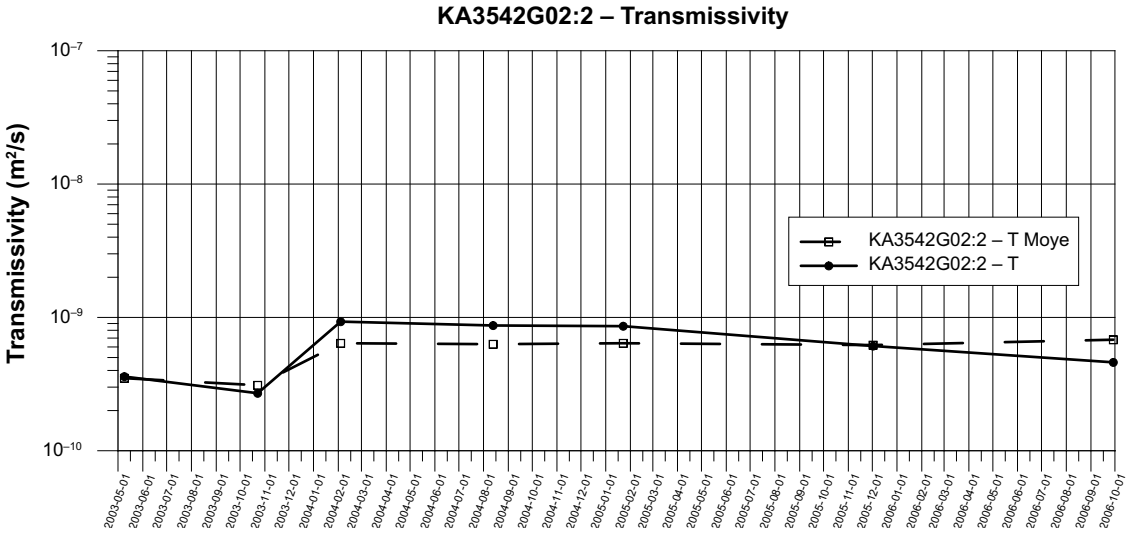

Figure 7-32. *Transmissivity change during the period 2003-05-01 to 2006-10-01.*

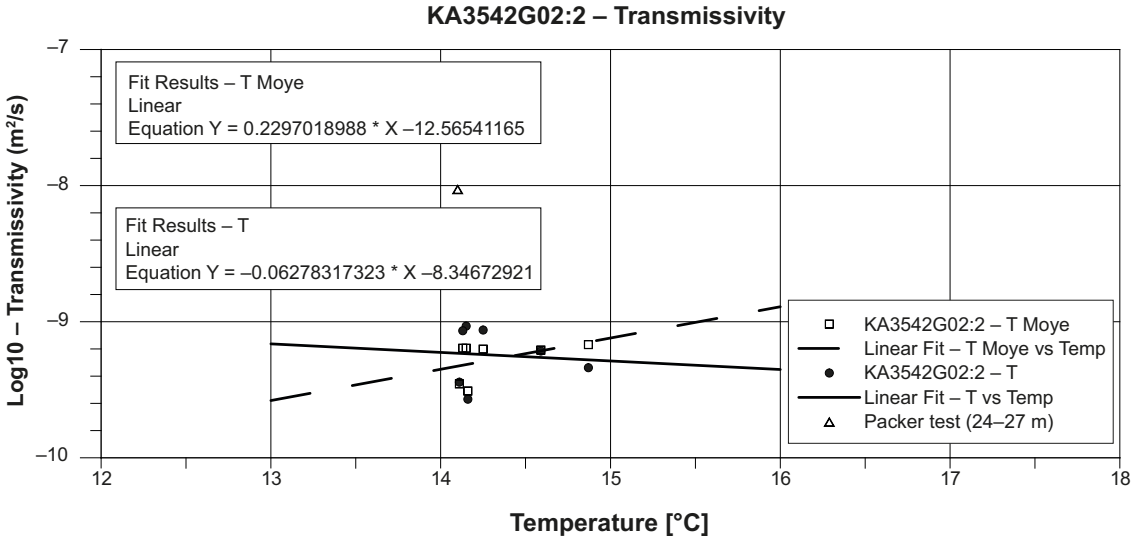

Figure 7-33. *Transmissivity versus temperature in KA3542G02:2 (25.60–27.20 m).*

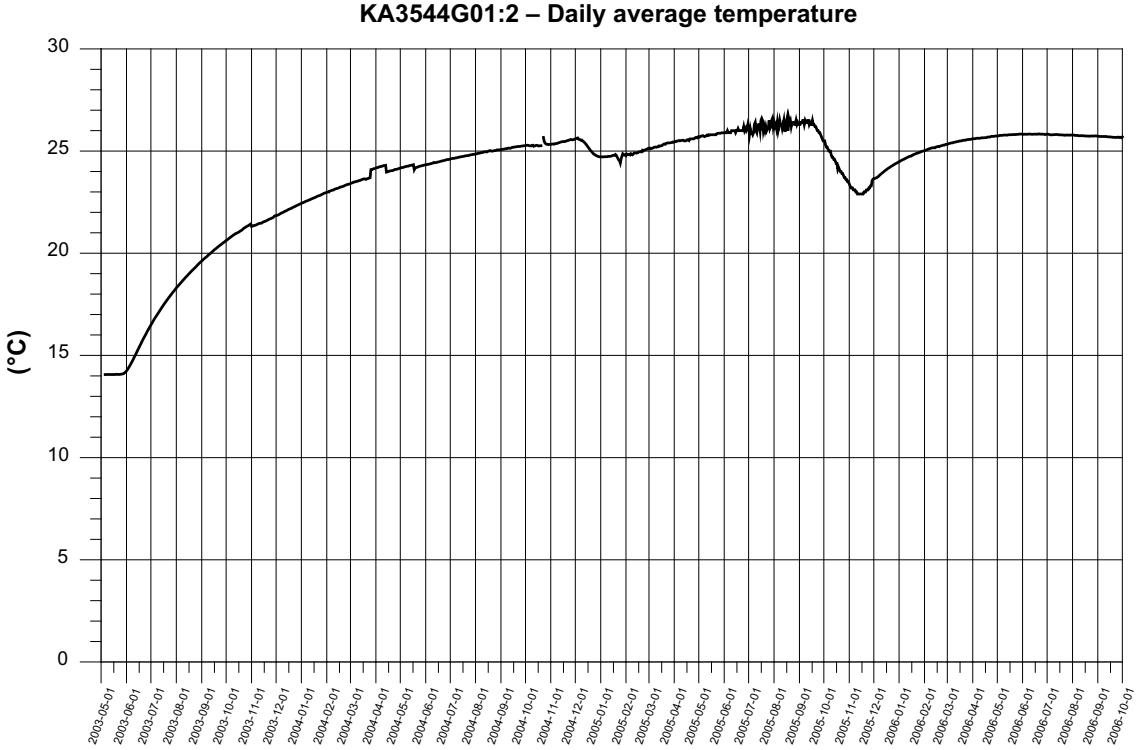

Figure 7-34. *KA3544G01:2. Average temperature.*

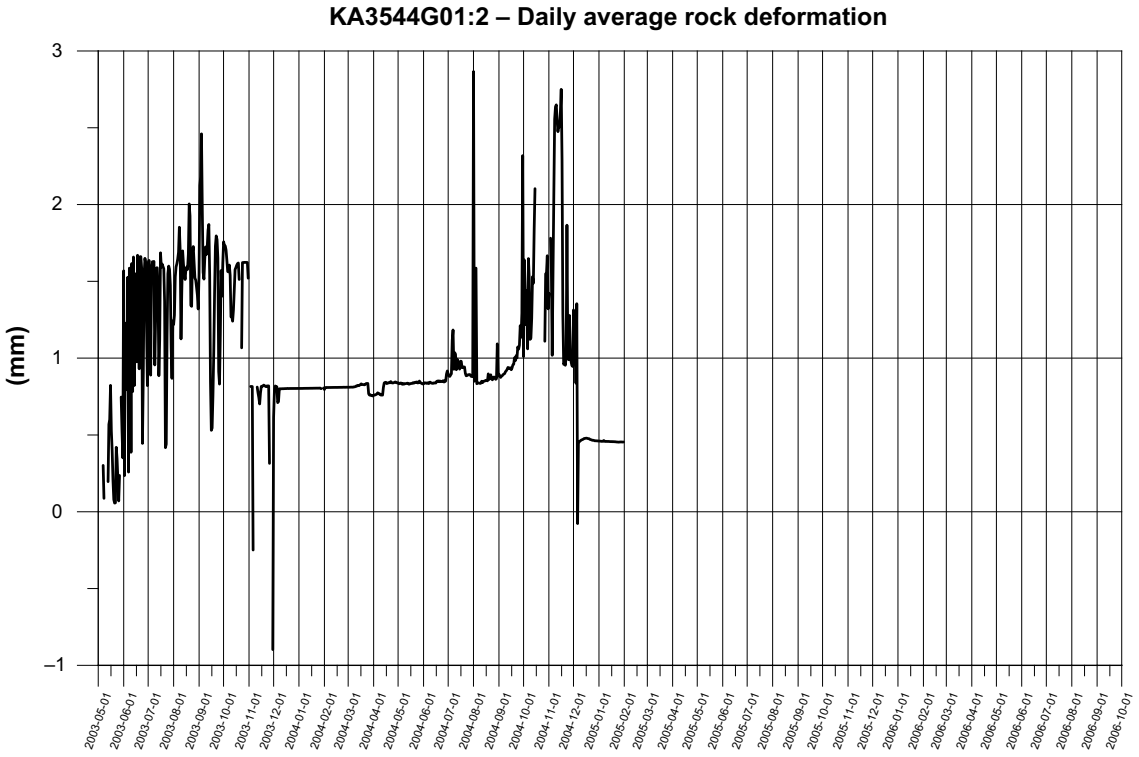

Figure 7-35. *KA3544G01:2. Rock deformation – intact rock section.*

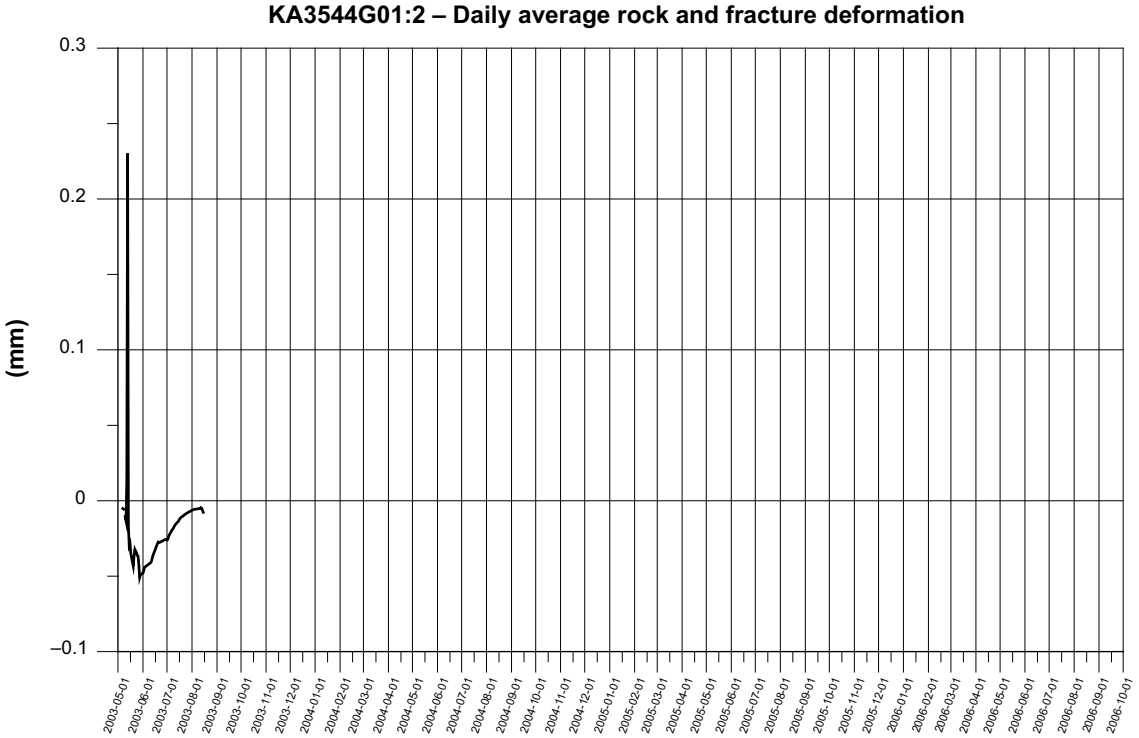

Figure 7-36. *KA3544G01:2. Rock and fracture deformation.*

Transmissivity

The change of the transmissivity during the period is shown below (Forsmark and Rhén 2004a, b, c, 2005a, b, c, Forsmark 2006, 2007a). Unfortunately only two tests were made before packer failure. (T-Moye: stationary assumption, T: evaluation based on transient data). Undisturbed pressure 2003-05 c. 2,000 kPa and 2006-10 c. 600 kPa, see Appendix 2.

- The decreasing trend is apparent. However, Chapter 7.5, Figure 7-104 indicates that log10 T may decrease up to c. 0.05 for a pressure drop of c. 1,000 kPa and it is possible that the pressure decrease also influence the possible transmissivity change.
- An earlier packer test for section 9.7–10.7 m gives T = $1.3 \cdot 10^{-8}$ m^2/s (in log10 format: –7.89) (Rhén and Forsmark 2001).

(Figure 7-37, Figure 7-38).

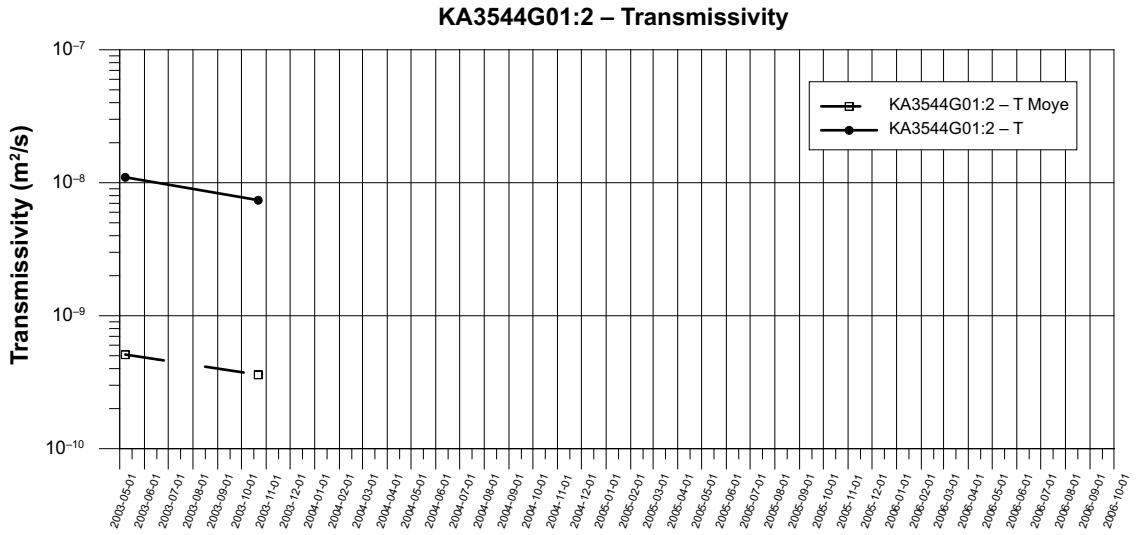

Figure 7-37. *Transmissivity change during the period 2003-05-01 to 2006-10-01.*

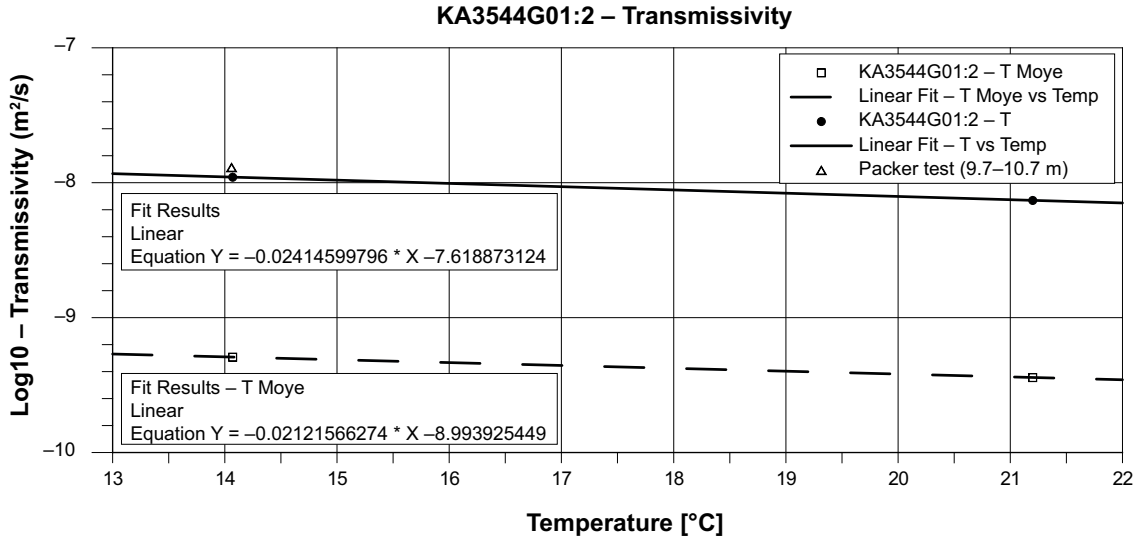

Figure 7-38. *Transmissivity versus temperature in KA3544G01:2 (8.90–10.65 m).*

7.3.6 KA3546G01:2 (6.75–8.30 m)

Temperature

- The zero value from May (2003) and the 20°C decrease between 2003-05-23 and 2003-06-17 have been removed. Thereafter the average value of the two thermistors is used.
- Data after 2004-05-22 is considered as non-realistic when compared to another temperature data is the close vicinity of the deposition hole.
- Data between 2004-05-22 and 2004-12-29 is replaced by data calculated as the temperature data in TR6012 (Ghoudarzi and Johannesson 2006) (which is a temperature sensor in a hole drilled from inside the deposition hole DA3545G01 located 1.8 m from the HM section in KA3546G01) plus 1.6 degrees which was the temperature difference 2004-05-22.

(Figure 7-39).

Long-term deformation

- The rock expands until the sensor fails in mid-december 2003.
- The reason for the large fracture expansion during the autumn 2003 is unknown.

(Figure 7-40, Figure 7-41, Figure 7-42).

Transmissivity

The change of the transmissivity during the period is shown below (Forsmark and Rhén 2004a, b, c, 2005a, b, c, Forsmark 2006, 2007a). (T-Moye: stationary assumption, T: evaluation based on transient data). Undisturbed pressure 2003-05 c. 0 kPa and 2006-10 c. 700 kPa, see Appendix 2.

- T_Moye and T decrease when the temperature increases for the three last tests in the figure above. Chapter 7.5, Figure 7-104 indicates that log10 T may decrease up to c. 0.05 for a pressure drop of c. 1,000 kPa and as the water pressure increase one can assume that the T decrease is due to the temperature increase.
- Possibly van the increased transmissivity at an early stage indicate a fracture slip?
- An earlier packer test for section 6.7–7.7 m gives $T = 3.9 \cdot 10^{-11}$ m^2/s (in log10 format: –10.41) (Forsmark and Rhén 2001).
- An earlier packer test for section 7.7–8.7 m gives $T = 1.7 \cdot 10^{-9}$ m^2/s (in log10 format: –8.77) (Rhén and Forsmark 2001).

(Figure 7-43, Figure 7-44).

7.3.7 KA3548A01:3 (8.80–10.75 m)

Temperature

- The outer thermistor is out of order so data from the inner thermistor is presented.
- Data between 2005-01-20 and 2005-01-24 is replaced by interpolated data.
- Data between 2005-02-01 and 2005-11-28 is replaced by interpolated data.

(Figure 7-45).

Long-term deformation

The intact rock sensor has failed as well. Therefor no fracture deformation can be presented.

(Figure 7-46).

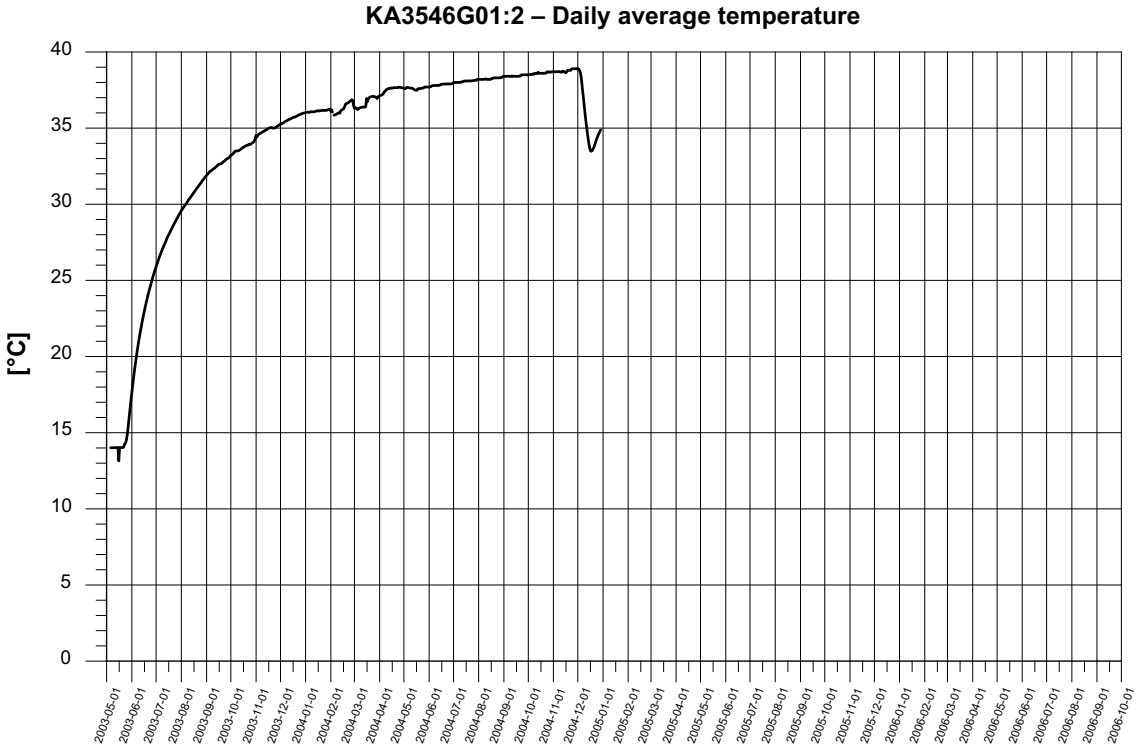

Figure 7-39. *KA3546G01:2. Average temperature.*

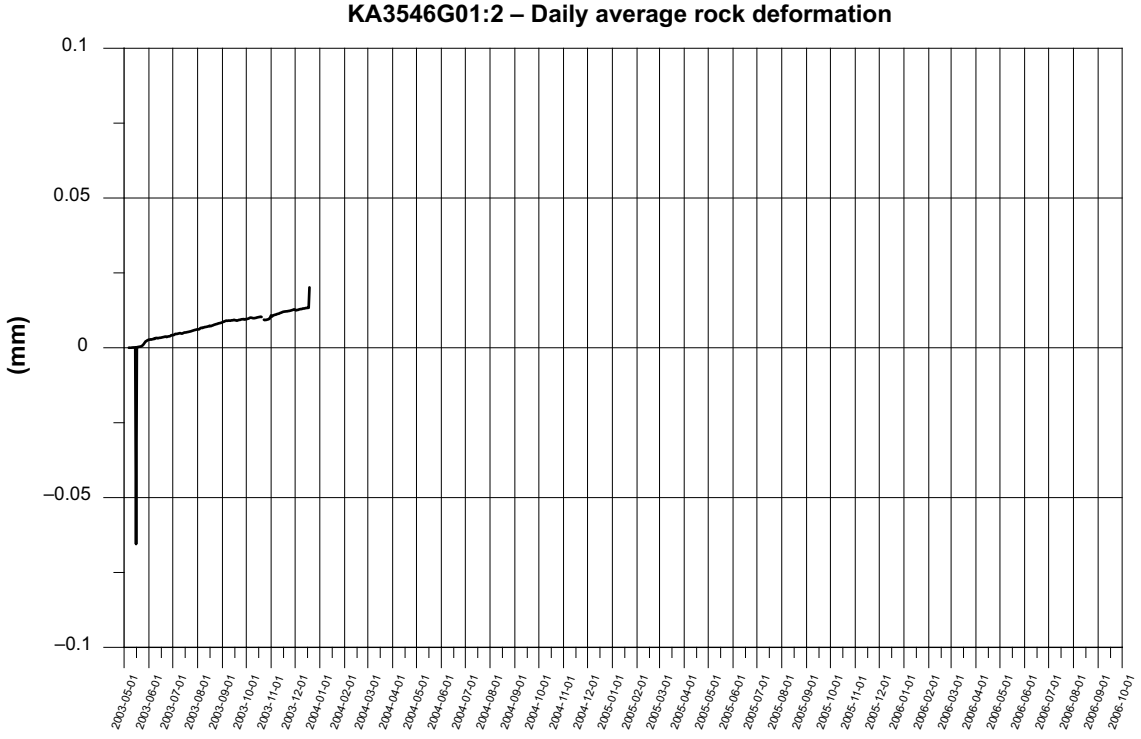

Figure 7-40. *KA3546G01:2. Rock deformation – intact rock section.*

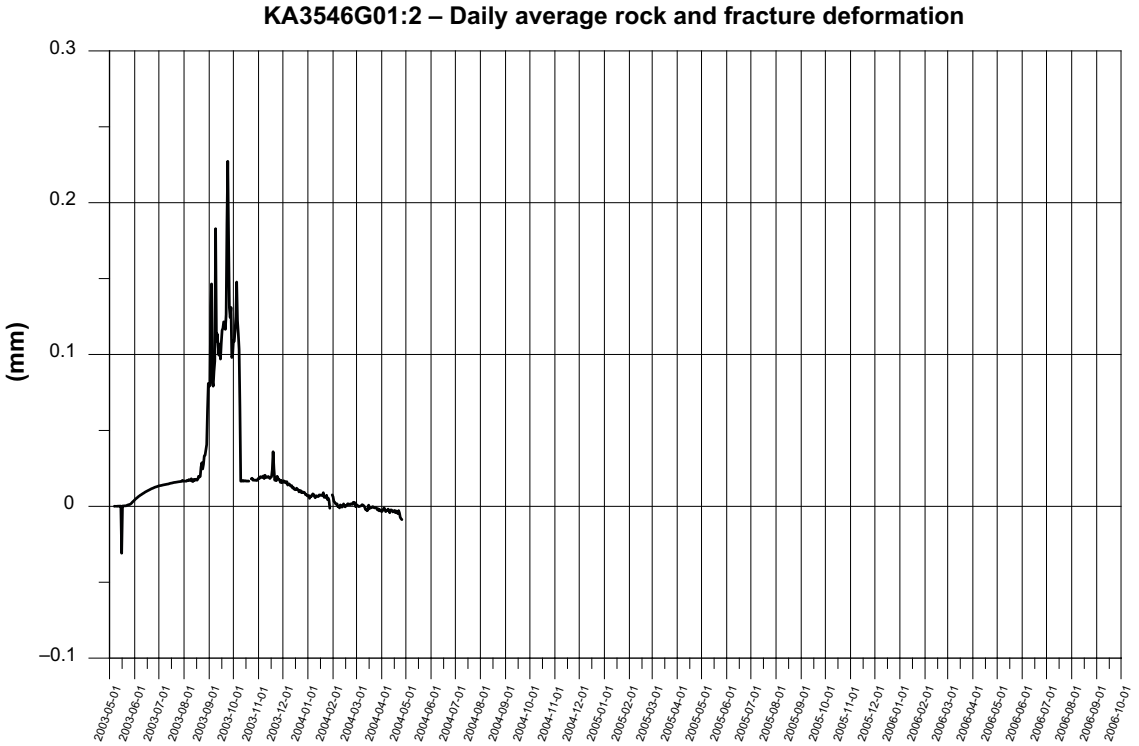

Figure 7-41. *KA3546G01:2. Rock and fracture deformation.*

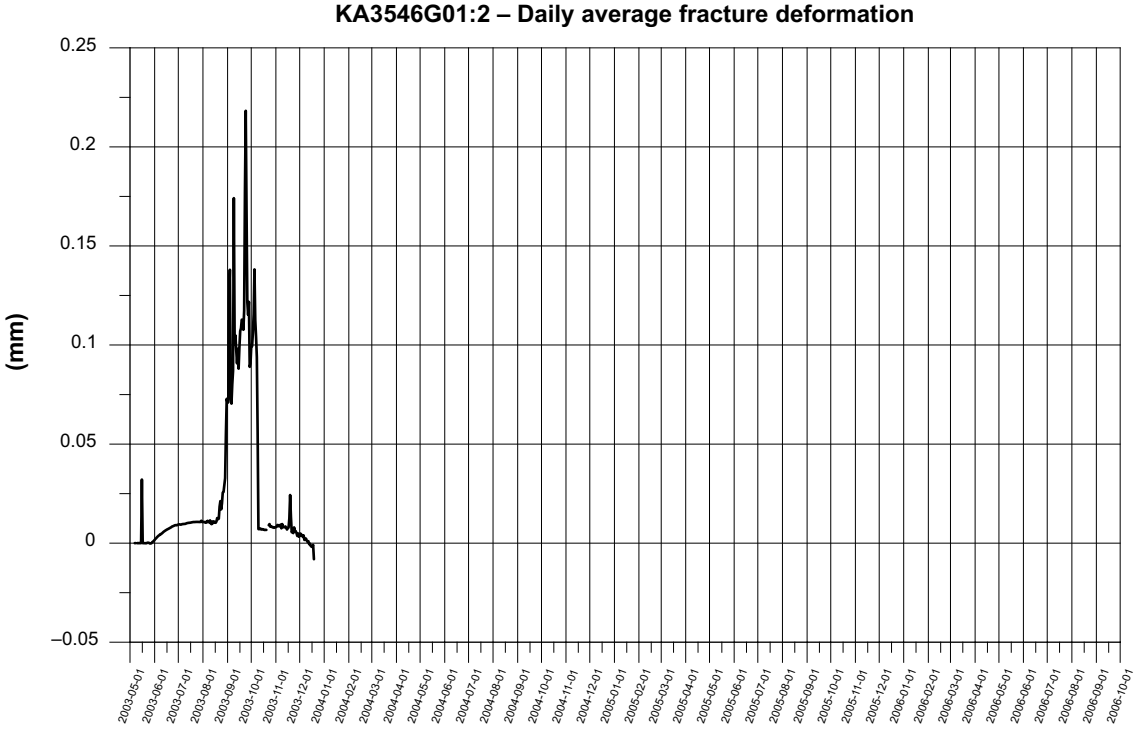

Figure 7-42. *KA3546G01:2. Single fracture deformation.*

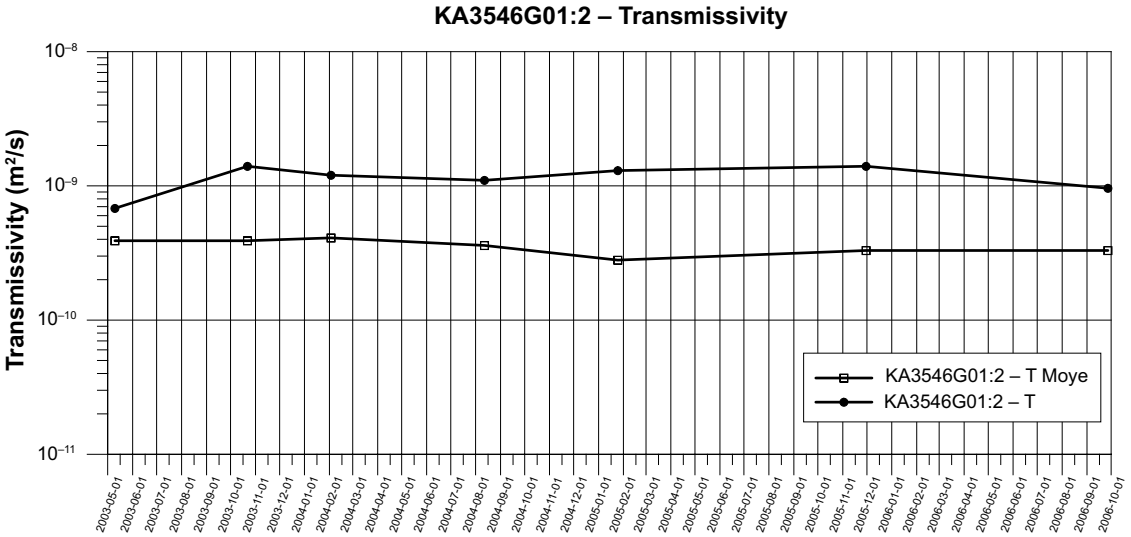

Figure 7-43. *Transmissivity change during the period 2003-05-01 to 2006-10-01.*

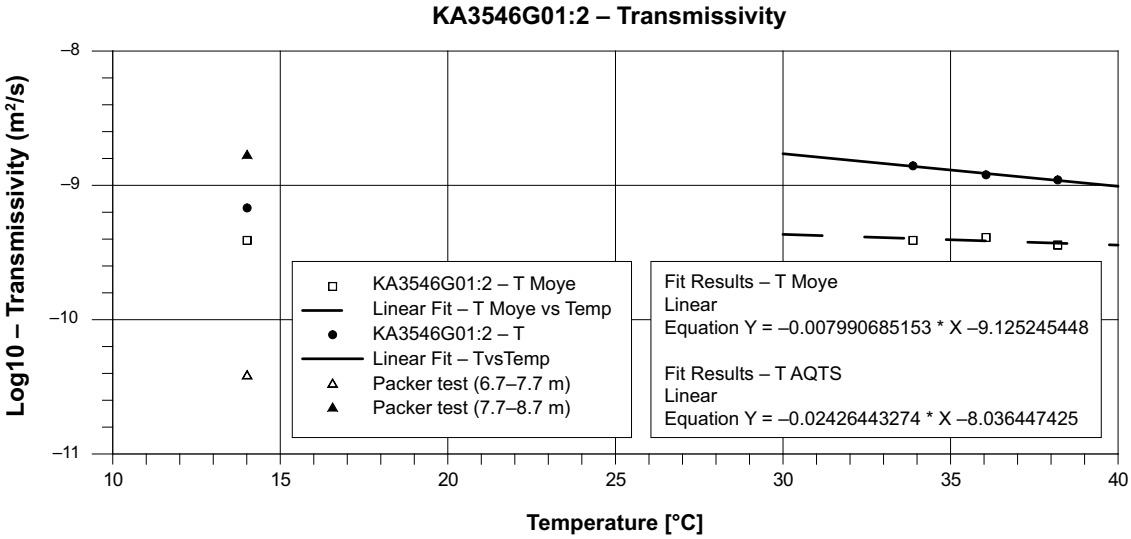

Figure 7-44. *Transmissivity versus temperature in KA3546G01:2 (6.75–8.30 m). No temperature measurements are available after 2005-01-01.*

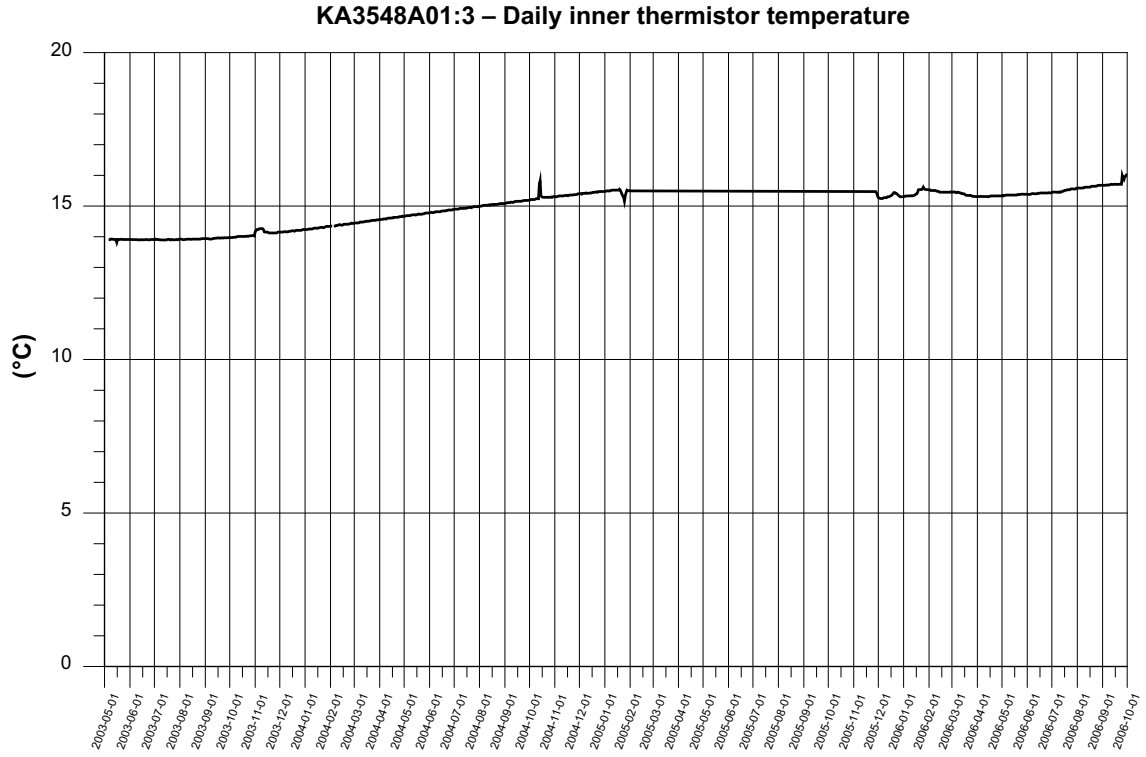

Figure 7-45. *KA3548A01:3. Average temperature.*

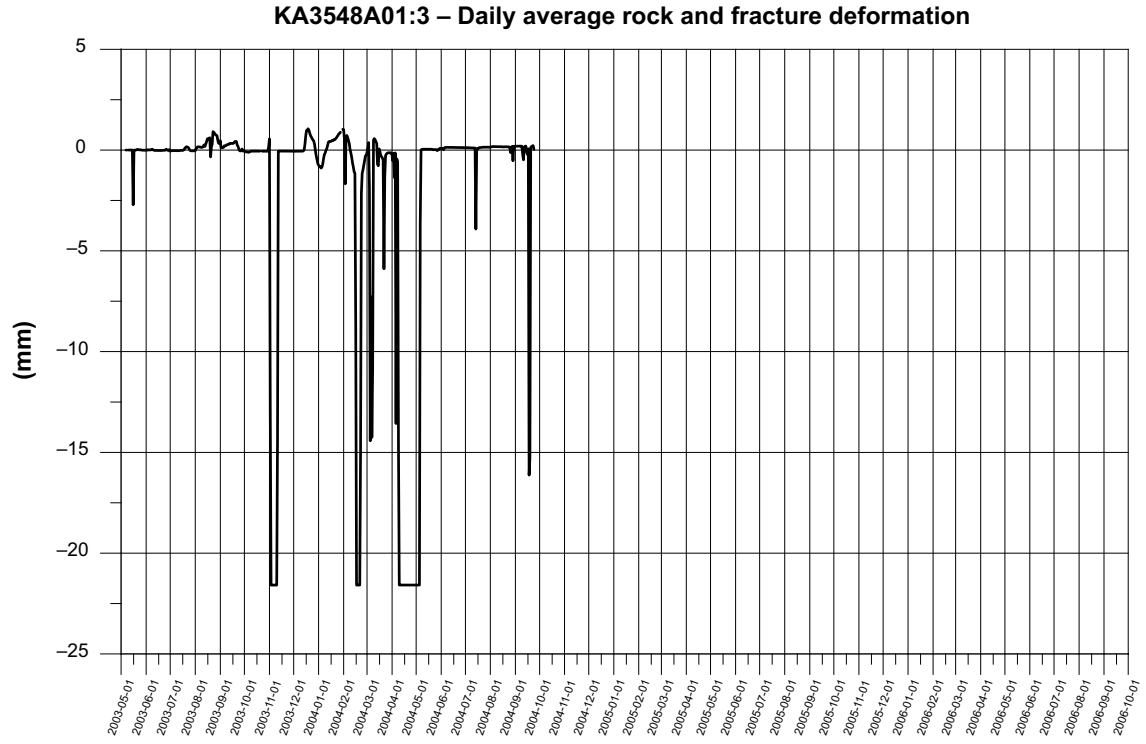

Figure 7-46. *KA3548A01:3. Rock and fracture deformation.*

Transmissivity

The change of the transmissivity during the period is shown below (Forsmark and Rhén 2004a, b, c, 2005a, b, c, Forsmark 2006, 2007a). (T-Moye: stationary assumption, T: evaluation based on transient data). Undisturbed pressure 2003-07 c. 3,500 kPa and 2006-10 c. 2,500 kPa, see Appendix 2.

- Both T and T_Moye decreases when the temperature increases. Chapter 7.5, Figure 7-104 indicates that log10 T may decrease up to c. 0.05 for a pressure drop of c. 1,000 kPa. The figure above includes effect from stress changes due to temperature and effective stress changes due to water pressure changes in the fracture and the effect of the temperature seem to dominate in this case.
- An earlier packer test for section 9–10 m gives T = $1.1 \cdot 10^{-7}$ m^2/s (in log10 format: –6.96) (Rhén and Forsmark 2001).

(Figure 7-47, Figure 7-48).

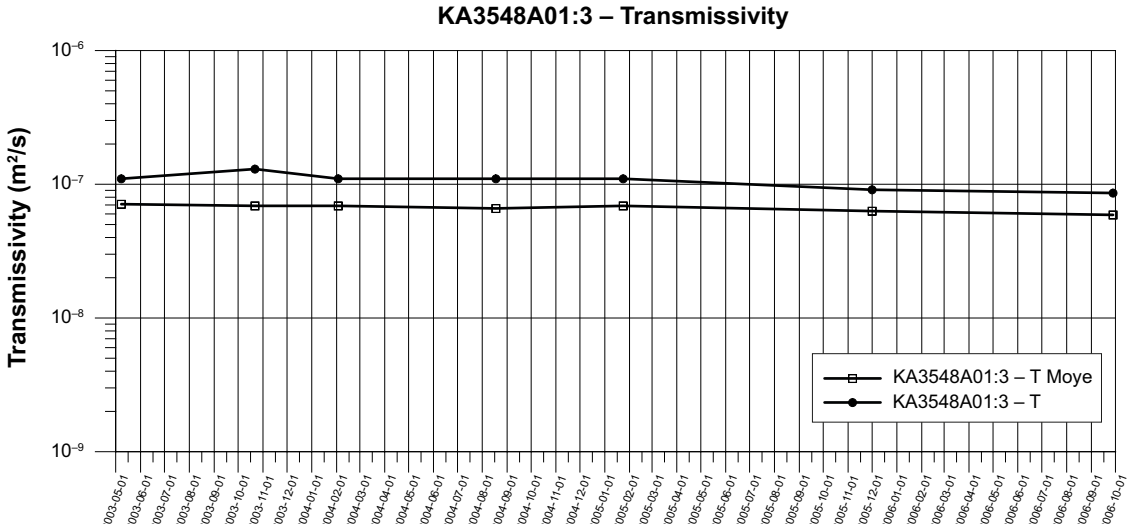

Figure 7-47. *Transmissivity change during the period 2003-05-01 to 2006-10-01.*

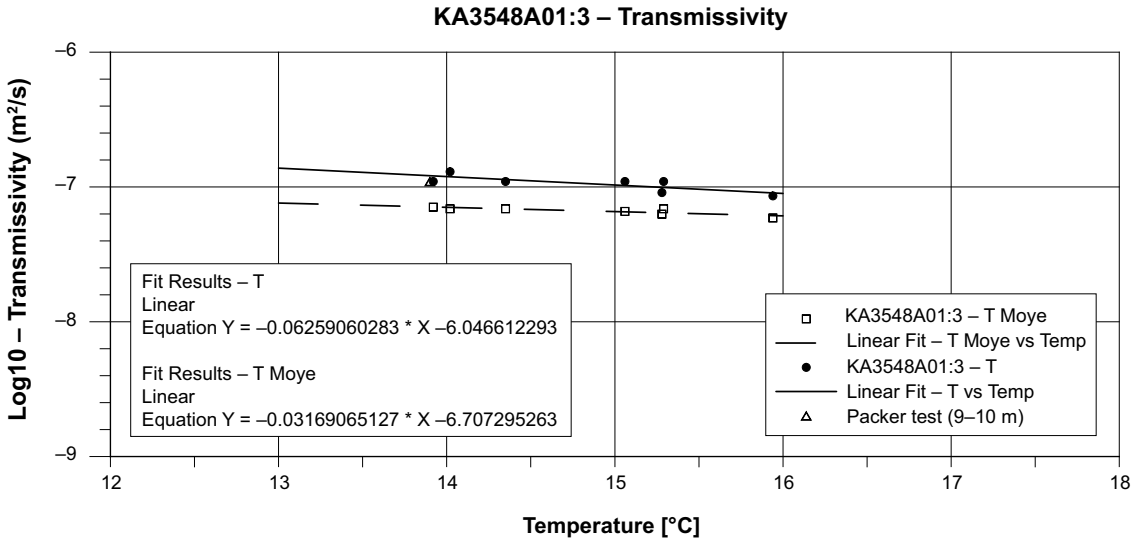

Figure 7-48. *Transmissivity versus temperature in KA3548A01:3 (8.80–10.75 m).*

7.3.8 KA3550G01:2 (5.20–7.30 m)

Temperature

- The temperature differs from the temperature in holes in the same area.
- Data between 2003-10-31 and 2006-10-01 is replaced by data calculated as the temperature data in TR5034 (Ghoudarzi and Johannesson 2006) (which is a temperature sensor in a hole drilled from inside the deposition hole DA3551G01 located 2.4 m from the HM section in KA3550G01) plus 9.5 degrees which was the temperature difference 2003-10-31.

(Figure 7-49).

Long-term deformation

- The intact rock expands as a result of the temperature increase until the sensor fails in October 2003.
- The fracture is being compressed until sensor failure.

(Figure 7-50, Figure 7-51, Figure 7-52).

Transmissivity

No hydraulic tests have been done in this borehole (Forsmark and Rhén 2004a, b, c, 2005a, b, c, Forsmark 2006, 2007a) due to packer failure. Undisturbed pressure 2003-07 c. 0 kPa and 2006-10 c. 700 kPa, see Appendix 2.

7.3.9 KA3552G01:2 (4.35–6.05 m)

Temperature

- None of the temperature sensors is in function.
- The data is replaced with data from KA3550G01:2.

(Figure 7-53).

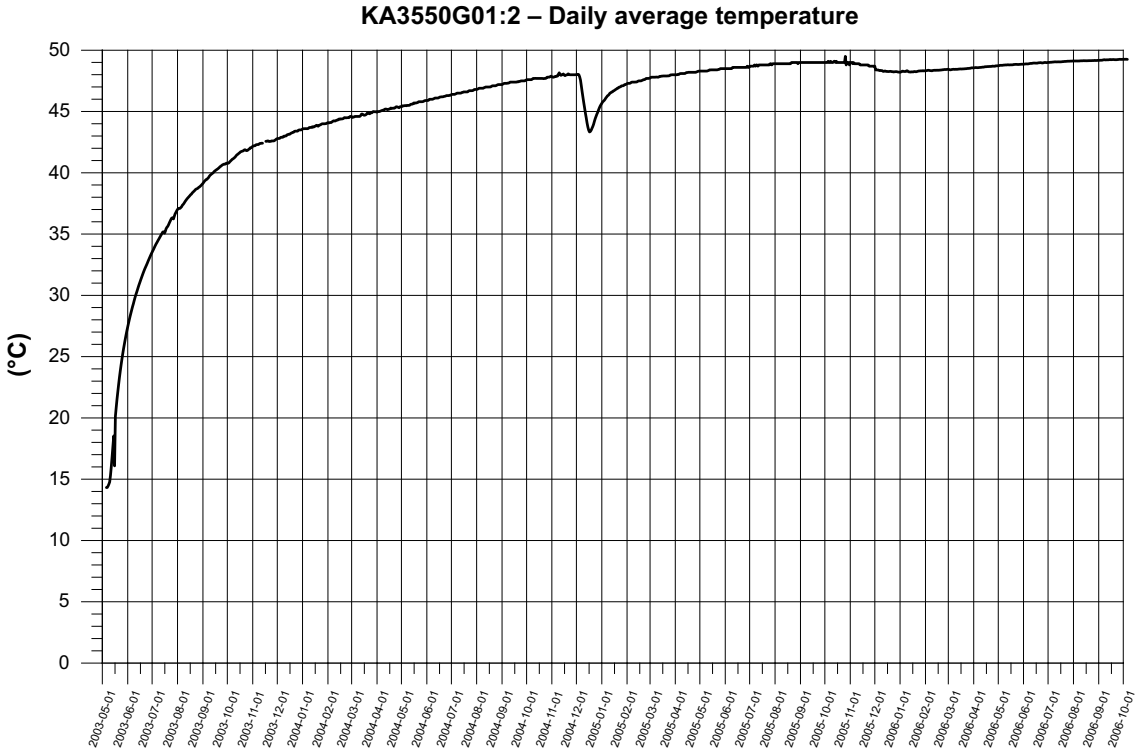

Figure 7-49. *KA3550G01:2. Average temperature.*

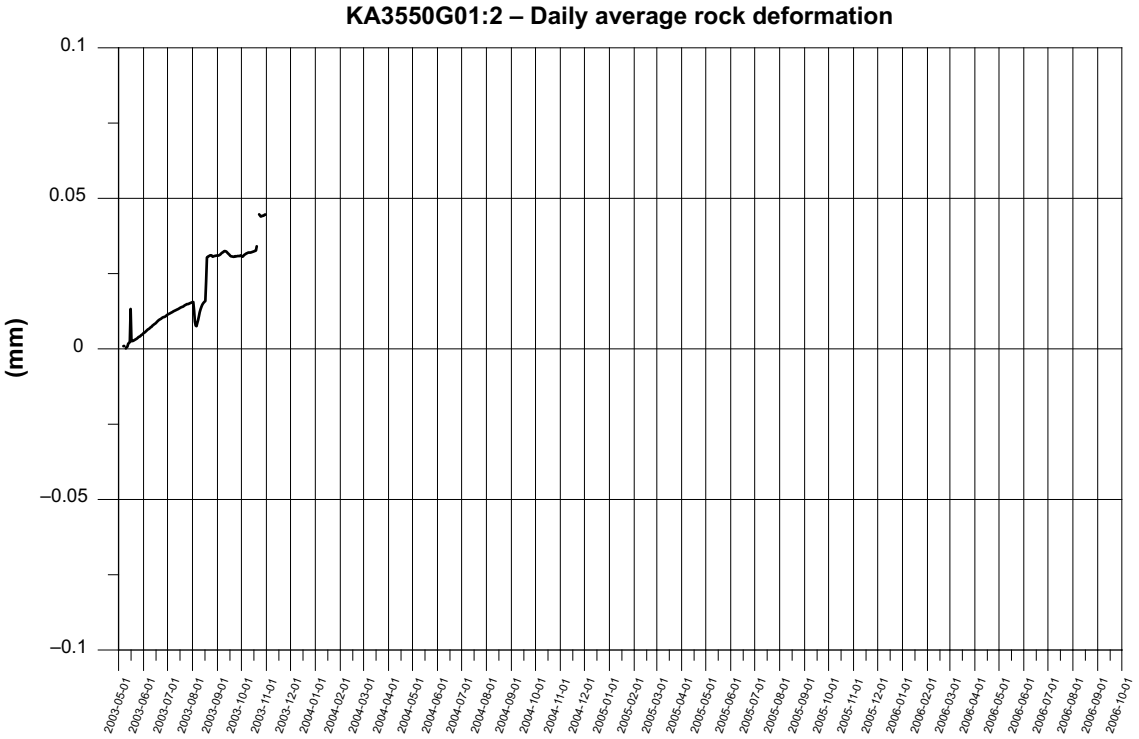

Figure 7-50. *KA3550G01:2. Rock deformation – intact rock section.*

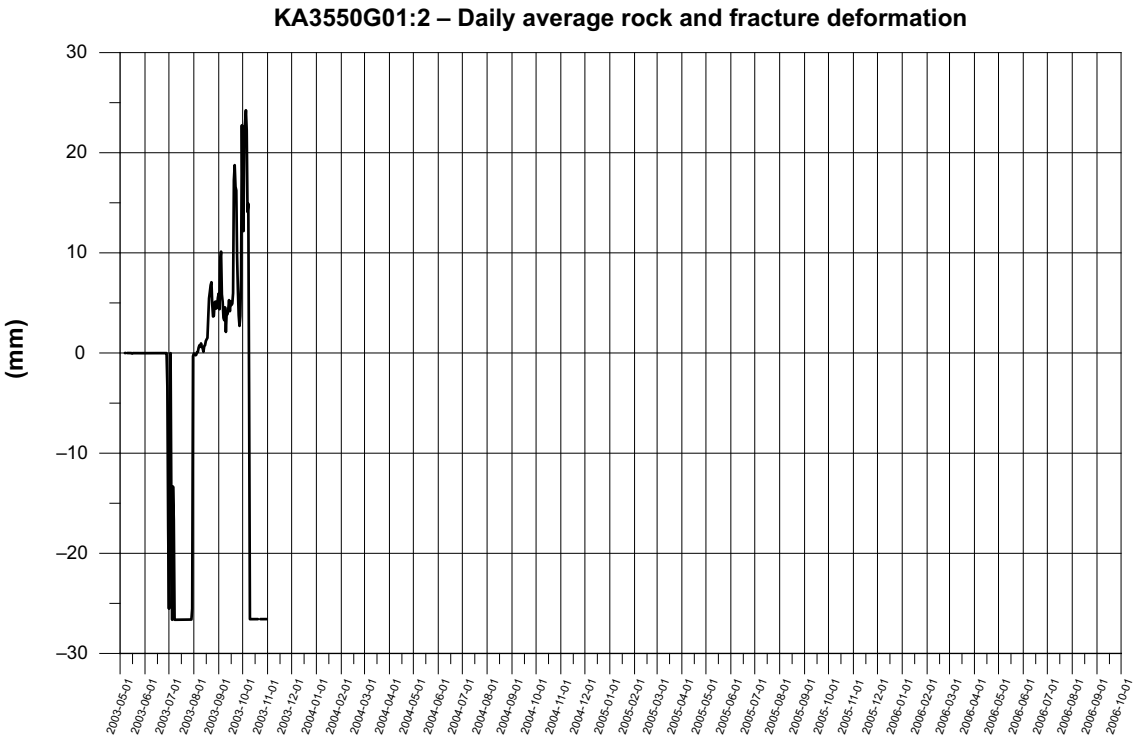

Figure 7-51. *KA3550G01:2. Rock and fracture deformation.*

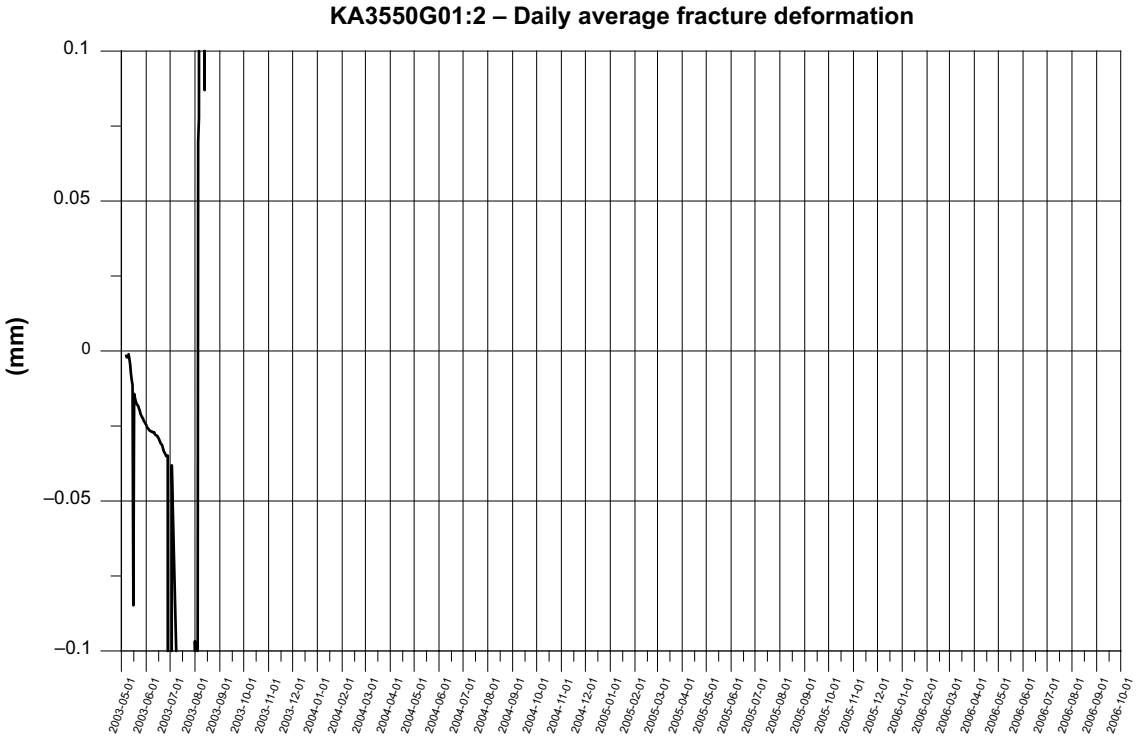

Figure 7-52. *KA3550G01:2. Single fracture deformation.*

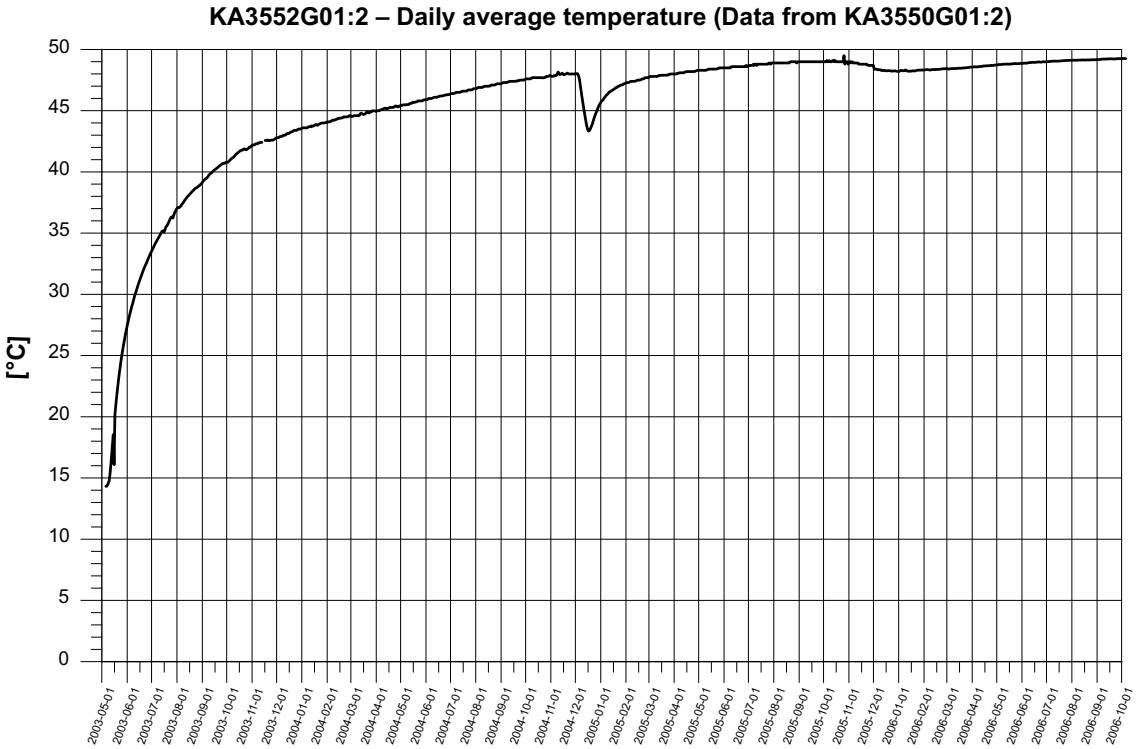

Figure 7-53. *KA3552G01:2. Average temperature.*

Long-term deformation

- The rock expansion ends up with a sensor failure in August 2003.

(Figure 7-54, Figure 7-55, Figure 7-56).

Transmissivity

The change of the transmissivity during the period is shown below (Forsmark and Rhén 2004a, b, c, 2005a, b, c, Forsmark 2006, 2007a). (T-Moye: stationary assumption, T: evaluation based on transient data). Undisturbed pressure 2003-05 c. 0 kPa and 2006-10 c. 800 kPa, see Appendix 2.

- The test section is very close to the canister and, together with KA3550G01:2, should be most affected by stress changes due to temperature increase in the rock mass.
- T_Moye and T decreases when the temperature increases. Chapter 7.5, Figure 7-104 indicates that log10 T may decrease up to c. 0.05 for a pressure drop of c. 1,000 kPa. In KA3552G01:2 the water pressure increases. The figure above includes effect from stress changes due to temperature and effective stress changes due to water pressure changes in the fracture and the effect of the temperature is clear in this case. The fracture orientation is 193/44, see Table 5-8.
- The "sudden" change in transmissivity between first and second test campaigns may be due to a fracture slip, see Figure 7-56 or only dependent on compression of the fracture due to the increased stress?
- An earlier packer test for section 4.7–5.7 m gives T (specific capacity) = $4.8 \cdot 10^{-9}$ m^2/s (in log10 format: –8.32) (Rhén and Forsmark 2001). Using measured parameters from that test gives a value of $T_{Moye} = 7.0 \cdot 10^{-10}$ m^2/s. This is in the same order of magnitude as the majority of the test results shown above.
- The pressure head in KA3552G01:3, is very high in the beginning of the test period, see Appendix 2. The reason may be that the section has a very low hydraulic conductivity, as can be seen in Rhén and Forsmark (2001), and during inflation of the packers the pressure increases to high levels followed by a slow leakage period lowering the pressure.

(Figure 7-57, Figure 7-58).

7.3.10 KA3554G01:2 (22.60–24.15 m)

Temperature

- Data between 2004-08-01 and 2006-10-01 is replaced by data from KA3542G01:3.

(Figure 7-59).

Long-term deformation

- The rock shows a slight compression since the measurement start.
- The expansion of both sensors at the beginning of the test period can be a result of that the anchors have settled down. After that there has been a small but clear compression of the system.
- At the end of February 2004 something happens that affect both sensors. No explanation for the sudden deformation change can be found.

(Figure 7-60).

Long-term deformation

(Figure 7-61, Figure 7-62).

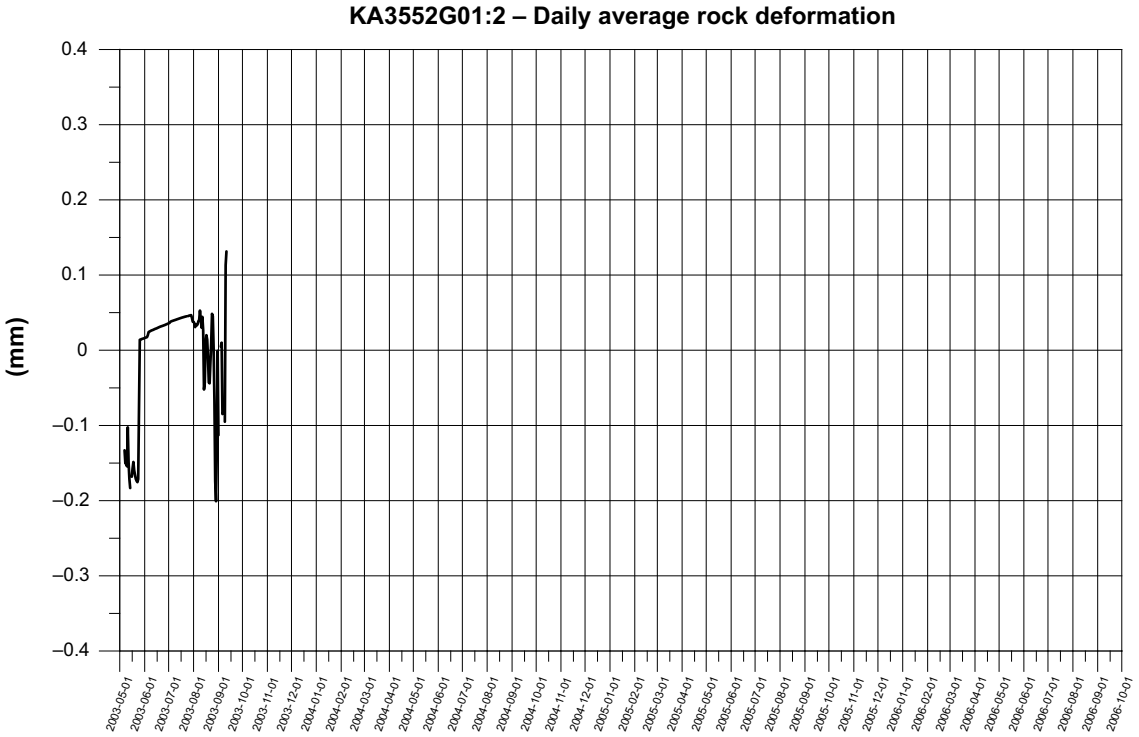

Figure 7-54. *KA3552G01:2. Rock deformation.*

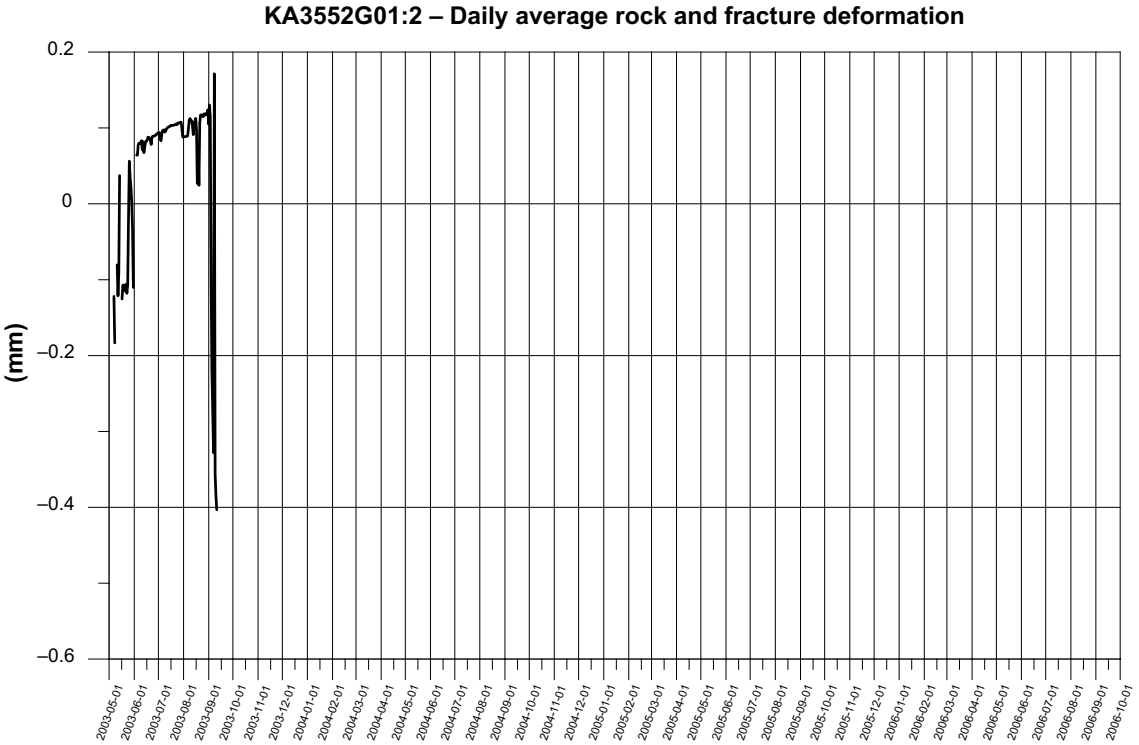

Figure 7-55. *KA3552G01:2. Rock and fracture deformation.*

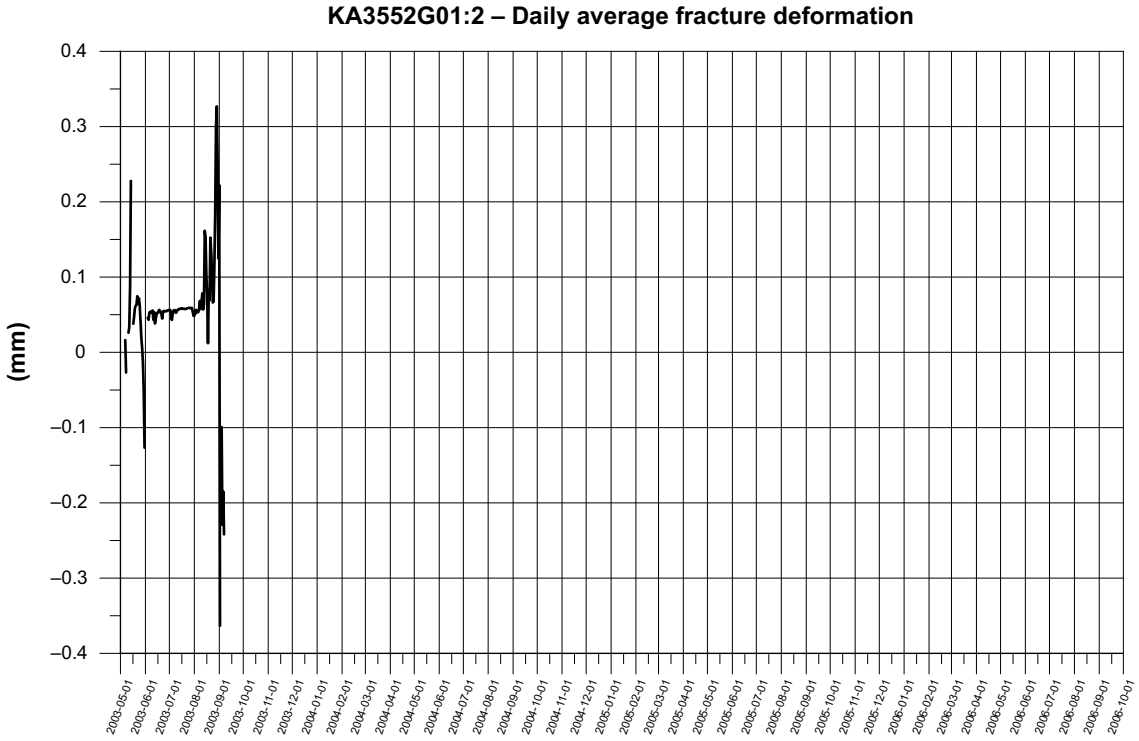

Figure 7-56. *KA3552G01:2. Single fracture deformation.*

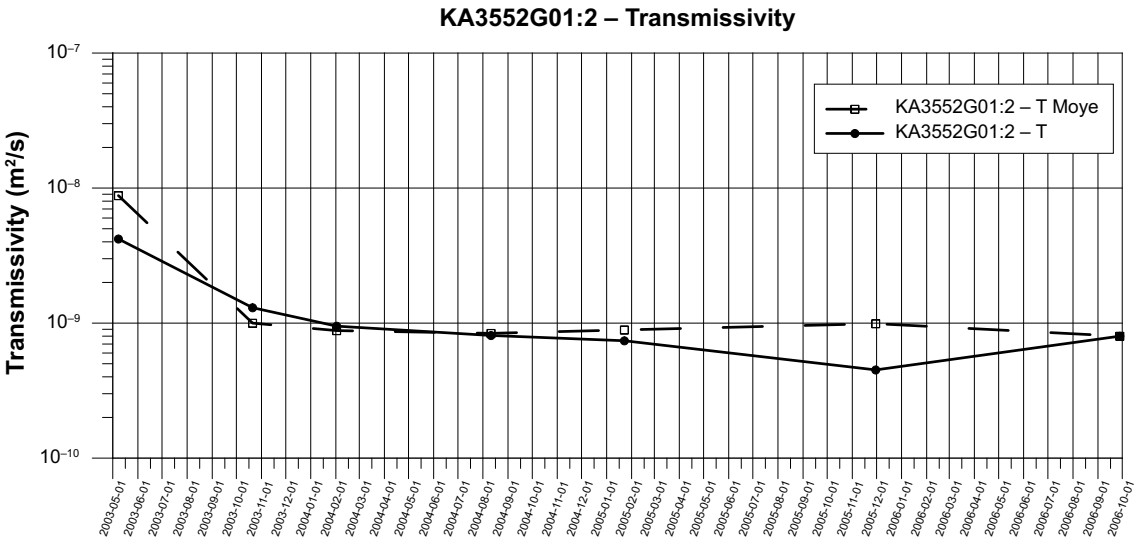

Figure 7-57. *Transmissivity change during the period 2003-05-01 to 2006-02-01.*

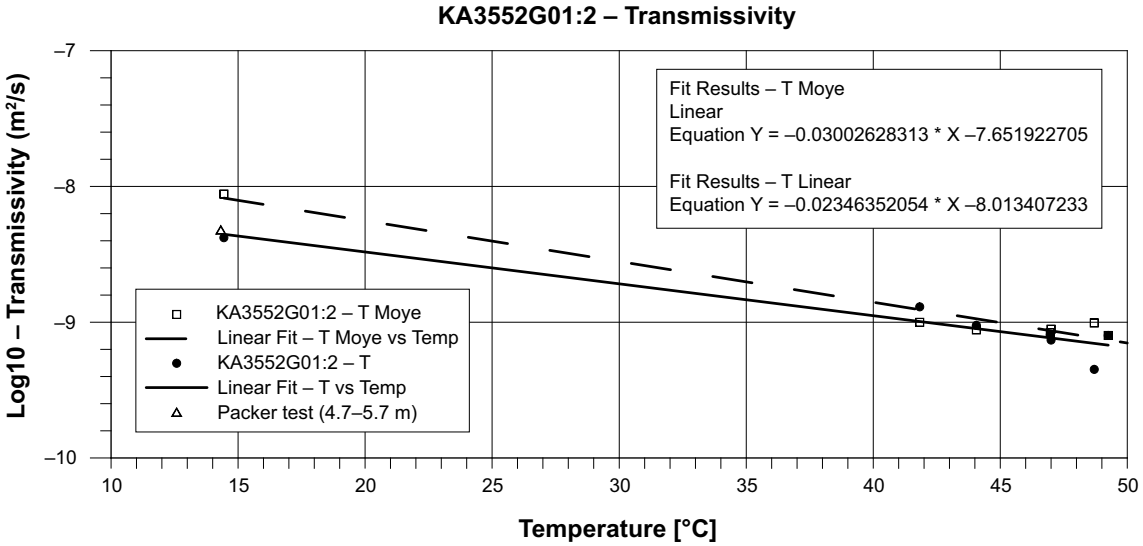

Figure 7-58. *Transmissivity versus temperature in KA3552G01:2 (4.35–6.05 m).*

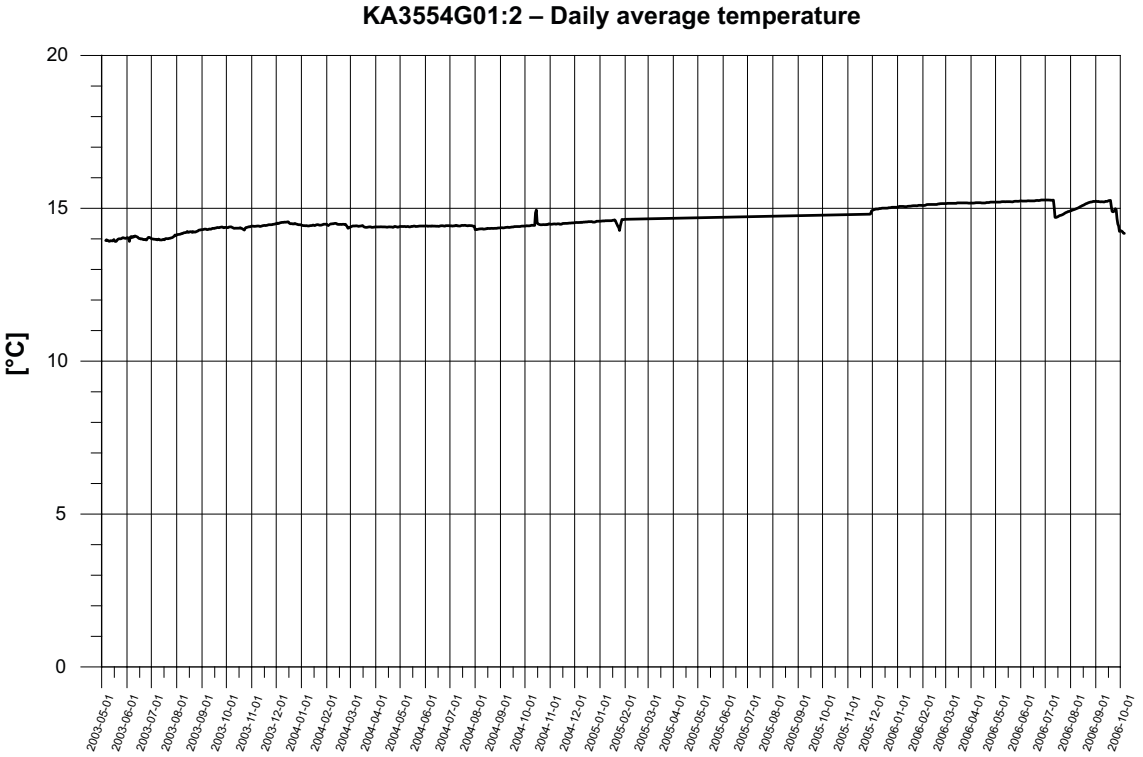

Figure 7-59. *KA3554G01:2. Average temperature.*

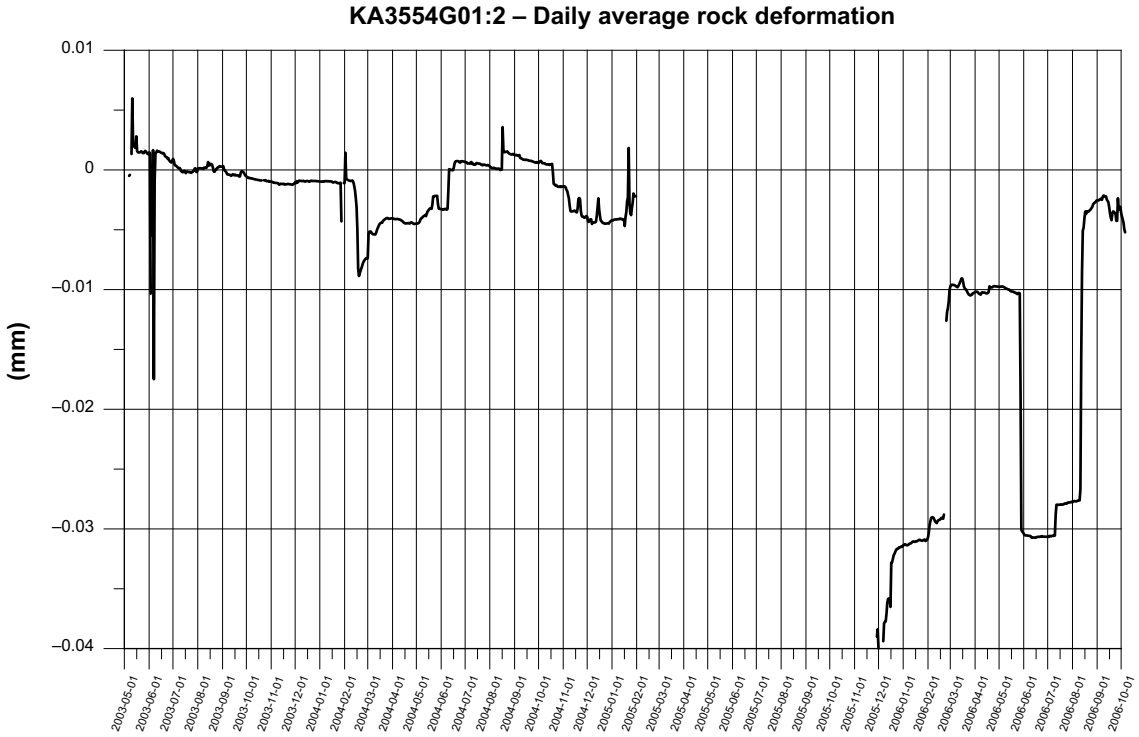

Figure 7-60. *KA3554G01:2. Rock deformation.*

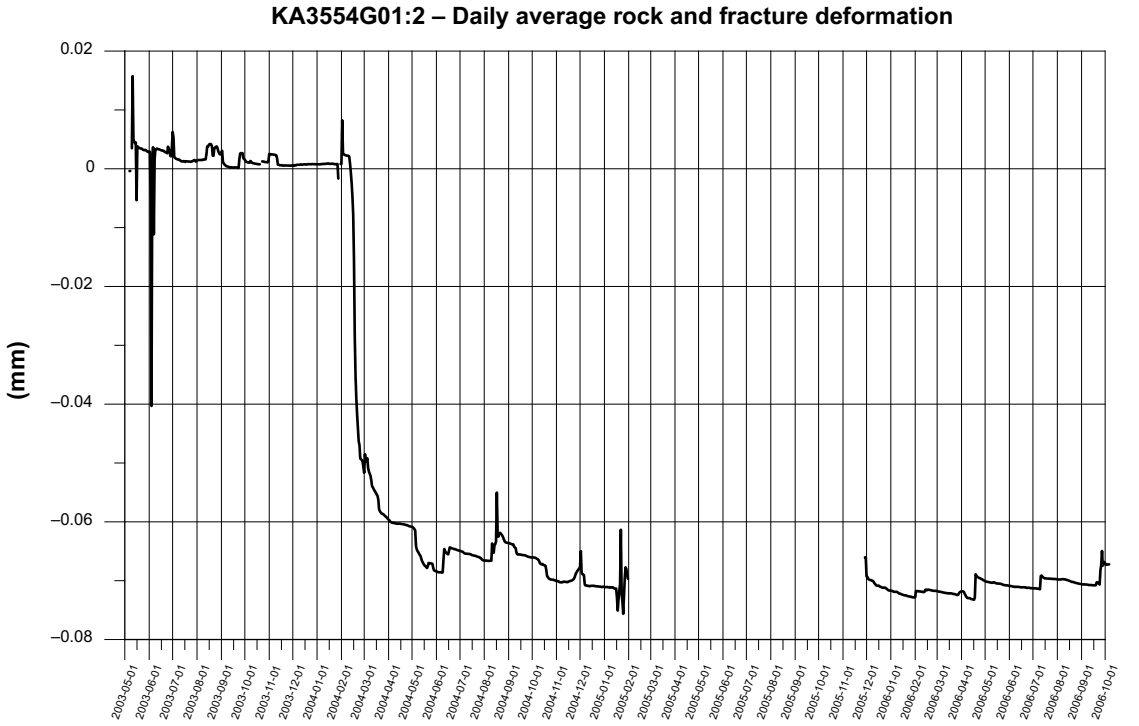

Figure 7-61. *KA3554G01:2. Rock and fracture deformation.*

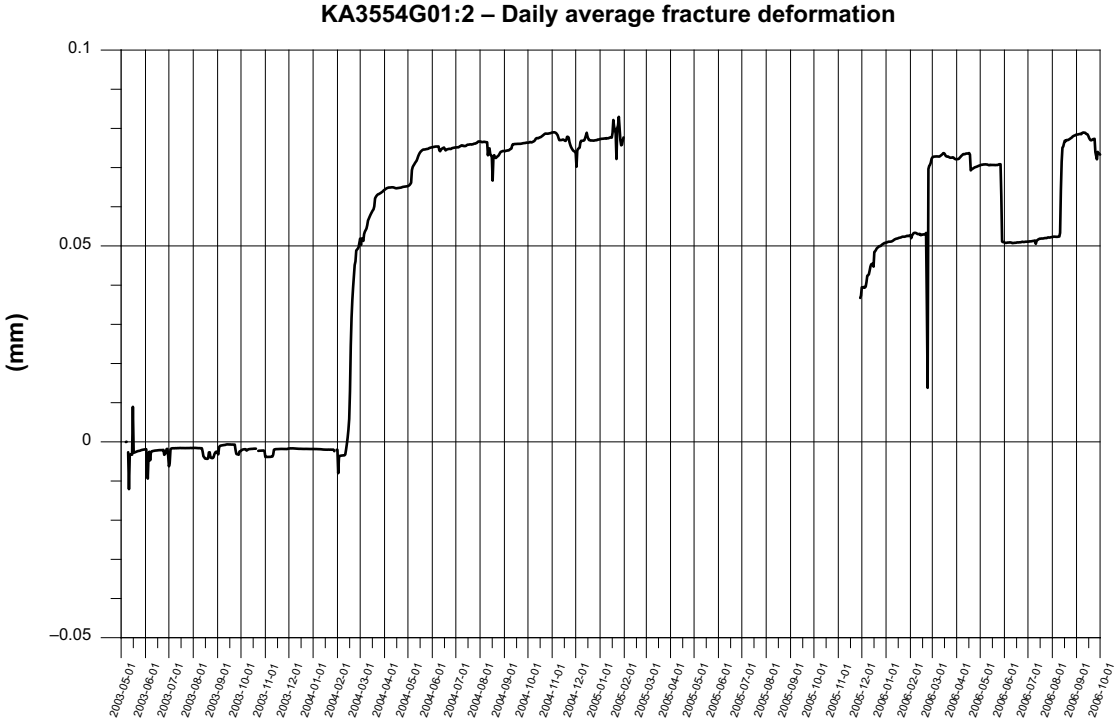

Figure 7-62. *KA3554G01:2. Single fracture deformation.*

Transmissivity

The change of the transmissivity during the period is shown below (Forsmark and Rhén 2004a, b, c, 2005a, b, c, Forsmark 2006, 2007a). (T-Moye: stationary assumption, T: evaluation based on transient data.). Undisturbed pressure 2003-05 c. 3,600 kPa and 2006-10 c. 2,800 kPa, see Appendix 2.

- Both T and T_Moye decreases when the temperature increases. Chapter 7.5, Figure 7-104 indicates that log10 T may decrease up to c. 0.05 for a pressure drop of c. 1,000 kPa. The figure above includes effect from stress changes due to temperature and effective stress changes due to water pressure changes in the fracture and the effect of the temperature seem to dominate in this case according to transient T but questionable according to T-Moye.
- An earlier packer test for section 21–24 m gives $T = 1.3 \cdot 10^{-6}$ m^2/s (in log10 format: –5.89) (Rhén and Forsmark 2001).

(Figure 7-63, Figure 7-64).

7.3.11 KA3554G02:4 (10.50–12.20 m)

Temperature

- Data between 2005-01-20 and 2005-01-24 is replaced by interpolated data.
- Data between 2005-02-01 and 2005-11-28 is replaced by interpolated data.

(Figure 7-65).

Long-term deformation

- The rock expands until sensor failure in February 2005.
- The fracture seems to be closing slowly the first year, but it appears strange as both the intact rock section and the intact rock+fracture section expands.

(Figure 7-66, Figure 7-67, Figure 7-68).

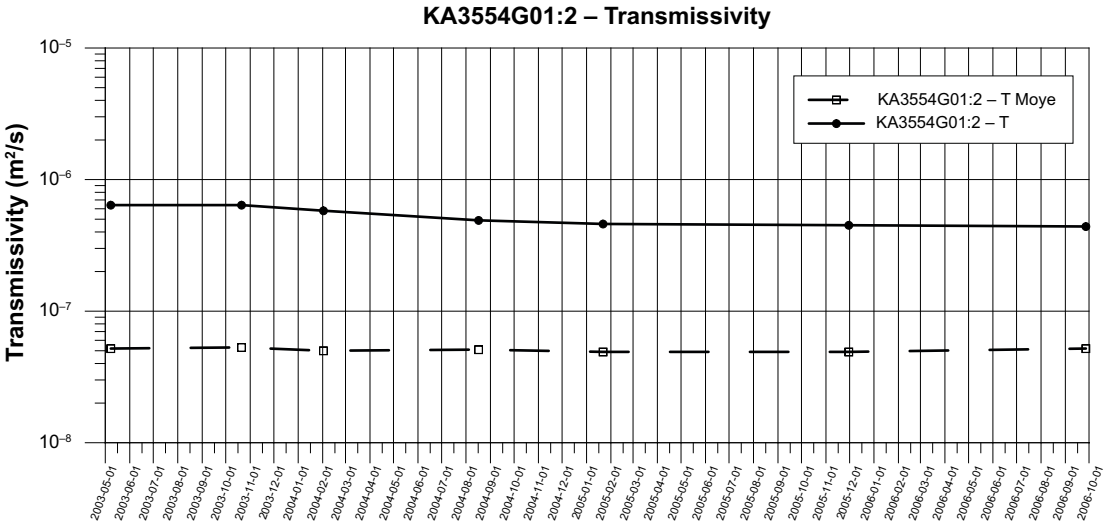

Figure 7-63. *Transmissivity change during the period 2003-05-01 to 2006-10-01.*

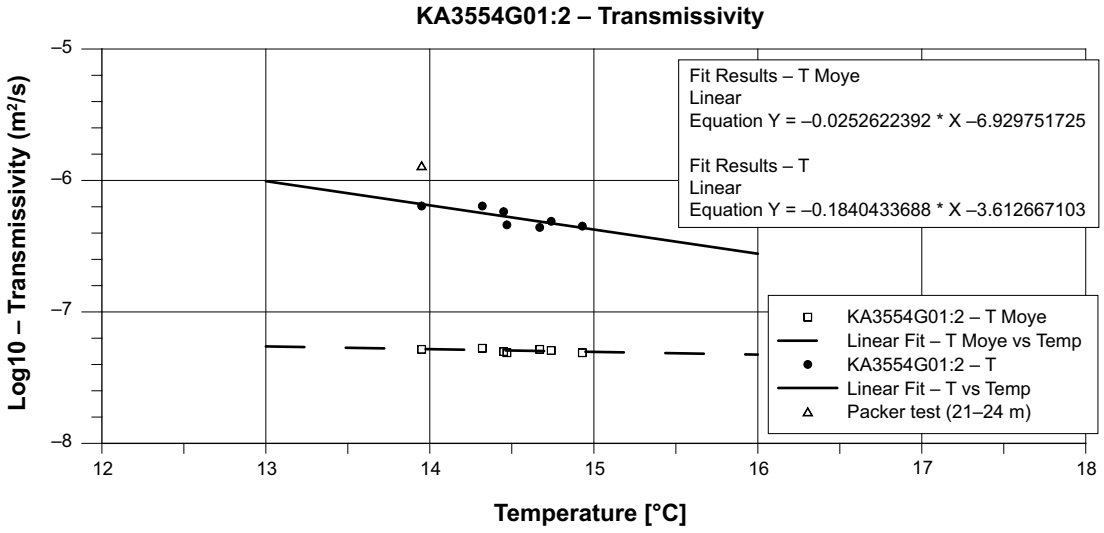

Figure 7-64. *Transmissivity versus temperature in KA3554G01:2 (22.60–24.15 m).*

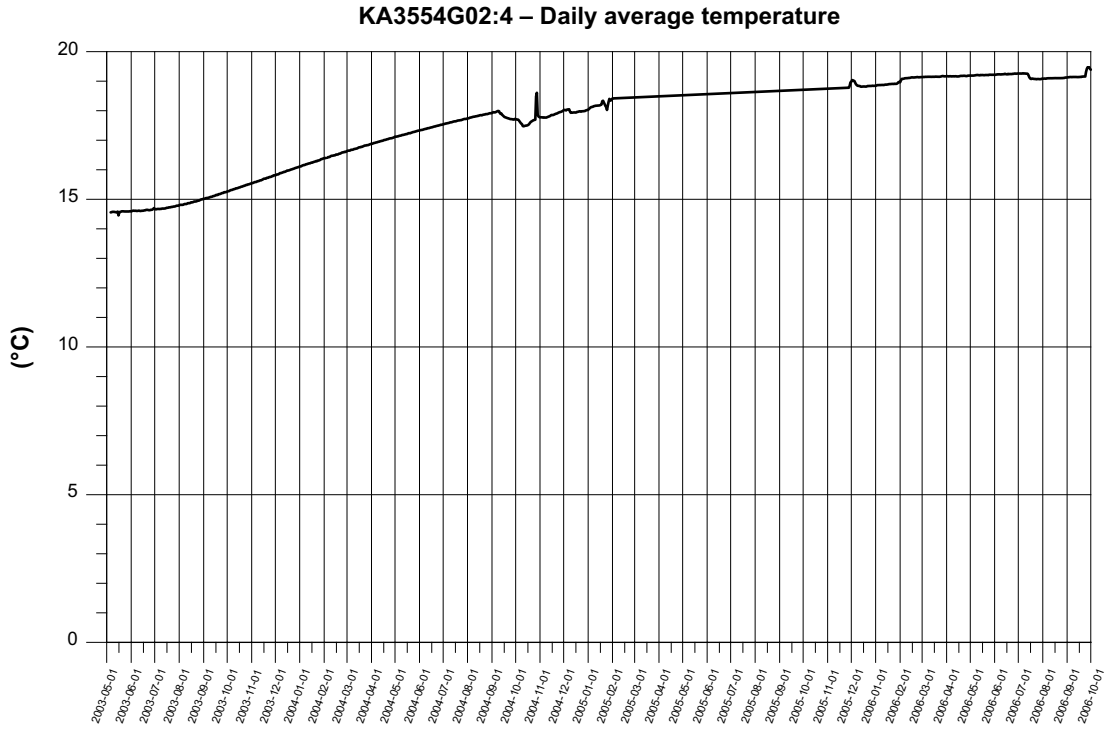

Figure 7-65. *KA3554G02:4. Average temperature.*

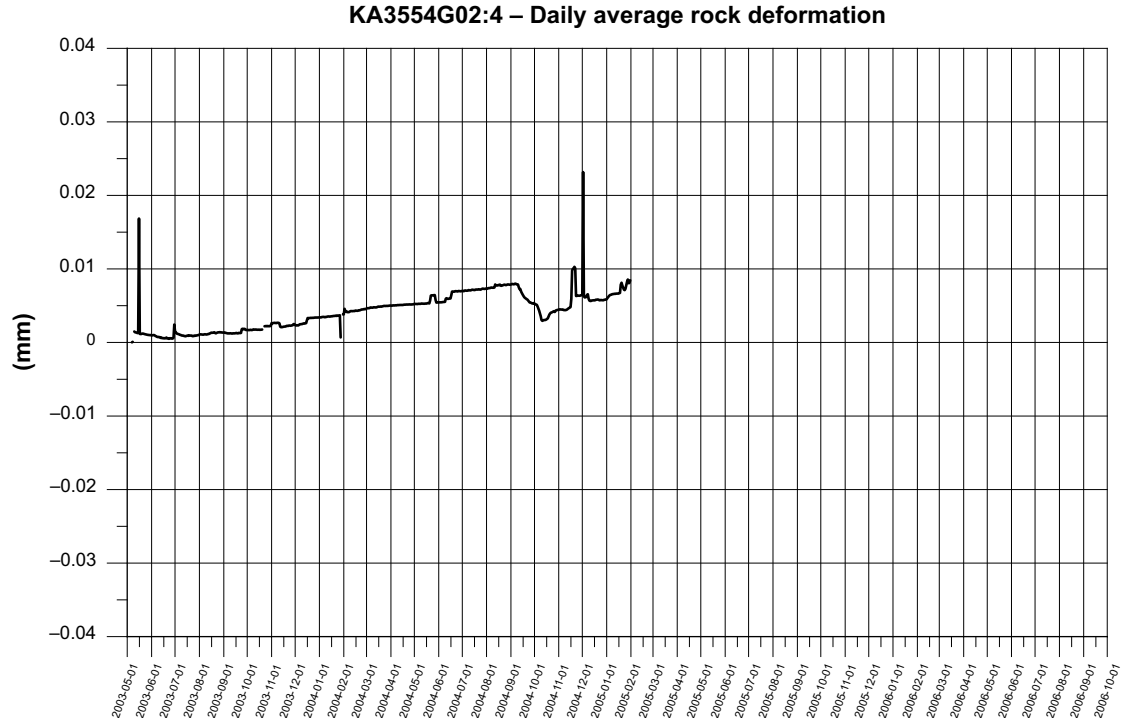

Figure 7-66. *KA3554G02:4. Rock deformation – intact rock section.*

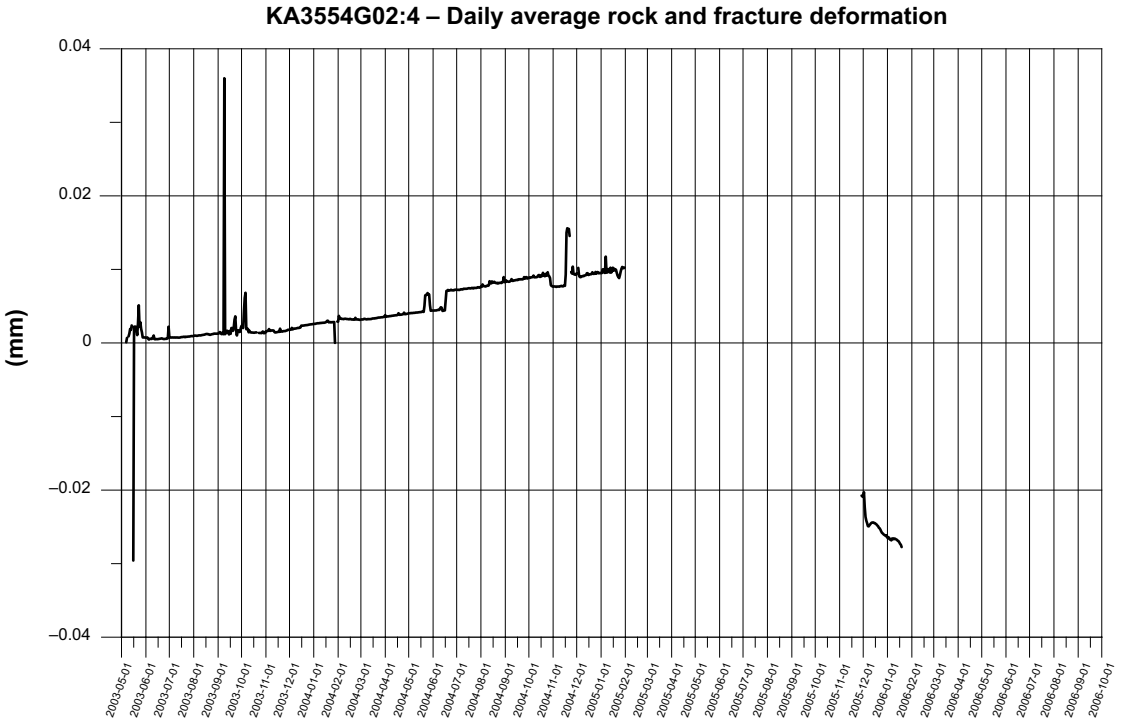

Figure 7-67. *KA3554G02. Rock and fracture deformation.*

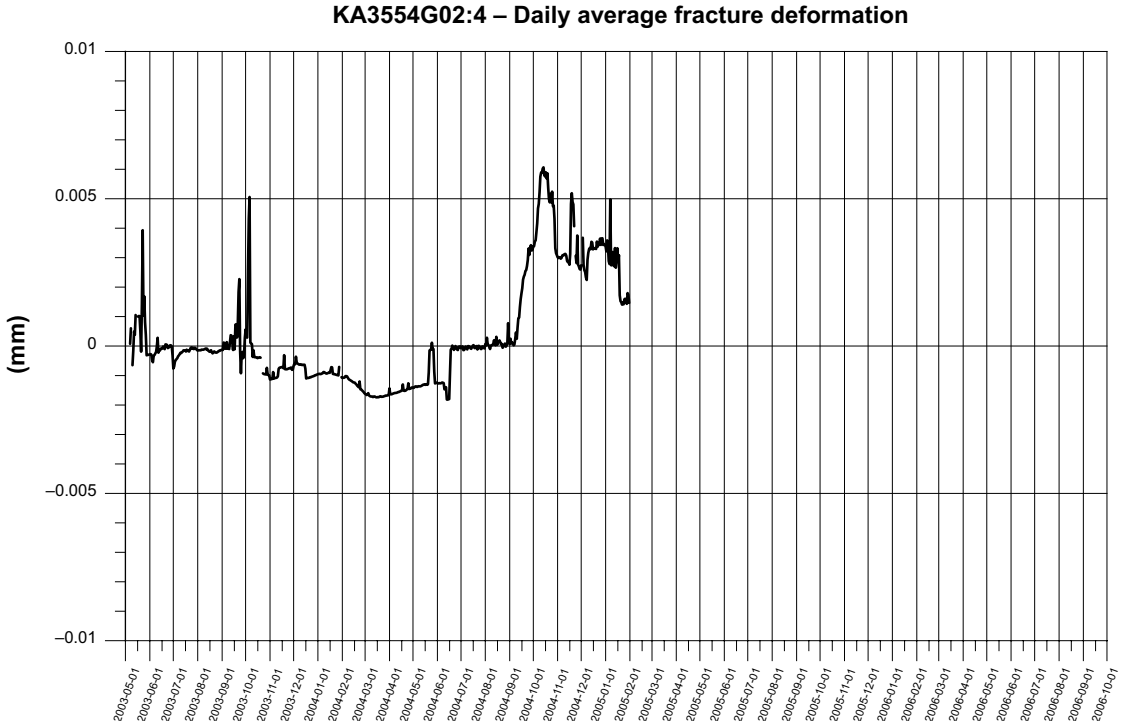

Figure 7-68. *KA3554G02:4. Single fracture deformation.*

Transmissivity

The change of the transmissivity during the period is shown below (Forsmark and Rhén 2004a, b, c, 2005a, b, c, Forsmark 2006, 2007a). (T-Moye: stationary assumption, T: evaluation based on transient data). Undisturbed pressure 2003-05 c. 2,400 kPa and 2006-10 c. 1,400 kPa, see Appendix 2.

- T_Moye increases slightly when the temperature decreases which is not what is expected. T decreases as expected. Chapter 7.5, Figure 7-104 indicates that log10 T may decrease up to c. 0.05 for a pressure drop of c. 1,000 kPa. The figure above includes effect from stress changes due to temperature and effective stress changes due to water pressure changes in the fracture and the effect of the temperature seem to dominate in this case according to transient T but questionable according to T-Moye.
- An earlier packer test for section 11–12 m gives T = $2.9 \cdot 10^{-7}$ m^2/s (in log10 format: –6.54) (Rhén and Forsmark 2001).

(Figure 7-69, Figure 7-70).

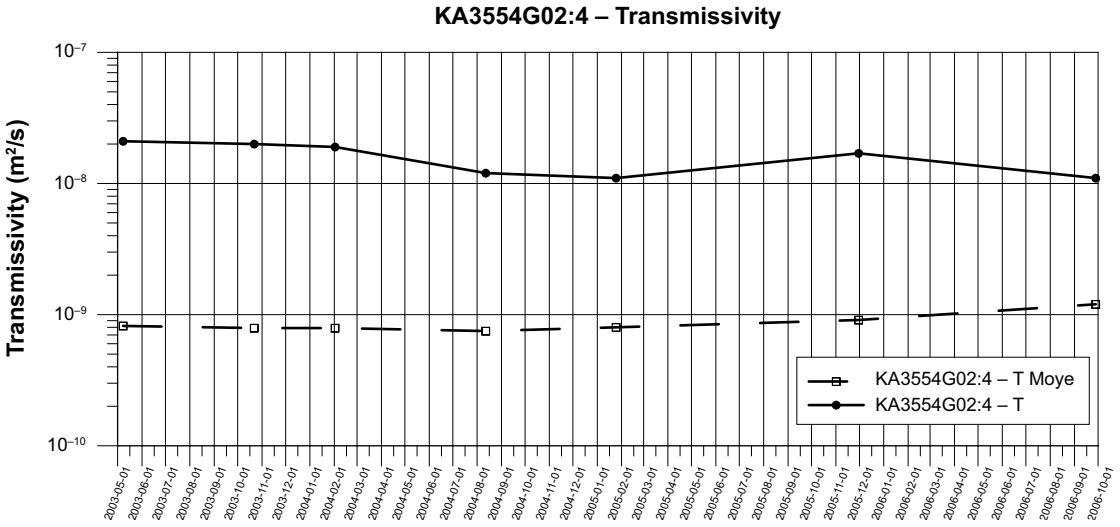

Figure 7-69. *Transmissivity change during the period 2003-05-01 to 2006-10-01.*

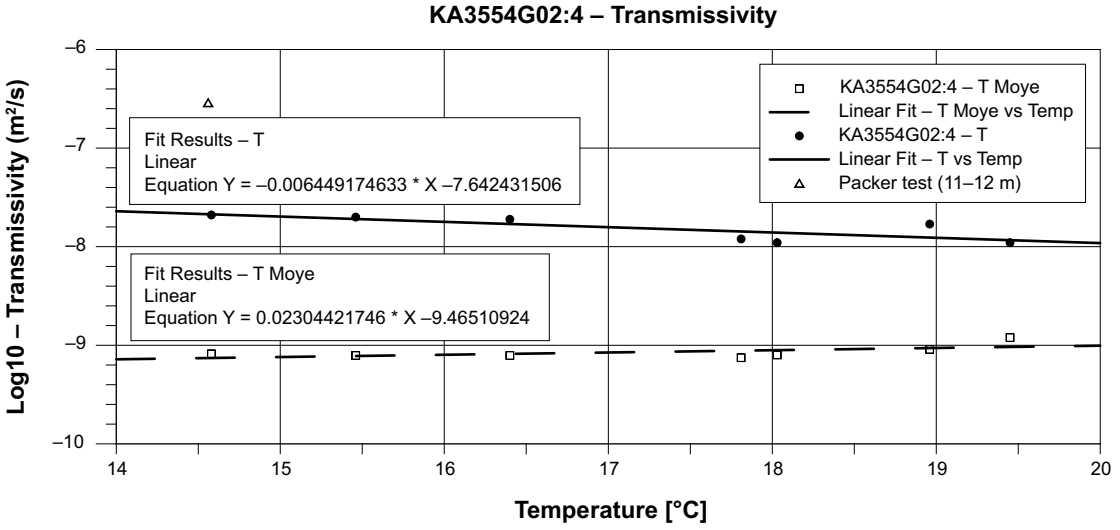

Figure 7-70. *Transmissivity versus temperature in KA3554G02:4 (10.50–12.20 m).*

7.3.12 Comments to expected behaviour

The expected behaviour has been that during temperature increase the intact rock expands while a fracture width decreases. In Table 7-1 below a summary of increases and decreases are presented. In a majority of tested boreholes the T_{MOYE} and the transient transmissivity are slightly decreasing when the temperature rise, the changes are however small. The measuring period is however rather short.

Table 7-1. Summary of temperature and deformation changes (ND = no data, Deformation; + : expansion, – : compression).

Borehole	Start date	Stop date	Temp. change (°C)	Total deformation intact rock (µm)	Total deformation fracture (µm)	T(TC1) May 2003 (m^2/s)	T(TC2) October 2003 (m^2/s)	T_{MOYE}(TC1) May 2003 (m^2/s)	T_{MOYE}(TC2) October 2003 (m^2/s)
KA3539G:2	**030510**	**040401**	**+0.9**	**–2.5**	**3.5**	**$1.3\cdot10^{-6}$**	**$1.5\cdot10^{-6}$**	**$1.3\cdot10^{-7}$**	**$2.0\cdot10^{-7}$**
KA3542G01:3	030510	040601	+0.4	–2.0	–6.6	$4.5\cdot10^{-8}$	$3.0\cdot10^{-8}$	$3.6\cdot10^{-8}$	$3.2\cdot10^{-8}$
KA3542G02:4	030510	031020	+0.1	–0.3	–2.8	$3.6\cdot10^{-10}$	$2.7\cdot10^{-10}$	$3.5\cdot10^{-10}$	$3.1\cdot10^{-10}$
KA3544G01:2	030510	031101	+7.4	+1,500?	ND	$1.1\cdot10^{-8}$	$7.4\cdot10^{-9}$	$5.1\cdot10^{-10}$	$3.6\cdot10^{-10}$
KA3546G01:2	030510	031215	+21.6	+13	–1.4	$6.8\cdot10^{-10}$	$1.4\cdot10^{-9}$	$3.9\cdot10^{-10}$	$3.9\cdot10^{-10}$
KA3548A01:3				ND	ND	$1.1\cdot10^{-7}$	$1.3\cdot10^{-7}$	$7.1\cdot10^{-8}$	$6.9\cdot10^{-8}$
KA3550G01:2	030510	030628	+18.8	+10.7	–35	No test	No test	No test	No test
KA3552G01:2				ND	ND	$4.2\cdot10^{-9}$	$1.3\cdot10^{-9}$	$8.8\cdot10^{-9}$	$1.0\cdot10^{-9}$
KA3554G01:2	030510	040127	+0.5	–1.0	–2.0	$6.4\cdot10^{-7}$	$6.4\cdot10^{-7}$	$5.2\cdot10^{-8}$	$5.3\cdot10^{-8}$
KA3554G02:4	030510	040201	+1.8	+3.8	–1.1	$2.1\cdot10^{-8}$	$2.0\cdot10^{-8}$	$8.2\cdot10^{-10}$	$7.9\cdot10^{-10}$

Several of the sudden changes in the deformation curves can probably be explained by a slip of one or several anchors. Some sudden changes can possibly be related to slip in fractures but it is difficult to be certain as it is believed that some slips are probably slip of the anchors.

7.4 Short term study during hydraulic test campaigns

Test campaigns

Until October 2006 seven test campaigns have been carried out:

- Campaign 1, May 8–11, 2003 (no deformation data is available)
- Campaign 2, October 21–23, 2003 (deformation data is missing between October 20 16:00 and October 22 15:08 due to logger problem).
- Campaign 3, February 2–4, 2004.
- Campaign 4, August 11–18, 2004.
- Campaign 5, January 19–25, 2005.
- Campaign 6, November 28–December 02, 2005.
- Campaign 7, September 25–September 29, 2006.

A further three test campaigns have been carried out after October 2006. Since the mechanical sensors didn't work properly during the period after campaign 7, the results are only mentioned briefly in the plots of Chapter 8:

- Campaign 8, October 15–19, 2007.
- Campaign 9, October 20–24, 2008.
- Campaign 10, November 10–19, 2009.

In Appendix 3 an overview of the test campaigns is given in more detail.

Expected behaviour

Pressure build-up test:

- The fracture is compressed when the water pressure inside the fracture is released (the flow period).
- The intact rock expands when the surrounded pressure is released (the flow period).
- The fracture width will increase when the flow period stops and the water pressure increases during pressure build-up.
- The intact rock is compressed when the flow period stops and the water pressure increases during pressure build-up.

7.4.1 KG0010B01

The borehole is not used in the test campaigns.

7.4.2 KA3539G:2

Deformation during test campaigns

Campaign 1

No data available.

Campaign 2 (October 21–23, 2003)

Flow start: October 23 10:15 (winter time correspond to 11:15 in figures).
Flow stop: October 23 10:45 (correspond to 11:45 in figures).

- The mechanical response of the pressure build-up test is very clear.
- The behaviour of the fracture is according to the expected behaviour.
- The measurement indicates that the test cause a permanent deformation of the fracture or movement of the whole measurement equipment or the outer anchor for Rock+Fracture section.
- The mechanical response is roughly 1.3 µm compression of fracture at a pressure drop of 1,364 kPa.

(Figure 7-71, Figure 7-72).

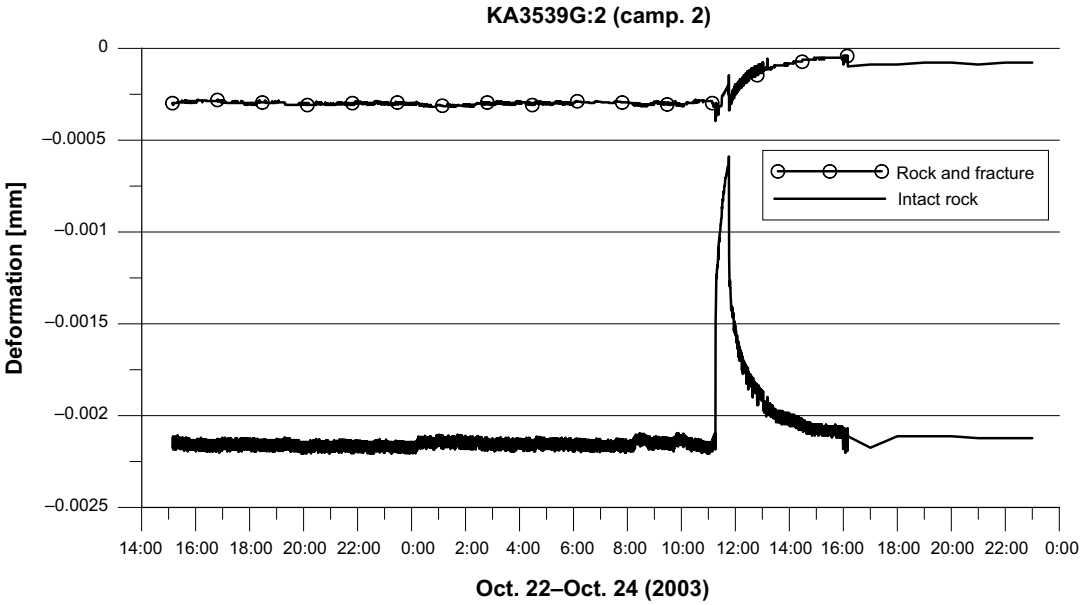

Figure 7-71. *Rock and fracture and intact rock deformation in KA3539G:2 during test campaign 2.*

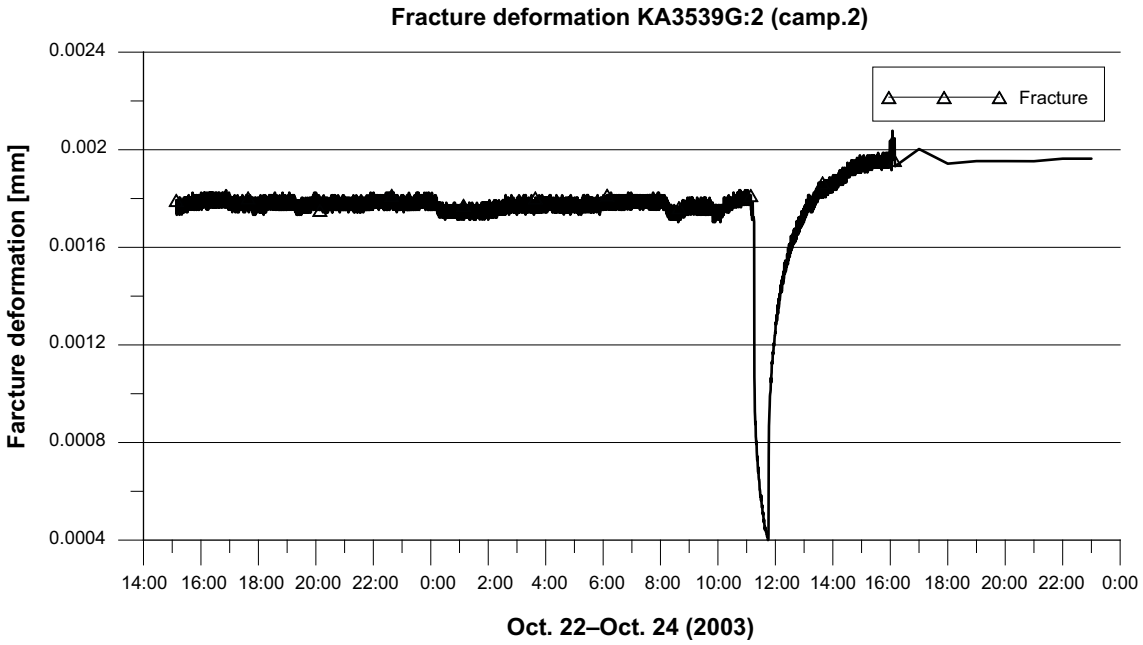

Figure 7-72. *Single fracture deformation in KA3539G:2 during test campaign 2.*

Campaign 3 (February 2–4, 2004)

Flow start: February 4 12:30.
Flow stop: February 4 13:30.

- The intact rock behaves like the expected behaviour.
- A permanent deformation is noticed in both intact rock and rock and fracture.
- The mechanical response is roughly 1.6 µm compression of fracture at a pressure drop of 1,465 kPa.

(Figure 7-73, Figure 7-74).

Campaign 4 (August 11–18, 2004)

Flow start and stop: August 18 10:00–11:00.
Flow start and stop: August 18 12:30–13:30.

- During the flow period the temperature decreases c. 0.2°C in the section with the fractures and in the section with "intact rock" the temperature decreases c. 0.05°C. The temperature corrections applied (deformation shown in the figure is the temperature corrected deformation), are then approximately 0.8 µm in the section with the fractures and in the section with "intact rock" approximately 0.2 µm.
- The mechanical response is roughly 1.4 µm compression of fracture at a pressure drop of 1,035 kPa.
- The mechanical response is roughly 1.3 µm compression of fracture at a pressure drop of 1,242 kPa.

(Figure 7-75, Figure 7-76).

Campaigns 5–7

No data available.

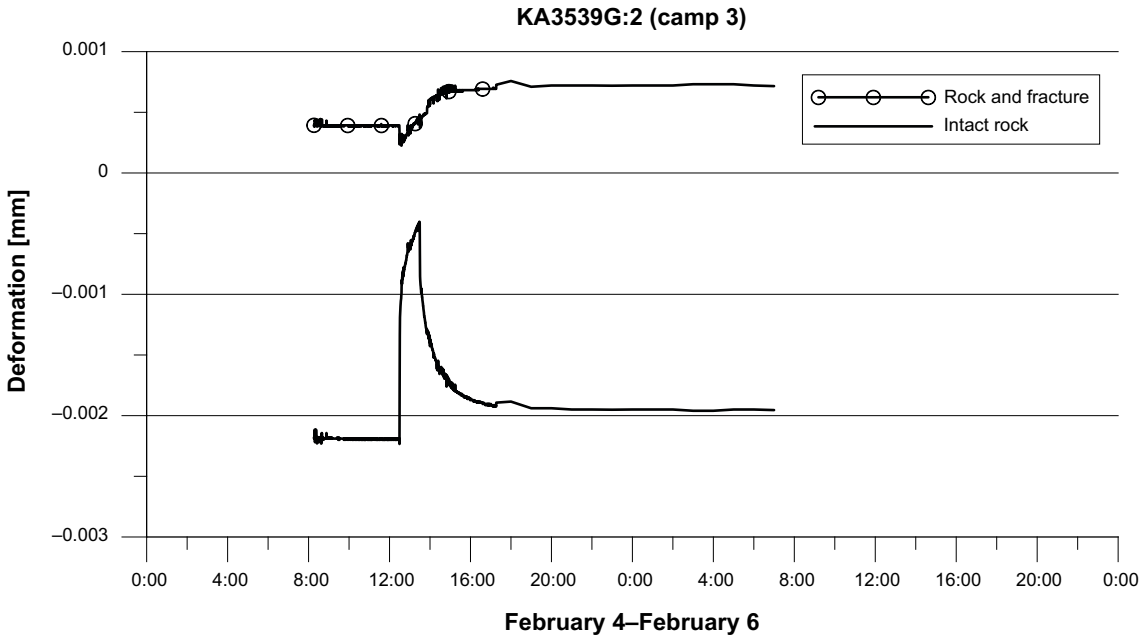

Figure 7-73. *Rock and fracture and intact rock deformation in KA3539G:2 during test campaign 3.*

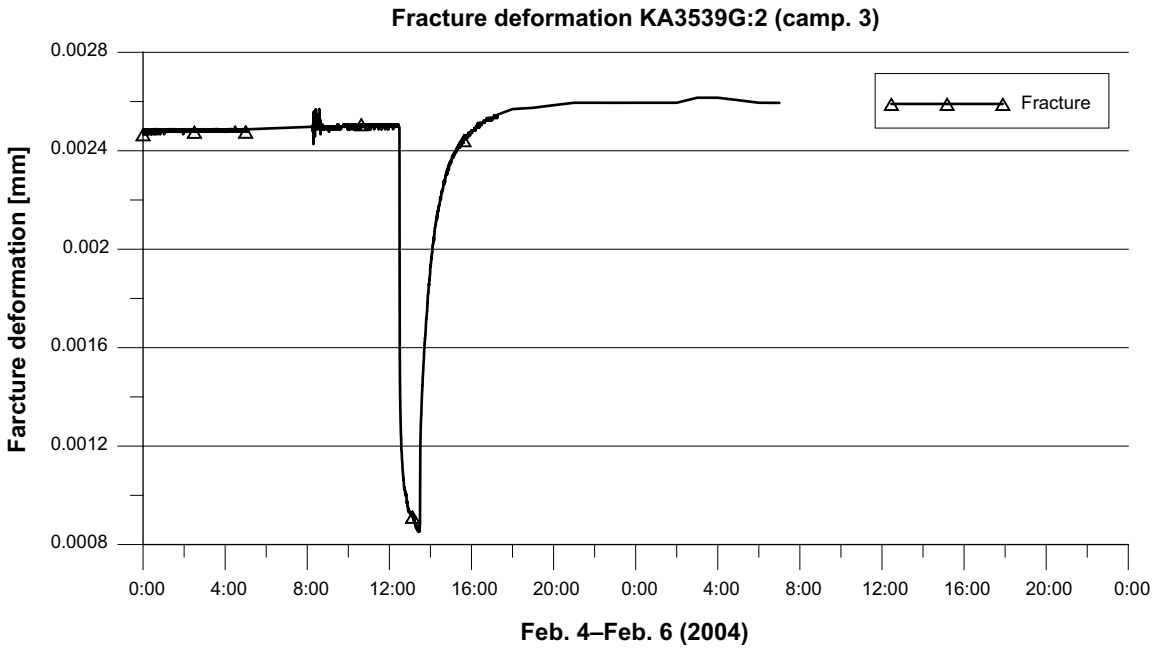

Figure 7-74. *Single fracture deformation in KA3539G:2 during test campaign 3.*

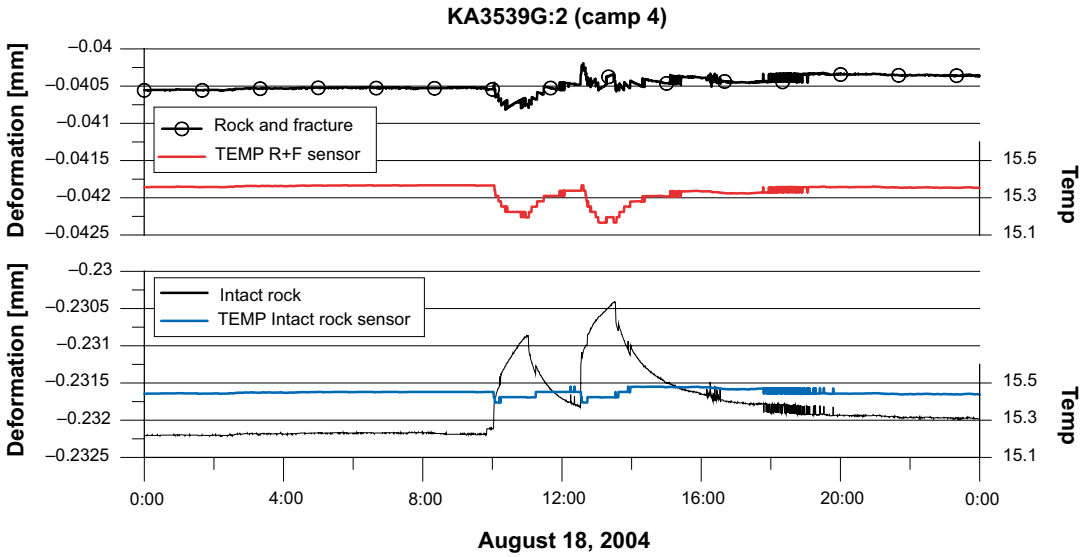

Figure 7-75. *Rock and fracture and intact rock deformation in KA3539G:2 during test campaign 4.*

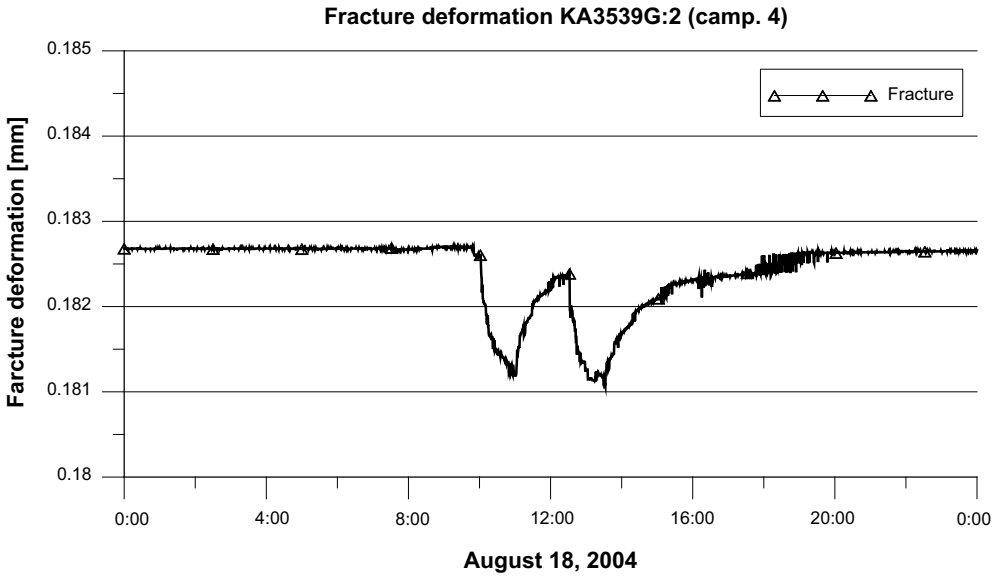

Figure 7-76. *Single fracture deformation in KA3539G:2 during test campaign 4.*

7.4.3 KA3542G01

Deformation during test campaigns

Campaign 1

No data available.

Campaign 2 (October 21–23, 2003)

Flow start: October 22 16:45 (winter time correspond to 17:45 in figures).
Flow stop: October 22 17:15 (correspond to 18:15 in figures).

- Both intact rock and rock and fracture behave as expected.
- The second dip and peak (19:15–19:45) is the response of the test performed in KA3548A01.
- The fracture deformation during the pressure build-up test is approximately 36 µm compression of fracture at a pressure drop of 3,238 kPa.
- The second pulse generates a pressure drop in KA3542G01:3 of 542 kPa and a fracture deformation approximately 7 µm compression of fracture in magnitude.

(Figure 7-77, Figure 7-78).

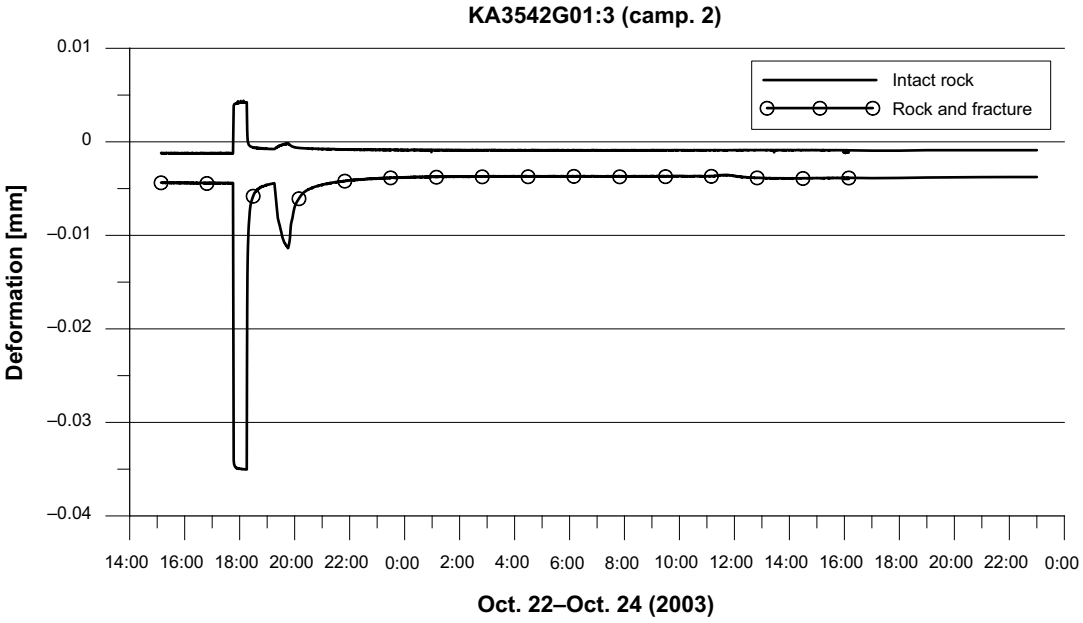

Figure 7-77. *Rock and fracture and intact rock deformation in KA3542G01:3 during test campaign 2.*

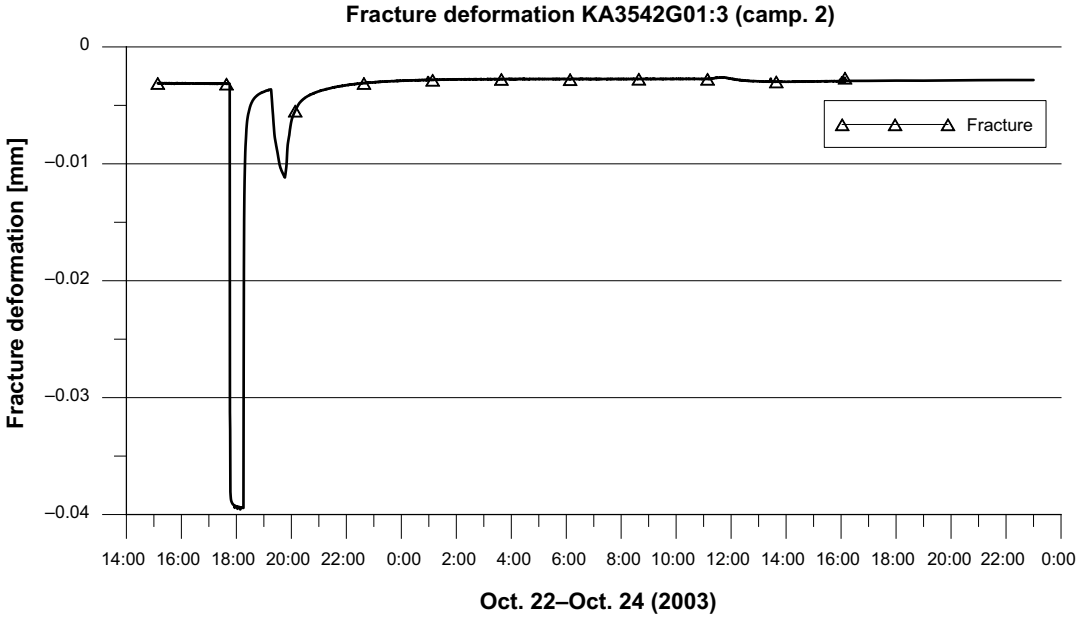

Figure 7-78. *Single fracture deformation in KA3542G01:3 during test campaign 2.*

Campaign 3 (February 2–4, 2004)

Flow start: February 3 13:00.
Flow stop: February 3 14:00.

- Both intact rock and rock and fracture behave as expected.
- The second dip and peak (16:00–17:00) is the response of the test performed in KA3548A01:3.
- The fracture deformation during the pressure build-up test is approximately 35 µm compression of fracture at a pressure drop of 3,117 kPa.
- The second pulse generates a pressure drop in KA3542G01:3 of 729 kPa and a fracture deformation approximately 10 µm compression of fracture in magnitude.

(Figure 7-79, Figure 7-80).

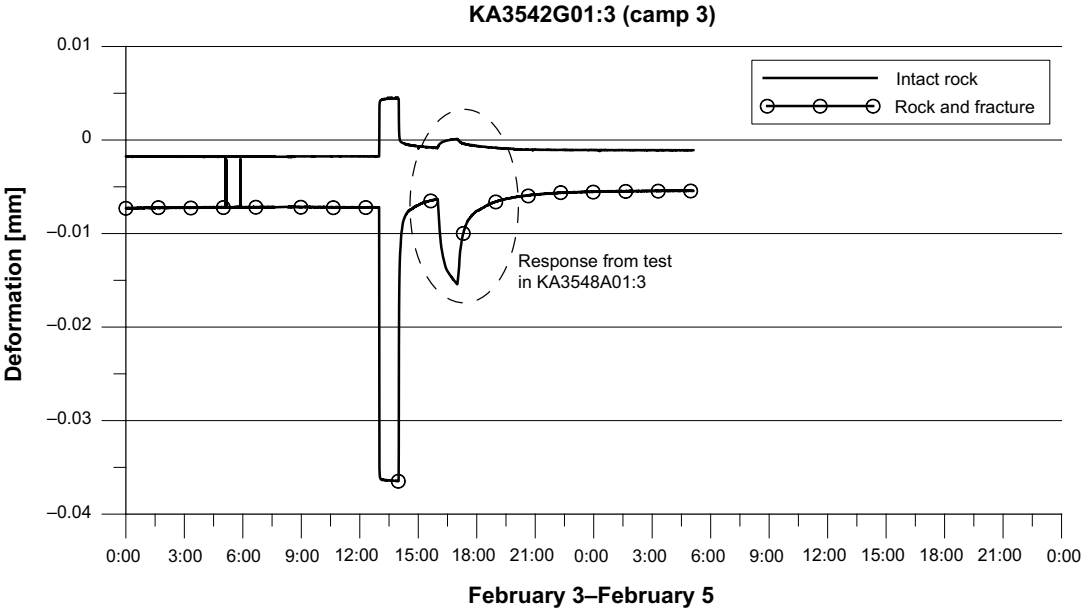

Figure 7-79. *Rock and fracture and intact rock deformation in KA3542G01:3 during test campaign 3.*

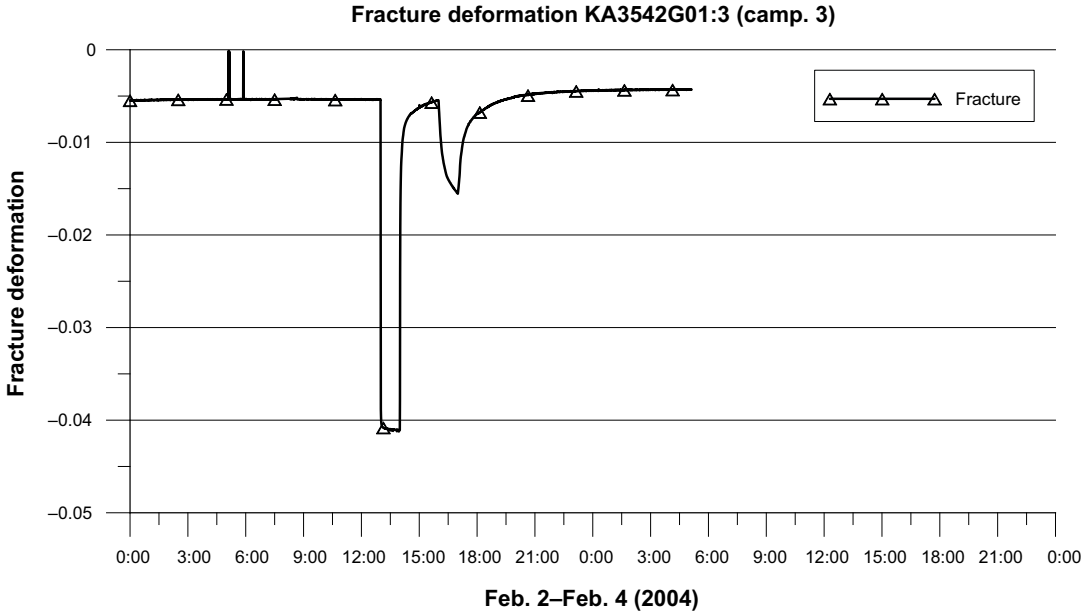

Figure 7-80. *Single fracture deformation in KA3542G01:3 during test campaign 3.*

Campaign 4 (August 11–18, 2004)

Flow start and stop: August 16 11:05–12:05 (correspond to 10:05–11:05 in figure).
Flow start and stop: August 16 14:35–15:35 (correspond to 13:35–14:35 in figure).
Flow start and stop: August 16 17:35–18:35 (correspond to 16:35–17:35 in figure).

- During the flow period the temperature decreases c. 0.01°C (Very uncertain observation) in the section with the fractures and in the section with "intact rock" the temperature increases less than c. 0.01°C (Very uncertain observation). The temperature corrections applied (deformation shown in the figure is the temperature corrected deformation), are then approximately 0.04 µm in the section with the fractures and in the section with "intact rock".
- The fracture deformation during the pressure build-up test is approximately 20 µm compression of fracture at a pressure drop of 1,430 kPa.
- The fracture deformation during the pressure build-up test is approximately 26 µm compression of fracture at a pressure drop of 2,432 kPa.
- The fracture deformation during the pressure build-up test is approximately 33 µm compression of fracture at a pressure drop of 2,992 kPa.

When the test section in KA3548A01:3 was flowed 2004-08-18 07:35–08:35 the pressure drop in KA3542G01:3 was 771 kPa and a fracture deformation approximately 11 µm compression of fracture in magnitude.

(Figure 7-81, Figure 7-82, Figure 7-83).

Campaigns 5–7

No data available.

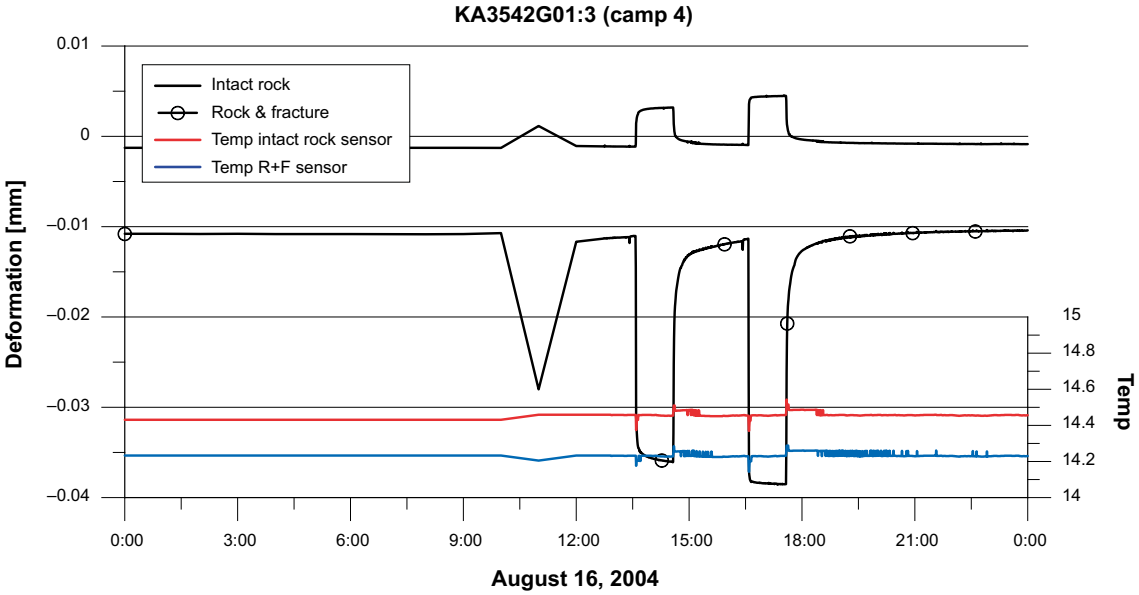

Figure 7-81. *Rock and fracture and intact rock deformation in KA3542G01:3 during test campaign 4.*

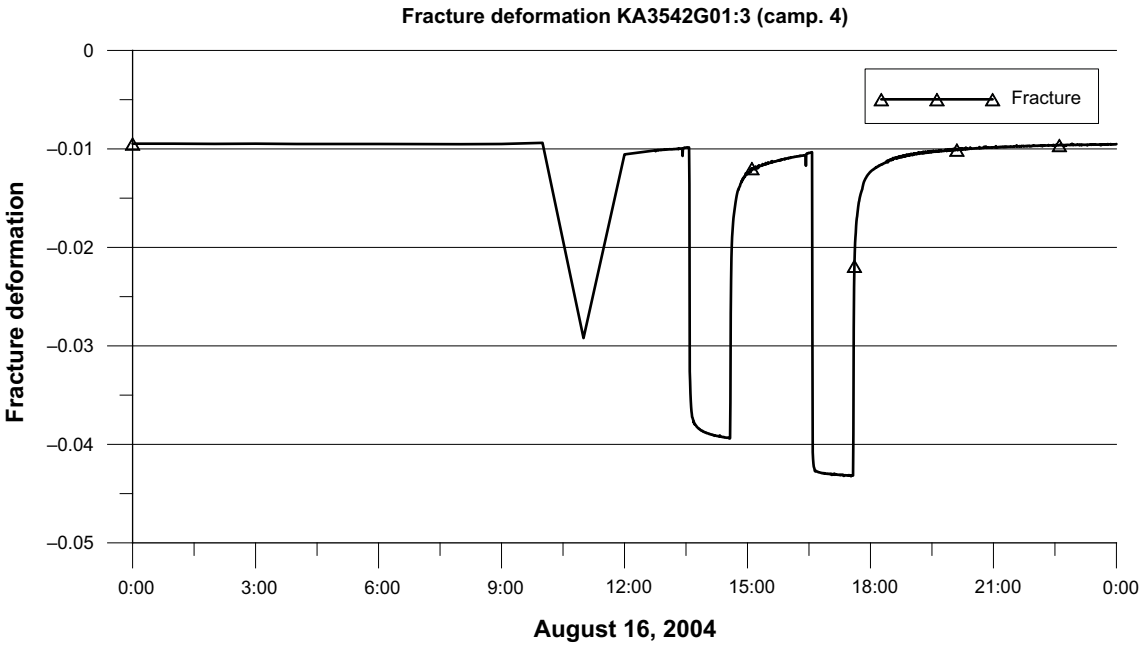

Figure 7-82. *Single fracture deformation in KA3542G01:3 during test campaign 4.*

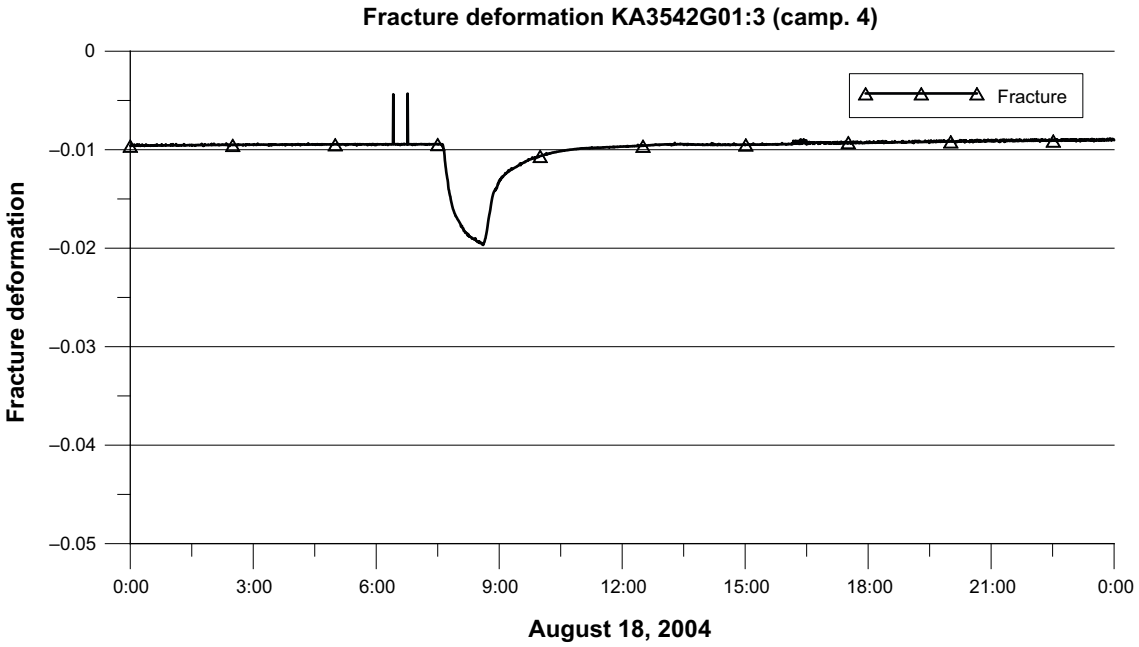

Figure 7-83. *Single fracture deformation in KA3542G01:3 during test campaign 4. The effect of the flowing of KA3548A01:3 is shown in the diagram.*

7.4.4 KA3542G02

Deformation during test campaigns

Campaign 1

No data available.

Campaign 2 (October 21–23, 2003)

Flow start: October 23 7:15 (winter time correspond to 8:15 in figures).
Flow stop: October 23 9:15 (correspond to 10:15 in figures).

- The response is larger in that part that includes the fracture.
- The intact rock expands during the release of the hydrostatic pressure and that is in accordance with the expected behaviour.
- The fracture behaviour is hard to explain since it seems that the fracture width has increased when the hydrostatic pressure is released. It is considered as unrealistic.

(Figure 7-84, Figure 7-85).

Campaigns 3–7

No data available.

7.4.5 KA3544G01

Deformation during test campaigns

Campaigns 1–7

No data available.

7.4.6 KA3546G01

Deformation during test campaigns

Campaigns 1–7

No data available.

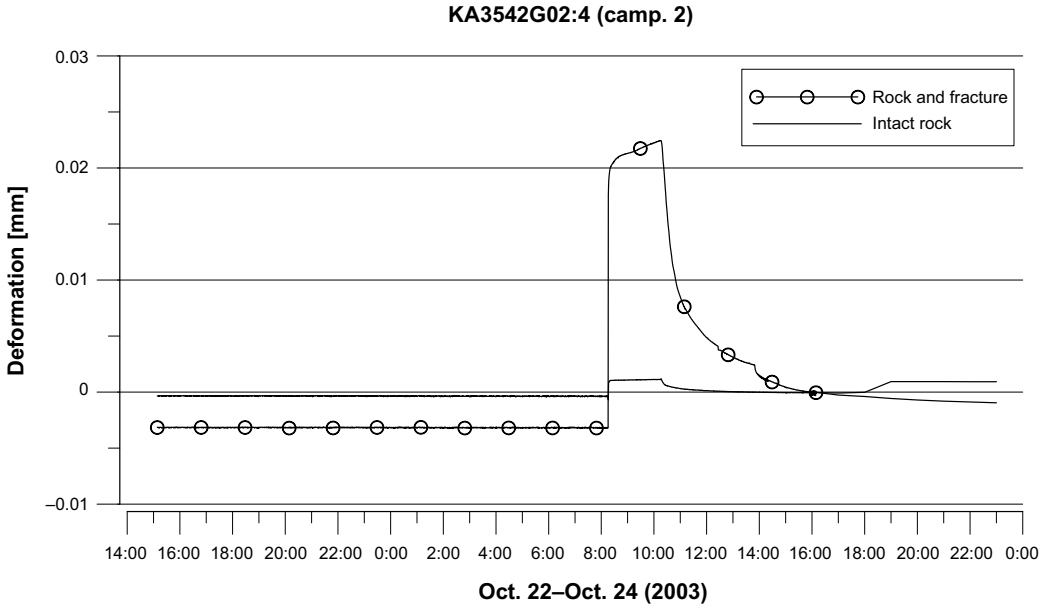

Figure 7-84. *Rock and fracture and intact rock deformation in KA3542G02:4 during test campaign 2.*

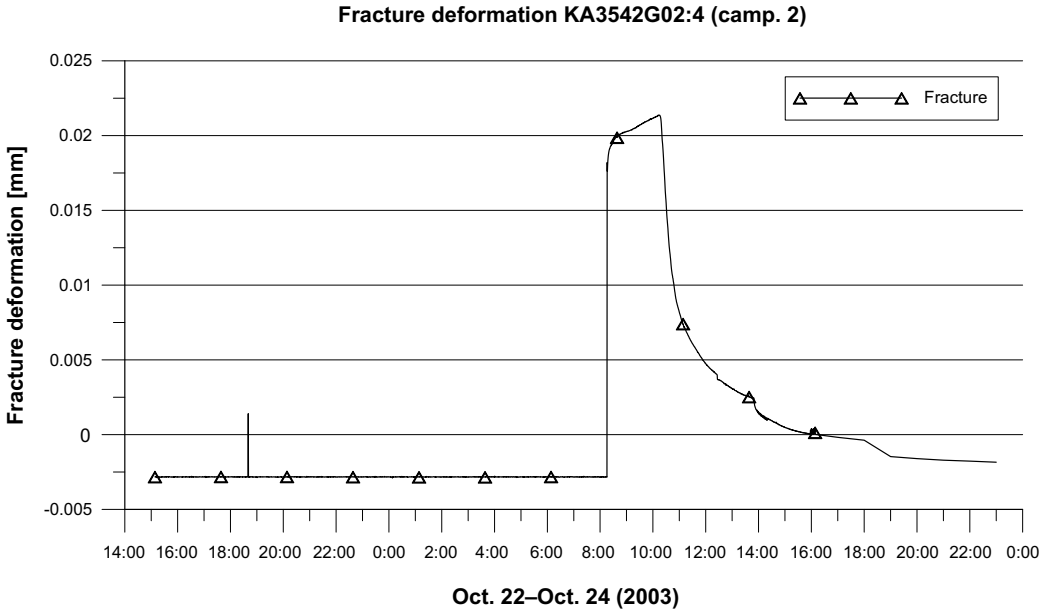

Figure 7-85. *Single fracture deformation in KA3542G02:4 during test campaign 2.*

7.4.7 KA3548A01

Deformation during test campaigns

Campaign 1

No data available.

Campaign 2 (October 21–23, 2003)

Flow start: October 22 18:15 (winter time correspond to 19:15 in figures).
Flow stop: October 22 18:45 (correspond to 19:45 in figures).

- The behaviour of the rock and fracture deformation curve during the pressure build-up tests is unstable and is hard to evaluate.

(Figure 7-86, Figure 7-87).

Campaign 3 (February 2–4, 2004)

Flow start: February 3 16:00.
Flow stop: February 3 17:00.

- The behaviour of the rock and fracture deformation curve during the pressure build-up tests is unstable and is hard to evaluate.

Campaign 4–7

No data available.

7.4.8 KA3550G01

Deformation during test campaigns

Campaigns 1–7

No data available.

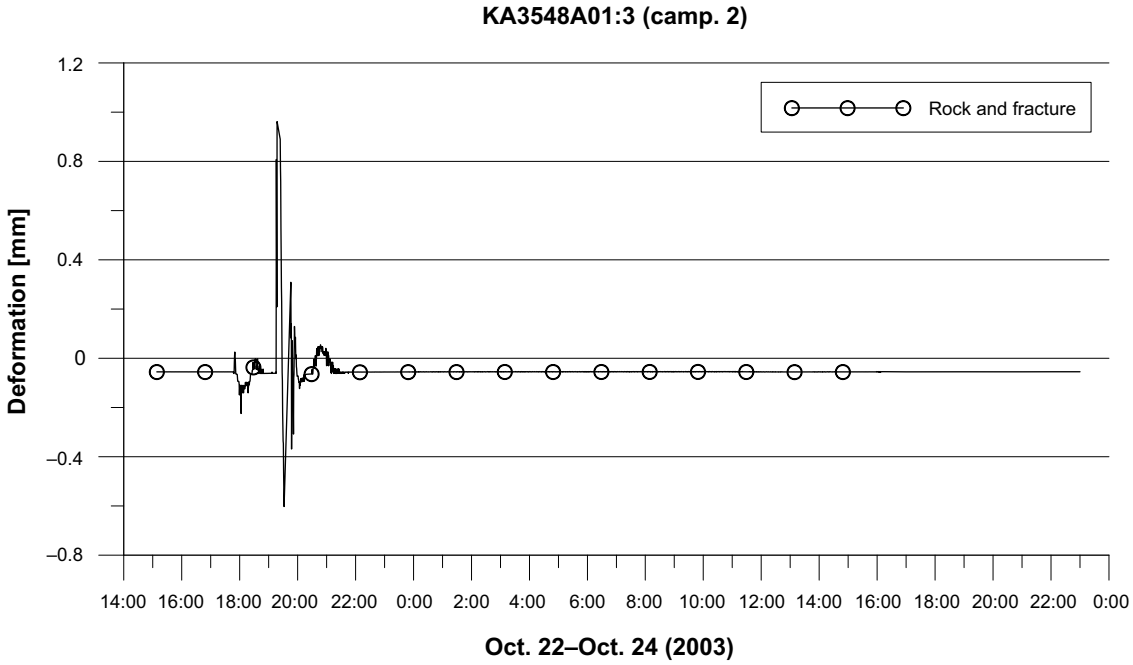

Figure 7-86. *Rock and fracture deformation in KA3548A01:3 during test campaign 2.*

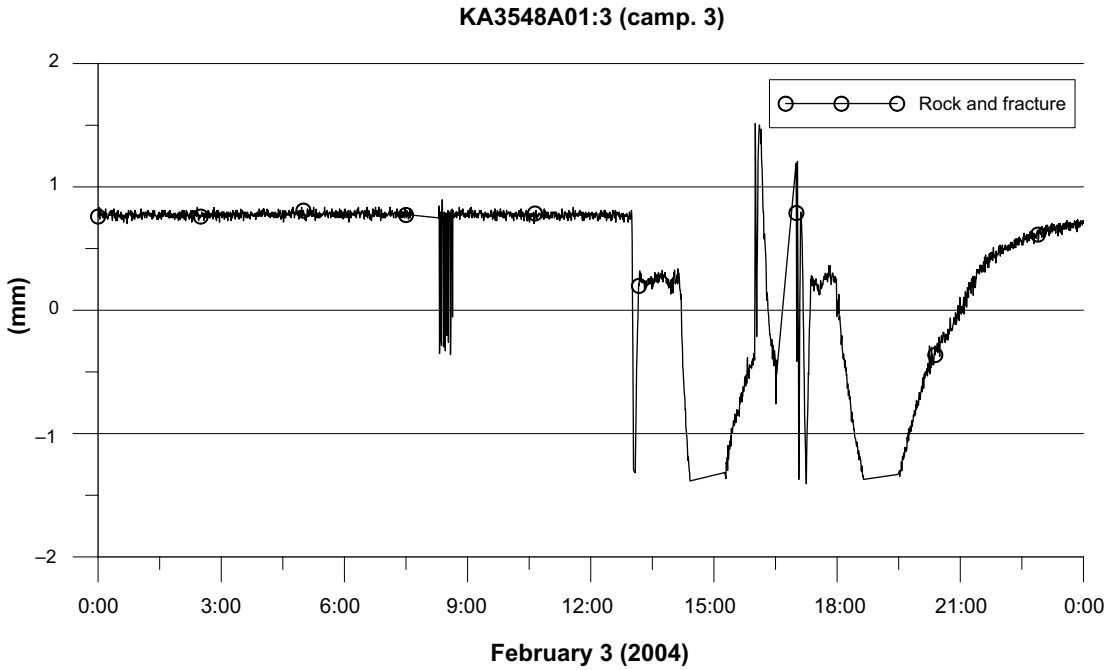

Figure 7-87. *Rock and fracture deformation in KA3548A01:3 during test campaign 3.*

7.4.9 KA3552G01

Deformation during test campaigns

Campaigns 1–7

No data available.

7.4.10 KA3554G01

Deformation during test campaigns

Campaigns 1–2

No data available.

Campaign 3 (February 2–4, 2004)

Flow start: February 2 17:30.
Flow stop: February 2 19:30.

- During the pressure build-up test the fracture behave as expected with compression after the hydrostatic pressure is released.
- The fracture deformation during the pressure build-up test is approximately 33 µm compression of fracture at a pressure drop of 3,159 kPa.
- A permanent deformation of 2 µm compression of fracture remains after the pressure build-up test.

(Figure 7-88, Figure 7-89).

Campaign 4 (August 11–18, 2004)

Flow start and stop: August 17 08:50–10:50 (correspond to 07:50–09:50 in figure).
Flow start and stop: August 17 13:10–15:10 (correspond to 12:10–14:10 in figure).
Flow start and stop: August 17 16:10–18:10 (correspond to 15:10–17:10 in figure).

- During the flow period the temperature is more or less constant in the section with the fractures and in the section with "intact rock" the temperature decreases more or less linearly c. 0.25°C during the test period. (The decrease related to the stop of the heaters, 2004-11-01 to 2004-12-06?) The temperature corrections applied (deformation shown in the figure is the temperature corrected deformation), for a single test are then approximately 0 µm in the section with the fractures and in the section with "intact rock" approximately 0.4 µm during a single test.
- For some reason the fracture width does not decrease after the flow stops at 18:10. It remains "open" for approximately an hour until its "closes". Since the hydrostatic pressure in the section recovers following a normal pattern it is probably due to some kind of equipment problem. It is not re-observed during TC 5 or TC 6.
- The fracture deformation during the pressure build-up test is approximately 11 µm compression of fracture at a pressure drop of 1,282 kPa.
- The fracture deformation during the pressure build-up test is approximately 22 µm compression of fracture at a pressure drop of 2,095 kPa.
- The fracture deformation during the pressure build-up test is approximately 33 µm compression of fracture at a pressure drop of 3,072 kPa.

(Figure 7-90, Figure 7-91).

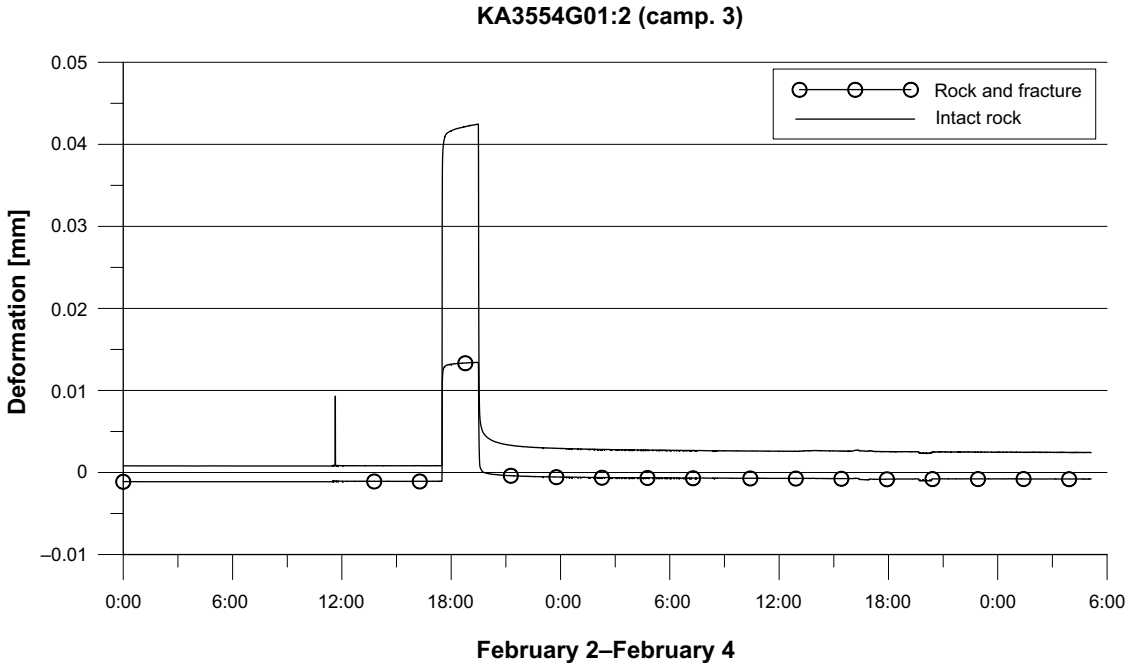

Figure 7-88. *Rock and fracture and intact rock deformation in KA3554G01:2 during test campaign 3.*

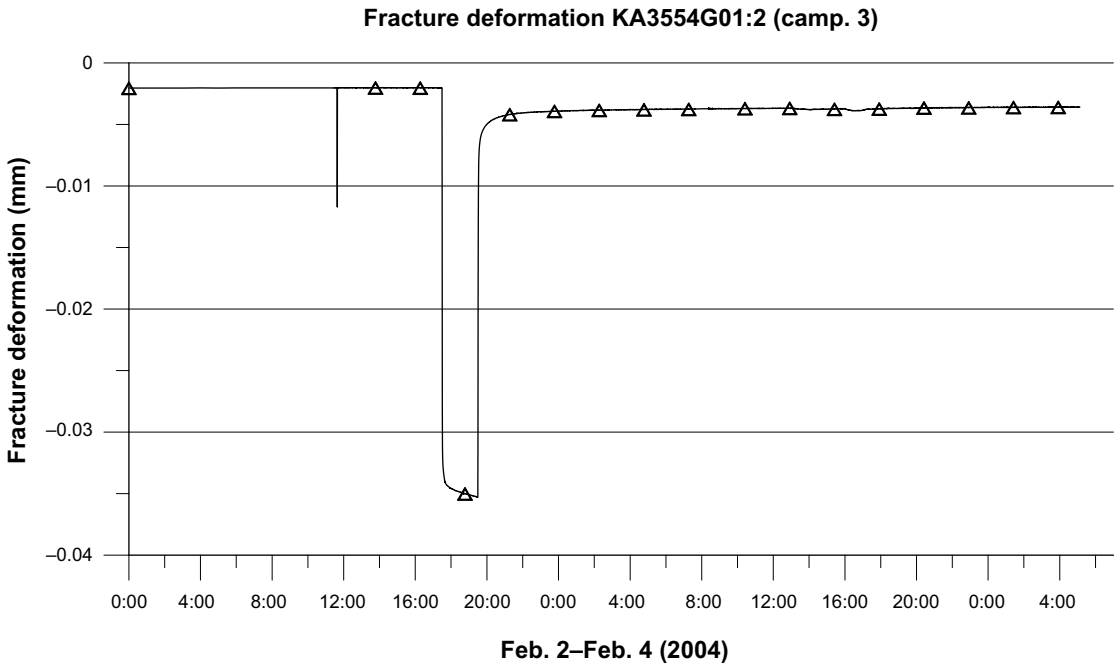

Figure 7-89. *Single fracture deformation in KA3554G01:2 during test campaign 3.*

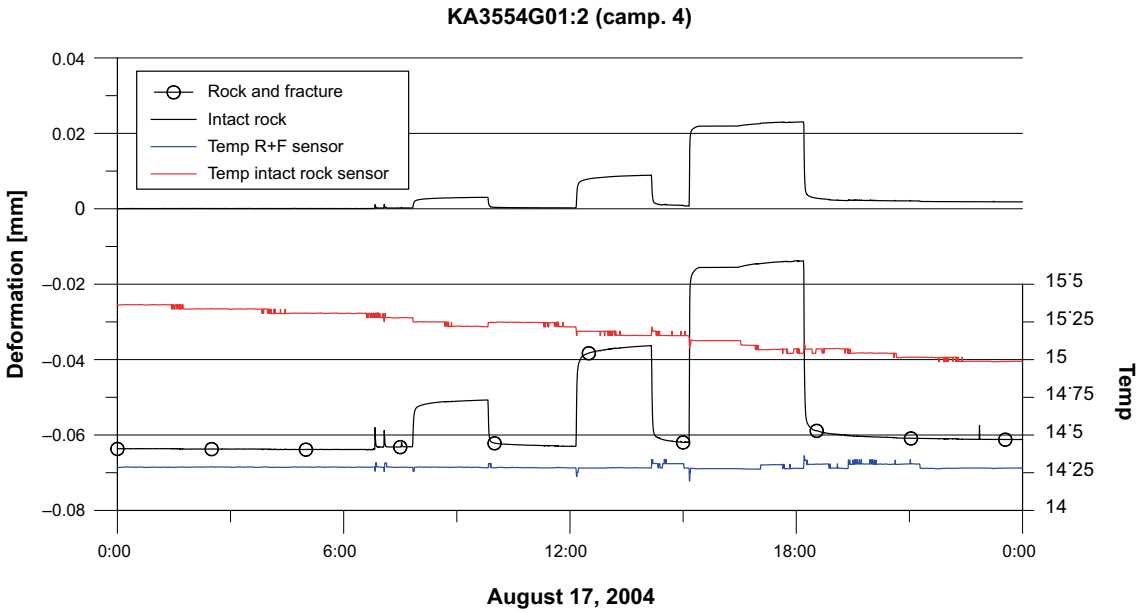

Figure 7-90. *Rock and fracture and intact rock deformation in KA3554G01:2 during test campaign 4.*

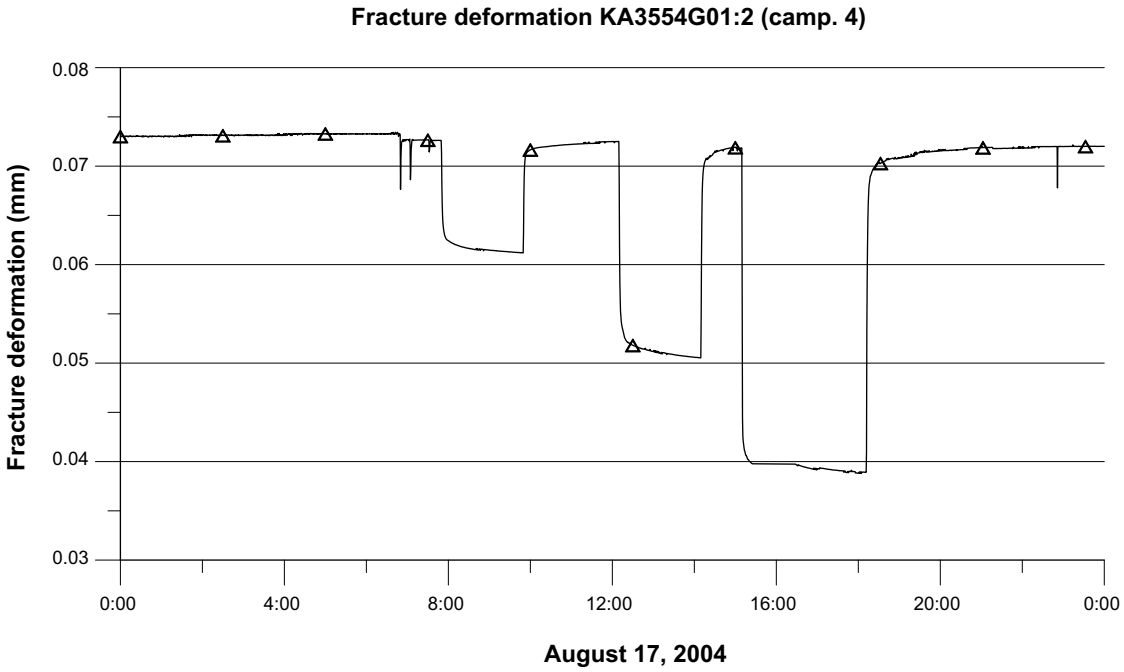

Figure 7-91. *Single fracture deformation in KA3554G01:2 during test campaign 4.*

Campaign 5 (January 19–25, 2005)

Flow start and stop: January 20 12:30–14:30.
Flow start and stop: January 21 12:00–14:00.
Flow start and stop: January 22 15:00–21:00 (Interference test).

- During the flow period the temperature decreases linearly c. 0.3°C in the section with the fractures and in the section with "intact rock" the temperature decreases c. 0.4°C. (The decrease related to the stop of the heaters, 2004-11-01 to 2004-12-06?) The temperature corrections applied (deformation shown in the figure is the temperature corrected deformation), for a single test are then less than approximately 0.2 µm in the section with the fractures and in the section with "intact rock".
- The fracture deformation during the pressure build-up test is approximately 6 µm compression of fracture at a pressure drop of 728 kPa.
- The fracture deformation during the pressure build-up test is approximately 21 µm compression of fracture at a pressure drop of 1,990 kPa.
- The fracture deformation during the pressure build-up test is approximately 32 µm compression of fracture at a pressure drop of 2,950 kPa.

(Figure 7-92, Figure 7-93).

Campaign 6 (November 28–December 2, 2005)

Flow start and stop: November 28 19:00–21:00.
Flow start and stop: November 29 18:00–20:00.
Flow start and stop: November 30 18:00–20:00.

- During the flow period the temperature decreases maximum c. 0.1°C in the section with the fractures and in the section with "intact rock" the temperature change is more or less c. 0°C during a test. The temperature corrections applied (deformation shown in the figure is the temperature corrected deformation), for a single test are then less than approximately 0.4 µm in the section with the fractures and 0 µm in the section with "intact rock".
- The fracture deformation during the pressure build-up test is approximately 10 µm compression of fracture at a pressure drop of 1,077 kPa.
- The fracture deformation during the pressure build-up test is approximately 21 µm compression of fracture at a pressure drop of 2,020 kPa.
- The fracture deformation during the pressure build-up test is approximately 28 µm compression of fracture at a pressure drop of 2,868 kPa.

(Figure 7-94, Figure 7-95).

Campaign 7 (September 25–September 29, 2006)

Flow start and stop: September 25 13:00–15:00.
Flow start and stop: September 26 10:00–12:00.
Flow start and stop: September 27 09:00–11:00.

- The fracture deformation during the pressure build-up test is approximately 6 µm compression of fracture at a pressure drop of 656 kPa.
- The fracture deformation during the pressure build-up test is approximately 12 µm compression of fracture at a pressure drop of 1,370 kPa.
- The fracture deformation during the pressure build-up test is approximately 25 µm compression of fracture at a pressure drop of 2,310 kPa.

(Figure 7-96, Figure 7-97).

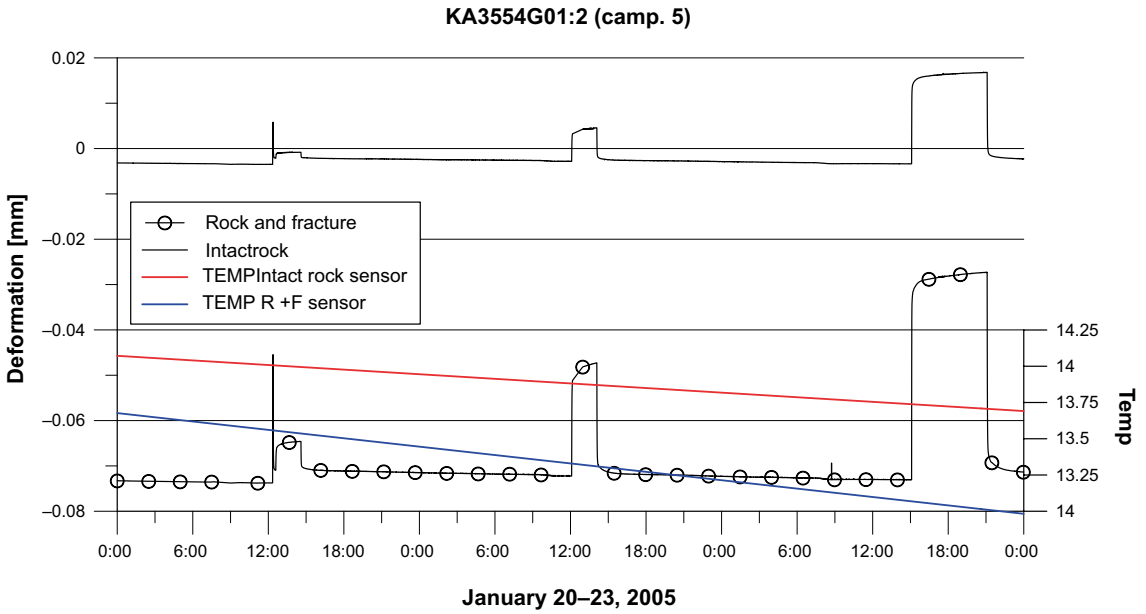

Figure 7-92. *Rock and fracture and intact rock deformation in KA3554G01:2 during test campaign 5.*

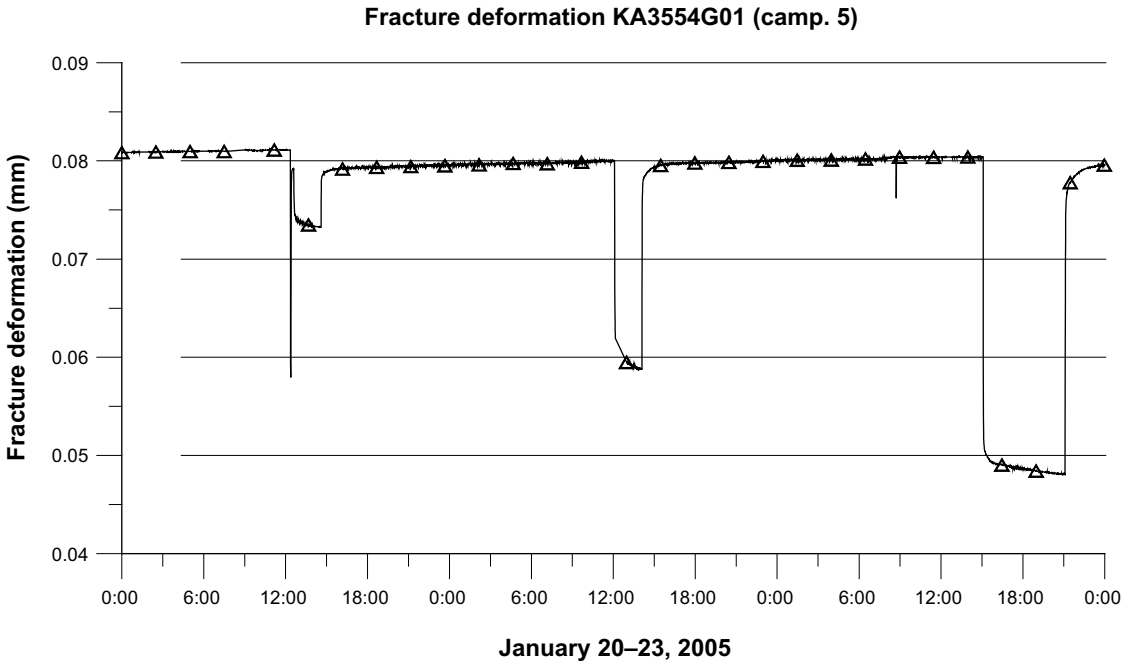

Figure 7-93. *Single fracture deformation in KA3554G01:2 during test campaign 5.*

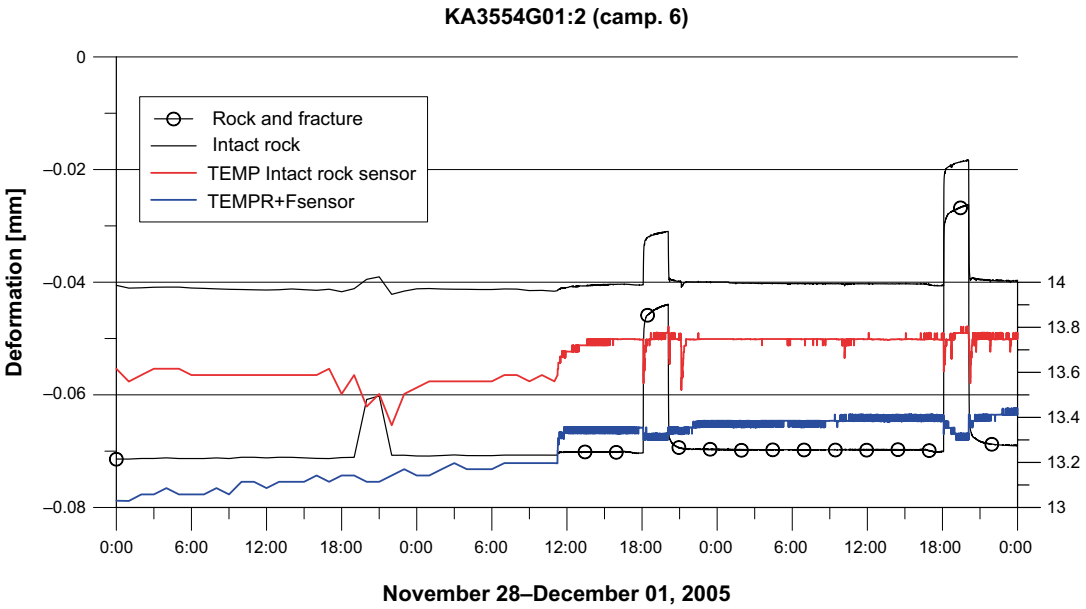

Figure 7-94. *Rock and fracture and intact rock deformation in KA3554G01:2 during test campaign 6.*

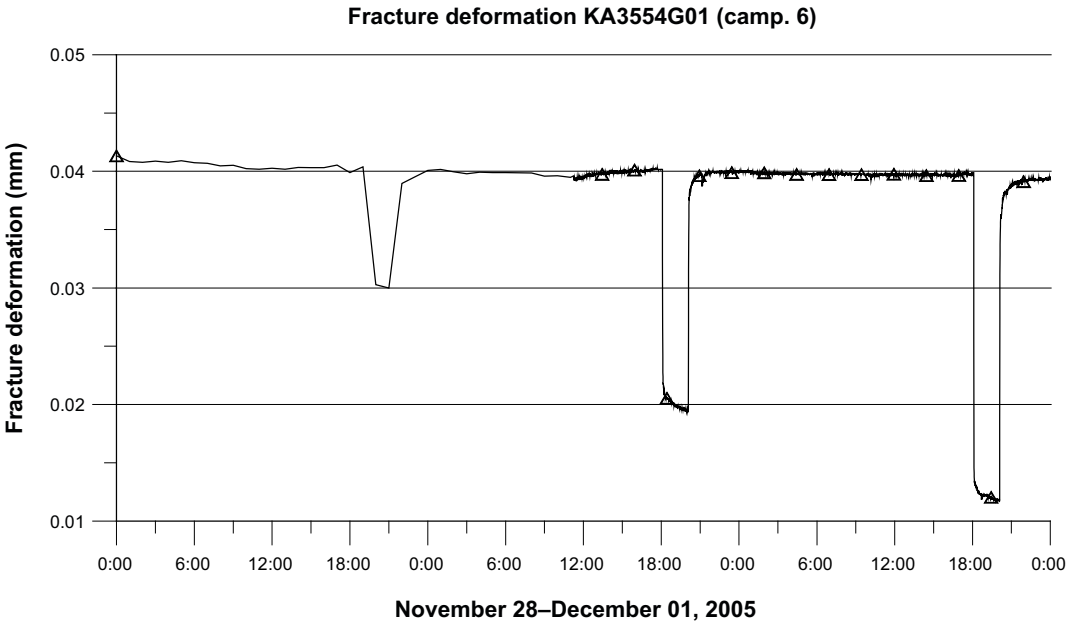

Figure 7-95. *Single fracture deformation in KA3554G01:2 during test campaign 6.*

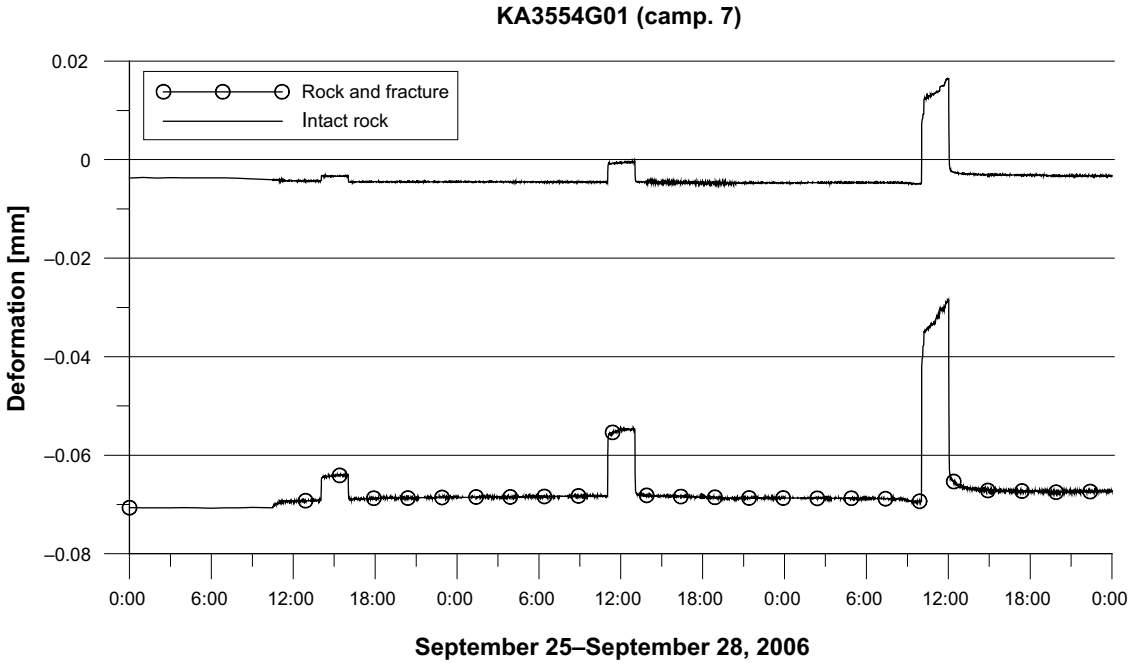

Figure 7-96. Rock and fracture and intact rock deformation in KA3554G01:2 during test campaign 7.

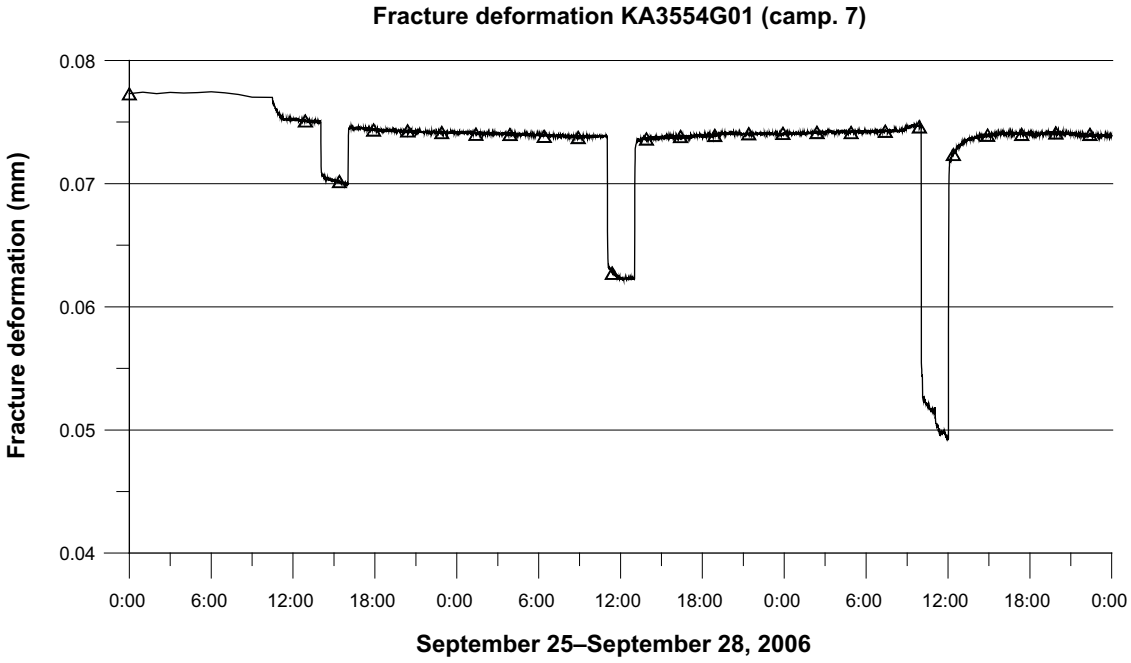

Figure 7-97. Single fracture deformation in KA3554G01:2 during test campaign 7.

7.4.11 KA3554G02

Deformation during test campaigns

Campaigns 1–2

No data available.

Campaign 3 (February 2–4, 2004)

Flow start: February 2 14:30.
Flow stop: February 2 16:30.

- A momentary expansion of the fracture followed by a period of both decreasing and increasing width. It is difficult to explain the behaviour.

(Figure 7-98, Figure 7-99).

Campaign 4 (August 11–18, 2004)

Flow start and stop: August 12 14:10–16:10
Flow start and stop: August 12 17:10–19:10

- The fracture behaviour is hard to explain since it seems that the fracture width has increased when the hydrostatic pressure is released. It is considered as unrealistic.

(Figure 7-100, Figure 7-101).

Campaign 5–7

No data available.

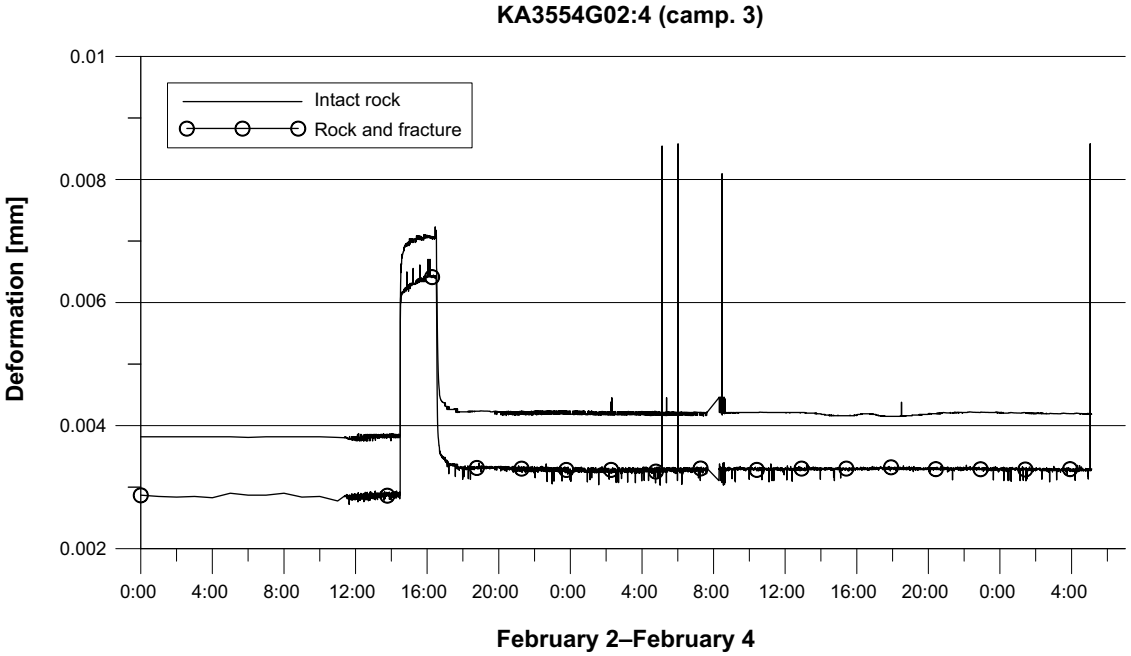

Figure 7-98. *Rock and fracture and intact rock deformation in KA3554G02:4 during test campaign 3.*

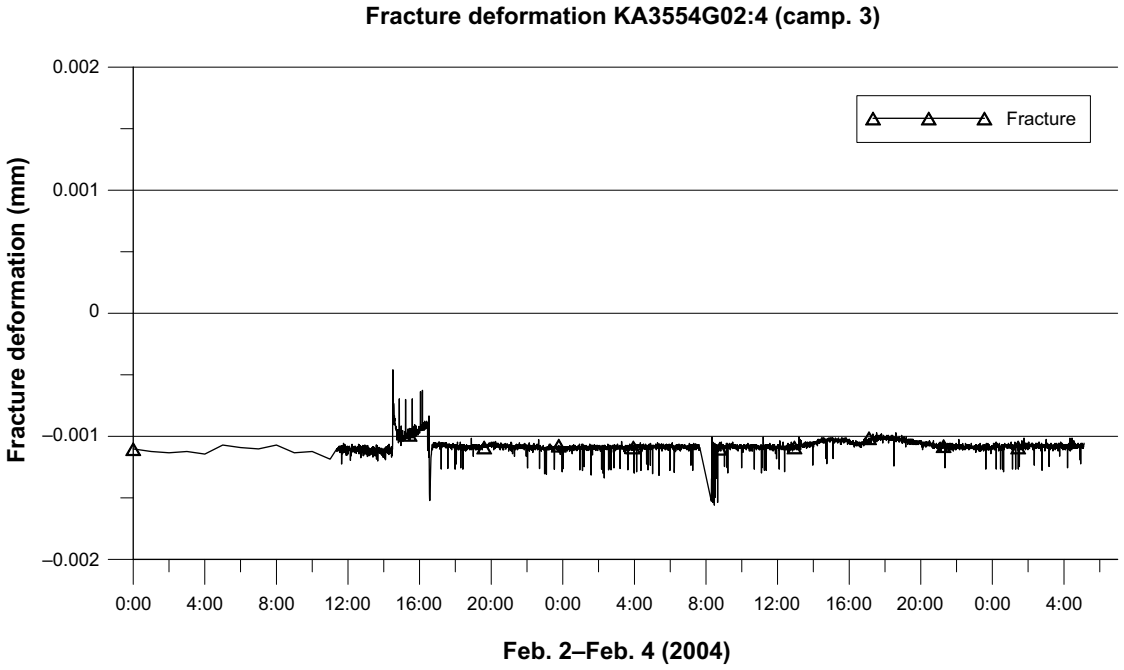

Figure 7-99. *Single fracture deformation in KA3554G02:4 during test campaign 3.*

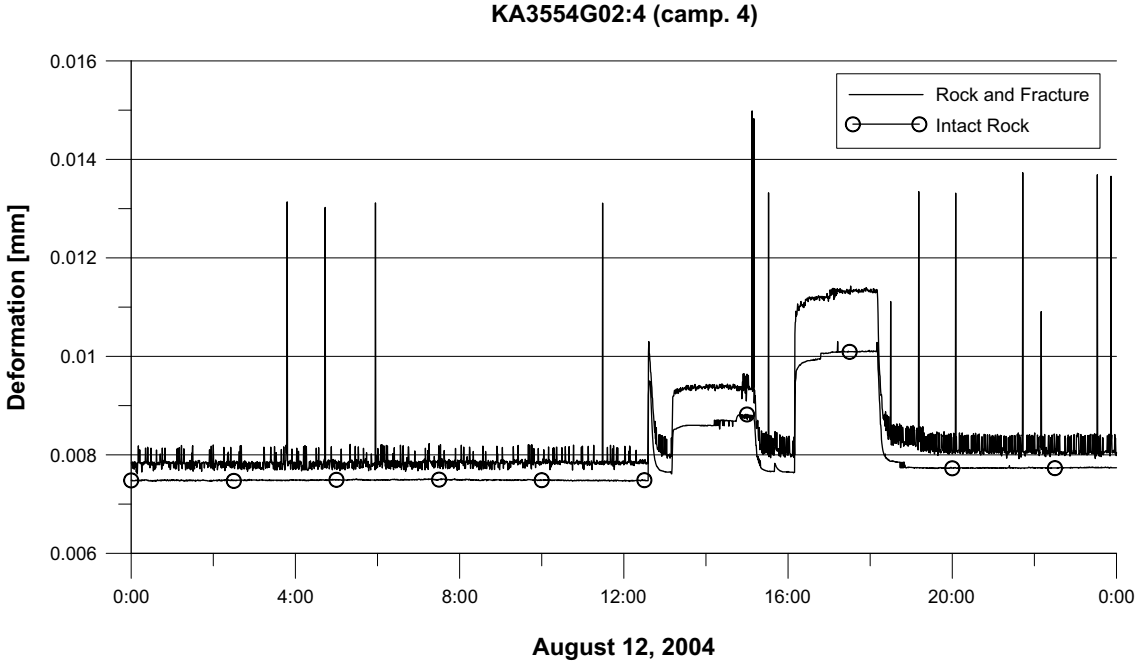

Figure 7-100. *Rock and fracture and intact rock deformation in KA3554G02:4 during test campaign 4.*

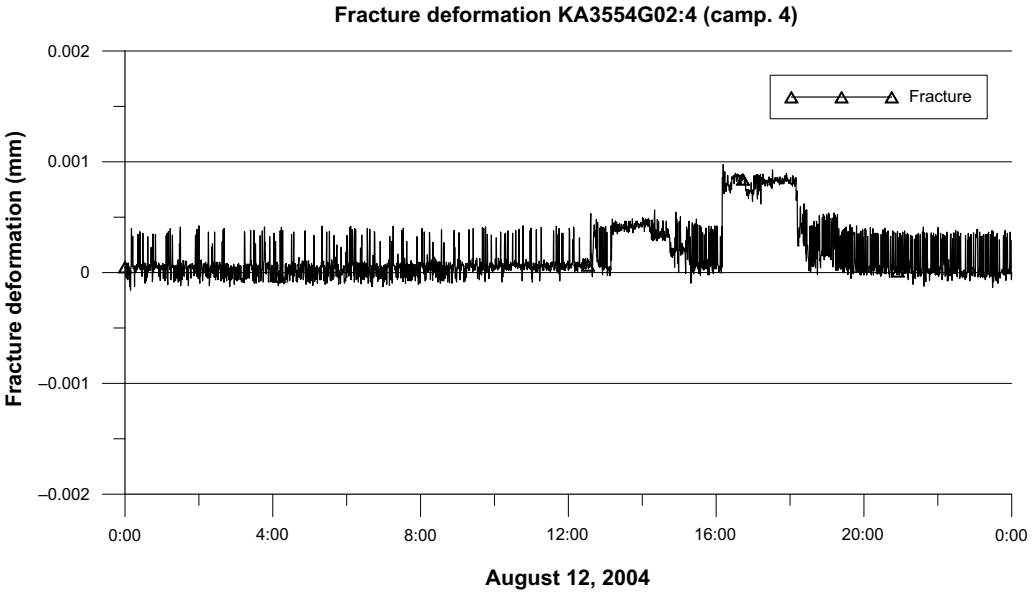

Figure 7-101. *Single fracture deformation in KA3554G02:4 during test campaign 4.*

7.5 Summary of measurements and comments to expected behaviour

A summary of the hydromechanical measurements (July 2009) is done in the table below. Dates for the hydraulic measurement campaigns were presented in Chapter 2.

Out of 22 temperature sensors within the hydromechanical equipment only 13 are still working 2006-10-01.

By 2010-01-01 only 4 out of the 22 temperature sensors were working and of the HM sensors only the rock and fracture sensor in KA3542G02:4 was in operation.

Table 7-2. Status of the long-term measurements 2009-07-01. An OK means that it has been possible to evaluate the measurement data. To evaluate the fracture properties it is necessary to have good data from both the intact rock and the rock and fracture sensor.

Borehole	Intact rock sensor	Rock and fracture sensor	Fracture def. calc.	Comments
KG0010B01	–	–		The temperature is affected of the air temperature in the tunnel. The borehole is a reference hole for undisturbed conditions (i.e. undisturbed by the heaters). The rock and fracture deformation is not evaluated. Measurements failed 2006-09-30.
KA3539G:2	–	–		The rock and fracture measurements failed in February 2005 and the intact rock sensor in mid-2008.
KA3542G01:3	–	–		The rock and fracture measurements failed in February 2005.
KA3542G02:4	–	OK		The rock measurements failed in February 2005 and only one sensor operates October 2006.
KA3544G01:2	–	–		The rock and fracture measurements failed in November 2003.
KA3546G01:2	–	–		The rock and fracture measurements failed in November 2003.
KA3548A01:3	–	–		The rock and fracture measurements failed in November 2003.
KA3550G01:2	–	–		Expansion of intact rock observed. The “rock and fracture”-sensor failed at July 2003. The “intact rock”-sensor failed in January 2004.
KA3552G01:2	–	–		The temperature data is replaced with data from KA3550G01:2. Both sensors failed in September 2003.
KA3554G01:2	–	–		The rock and fracture measurements failed in October 2006.
KA3554G02:4	–	–		The rock and fracture measurements failed in February 2005.

Table 7-3. Summary of the maximum fracture deformation during pressure build-up test (Test campaigns 2–4).

Borehole	Camp. 2 ΔP [kPa]	Δδ [mm]	Camp. 3 ΔP [kPa]	Δδ [µm]	Camp. 4a ΔP [kPa]	Δδ [µm]	Camp. 4b ΔP [kPa]	Δδ [µm]	Camp. 4c ΔP [kPa]	Δδ [µm]	Comments
KA3539G:2	1,364	–1.3	1,465	–1.6	1,035	–1.4	1,242	–1.3	–	–	
KA3542G01:3	3,238	–36	3,117	–35	1,430	–20?	2,432	–26	2,992	–33	This section is influenced by the flowing of KA3548A01:3.
Flowing of KA3548A01:3	542	–7	729	–10	771	–11	–	–	–	–	
KA3542G02:2	1,849	+25?	–	–	–	–	–	–	–	–	The fracture width increases which is unrealistic!?
KA3544G01:2	–	–	–	–	–	–	–	–	–	–	Logger problem during camp. 2. The inner sensor failed in mid August (camp. 3).
KA3546G01:2	–	–	–	–	–	–	–	–	–	–	Logger problem during camp. 2. The outer sensor failed in February 2004.
KA3548A01:3	–	–	–	–	–	–	–	–	–	–	Bad data quality.
KA3550G01:2	–	–	–	–	–	–	–	–	–	–	Failure of packer system.
KA3552G01:2	–	–	–	–	–	–	–	–	–	–	Failure of sensors in Sept 2003.
KA3554G01:2	–	–	3,159	–33	1,282	–11	2,095	–22	3,072	–33	Good test series.
KA3554G02:4	–	–	2,032	+0.4	1,017	+0.5	1,908	+0.8	–	–	The fracture width increases which is unrealistic!?

Table 7-4. Summary of the maximum fracture deformation during pressure build-up test (Test campaigns 5–6).

Borehole	Camp. 5a ΔP [kPa]	Δδ [µm]	Camp. 5b ΔP [kPa]	Δδ [µm]	Camp. 5c ΔP [kPa]	Δδ [µm]	Camp. 6a ΔP [kPa]	Δδ [µm]	Camp. 6b ΔP [kPa]	Δδ [µm]	Camp. 6c ΔP [kPa]	Δδ [µm]	Comments
KA3539G:2	–	–	–	–	–	–	–	–	–	–	–	–	
KA3542G01:3	–	–	–	–	–	–	–	–	–	–	–	–	
KA3542G02:2	–	–	–	–	–	–	–	–	–	–	–	–	
KA3544G01:2	–	–	–	–	–	–	–	–	–	–	–	–	
KA3546G01:2	–	–	–	–	–	–	–	–	–	–	–	–	
KA3548A01:3	–	–	–	–	–	–	–	–	–	–	–	–	
KA3550G01:2	–	–	–	–	–	–	–	–	–	–	–	–	
KA3552G01:2	–	–	–	–	–	–	–	–	–	–	–	–	
KA3554G01:2	728	–6	1,990	–21	2,950	–32	1,077	–10	2,020	–21	2,868	–28	Good tests.
KA3554G02:4	–	–	–	–	–	–	–	–	–	–	–	–	

Table 7-5. Summary of the maximum fracture deformation during pressure build-up test (Test campaign 7).

Borehole	Camp. 7a ΔP [kPa]	Δδ [µm]	Camp. 7b ΔP [kPa]	Δδ [µm]	Camp. 7c ΔP [kPa]	Δδ [µm]	Comments
KA3539G:2	–	–	–	–	–	–	
KA3542G01:3	–	–	–	–	–	–	
KA3542G02:2	–	–	–	–	–	–	
KA3544G01:2	–	–	–	–	–	–	
KA3546G01:2	–	–	–	–	–	–	
KA3548A01:3	–	–	–	–	–	–	
KA3550G01:2	–	–	–	–	–	–	
KA3552G01:2	–	–	–	–	–	–	
KA3554G01:2	656	–5	1,370	–12	2,310	–25	Good tests.
KA3554G02:4	–	–	–	–	–	–	

The measurements in KA3542G02:2 and KA3554G02:4 show increasing fracture width, during flow phase, which is unrealistic. The reason for this is unknown.

The measurement section in KA3554G01:2 is the only functional one during TC3–TC7. The results are very good in regard to quality.

In Figure 7-102 the deformation is plotted against hydrostatic water pressure loss, dPmax, in Figure 7-103 the transmissivity is plotted against deformation and in Figure 7-104 the transmissivity is plotted against hydrostatic water pressure loss, dPmax.

In Figure 7-102 there is a more or less linear relationship between hydrostatic water pressure loss and fracture width in the data from KA3542G01:3 and KA3554G01:2. The few observations in KA3539G:2 does not indicate that the deformation changes when the pressure changes, but the observations are in a narrow pressure range.

One of the questions considered is:

- If fracture transmissivities have changed, can it be correlated to measured deformations of fractures?

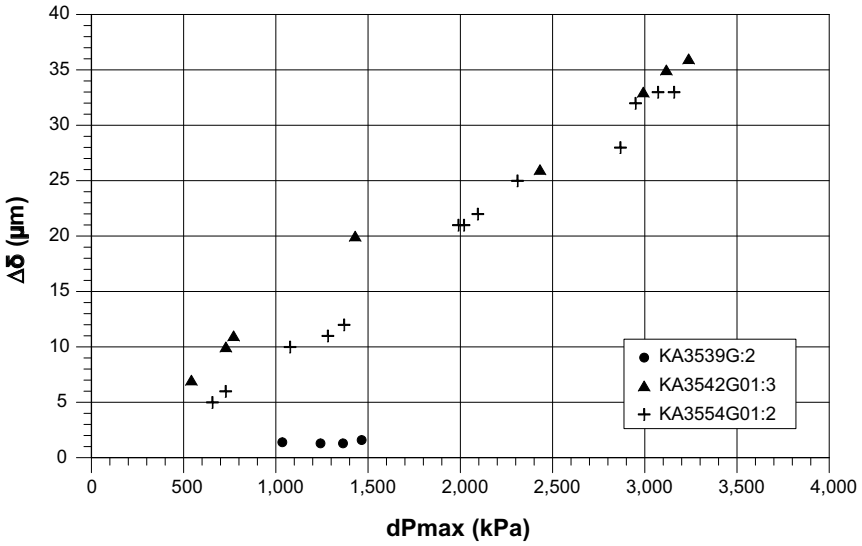

Figure 7-102. *dPmax versus maximum fracture width (Δδ) decrease during the flow period of a test.*

The Figure 7-103 show that there is a correlation as expected between the fracture width change and transmissivity but the deformations are small and the transmissivity changes are small. At the depth that the experiments were performed one can expect that all fractures are under a high stress from the outset and a stress increase due to temperature load or decrease in water pressure should just cause small deformations of the fractures. Figure 7-104 shows also that the transmissivity change is small for the applied water pressure changes.

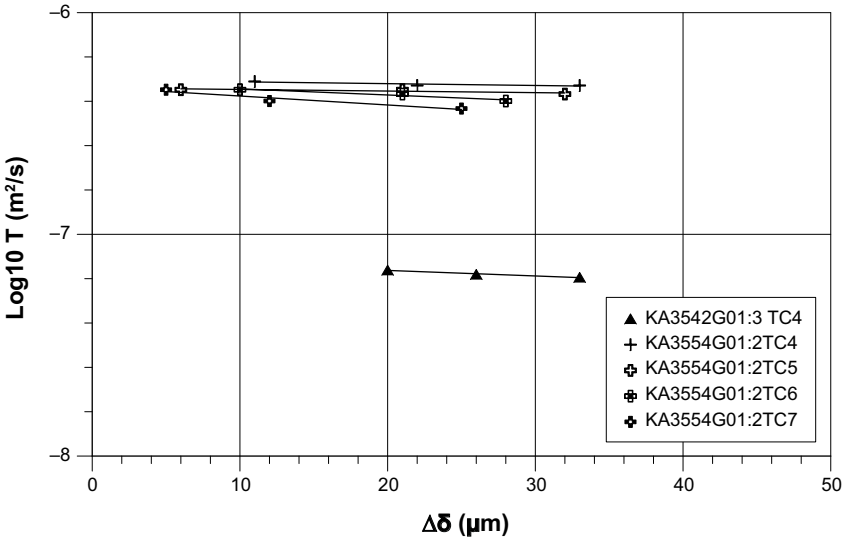

Figure 7-103. *Maximum change in fracture width (Δδ) during flowing of section versus corresponding T (data from test campaigns 4, 5, 6 and 7).*

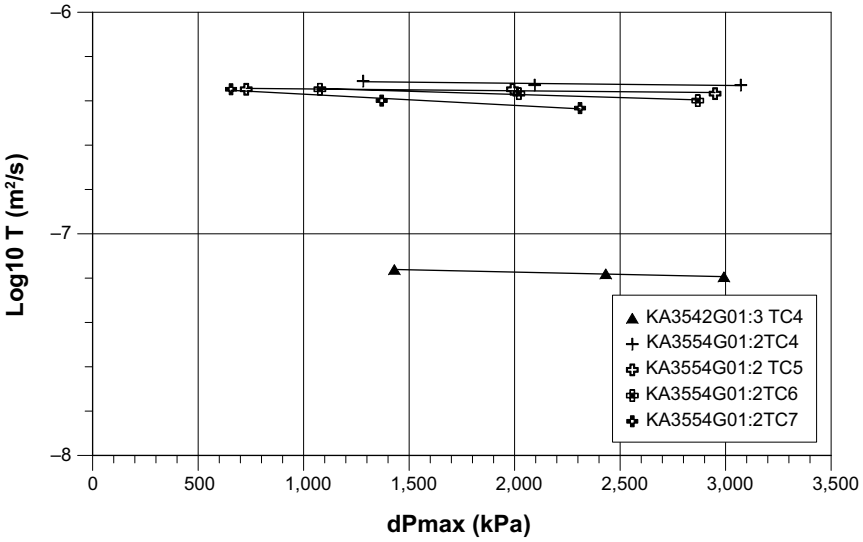

Figure 7-104. *dPmax during flowing of section versus corresponding T (data from test campaigns 4, 5, 6 and 7).*

8 Transmissivity changes until 2010-02-01

This chapter shows plots of the transmissvity changes during the operation phase period of section I and II of the Prototype repository (Appendix 4 shows all boreholes). In the plots the data is updated with the results from the last three test campaigns 8–10. Also included in this chapter are the results from certain boreholes tested which were not equipped with hydromechanical sensors. Results are commented in Chapter 9.

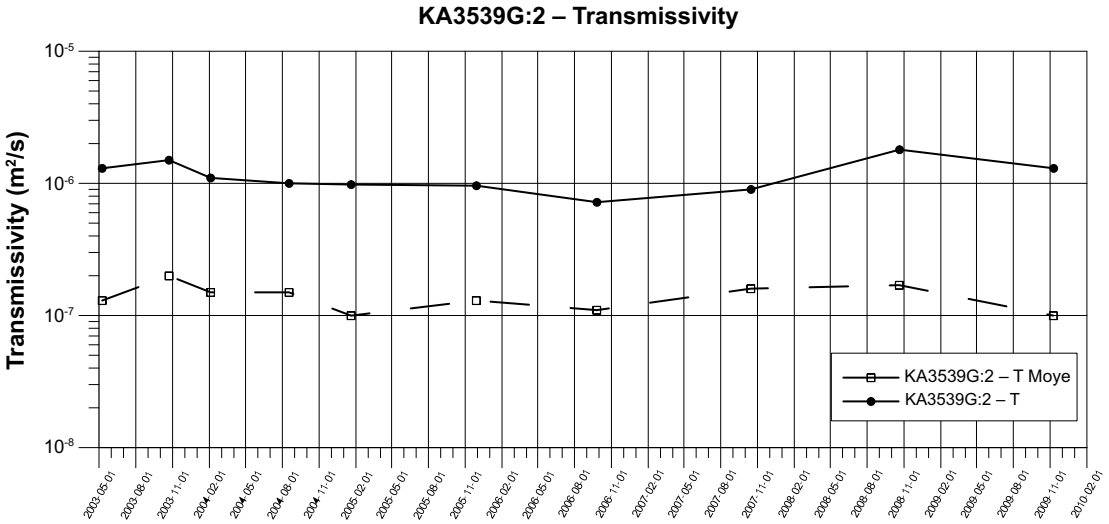

Figure 8-1. *Transmissivity change during the period 2003-05-01 to 2010-02-01 of KA3539G:2.*

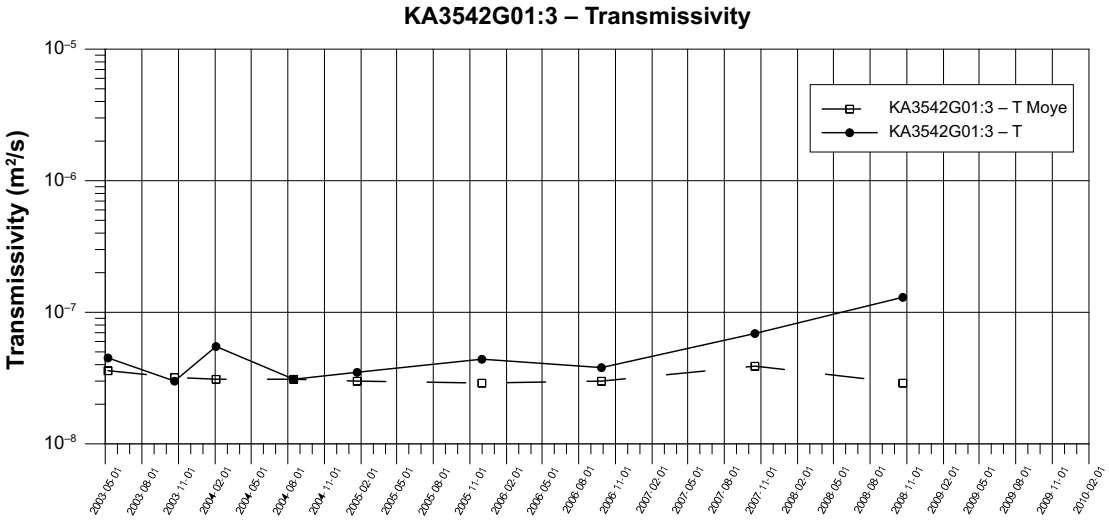

Figure 8-2. *Transmissivity change during the period 2003-05-01 to 2010-02-01 of KA3542G01:3.*

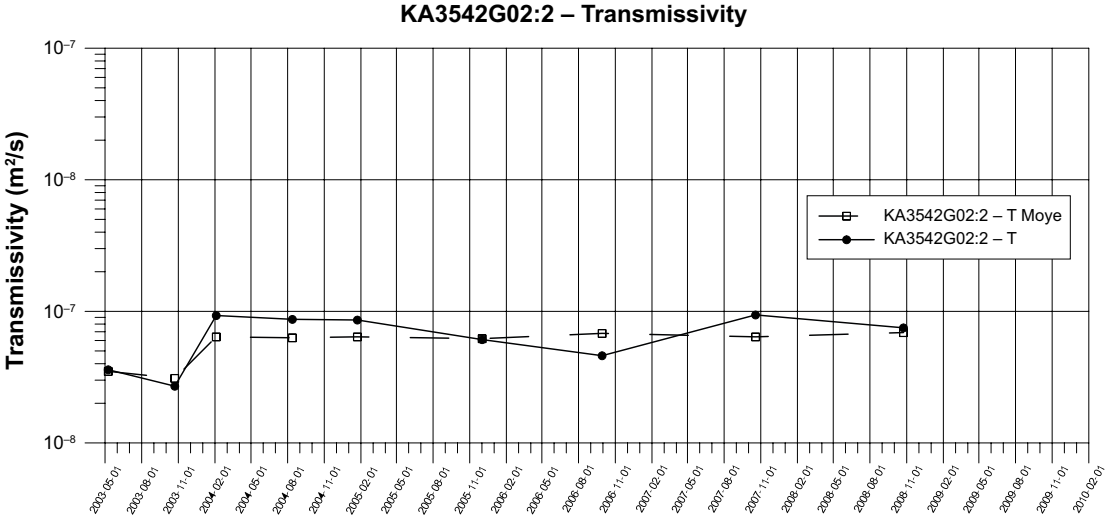

Figure 8-3. *Transmissivity change during the period 2003-05-01 to 2010-02-01 of KA3542G02:2.*

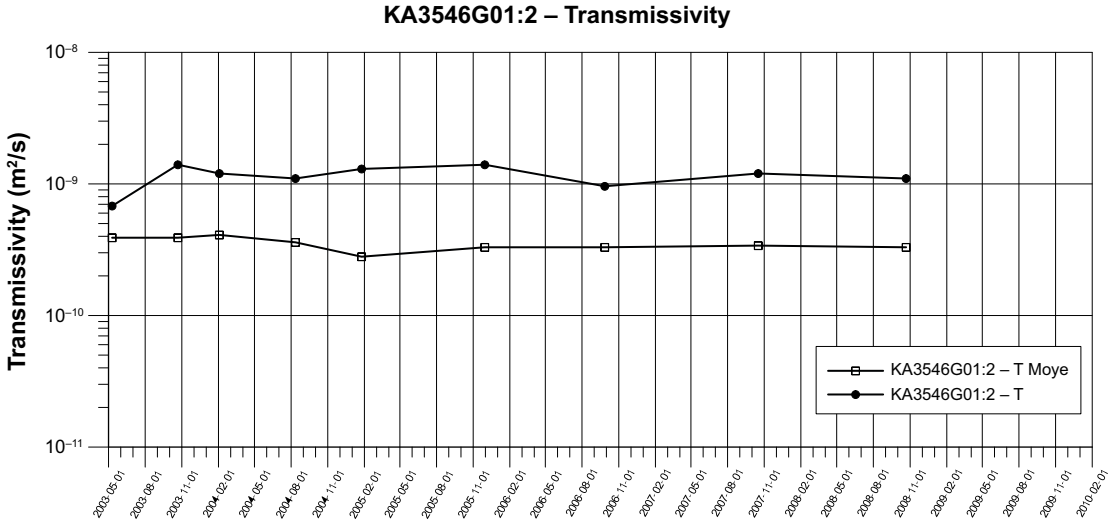

Figure 8-4. *Transmissivity change during the period 2003-05-01 to 2010-02-01 of KA3546G01:2.*

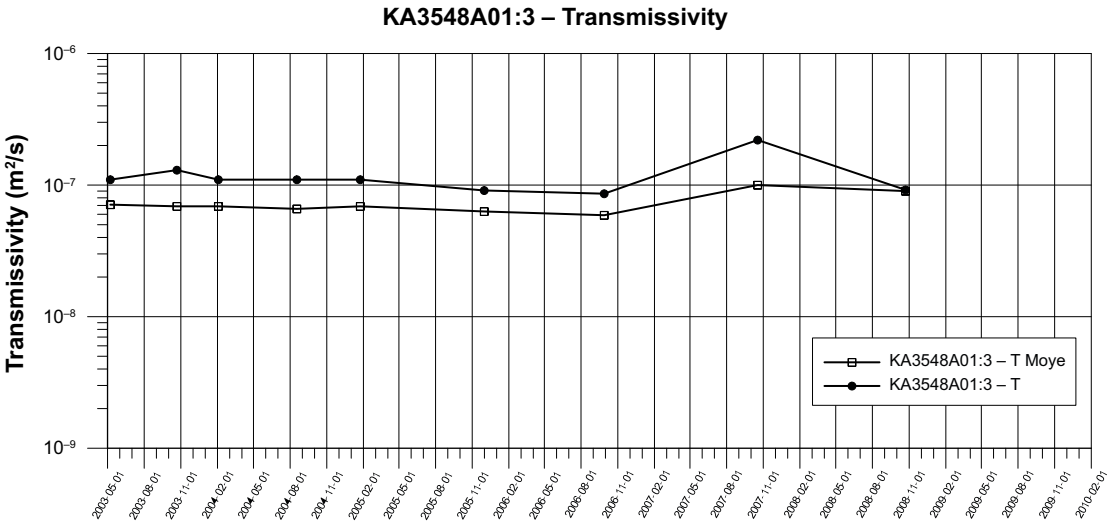

Figure 8-5. *Transmissivity change during the period 2003-05-01 to 2010-02-01 of KA3548A01:3.*

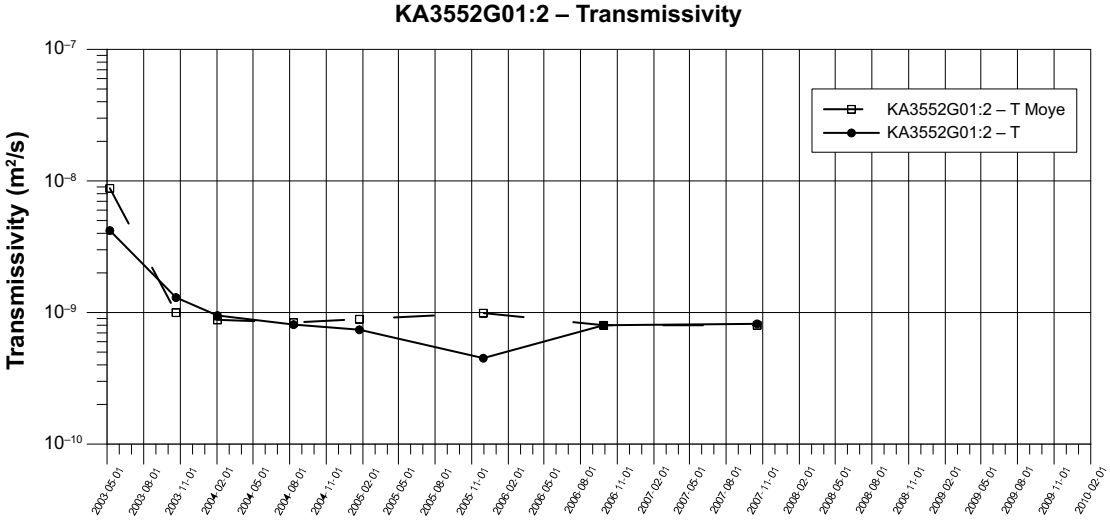

Figure 8-6. *Transmissivity change during the period 2003-05-01 to 2010-02-01 of KA3552G01:2.*

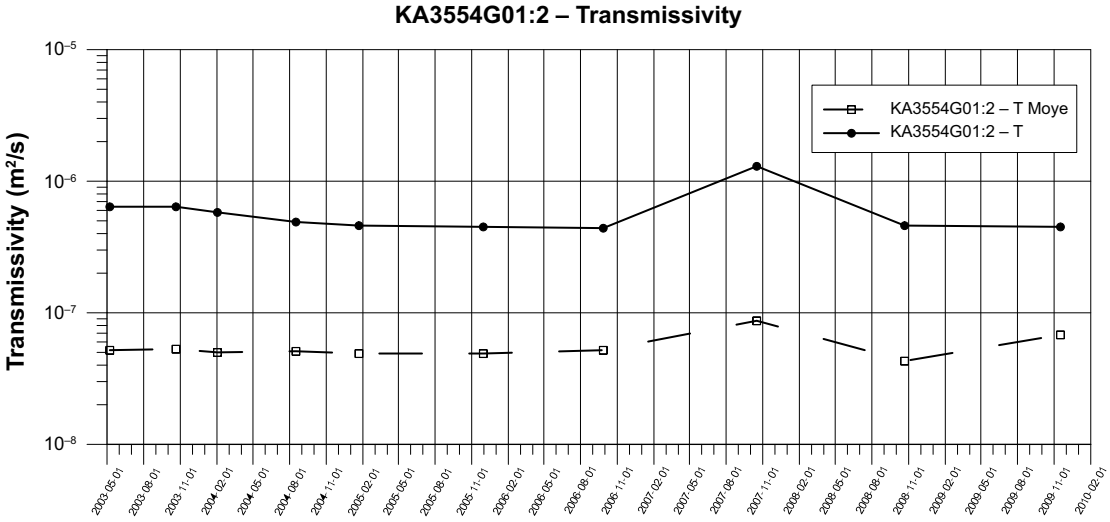

Figure 8-7. *Transmissivity change during the period 2003-05-01 to 2010-02-01 of KA3554G01:3.*

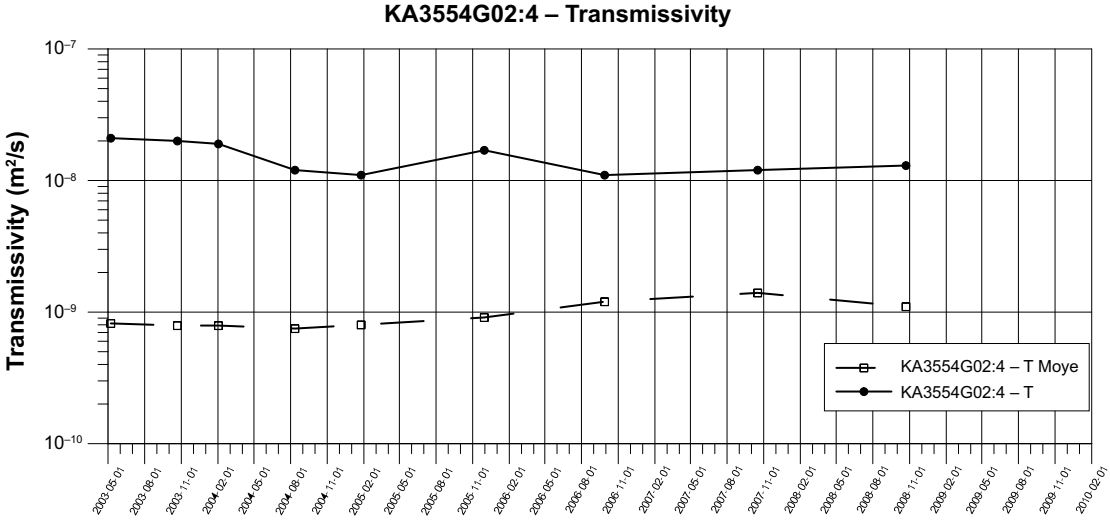

Figure 8-8. *Transmissivity change during the period 2003-05-01 to 2010-02-01 of KA3554G02:4.*

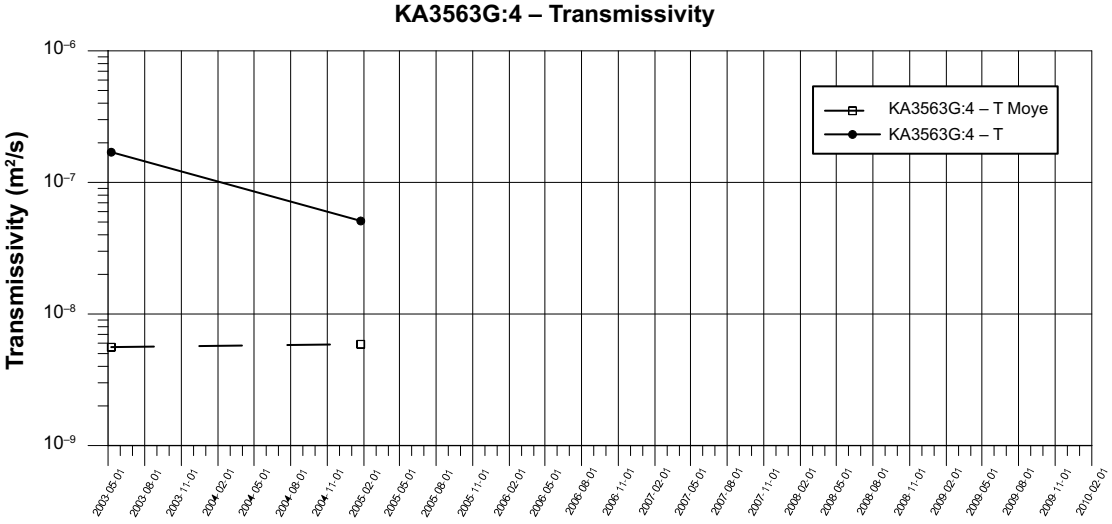

Figure 8-9. *Transmissivity change during the period 2003-05-01 to 2010-02-01 of KA3563G:4.*

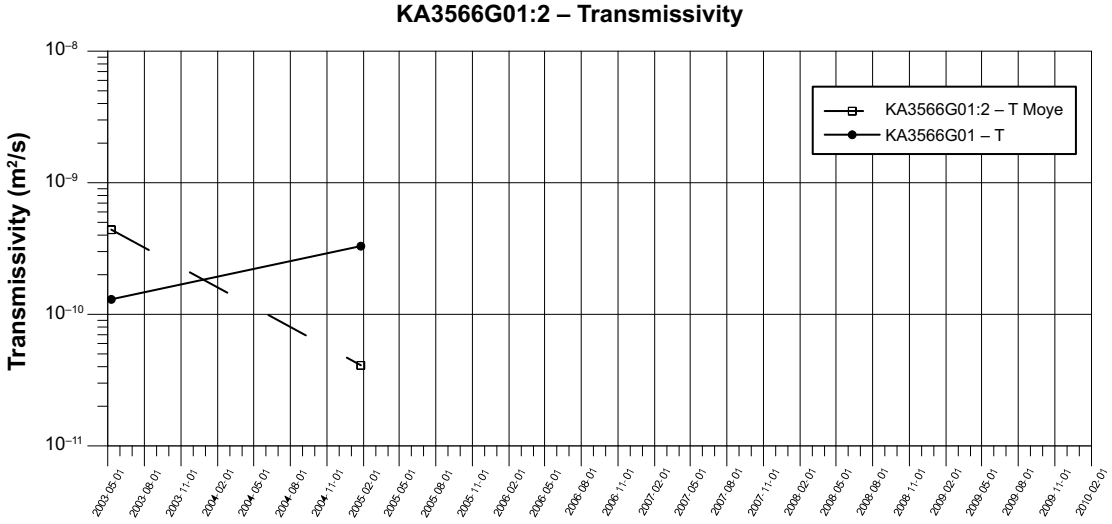

Figure 8-10. *Transmissivity change during the period 2003-05-01 to 2010-02-01 of KA3566G01:2.*

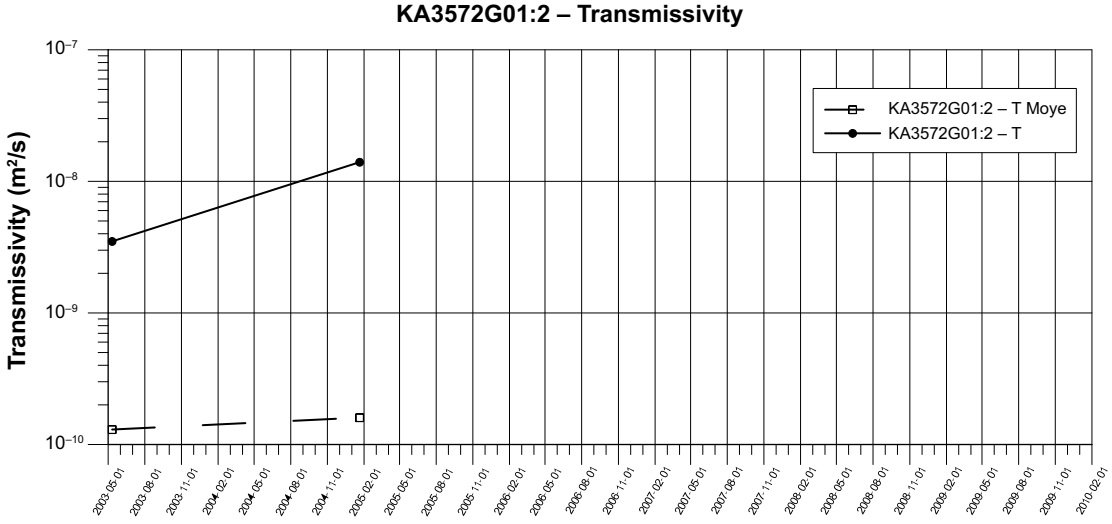

Figure 8-11. *Transmissivity change during the period 2003-05-01 to 2010-02-01 of KA3572G01:2.*

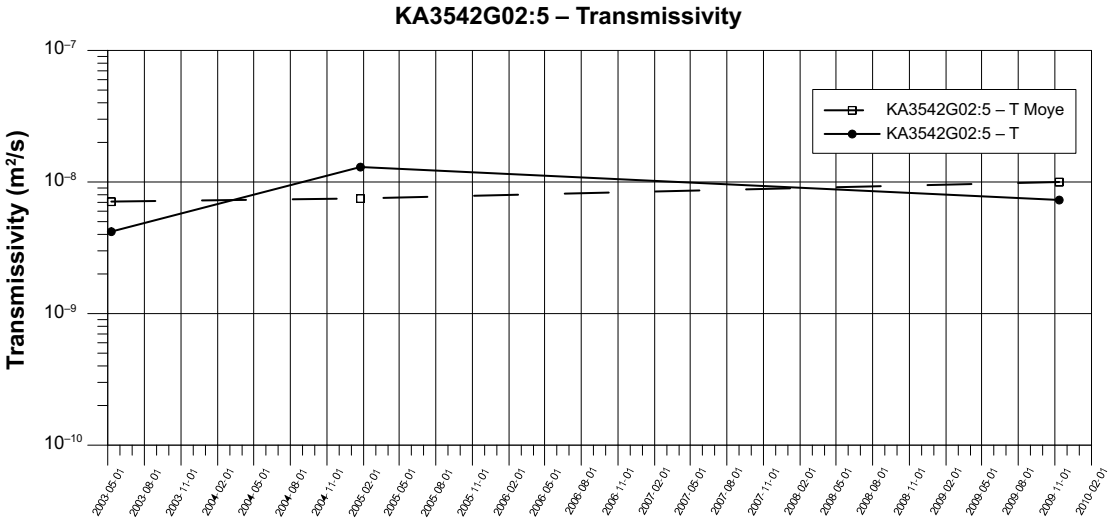

Figure 8-12. *Transmissivity change during the period 2003-05-01 to 2010-02-01 of KA3542G02:5.*

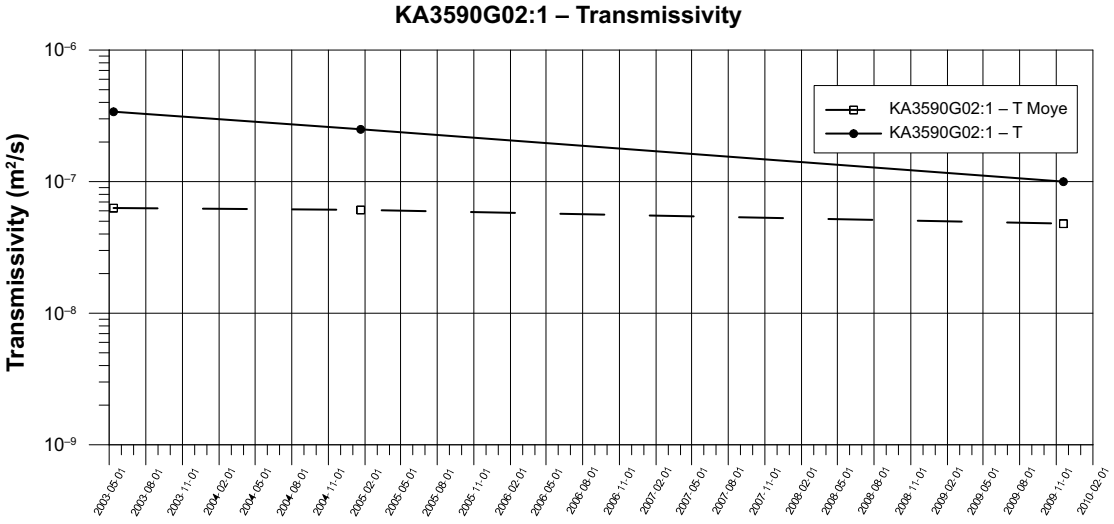

Figure 8-13. *Transmissivity change during the period 2003-05-01 to 2010-02-01 of KA3592G02:1.*

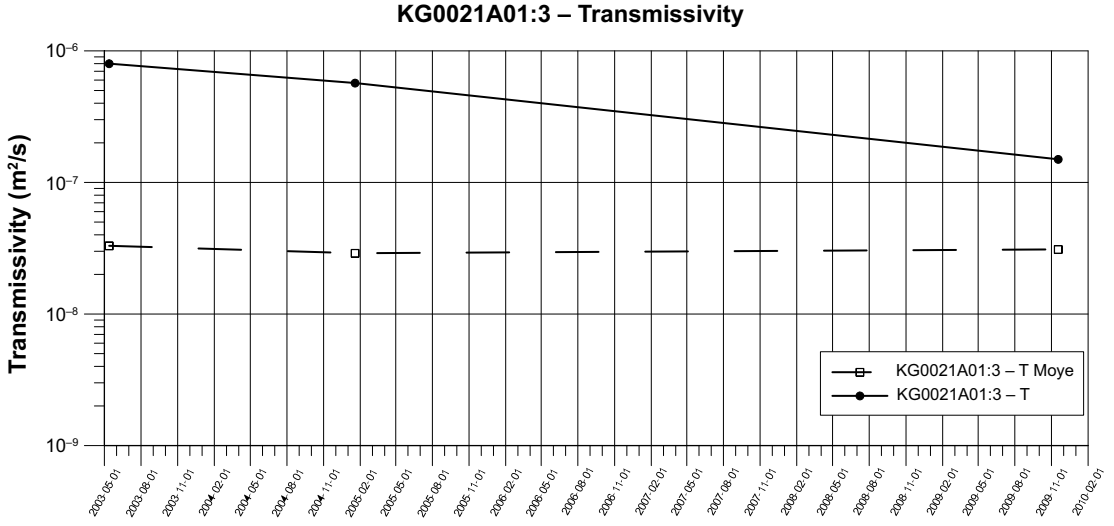

Figure 8-14. *Transmissivity change during the period 2003-05-01 to 2010-02-01 of KG0021A01:3.*

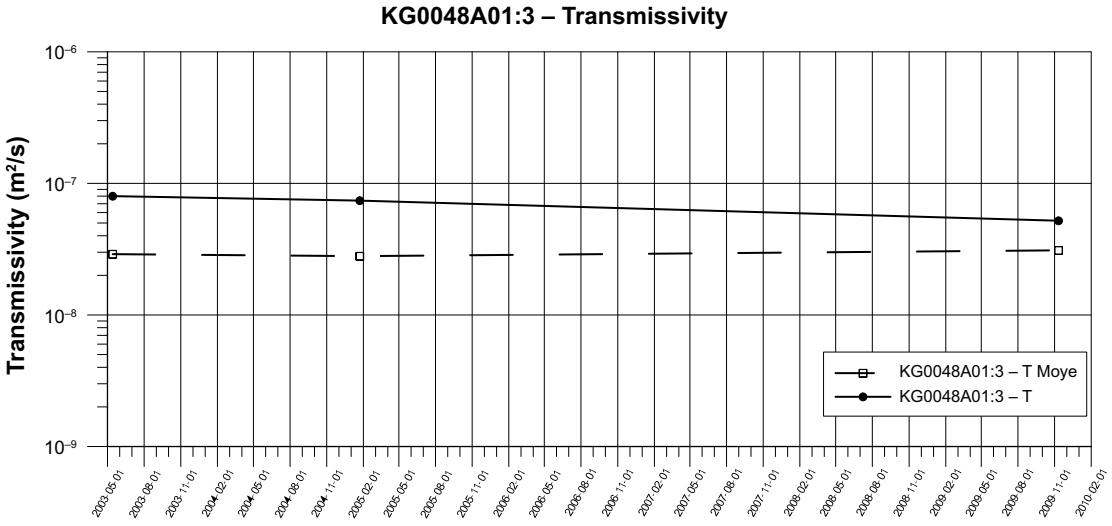

Figure 8-15. *Transmissivity change during the period 2003-05-01 to 2010-02-01 of KG0048A01:3.*

9 Comments and conclusions

Comments and conclusions made from the deformation measurements within the prototype project are divided into the following parts:

- Hydromechanical sensor performance.
- Temperature measurements.
- Long-term deformation measurements.
- Short-term measurements (hydraulic test campaigns).
- Hydraulic head changes.
- Flow into the deposition holes.
- Main conclusions.

9.1 Hydromechanical sensor performance

The best hydromechanical sensor performances are the ones in KA3554G01:2. Both sensors were functional during the major part of the period 2003–2006 with the exception of the total breakdown in 2005 which occurred in all holes, see Chapter 5. The equipment in the reference hole KG0010B01 were also in operation 2006. Otherwise the equipment, one or both sensors, see Figures 6-1 and 6-2, in the remaining 9 boreholes had stopped functioning at the beginning of October 2006.

Out of 22 temperature sensors within the hydromechanical equipment only 13 were still working 2006-10-01.

By 2010-01-01 only 4 out of the 22 temperature sensors were working and of the HM sensors only the rock and fracture sensor in KA3542G02:4 was in operation.

- The measurements indicate sudden “jumps” which could be caused by either expansion or compression of a fracture. This is the general pattern for both the sections with intact rock only and for the sections one or several fractures. The reason can either be that the anchor itself has slipped which is the plausible explanation for sections with intact rock only, or that a movement in a fracture suddenly occurs, which may be the explanation for fracture sections.
- When the backfilling of section II in the Prototype repository was in progress of vibrations were generated in the process of packing the backfill during the period 2003-04-29–2003-06-27. It is an open question whether the energy from this vibration could have been large enough to cause the observed fast “deformations” that could possibly be micro slips of the anchors or micro-movements in fractures. The first explanation, slips of the anchor, is the most probable reason as there are sudden movements later in the project, see below.
- Due to the fact that many sections with intact rock show sudden displacements, it appears that the anchor construction is not optimal to the current conditions. There are very small displacements involved and perhaps the anchors would have performed better with a larger area (and softer) in contact with the rock surface compared to the steel pin and steel edge collar on the anchor that were in contact with the borehole wall in this experiment. cf. Figure 4-1 and Figures 2-6 and 2-7 in Rhén et al. (2003). The original design with expandable copper bladders on the anchors, as delivered from Geokon Inc., was tested in laboratory and was found to not work properly for measuring small deformations. The anchors was therefore modified and tested in the laboratory, but as indicated above, the new design did not perform satisfactory and should probably be developed further if new tests are to be made.

9.2 Temperature measurements

The temperature increases to more than 40°C in the test sections closest to a canister hole, while the increase is more modest in holes more distant to the heating source. The tested sections can be divided into classes with “thermal” distances, where the distance is the closest distance to a heating canister, see Figure 9-1:

- approx. 1 m : KA3550G01:2 and KA3552G01:2,
- approx. 1.5 m : KA3544G01:2 and KA3546G01:2,
- approx. 10 m : KA3539G:2 and KA3554G02:4,
- approx. 15 m : KA3542G01:3 and KA3548A01:3,
- approx. 20 m : KA3542G02:2 and KA3554G01:2.

The temperature increase is rather small in most sections except for KA3544G01:2, KA3546G01:2, KA3550G01:2 and KA3552G01:2.

The temperature correction of the measured deformation over a long time period with significant temperature increase is essential for an experiment like the Prototype experiment. As many temperature sensors, mounted within the deformation sensor equipment, failed, one could possibly in a future experiment install one extra temperature sensor near the anchors for the deformation measurement.

For the long term observations the temperature corrections are important. As an example the applied temperature corrections on the deformation for 5, 10 and 30°C increase are 20 µm, 40 µm and 120 µm, compare with Figure 9-1. The observed long term deformations, although irregular (which is discussed in the next section), are generally larger than the temperature corrections indicated above, thus indicating that incorrect temperature corrections generally should not be expected to produce artificial deformations. However, if the observed deformation small and the temperature change large, the uncertainty in the small observed deformation can be large if there is a significant uncertainty in the correction of the deformation related to the temperature change.

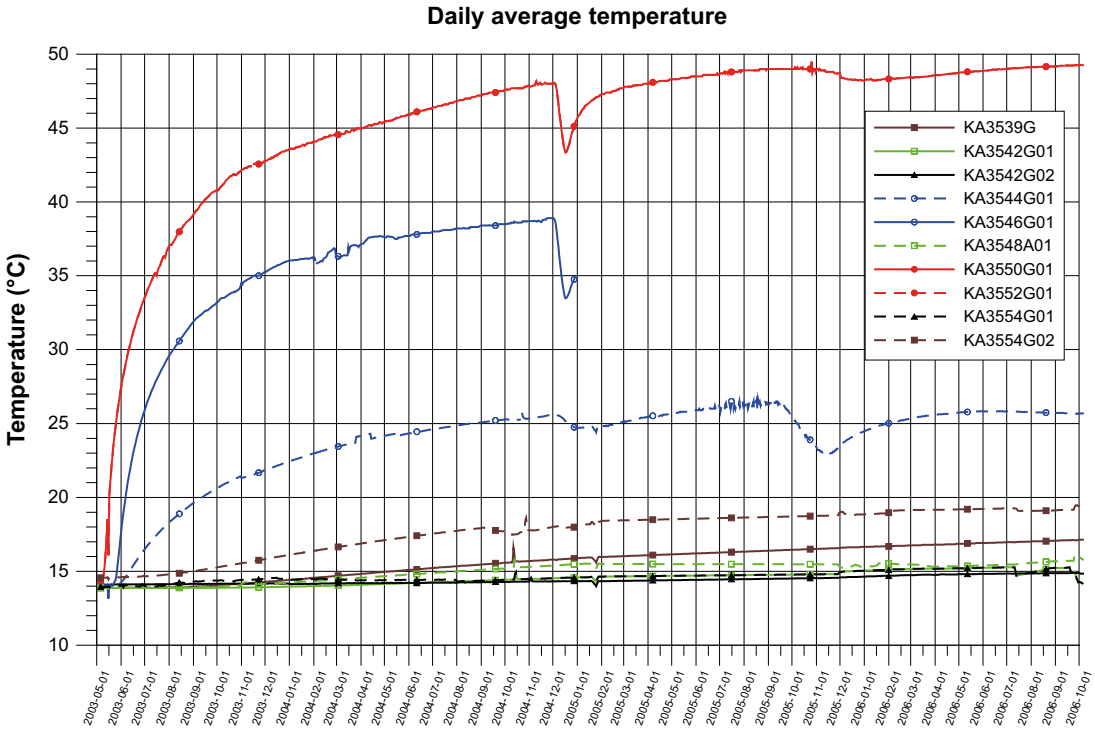

Figure 9-1. *Temperature development in the boreholes. The temperature drop is due to that the heaters were shut down for a period.*

During the short term tests it was possible to observe small temperature changes in some cases, up to c. 0.4°C during a test. In some case the change was observed in a section with fractures, the change was probably caused by the flowing water. Other causes were probably related to that one heater was stopped for a period, and that caused a temperature pulse in the rock mass. The temperature corrections of the deformations during the short term tests are small compared to the deformations observed. So, even though the temperature correction should be accurate considering how the equipment is constructed, the observed deformations during the short term tests is not considered to be an artefact of just temperature corrections, assuming that it is time delay between when the temperature pulse affects the strain gauge and the sensor for the temperature measurements. However, as there have been a large number of failures of temperature gauges it cannot be excluded that in some cases where data is missing that there is a noticeable effect of the temperature correction on the measured deformation, but still it seems from the available results that the effect may be relatively small.

According to Chapter 3 the temperature sensor, thermistor, with measurement range –80 to +150°C has an accuracy ±0.5°C. The measured temperatures, as shown in Figure 9-1, should be accurate.

9.3 Evaluated transmissivities

The evaluated transmissivities (T) are based on two evaluation methods;

1 The method suggested by Moye (1967) assumes a steady state radial flow near the tested section and spherical flow at some distance.

2 For the transient evaluation the measured flow rate for the flowing phase is used (multirate approach) and the pressure from the pressure build-up period is used for the evaluation. Evaluating the transient data, the pressure change, Δp, is plotted versus the equivalent time, dt_e, in minutes. The solution used in the analysis is the Dougherty-Babu model for a pumping test in a confined aquifer (Dougherty and Babu 1984).

The methods are described in Section 4.3.4. For method 1 only borehole geometry, test section length, flow rate and pressure difference are and no subjective judgment of the data is needed to calculate the T. Geometrical factors do not change between the tests and the pressure measurements can be considered very accurate. The flow rate, however, can change if the test duration changes, as some test section may not reach fully steady state. To avoid major problem with this the chosen test duration was generally rather long; 120 minutes. In some cases were steady state was reached rather quickly, 60 minutes flow time was used and in some slow reacting sections 180 minutes flow time was used (some of the tests during test campaign 1 slightly different flow times). These individual test-section flow times were used for the repeated tests, with the purpose that the measured last flow rate would be close to steady state flow rate and if not fully developed steady state the same flow times should provide comparable conditions for evaluation of changes of T.

The benefits with method 2 are that near-borehole effects (skin factor) can be filtered out and the evaluated T can be considered to better represent the transmissivity of the fracture. The negative side is that the method demands more from the monitoring of the tests (high frequency of sampling of flow rate and pressure) and that there is some subjectivity in the evaluation process of fitting models to the measured data. In our case the monitoring has been made with a high frequency sampling rate, so data quality is good in that sense. Some tests show complicated flow regime developments and in such cases one can easily get differences in estimated T due to different judgments of what is a reasonable fit for parameter estimation. To minimise the problems of subjectivity in the evaluation, the flow regimes were carefully studied and all previous made tests for a specific test section were checked before the evaluation of a new test; in order to perform the evaluation in a similar manner. With this methodology it was believed that the relative changes of T could be described accurately.

In general one can say that evaluated transmissivities for a test section is dependent of test time, evaluations methods as well as effects from boundary conditions (some may be transient or constant head). As described above, the attempt has been to avoid major problems in order to get relative changes that should be accurate, the relative changes which were considered important for the

project. The changes observed for T can generally be considered small and within an estimated uncertainty for an absolute value of T. There are a few greater changes of T and one can be certain that there exist a change of the absolute T. On the other hand, the frequent observation of small changes of T is also an important result as it tells us that no major changes occurred when the rock was heated. These small changes can probably be within expected uncertainties for an absolute estimate of T and observed small trends of the relative changes are uncertain. In a few cases where there are several observations showing a trend one can probably be more certain that there is a trend although small relative changes. However, this assumes that the major changes are due to compression or extension of fractures related to a slow change of stresses. If there is a fracture slip one can have a sudden increase or a decrease of the fracture transmissivity. There are a few observations that possibly can be related to slips but it has not been possible to confirm this cause to the change.

9.4 Long-term deformation measurements

In the summer months of 2003 most of the measurement sensors were still working. During that period when there are valid measurement data, there is increasing temperature in the rock and the rock expands while the measured fractures are generally being compressed.

The normal accuracy for the hole measuring system including hysteresis, non-linearity, misalignment, batch factor variations etc is 1% F.S. according to Geokon. The accuracy based on individual calibration that were performed of the sensors were; Measurement range 0.76–2.1 mm, Resolution (logger) 0.10–0.28 µm, Accuracy 0.76–2.1 µm according to Chapter 3, which can be considered as a sufficient accuracy for the test.

In a majority of tested boreholes the transmissivity slightly decreases when the temperature rises. But there are also boreholes where the opposite result is received. However changes are generally very small. In several sections, but not all, the water pressure decreases c. 500 to 1,000 kPa during 2003 to 2006 but this change cannot explain the observed long-term deformations using transmissivity and pressure-change data from the short-term deformation measurements in some borehole sections. In a few sections the water pressure increased but the transmissivity decreased and one can conclude that the temperature increase has caused transmissivity decrease. In some cases possibly both the temperature increase and the water pressure decrease has caused the transmisssivity decrease.

In borehole KA3552G01:2, which is c. 1.2 m from the centre line of the heater (c. 0.6 m outside the deposition hole wall) with temperature increase from c. 14 to 49°C, there is a clear deformation and transmissivity decrease from c. $5 \cdot 10^{-9}$ m^2/s to c. $6 \cdot 10^{-10}$ m^2/s in the section with a fracture with orientation 193/44. KA3550G01:2 which is in a similar position as KA3552G01:2 but due to packer failure no data are available.

KA3544G01:2 and KA3546G01:2 are fairly close to the heaters, which are c. 1.2 m from the centre line of the heater (c. 0.6 m outside the deposition hole) but located near the bottom of the heater. The temperature increase is c. from c. 14 to 25°C (KA3544G01:2) and 38°C (KA3546G01:2) and the monitored sections have 3–4 fractures with different orientations. In KA3544G01:2the transmissivity decreases from c. c. $1 \cdot 10^{-8}$ m^2/s to c. $7 \cdot 10^{-9}$ m^2/s (only two measurements) but in KA3544G01:2 there seem to be no decrease in transmissivity.

There are a few observations that indicate a sudden transmissivity increase, e.g. KA3542G02:2, which possibly can indicate a fracture slip; a few months after the heater were started. After this sudden increase, the transmissivity decreases. In other borehole sections the transmissivity changes are small and not possible to judge if they are due to the decreasing water pressure or increasing load due to temperature increase.

The long-term deformation measurements are very difficult to evaluate due to a number of rapid changes that have not been possible to couple to a known cause, or the deformations seem unrealistic in some cases.

9.5 Short-term deformation measurements

During the seven hydraulic test campaigns (TC1–TC7) several of the test sections reacts as expected. During flow phase the fracture located within the tested section reacts with decreased fracture width in response to the lower hydrostatic pressure in the section. When the flow phase ends the fracture width increases once again. The best results are from KA3542G01:3 (TC2–TC4) and KA3554G01:2 (TC3–TC7). There is a more or less linear relationship between hydrostatic water pressure loss and fracture width in the data from the two boreholes.

The fracture transmissivity decreases slightly when the fracture or set of fractures are being compressed during the hydraulic tests.

It seems that in some cases the deformation during a short test does not come back to initial values before the sudden pressure decrease. This may indicate a permanent deformation of the fracture but it cannot be excluded that it is small anchor slips that is observed.

9.6 Hydraulic head changes

Appendix 2 shows the pressure measurements around the Prototype repository. There seem to be a slowly decreasing trend in the water pressure by time. At least partly, this cannot be explained as effects from the Prototype repository itself or nearby tunnels, as one can observe a decreasing trend en several of the boreholes in the Äspö HRL, exemplified in Figure 9-2. Borehole KA3105A is situated east of the TBM assembly hall and KA2162B is drill through the tunnel spiral, Figure 1-2 and Figure 1-3. During the same period the total inflow of water to the tunnels has decreased, see Figure 9-3. Explanations for the decreasing inflow rate to the tunnels, which has been observed at several underground facilities, has been near-tunnel effects causing a permeability decrease close to the tunnel as; Stress changes due to the excavation, chemical precipitation and/or gas release near the tunnel due to pressure decrease of the inflowing water. Fault gauge moving with the flowing water can also cause changes in the permeability, which has been observed within the Prototype experiment, then linked to changes observed when blasting rock nearby. As the pressure far away from the tunnels does not increase, as one would anticipate of the above reasons, there must be, at least also, other mechanisms involved causing the decreasing inflow rate to the tunnels. This mechanism cannot be explained at present but possibly can successive fault gauge movements and/or small and slow creep deformation of the rock cause very small changes of the permeability of the fracture system within long distances from the tunnels creating a slightly lower mean permeability.

9.7 Flow into the deposition holes

The inflow to the deposition holes DA3551G01 and DA3545G01 were measured 1999-12 to 2000-06 three times (Rhén and Forsmark 2001). In the winter 2012–2013, after the backfill and the buffer had been removed in tunnel section II, the flow measurements were repeated for two of the depositions holes. The measured flow rates for the two occasions are shown in Table 9-1. As can be seen the inflow rates has decreased.

Table 9-1. Result of inflow measurements to deposition boreholes DA3551G01 and DA3545G01.

Borehole	Q 2000-03-28–2000-03-31 (L/min)	Q 2012-12-20–2013-02-07 (L/min)
DA3551G01	0.00155	0
DA3545G01	0.00270	0.00045

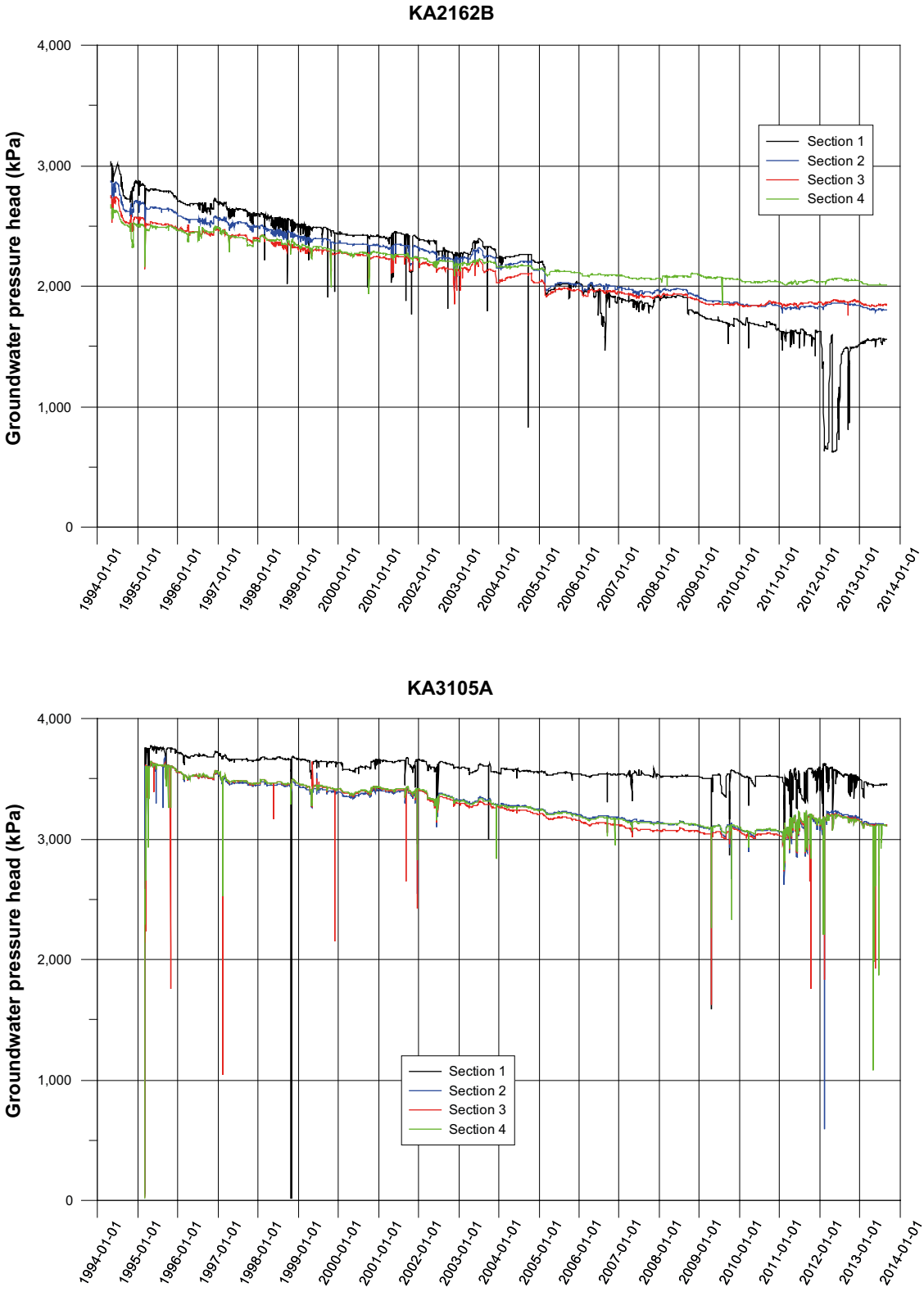

Figure 9-2. *Groundwater pressure in KA2162B and KA3105A.*

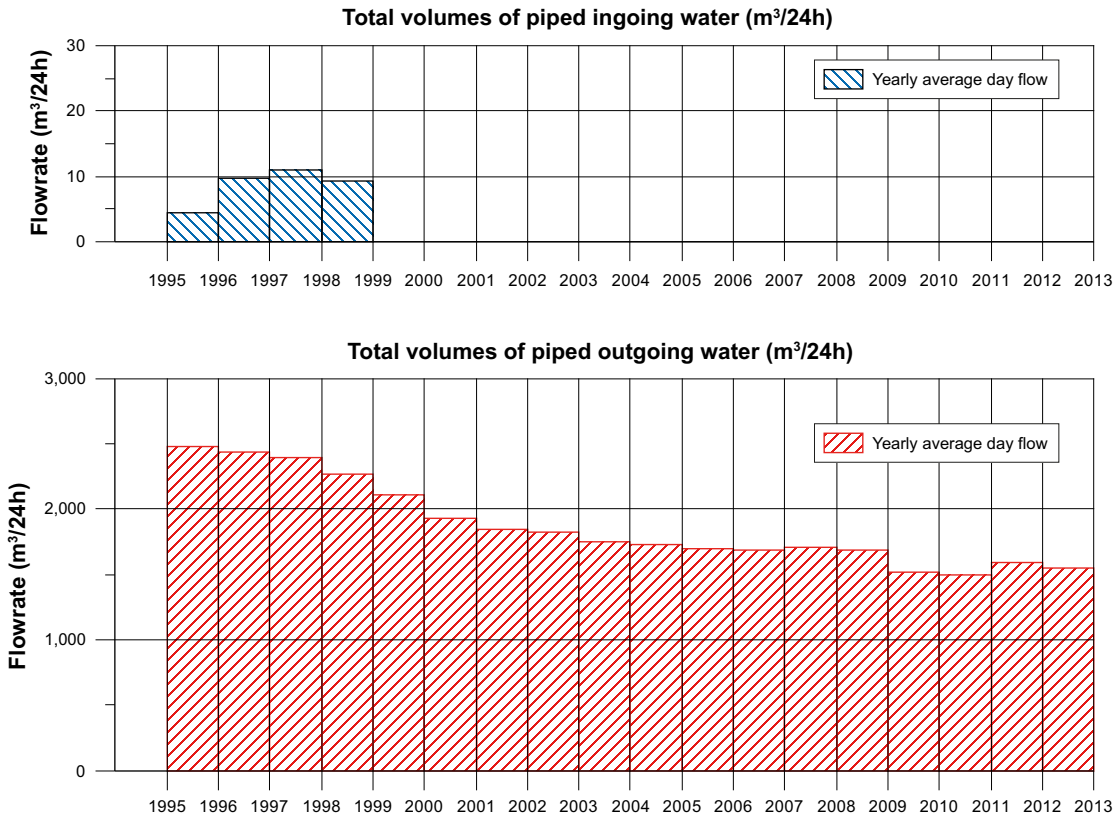

Figure 9-3. *Measurement of total inflow from the rock (outgoing water) to the Äspö HRL and total ingoing water for e.g drilling purpose. (Measurement of ingoing water was ended June 1999 after a failure in the flow meter.).*

9.8 Main conclusions

9.8.1 General

The following questions are considered in Section 1.2.3:

- Is there any deformation observed on the intact rock that can be correlated to temperature?
- Is there any deformation of open fractures that can be correlated to temperature?

Yes, deformation can be observed in both the intact rock and in sections with fractures, but the results are difficult to interpret as the anchors seem to slip on the rock surface in some cases and the amount of data is less than expected due to that sensors have stopped working during the project.

- Are there any changes of fracture transmissivities that can be correlated to temperature?

Yes, but the changes are generally small.

- If fracture transmissivities have changed, can it be correlated to measured deformations of fractures?

Yes, and the changes are small. However the amount of data is also small.

Below the main results are described in more detail:

- The observed deformations and transmissivity changes during the measurement period are small. This was expected as the initial rock stress before the heating is rather high at the depth for the Prototype repository. The transmissivity decrease is c. 0.1 of the initial transmissivity value for one observation just outside a deposition hole but all other observations near or distant from the deposition holes show fewer changes, but the changes show decreases as well as increases. The mall changes should be considered uncertain.

- Hydraulic tests with different water pressure decreases show that the evaluated transmissivity is dependent of the applied water pressure decrease. However, the transmissivity changes are small relative the pressure change. This is expected as the tests are performed at such large depth with relatively high initial rock stresses.
- Although the measurements in some respect have been successful (according to the point above) one can conclude that the deformation measurements are difficult. The deformations are small and one has to be very sure that the anchor does not slip on the rock wall. The sensors (strain gauge and temperature) in the deformation measurement equipment should also withstand the environment (temperature, water pressure, vibration (e.g. from packing the backfill in the tunnels)) in the borehole better than the equipment used. It is presently not known the reason for the deformation measurement-equipment failure.
- The methodology for performing hydraulic tests has worked well but in any future similar investigations one should perform several tests with different pressure drawdowns (e.g 200 kPa (or at least somewhat lower than used in the present study) as start value and then increase the differential pressure in a number of steps suitable for the project) during each test campaign in each test section already from the outset. Data will be useful for evaluating fracture compressibility and one can use the test with the lowest differential pressure when comparing long term behaviour, which would be preferable. To show permeability changes qualitative one can probably also use a third test (besides evaluation of T using stationary and transient methods) by plotting the specific drawdown versus time for all tests made in a specific test section.
- The characterisation of the Prototype tunnel before the tunnel was backfilled and the experiment started, was extensive and it was possible to do several types of geological and hydrogeological investigations that provided a good basis for planning the experiment. However, one method was excluded; the flow logging with Posiva flow log aiming to detect individual flowing fractures and estimate their transmissivity. Investigations in other projects later made by SKB using this tool has proven valuable as a compliment to geological characterisation and orientation of fractures and hydraulic tests with small and large test-section lengths.
- The installed hydraulic packers in tunnel section II have functioned well but unfortunately there have been a few packer failures that have spoiled the possibilities to perform hydraulic tests in those boreholes.
- The water pressure around the deposition tunnels did not increase as expected. First of all, section I was drained most of test period due to electrical problems with one canister heater when the water pressure increased, which also affect the pressure around section II. There also exists a general pressure decrease near the Prototype repository, but also in Äspö HRL in general. It does not have a main influence of the evaluation of the short-term deformations (other than it limits to use high differential pressures), but it can affect the long-term deformation measurements in that respect that the effective stress in the fractures changes. If the deformation due to the thermal load is limited, the observed small deformations may just be due to long term pressure changes.
- The nearby experiment in tunnel TASS has significantly disturbed the Prototype experiment. The drilling and the grouting for the Fine Sealing project (year 2007) as well as excavation of the TASS tunnel, disturbed the pressures and probably has grout affected at least one of the observation boreholes drilled from the Prototype tunnel. The drilling, the grouting and tunnel excavation have however not had an impact of most result related to hydraulic tests and deformation measurements, as the main part of the result are from the period before 2007. The boundary conditions for the Prototype project significantly changed after 2007 due to the TASS tunnel. Pressure levels and pressure trends have changed in several cases comparing data before drill start and after excavation.

9.8.2 Comparison with predictions

Before the experiment started, scoping calculations were made of the expected behaviour of the fractures, see Rhén and Alm (2004). The conclusions were:

- **Prediction:** The hydraulic response will in general be decreased transmissivity. The decrease will be larger the closer the fractures are to the canisters.

- **Outcome:** Correct prediction but the number of observations is small.
- **Prediction:** The transmissivity will be reduced to something between 10 and 80 percent of the in situ values.
- **Outcome:** Prediction fairly correct. One observation close to the deposition holes shows a decrease to 10% of initial value. Most other sections show only small changes or hardly any changes. However, the maximum distance from the deposition holes assumed in the predictions were 10 m and several of the observation are c. 15–25 m from the deposition holes, see Section 7.2, indicating that it is reasonable that the observations indicate less changes for many of the measured section.
- **Prediction:** The fracture closure will be in the range of 5–70 micrometre.
- **Outcome:** The deformation during short term tests with a decrease of the effective pressure of maximum c. 3,200 kPa generates a deformation of maximum 35 micrometre, see Figure 7-102. The measured long-term deformation is very uncertain due to that the anchors have probably in many cases slipped. In a few cases were there seem to be a more or less continuous deformations change, without sudden and permanent changes in deformation that is in the prediction range, see Section 7.3. It cannot be said that the measurements have confirmed the predictions, due to the fact that the measurement data for long-term monitoring of deformations are of low quality.
- **Prediction:** The hydraulic and mechanical responses on the fracture depend on the orientation of the fracture relative the stress field.
- **Outcome:** It cannot be said that the measurements have confirmed the predictions, due to the fact that the measurement data for long-term monitoring of deformations are of low quality, and it has not been consider possible to evaluate actual stress situation around each monitored section in order to validate the predictions. For future experiments one would like to have more measurement sections rather near deposition holes (probably <10 m) where probable stress effects more likely can be observed. Preferably that each borehole section having one or several fractures with approximately one orientation and that most of the borehole section have fracture(s) with different orientations compared to other borehole sections. One should also use the Posiva flow log, or similar equipment, to identify the flowing fractures and then using the geological mapping for orientation of the flowing fracture.
- **Prediction:** Major part (~80%) of the increase in stress and temperature is reached within two years.
- **Outcome:** After two years (2005-05) the temperature close to the deposition holes was c. 95% of the temperature 2006-10, see Section 6.3. After two years the temperature c. 10 m from the deposition holes was c. 70% of the temperature 2006, see Section 6.3. Deformation data are lacking for a longer period so no relevant comparison to prediction can be made.

References

SKB's (Svensk Kärnbränslehantering AB) publications can be found at www.skb.se/publications.

Alm P, Forsmark T, Rhén I, 2005. Äspö Hard Rock Laboratory. Prototype repository. Installations for measurements of flow into tunnels, water pressure in the rock and hydromechanical responses in boreholes during operation phase. SKB IPR-05-04, Svensk Kärnbränslehantering AB.

Dougherty D E, Babu D K, 1984. Flow to a partially penetrating well in a double-porosity reservoir. Water Resources Research 20, 1116–1122.

Forsmark T, 2006. Äspö Hard Rock Laboratory. Prototype repository. Hydraulic tests and displacement measurements during operation phase. Test campaign 6. Single hole tests. SKB IPR-06-01, Svensk Kärnbränslehantering AB.

Forsmark T, 2007a. Äspö Hard Rock Laboratory. Prototype repository. Hydraulic tests and displacement measurements during operation phase. Test campaign 7. Single hole tests. SKB IPR-07-02, Svensk Kärnbränslehantering AB.

Forsmark T, 2007b. Äspö Hard Rock Laboratory. Prototype repository. Hydraulic tests and displacement measurements during operation phase. Test campaign 8. Single hole tests. SKB IPR-07-17, Svensk Kärnbränslehantering AB.

Forsmark T, 2008. Äspö Hard Rock Laboratory. Prototype repository. Hydraulic tests and displacement measurements during operation phase. Test campaign 9. SKB IPR-08-22, Svensk Kärnbränslehantering AB.

Forsmark T, 2010. Äspö Hard Rock Laboratory. Prototype repository. Hydraulic tests during operation phase. Test campaign 10. Interference tests. SKB IPR-10-03, Svensk Kärnbränslehantering AB.

Forsmark T, Rhén I, 2004a. Äspö Hard Rock Laboratory. Prototype repository. Hydraulic tests and displacement measurements during operation phase, test campaign 1, single hole tests. SKB IPR-04-17, Svensk Kärnbränslehantering AB.

Forsmark T, Rhén I, 2004b. Äspö Hard Rock Laboratory. Prototype repository. Hydraulic tests and displacement measurements during operation phase, test campaign 2, single hole tests. SKB IPR-04-18, Svensk Kärnbränslehantering AB.

Forsmark T, Rhén I, 2004c. Äspö Hard Rock Laboratory. Prototype repository. Hydraulic tests and displacement measurements during operation phase, test campaign 3, single hole tests. SKB IPR-04-19, Svensk Kärnbränslehantering AB.

Forsmark T, Rhén I, 2005a. Äspö Hard Rock Laboratory. Prototype repository. Hydraulic tests and displacement measurements during operation phase, test campaign 4, single hole tests. SKB IPR-05-02, Svensk Kärnbränslehantering AB.

Forsmark T, Rhén I, 2005b. Äspö Hard Rock Laboratory. Prototype repository. Hydraulic tests and displacement measurements during operation phase. Test campaign 5. Single hole tests. SKB IPR-05-17, Svensk Kärnbränslehantering AB.

Forsmark T, Rhén I, 2005c. Äspö Hard Rock Laboratory. Prototype repository. Hydraulic tests and displacement measurements during operation phase. Test campaign 5. Interference tests. SKB IPR-05-18, Svensk Kärnbränslehantering AB.

Forsmark T, Forsman I, Rhén I, 2004. Äspö Hard Rock Laboratory. Prototype repository. Hydraulic tests and displacement measurements during operation phase, test campaign 1, interference tests. SKB IPR-04-16, Svensk Kärnbränslehantering AB.

Fälth B, Hökmark H, 2006. Mechanical and thermo-mechanical discrete fracture near-field analyses based on preliminary data from the Forsmark, Simpevarp and Laxemar sites. SKB R-06-89, Svensk Kärnbränslehantering AB.

Goudarzi R, Johannesson L-E, 2006. Äspö Hard Rock Laboratory. Prototype repository. Sensor data report (Period 010917–060601). Report No:15. SKB IPR-06-26, Svensk Kärnbränslehantering AB.

Horne R N, 1995. Modern well test analysis: a computer-aided approach. 2nd ed. Palo Alto, CA: Petroway Inc.

Hökmark H, Fälth B, Wallroth T, 2006. T-H-M couplings in rock. Overview of results of importance to the SR-Can safety assessment. SKB R-06-88, Svensk Kärnbränslehantering AB.

Moye D G, 1967. Diamond drilling for foundation exploration. Civil Engineering Transactions, Institute of Engineers (Australia), 95–100.

Rhén I, Alm P, 2004. Äspö Hard Rock Laboratory. Prototype repository. Hydromechanical behaviour of fractures due to excavation and thermal load. SKB IPR-04-22, Svensk Kärnbränslehantering AB.

Rhén I, Forsmark T, 2001. Äspö Hard Rock Laboratory. Prototype repository. Hydrogeology. Summary report of investigations before the operation phase. SKB IPR-01-65, Svensk Kärnbränslehantering AB.

Rhén I, Forsmark T, Torin L, Puigdomenech I, 2001. Äspö Hard Rock Laboratory. Prototype repository. Hydrogeological, hydrochemical and temperature measurements in boreholes during the operation phase of the Prototype repository. Tunnel section I. SKB IPR-01-32, Svensk Kärnbränslehantering AB.

Rhén I, Forsmark T, Magnusson J, Alm P, 2003. Äspö Hard Rock Laboratory. Prototype repository. Hydrogeolocical, hydrochemical, hydromechanical and temperature measurements in boreholes during the operation phase of the Prototype repository Tunnel section II. SKB IPR-03-22, Svensk Kärnbränslehantering AB.

Rhén I, Forsmark T, Hartley L, Jackson C P, Roberts D, Swan D, Gylling B, 2008. Hydrogeological conceptualisation and parameterisation. Site descriptive modelling, SDM-Site Laxemar. SKB R-08-78, Svensk Kärnbränslehantering AB.

SKB, 2011. Long-term safety for the final repository for spent nuclear fuel at Forsmark. Main report of the SR-Site project. SKB TR-11-01, Svensk Kärnbränslehantering AB.

Spane F A, Wurstner S K, 1993. DERIV: A computer program for calculating pressure derivatives for use in hydraulic tests. Groundwater 31, 814–822.

Appendix 1

Temperature in borehole sections with HM measurements

In the appendices the following plots are presented with all data available until 2009-07-01. Most of the sensors unfortunately malfunction by that date.

- Daily average temperature plot for inner deformation measurement section.
- Daily average temperature plot for outer deformation measurement section.

KG0010B01

Temperature

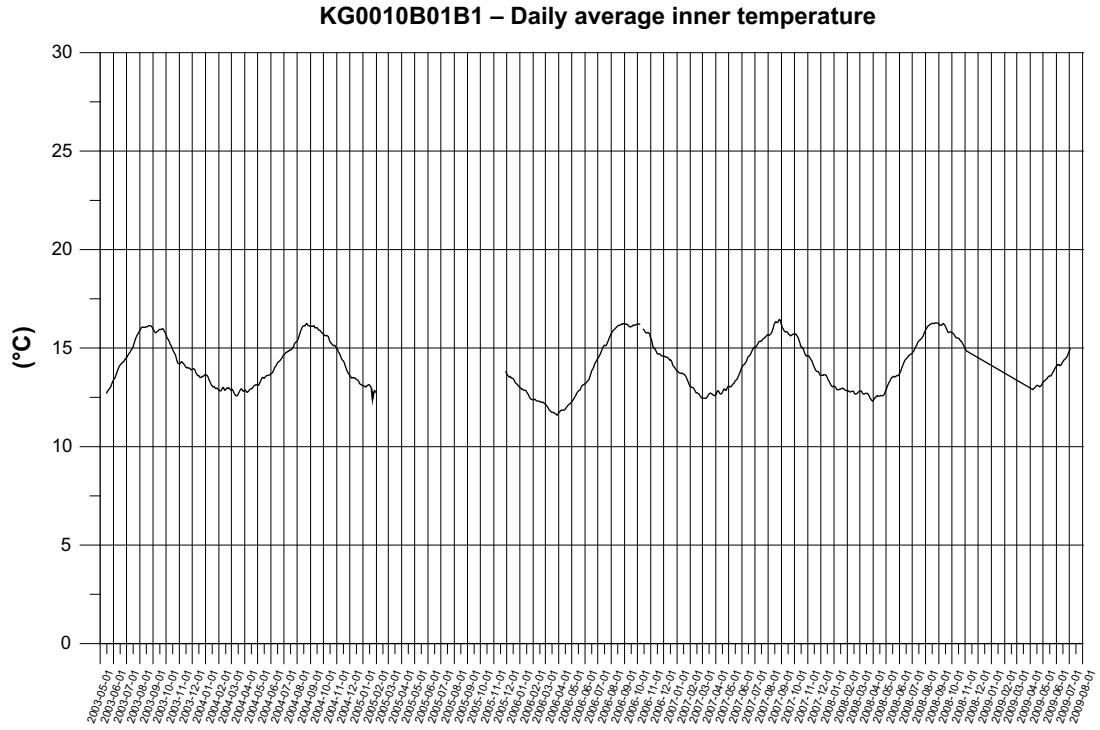

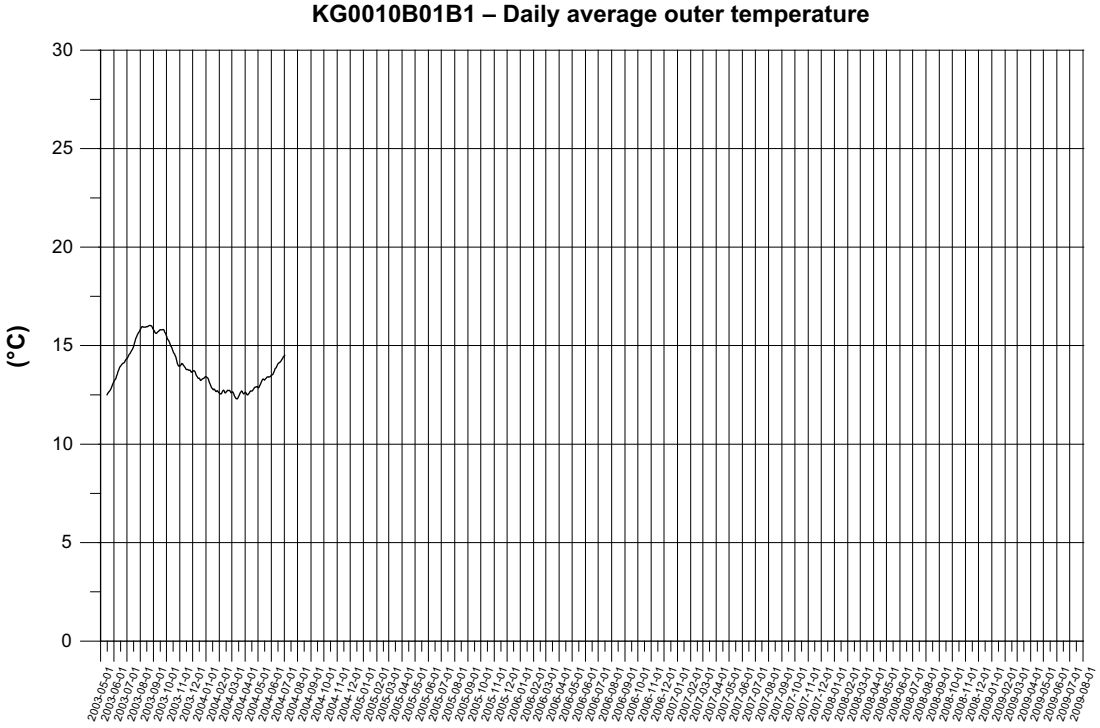

KG0010B01

Long-term deformation

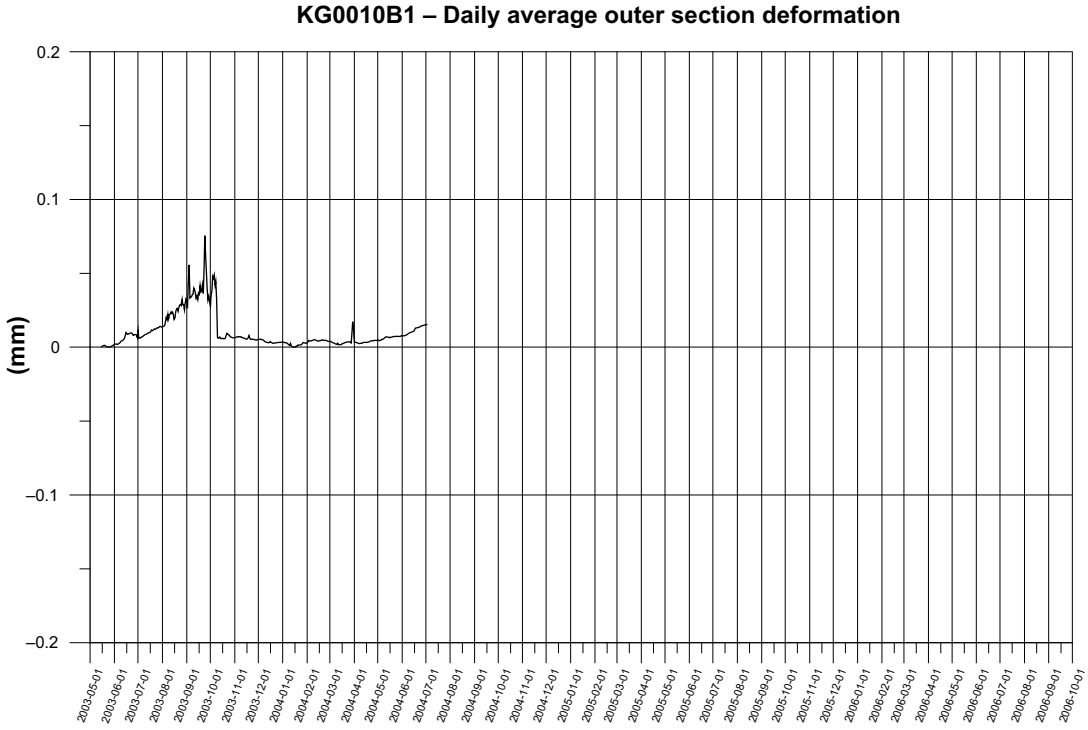

KA3539G

Temperature

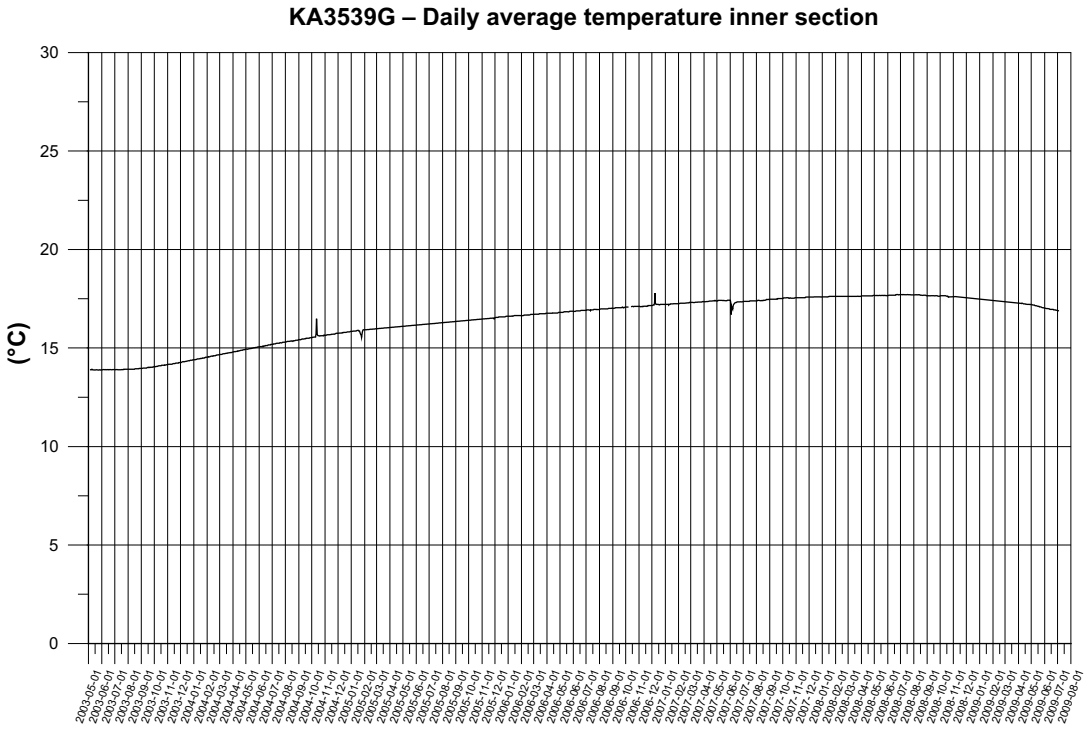

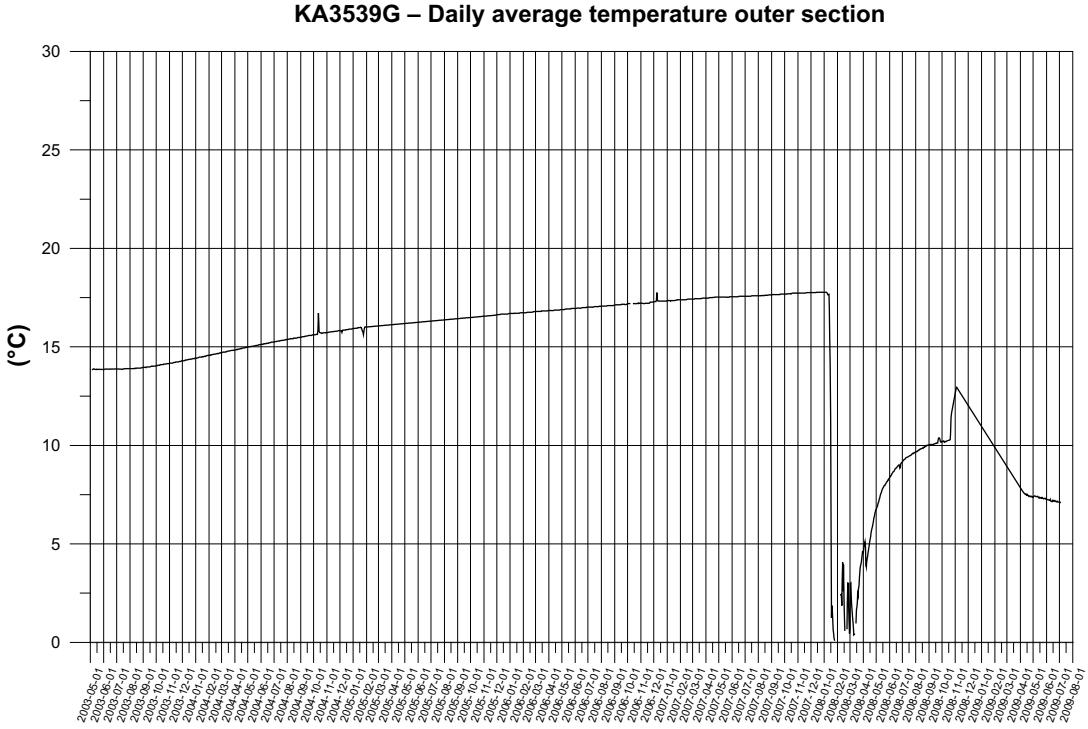

KA3542G01

Temperature

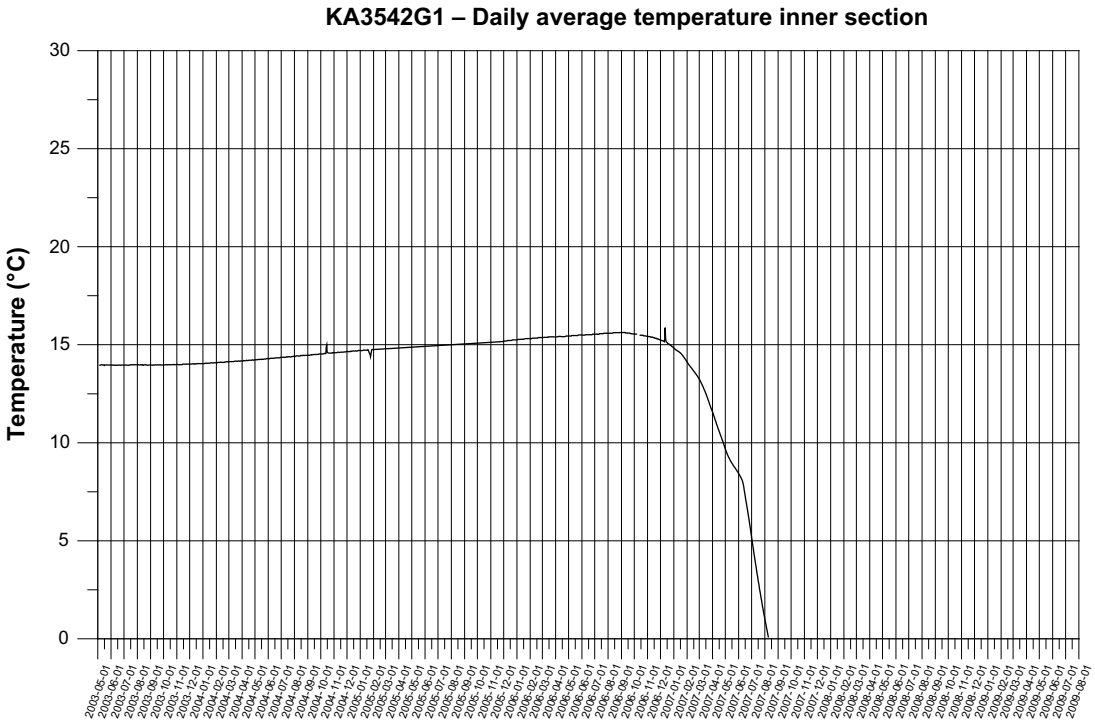

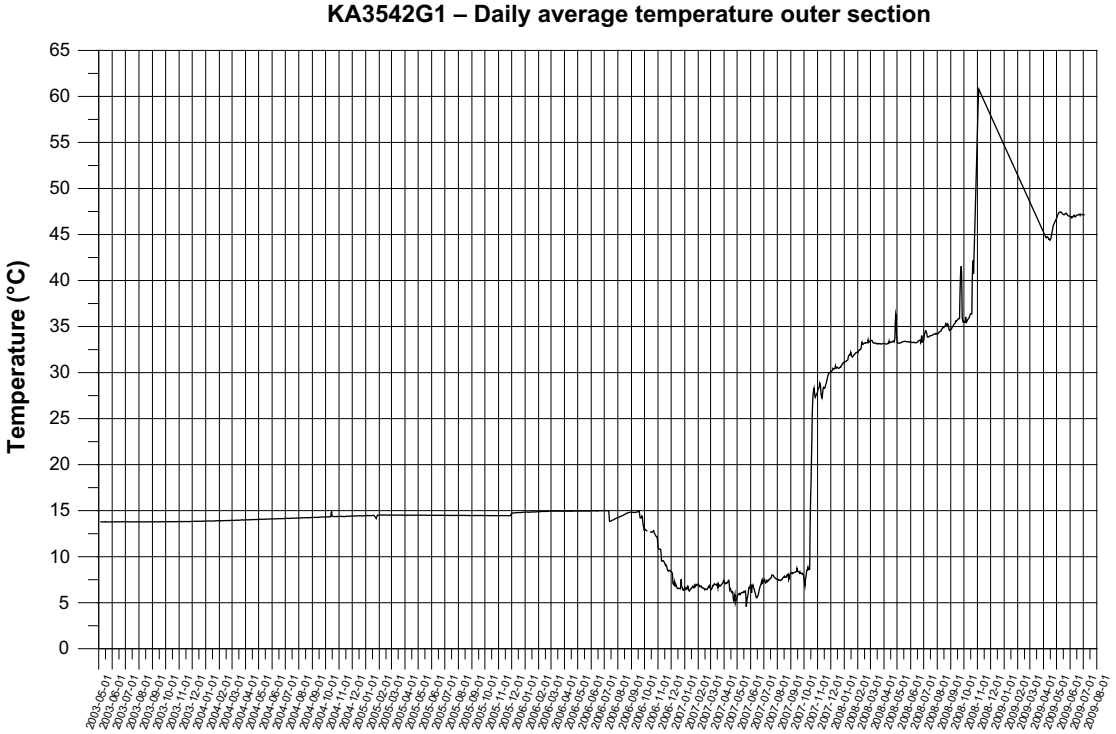

KA3542G02

Temperature

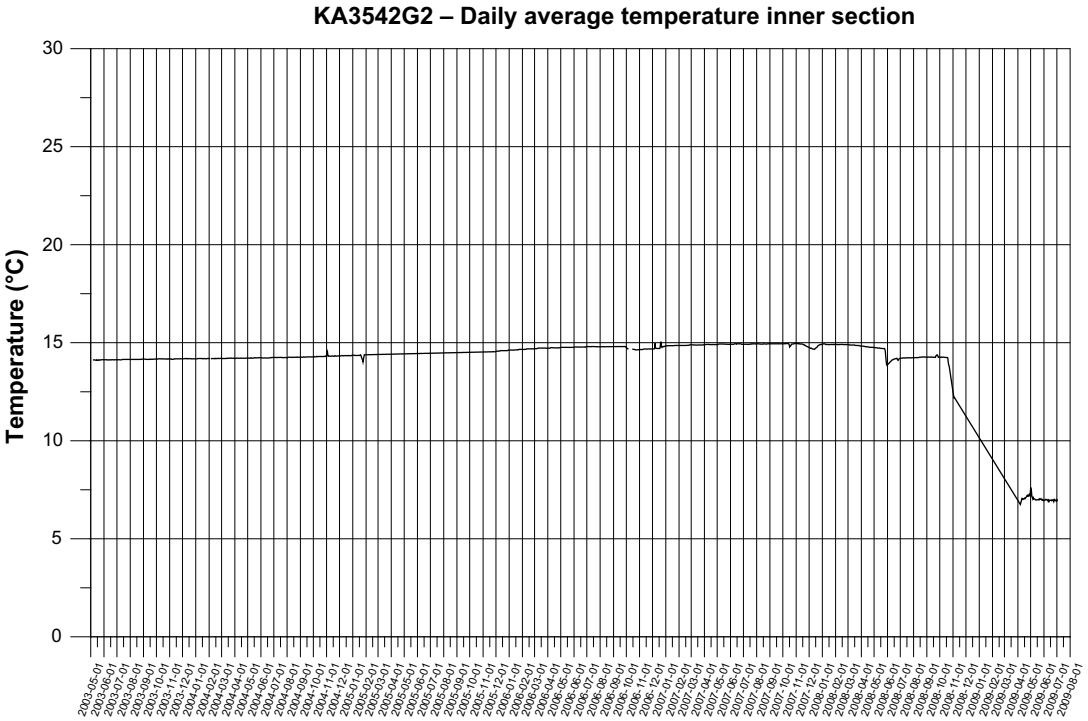

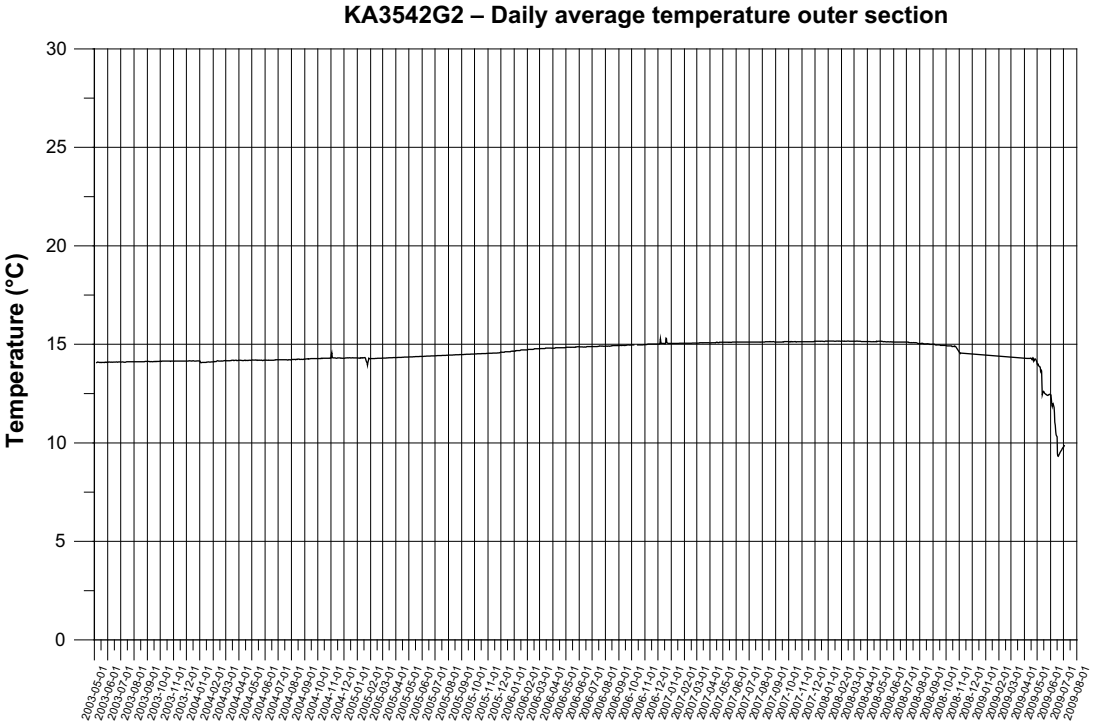

KA3544G01

Temperature

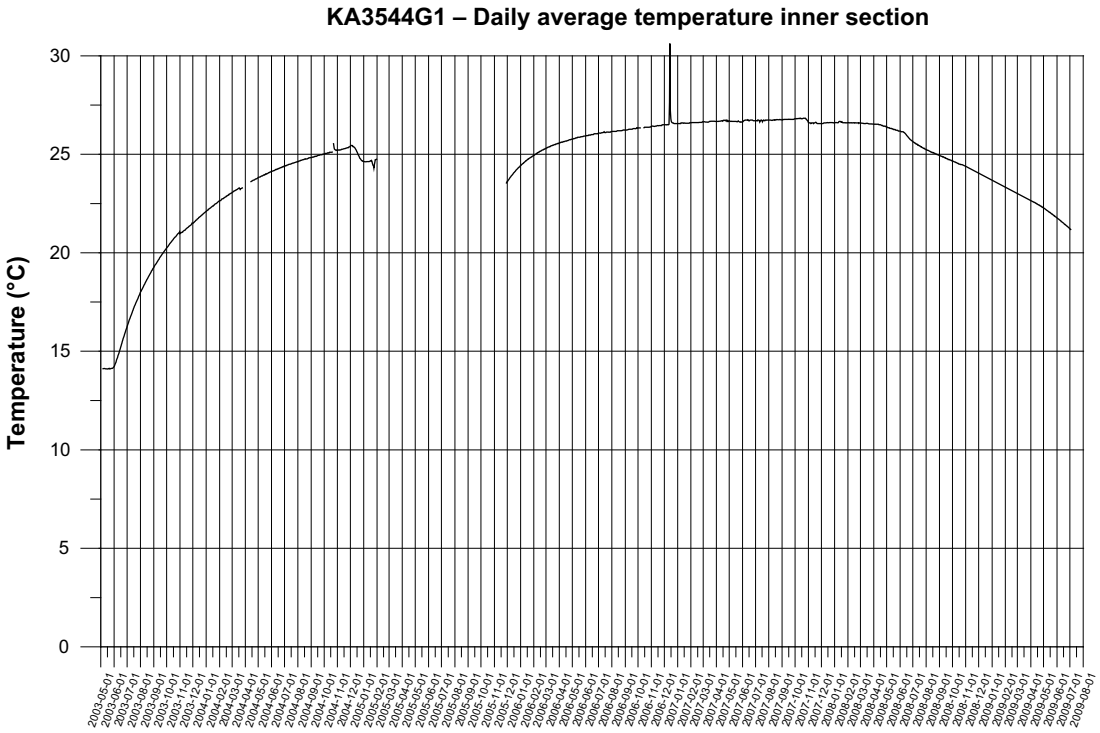

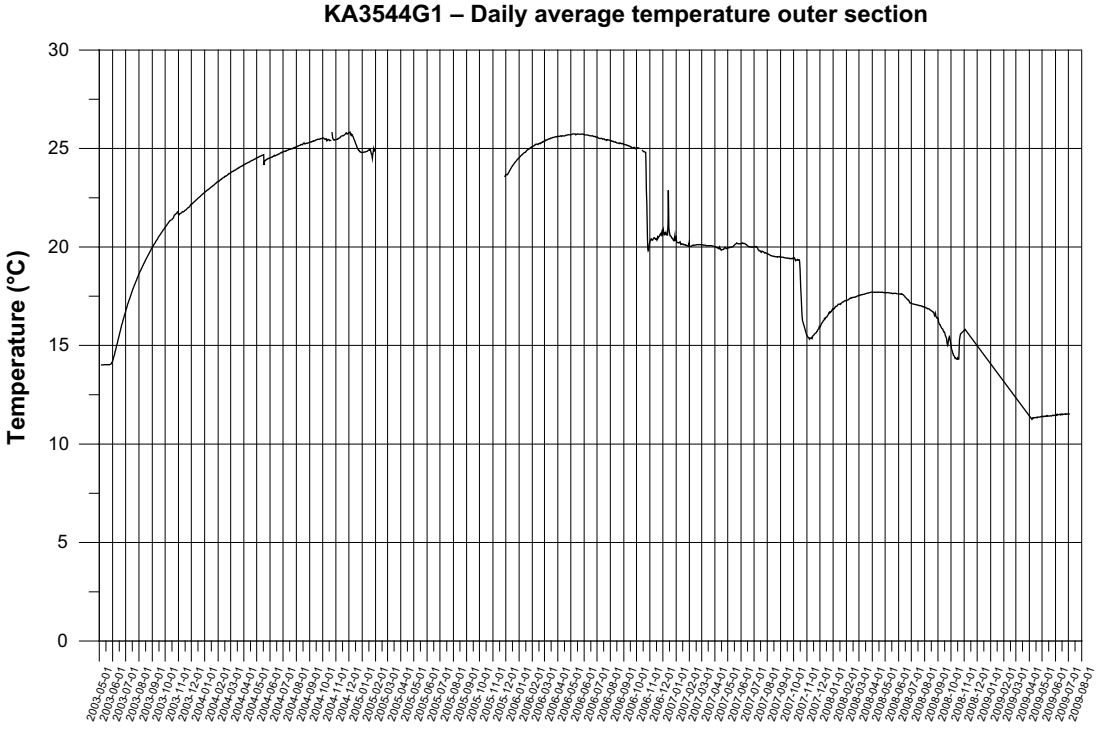

KA3546G01

Temperature

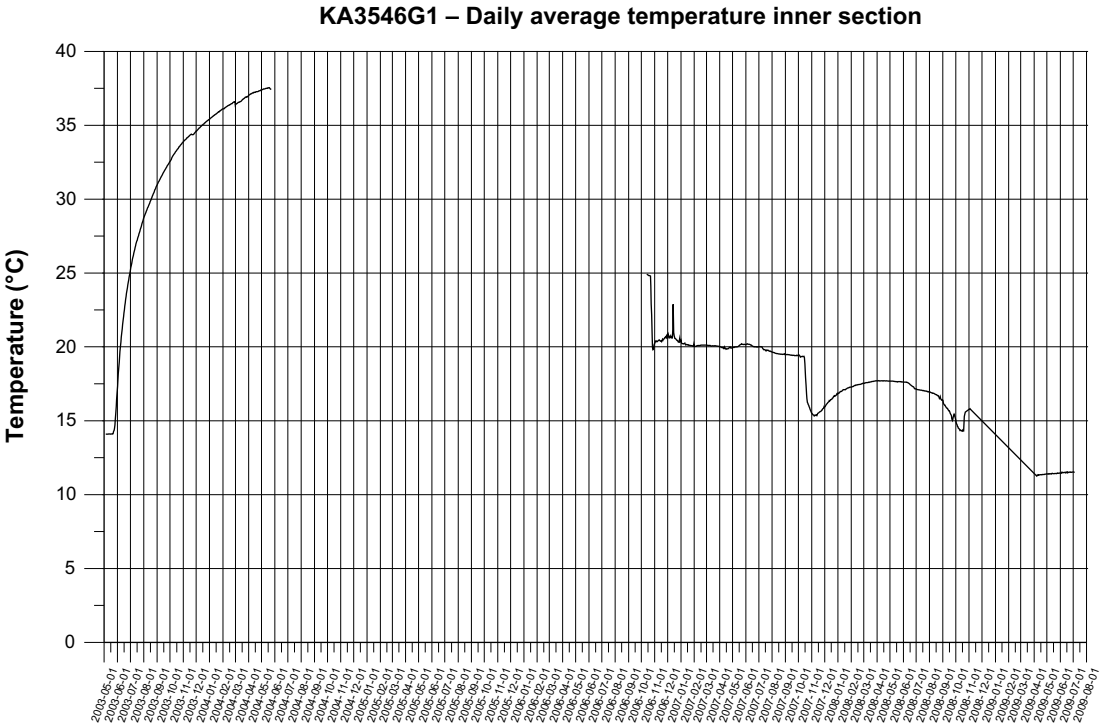

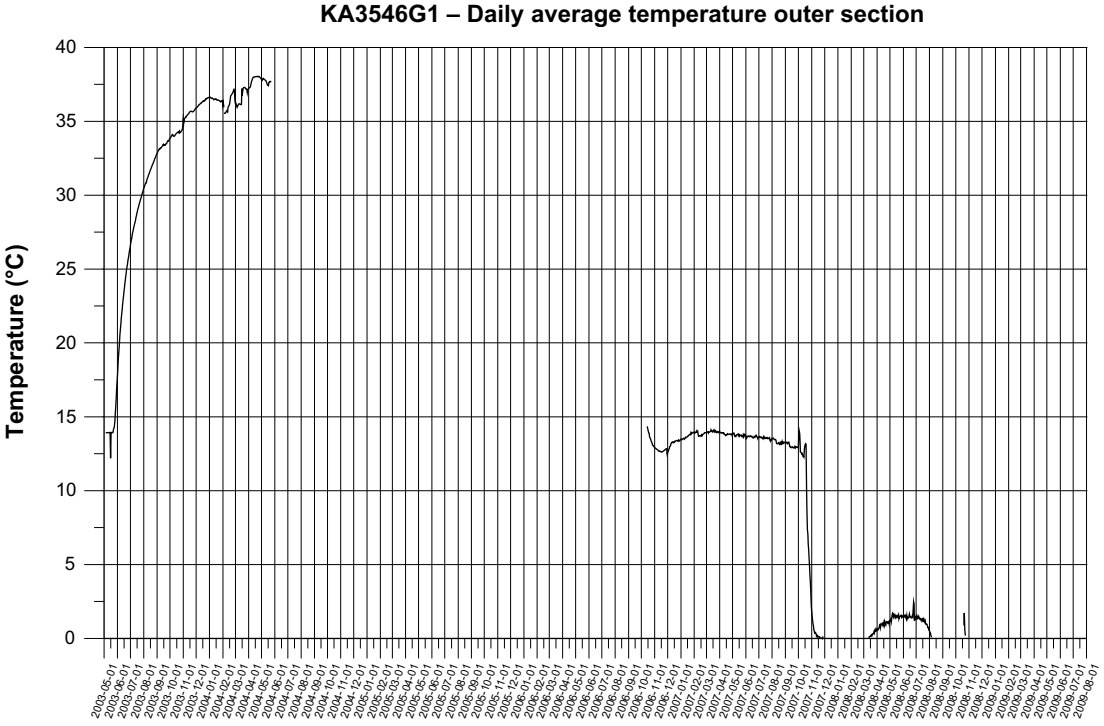

KA3548A01

Temperature

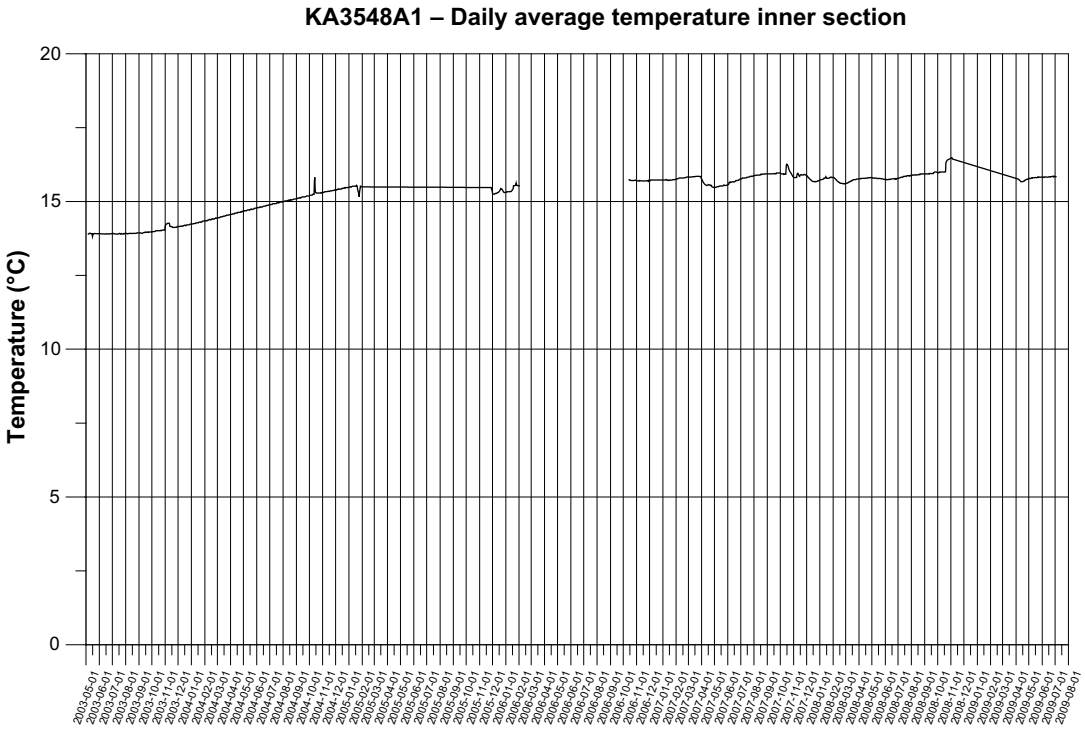

KA3550G01

Temperature

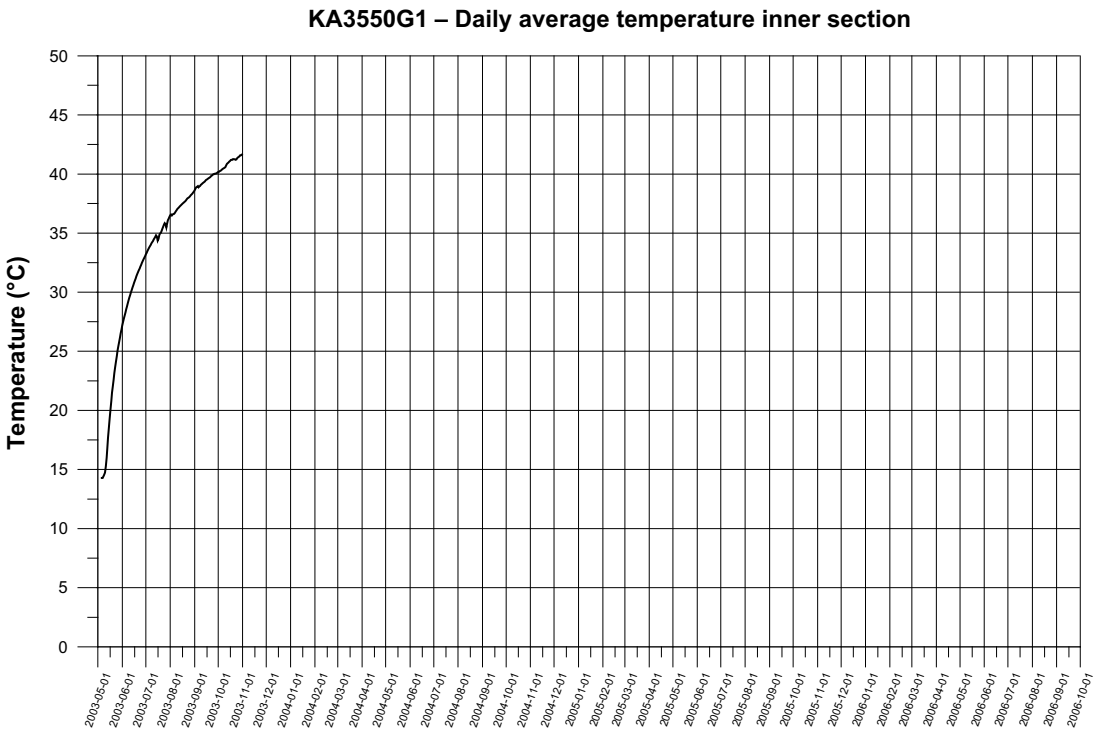

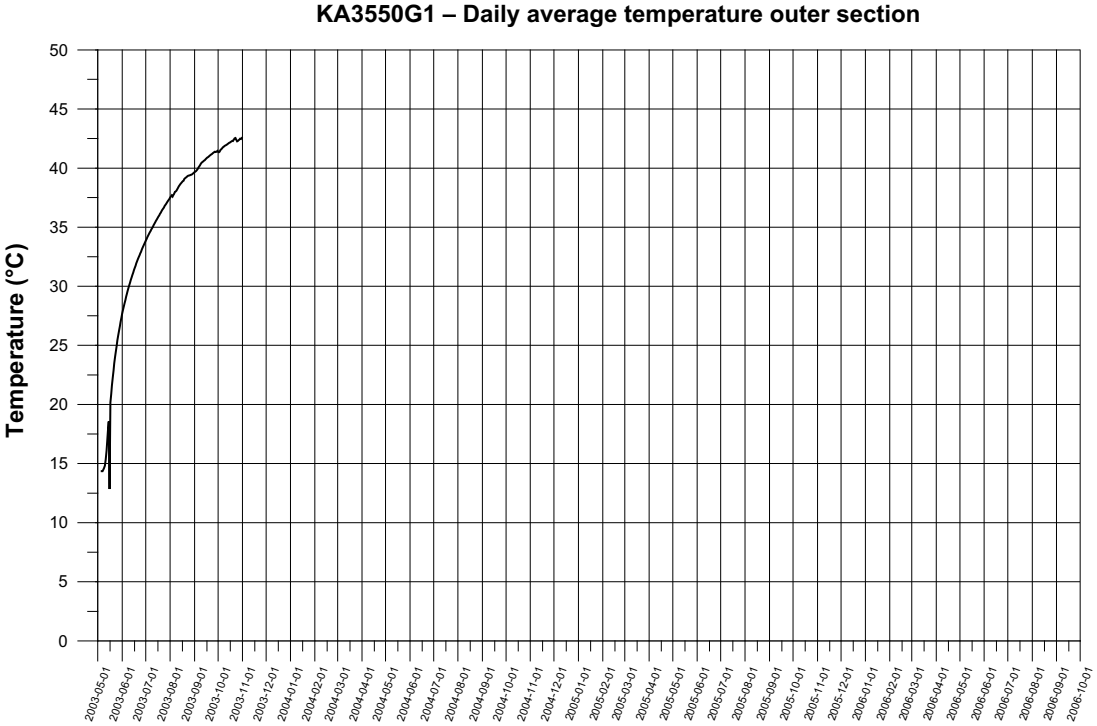

KA3552G01

Temperature

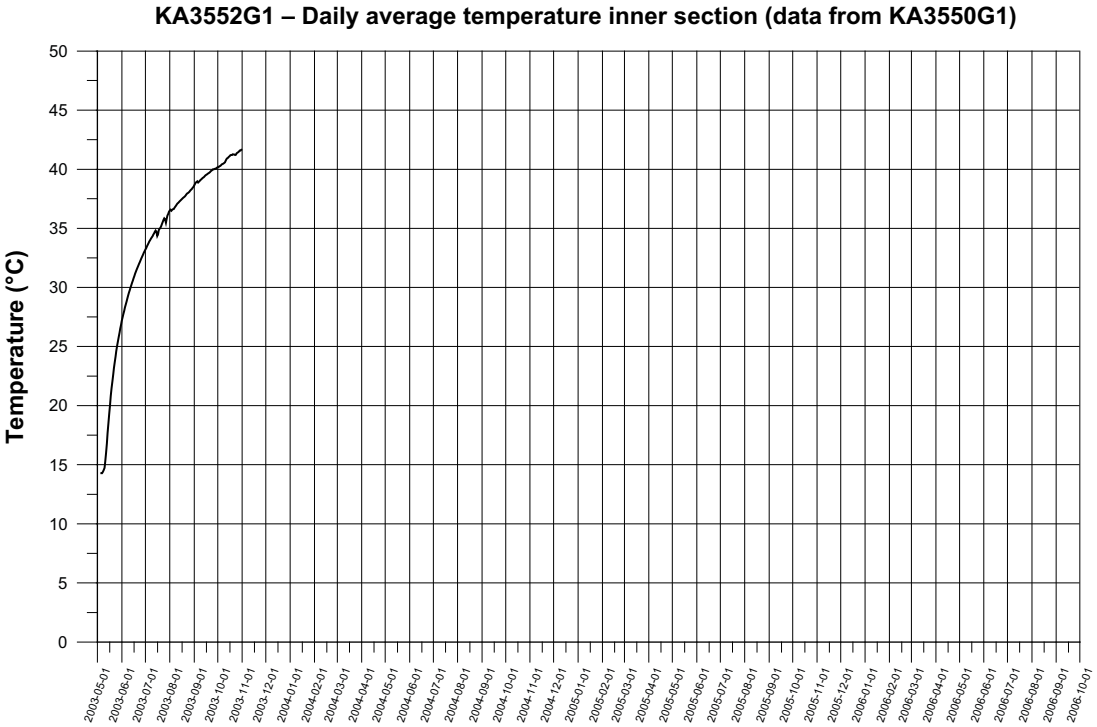

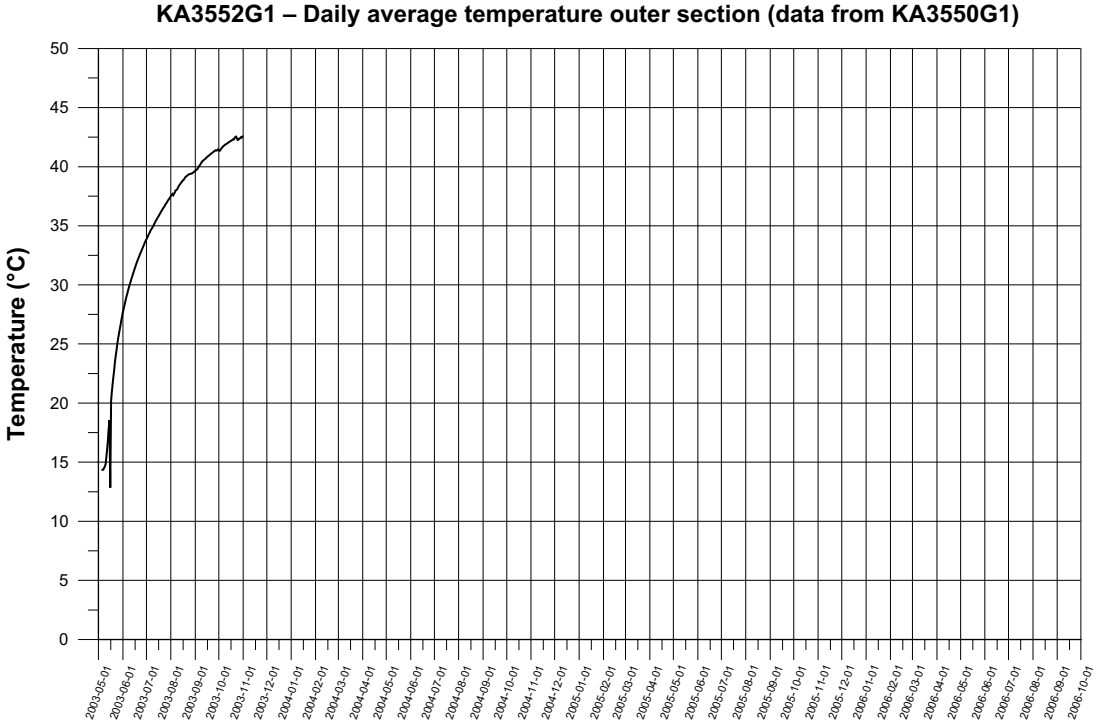

- The data is replaced with data from KA3550G01.

KA3554G01

Temperature

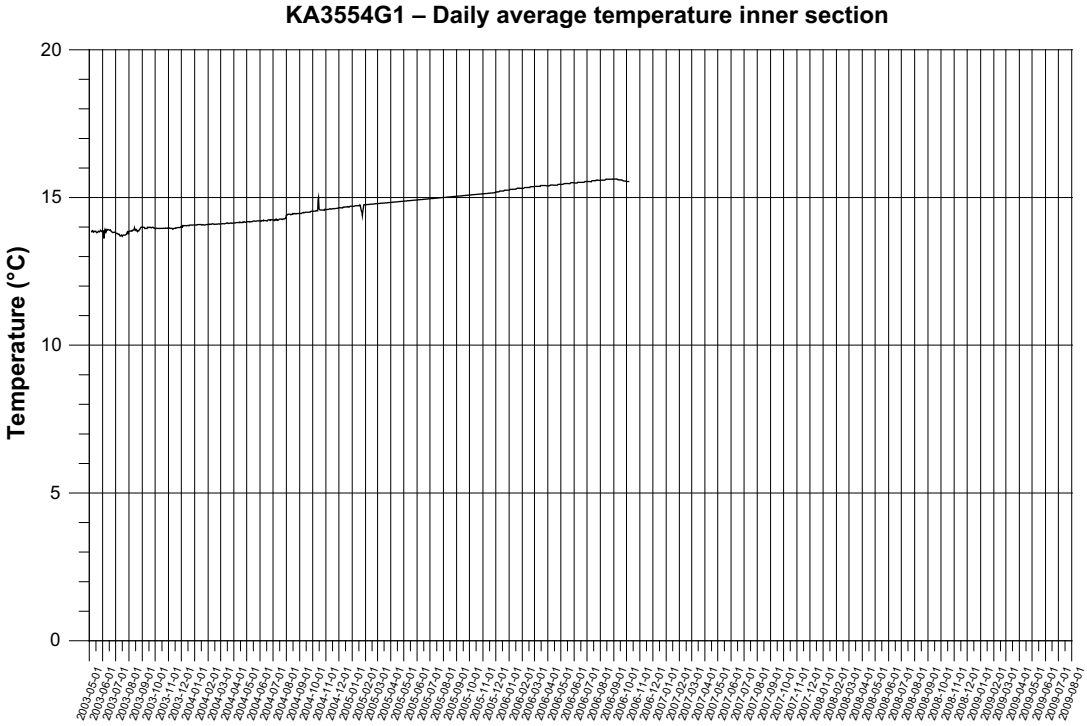

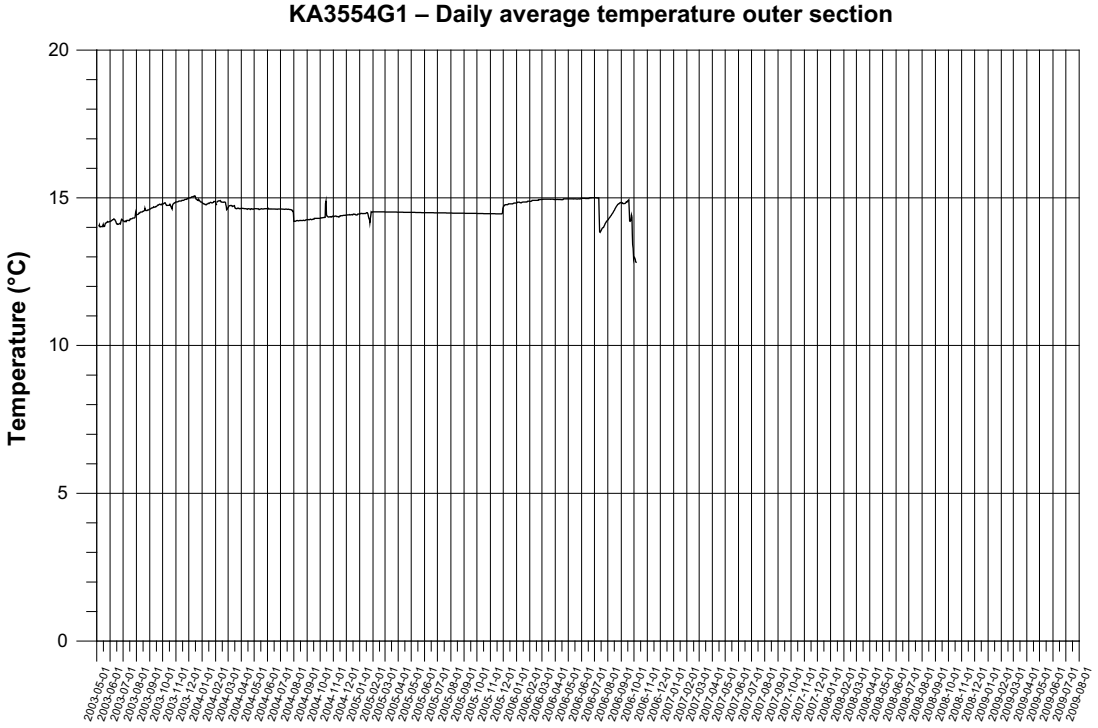

Data after 2004-08-01 is replaced by data from KA3542G01.

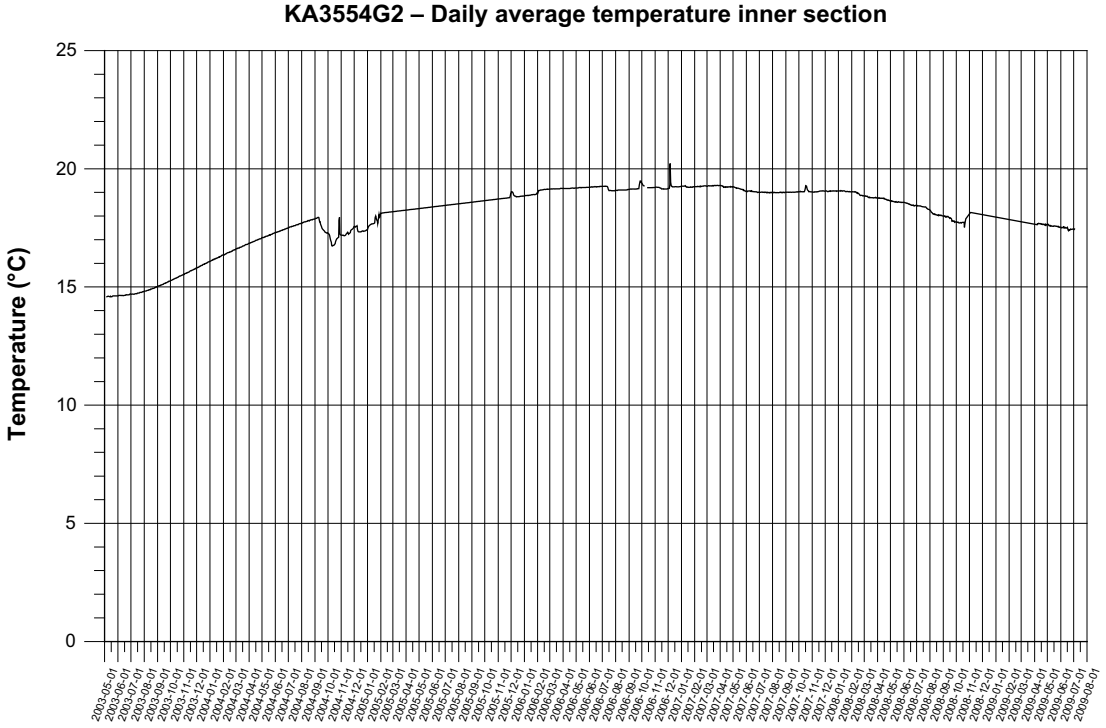

KA3554G02

Temperature

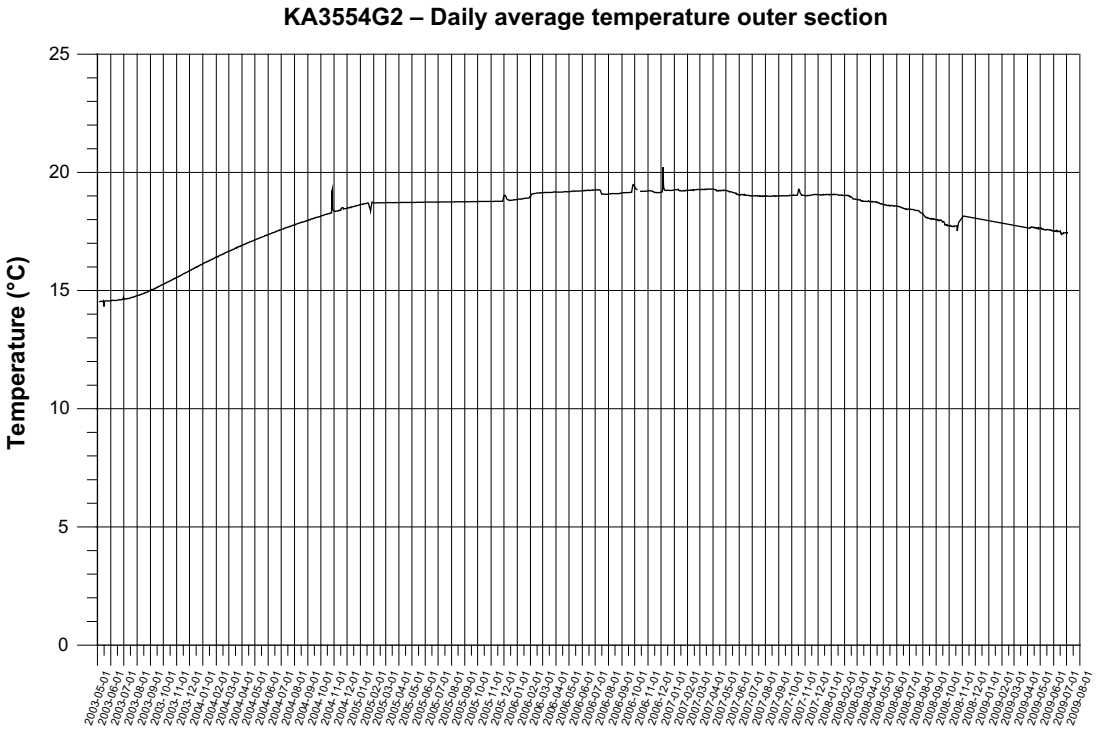

Pressure head in borehole sections

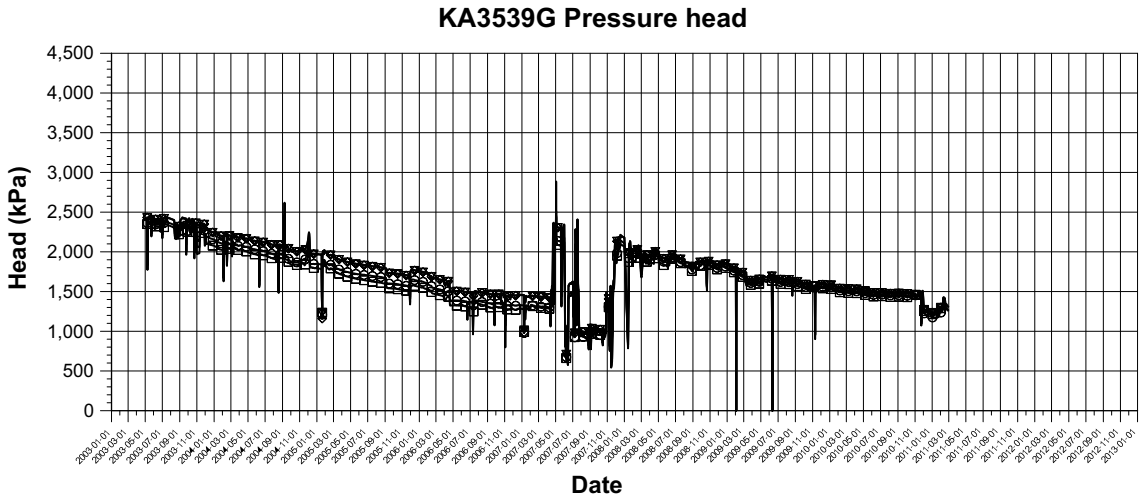

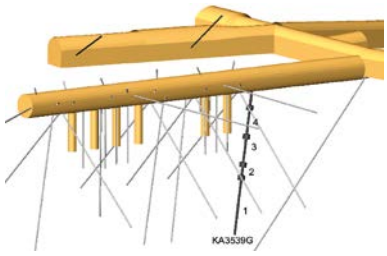

Events

Start backfilling of section I 2001-09-03
Stop backfilling of section I 2001-11-20
Casting of inner plug finalized 2001-12-19
Start backfilling of section II 2003-04-29
Stop backfilling of section II 2003-06-27
Casting of outer plug finalized 2003-09-11
Packer failure of KA3573A:3 2006-04-18
Startdrilling of Fine Sealing Project 2007-03-12
Start grouting of Fine Sealing Project 2007-11-19
Excavation start of TASS tunnel 2007-12-11
Excavation stop of TASS tunnel 2008-12-18

Borehole sections

G:1 18.6 m – 30 m
G:2 15.85 m – 17.6 m
G:3 10 m – 14.85 m
G:4 4 m – 9 m

P_KA3539G.GRF 2013-06-10

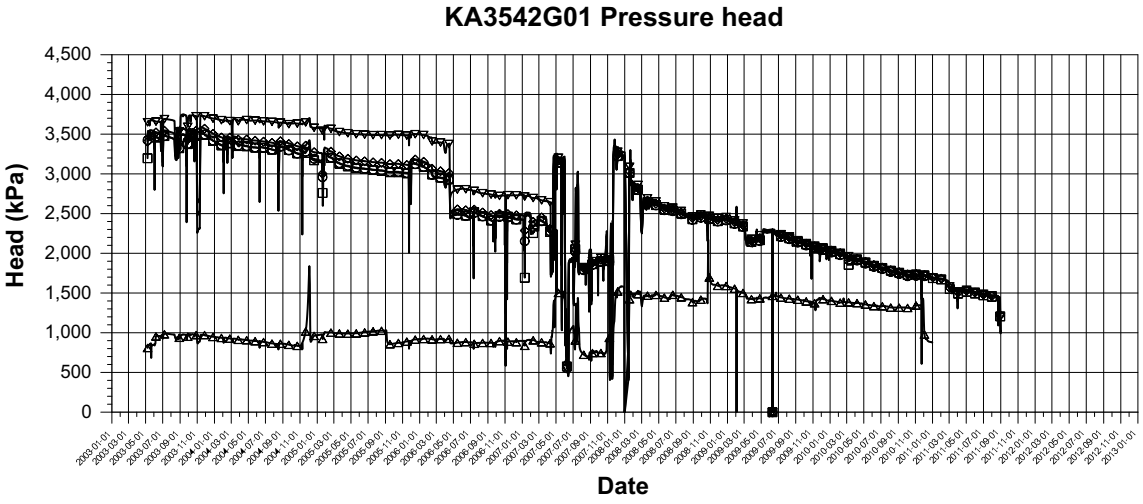

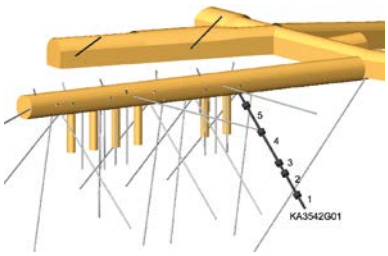

Events

Start backfilling of section I 2001-09-03
Stop backfilling of section I 2001-11-20
Casting of inner plug finalized 2001-12-19
Start backfilling of section II 2003-04-29
Stop backfilling of section II 2003-06-27
Casting of outer plug finalized 2003-09-11
Packer failure of KA3573A:3 2006-04-18
Start drilling of Fine Sealing Project 2007-03-12
Start grouting of Fine Sealing Project 2007-11-19
Excavation start of TASS tunnel 2007-12-11
Excavation stop of TASS tunnel 2008-12-18

Borehole sections

G01:1 27 m – 30 m
G01:2 21.3 m – 26 m
G01:3 18.6 m – 20.3 m
G01:4 10.5 m – 17.6 m
G01:5 3.5 m – 9.5 m

P_KA3542G01.GRF 2013-06-10

KA3542G02 Pressure head

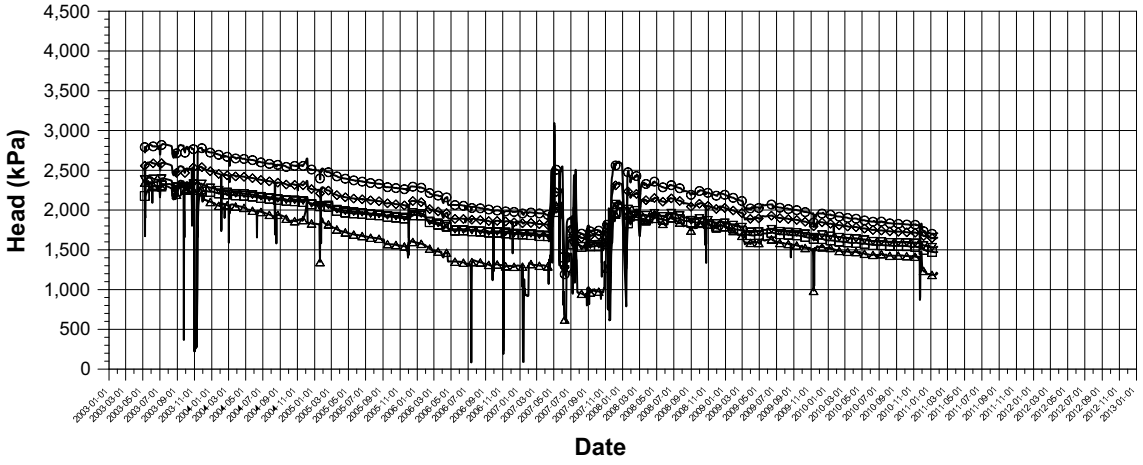

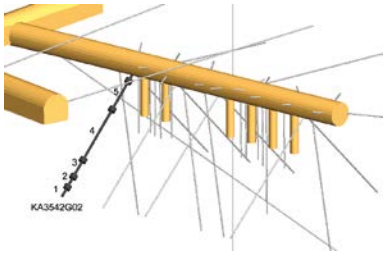

Events

Start backfilling of section I 2001-09-03
Stop backfilling of section I 2001-11-20
Casting of inner plug finalized 2001-12-19
Start backfilling of section II 2003-04-29
Stop backfilling of section II 2003-06-27
Casting of outer plug finalized 2003-09-11
Packer failure of KA3573A:3 2006-04-18
Start drilling of Fine Sealing Project 2007-03-12
Start grouting of Fine Sealing Project 2007-11-19
Excavation start of TASS tunnel 2007-12-11
Excavation stop of TASS tunnel 2008-12-18

Borehole sections

G02:1 28.2 m – 30.01 m
G02:2 25.6 m – 27.2 m
G02:3 21.5 m – 24.6 m
G02:4 9 m – 20.5 m
G02:5 2 m – 8 m

P-KA3542G02.GRF 2013-06-10

KA3544G01 Pressure head

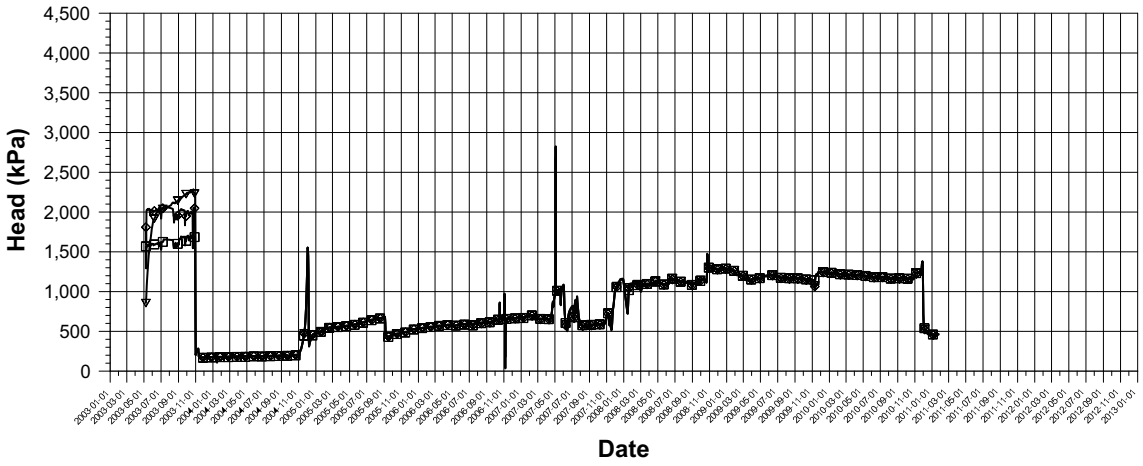

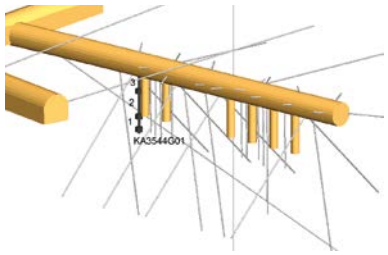

Events

Start backfilling of section I 2001-09-03
Stop backfilling of section I 2001-11-20
Casting of inner plug finalized 2001-12-19
Start backfilling of section II 2003-04-29
Stop backfilling of section II 2003-06-27
Casting of outer plug finalized 2003-09-11
Packer failure of KA3573A:3 2006-04-18
Start drilling of Fine Sealing Project 2007-03-12
Start grouting of Fine Sealing Project 2007-11-19
Excavation start of TASS tunnel 2007-12-11
Excavation stop of TASS tunnel 2008-12-18

Borehole sections

G01:1 11.65 m – 12 m
G01:2 8.9 m – 10.65 m
G01:3 3.5 m – 7.9 m

P-KA3544G01.GRF 2013-06-10

KA3546G01 Pressure head

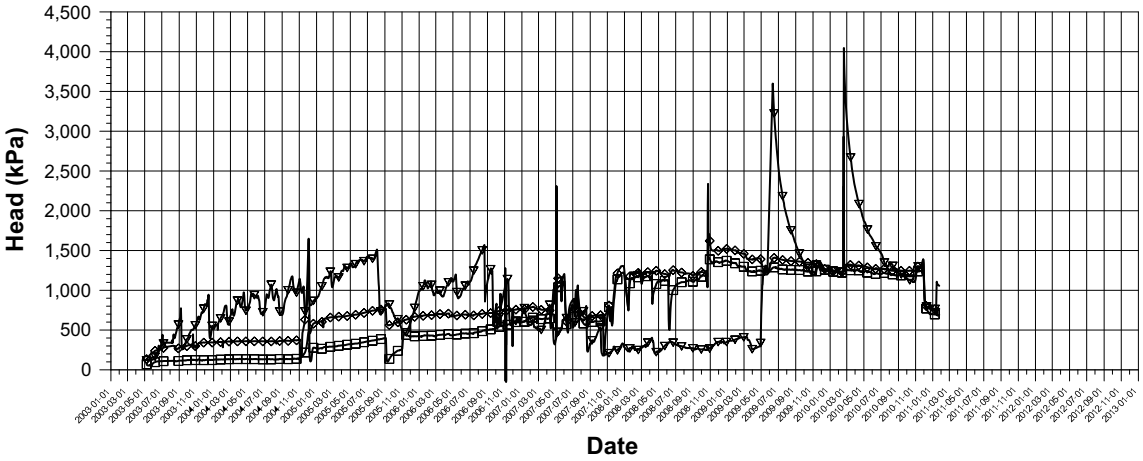

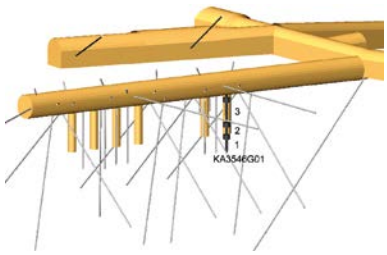

Events

Start backfilling of section I 2001-09-03
Stop backfilling of section I 2001-11-20
Casting of inner plug finalized 2001-12-19
Start backfilling of section II 2003-04-29
Stop backfilling of section II 2003-06-27
Casting of outer plug finalized 2003-09-11
Packer failure of KA3573A:3 2006-04-18
Start drilling of Fine Sealing Project 2007-03-12
Start grouting of Fine Sealing Project 2007-11-19
Excavation start of TASS tunnel 2007-12-11
Excavation stop of TASS tunnel 2008-12-18

Borehole sections

G01:1 9.3 m – 12 m
G01:2 6.75 m – 8.3 m
G01:3 1.5 m – 5.75 m

P_KA3546G01.GRF 2013-06-10

KA3548A01 Pressure head

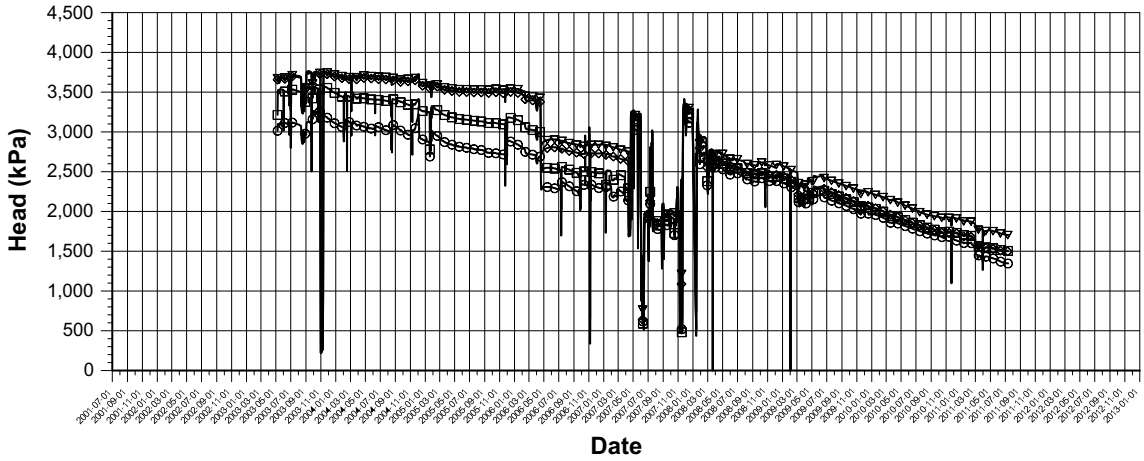

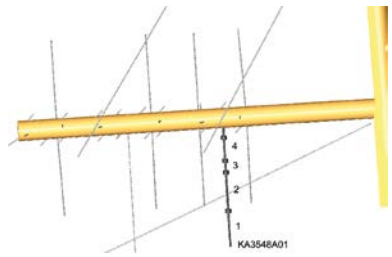

Events

Start backfilling of section I 2001-09-03
Stop backfilling of section I 2001-11-20
Casting of inner plug finalized 2001-12-19
Start backfilling of section II 2003-04-29
Stop backfilling of section II 2003-06-27
Casting of outer plug finalized 2003-09-11
Packer failure of KA3573A:3 2006-04-18
Start drilling of Fine Sealing Project 2007-03-12
Start grouting of Fine Sealing Project 2007-11-19
Excavation start of TASS tunnel 2007-12-11
Excavation stop of TASS tunnel 2008-12-18

Borehole sections

A01:1 21.5 m – 30 m
A01:2 11.75 m – 20.5 m
A01:3 8.8 m – 10.75 m
A01:4 3 m – 7.8 m

P_KA3548A01.GRF 2013-06-10

KA3550G01 Pressure head

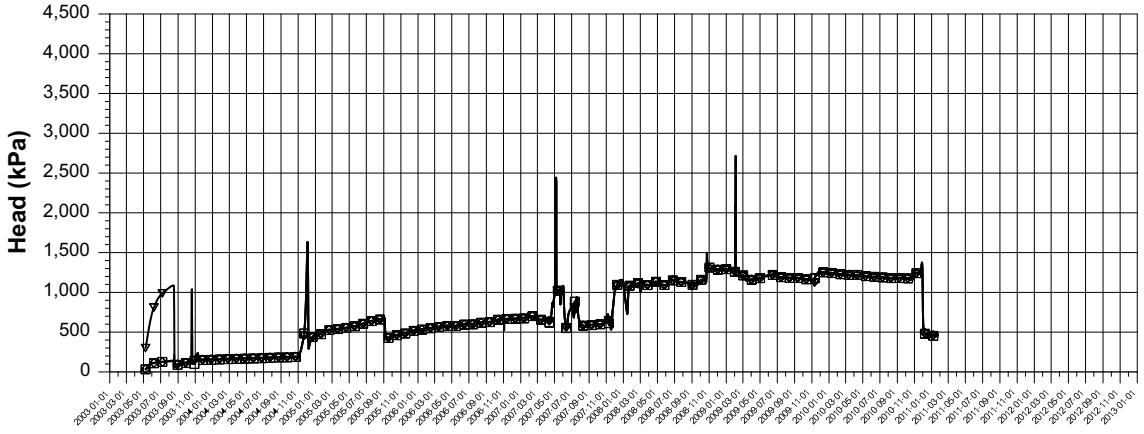

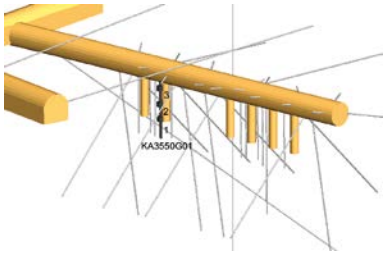

Events

Start backfilling of section I 2001-09-03
Stop backfilling of section I 2001-11-20
Casting of inner plug finalized 2001-12-19
Start backfilling of section II 2003-04-29
Stop backfilling of section II 2003-06-27
Casting of outer plug finalized 2003-09-11
Packer failure of KA3573A:3 2006-04-18
Start drilling of Fine Sealing Project 2007-03-12
Start grouting of Fine Sealing Project 2007-11-19
Excavation start of TASS tunnel 2007-12-11
Excavation stop of TASS tunnel 2008-12-18

Borehole sections

G01:1 8.3 m – 12.03 m
G01:2 5.2 m – 7.3 m
G01:3 1.8 m – 4.2 m

P_KA3550G01.GRF 2013-06-10

KA3552G01 Pressure head

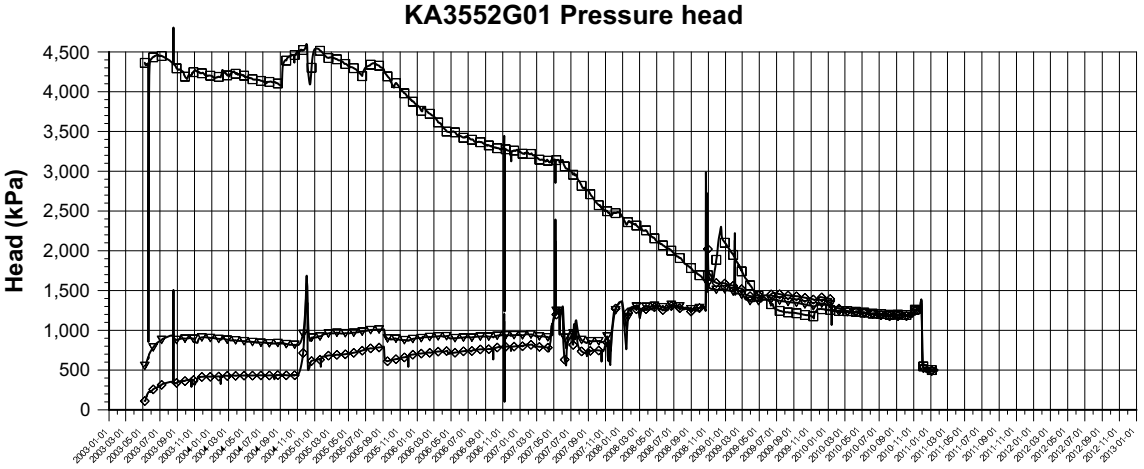

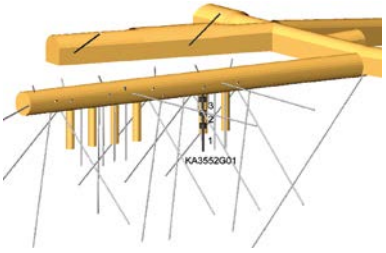

Events

Start backfilling of section I 2001-09-03
Stop backfilling of section I 2001-11-20
Casting of inner plug finalized 2001-12-19
Start backfilling of section II 2003-04-29
Stop backfilling of section II 2003-06-27
Casting of outer plug finalized 2003-09-11
Packer failure of KA3573A:3 2006-04-18
Start drilling of Fine Sealing Project 2007-03-12
Start grouting of Fine Sealing Project 2007-11-19
Excavation start of TASS tunnel 2007-12-11
Excavation stop of TASS tunnel 2008-12-18

Borehole sections

G01:1 7.05 m – 12 m
G01:2 4.35 m – 6.05 m
G01:3 1.5 m – 3.35 m

P_KA3552G01.GRF 2013-08-15

KA3554G01 Pressure head

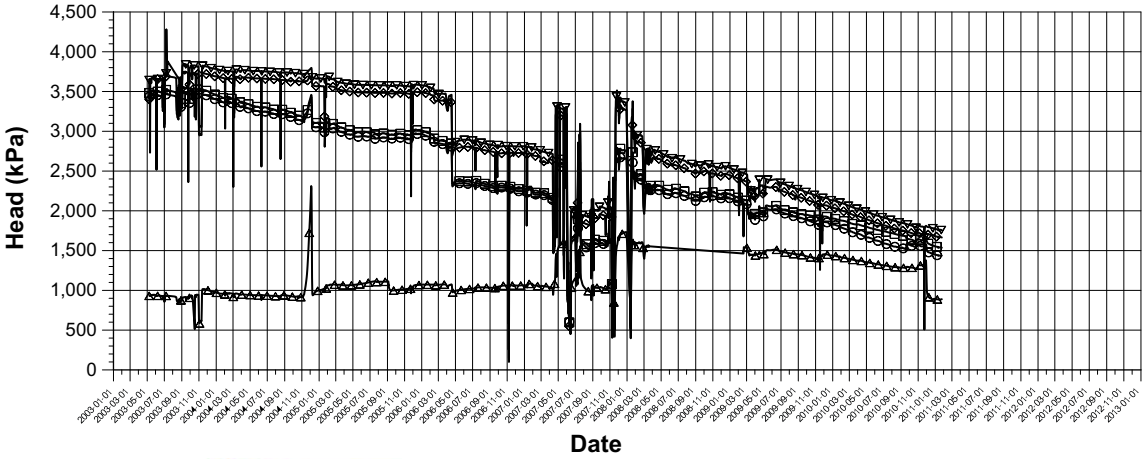

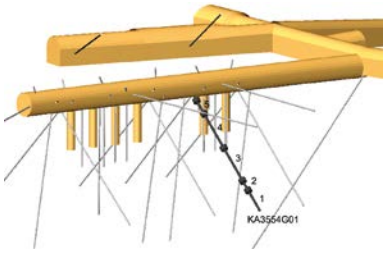

Events

Start backfilling of section I 2001-09-03
Stop backfilling of section I 2001-11-20
Casting of inner plug finalized 2001-12-19
Start backfilling of section II 2003-04-29
Stop backfilling of section II 2003-06-27
Casting of outer plug finalized 2003-09-11
Packer failure of KA3573A:3 2006-04-18
Start drilling of Fine Sealing Project 2007-03-12
Start grouting of Fine Sealing Project 2007-11-19
Excavation start of TASS tunnel 2007-12-11
Excavation stop of TASS tunnel 2008-12-18

Borehole sections

G01:1 25.15 m – 30.01 m
G01:2 22.6 m – 24.15 m
G01:3 14 m – 21.6 m
G01:4 5 m – 13 m
G01:5 1.5 m – 4 m

P~KA3554G01~GRF 2013-06-10

KA3554G02 Pressure head

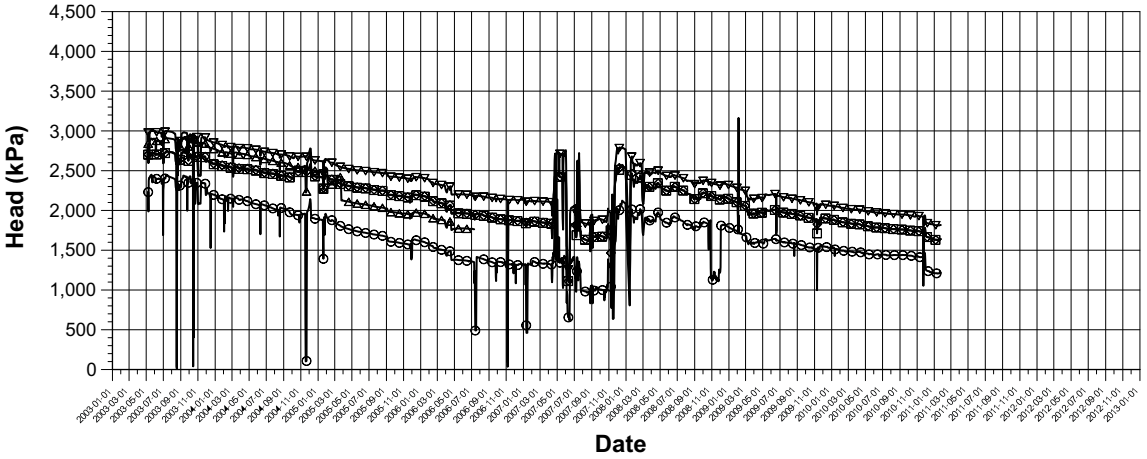

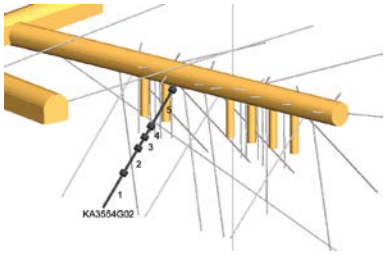

Events

Start backfilling of section I 2001-09-03
Stop backfilling of section I 2001-11-20
Casting of inner plug finalized 2001-12-19
Start backfilling of section II 2003-04-29
Stop backfilling of section II 2003-06-27
Casting of outer plug finalized 2003-09-11
Packer failure of KA3573A:3 2006-04-18
Start drilling of Fine Sealing Project 2007-03-12
Start grouting of Fine Sealing Project 2007-11-19
Excavation start of TASS tunnel 2007-12-11
Excavation stop of TASS tunnel 2008-12-18

Borehole sections

G02:1 22 m – 30.01 m
G02:2 15.9 m – 21 m
G02:3 13.2 m – 14.9 m
G02:4 10.5 m – 12.2 m
G02:5 1.5 m – 9.5 m

P~KA3554G02~GRF 2013-06-10

Appendix 3

Hydraulic tests, operation phase Prototype repository

Table A3-1. Single hole tests during the campaign in May 2003.

Borehole	Section (m)	HM section	Single hole test no.	Date of test	Start of test	Flow start	Flow stop	Test stop
KA3550G01:2[(1)]	5.20–7.30	X	–	–	–	–	–	–
KA3552G01:2	4.35–6.05	X	1:1	2003-05-08	10:00:00	10:52:00	11:39:00	13:58:00
KA3554G01:2	22.60–24.15	X	1:2	2003-05-08	13:15:00	13:46:00	14:16:00	16:00:00
KA3554G02:4	10.50–12.20	X	1:3	2003-05-08	14:45:00	15:16:00	15:46:00	18:00:00
KA3548A01:3	8.80–10.75	X	1:4	2003-05-08	16:15:00	16:46:00	17:16:00	20:00:00
KA3542G01:3	18.60–20.30	X	1:5	2003-05-08	17:53:00	18:23:00	18:53:00	21:00:00
KA3544G01:2	8.90–10.65	X	1:6	2003-05-08	19:23:00	19:53:00	20:43:00	23:00:00
KA3542G02:2	25.60–27.20	X	1:7	2003-05-09	05:55:00	06:25:00	07:25:00	10:00:00
KA3563G:4	1.50–3.00	–	1:8	2003-05-09	05:55:00	06:26:00	07:26:00	10:00:00
KA3546G01:2	6.75–8.30	X	1:9	2003-05-10	06:00:00	06:30:00	07:30:05	10:00:00
KA3566G01:2	20.0–21.5	–	1:10	2003-05-10	06:00:00	06:34:00	07:34:00	10:00:00
KA3572G01:2	2.70–5.30	–	1:11	2003-05-11	08:00:00	08:30:00	09:30:00	12:00:00
KA3574G01:3	1.80–4.10	–	1:12	2003-05-11	08:00:00	08:32:00	09:32:00	12:00:00
KA3539G:2	15.85–17.6	X	1:13	2003-05-09	08:00:00	08:40:00	14:50:00	06:30:00

[(1)] indicates packer system failure, “X” indicates that section is equipped with HM sensors.

Table A3-2. Interference tests during the campaign in May 2003.

Borehole	Section (m)	HM section	Test no.	Date of test	Start of test	Flow start	Flow stop	Test stop (Next day)
KA3539G:2	15.85–17.60	X	1:21	2003-05-09	06:40:00	08:40:00	14:50:00	06:30:00
KA3542G02:5	2.00–8.00	–	1:22	2003-05-10	06:55:00	08:55:00	14:55:00	08:30:00
KA3554G01:2	22.60–24.15	X	1:23	2003-05-11	08:35:00	10:35:00	16:35:00	09:41:00
KA3590G02:1	25.50–30.01	–	1:24	2003-05-12	07:41:00	09:41:00	15:41:00	09:40:00
KG0021A01:3	35.00–36.00	–	1:25	2003-05-13	07:40:00	09:40:00	15:40:00	09:40:00
KG0048A01:3	32.80–33.80	–	1:26	2003-05-14	07:40:00	09:40:00	15:40:00	09:40:00
KA3573A:4	10.50–12.50	–	1:27	2003-05-15	07:40:00	09:40:00	15:40:00	09:40:00

Table A3-3. Single hole tests during the campaign in October 2003.

Borehole	Section (m)	HM section	Single hole test no.	Date of test	Start of test	Flow start	Flow stop	Test stop
KA3550G01:2[(1)]	5.20–7.30	X	–	–	–	–	–	–
KA3552G01:2	4.35–6.05	X	2:1	2003-10-21	10:30:00	12:30:00	14:30:00	15:30:00
KA3554G01:2	22.60–24.15	X	2:2	2003-10-21	13:30:00	15:30:00	16:00:00	17:00:00
KA3554G02:4	10.50–12.20	X	2:3	2003-10-22	05:45:00	07:45:00	09:45:00	10:45:00
KA3548A01:3	8.80–10.75	X	2:4	2003-10-22	16:15:00	18:15:00	18:45:00	19:45:00
KA3542G01:3	18.60–20.30	X	2:5	2003-10-22	14:45:00	16:45:00	17:15:00	18:15:00
KA3544G01:2	8.90–10.65	X	2:6	2003-10-22	08:45:00	10:45:00	12:45:00	13:45:00
KA3542G02:2	25.60–27.20	X	2:7	2003-10-23	05:15:00	07:15:00	09:15:00	10:15:00
KA3546G01:2	6.75–8.30	X	2:9	2003-10-22	11:45:00	13:45:00	15:45:00	16:45:00
KA3539G:2	15.85–17.6	X	2:13	2003-10-23	08:15:00	10:15:00	10:45:00	12:45:00

[(1)] indicates packer system failure, “X” indicates that section is equipped with HM sensors.

Table A3-4. Single hole tests during the campaign in February 2004.

Borehole	Section (m)	HM section	Single hole test no.	Date of test	Start of test	Flow start	Flow stop	Test stop
KA3550G01:2[(1)]	5.20–7.30	X	–[(1)]	–	–	–	–	–
KA3552G01:2	4.35–6.05	X	3:1	2004-02-02	09:30:00	10:30:00	13:30:00	14:30:00
KA3554G01:2	22.60–24.15	X	3:2	2004-02-02	15:30:00	17:30:00	19:30:00	21:30:00
KA3554G02:4	10.50–12.20	X	3:3	2004-02-02	12:30:00	14:30:00	16:30:00	17:30:00
KA3548A01:3	8.80–10.75	X	3:4	2004-02-03	14:00:00	16:00:00	17:00:00	19:00:00
KA3542G01:3	18.60–20.30	X	3:5	2004-02-03	11:00:00	13:00:00	14:00:00	16:00:00
KA3544G01:2[(1)]	8.90–10.65	X	–[(1)]	–	–	–	–	–
KA3542G02:2	25.60–27.20	X	3:7	2004-02-04	06:00:00	08:00:00	11:00:00	12:30:00
KA3546G01:2	6.75–8.30	X	3:9	2004-02-03	06:30:00	08:30:00	11:30:00	13:00:00
KA3539G:2	15.85–17.6	X	3:13	2004-02-04	10:30:00	12:30:00	13:30:00	15:30:00

[(1)] indicates packer system failure, “X” indicates that section is equipped with HM sensors.

Table A3-5. Single hole tests during the campaign in August 2004.

Borehole	Section (m)	HM section	Single hole test no.	Date of test	Start of test	Flow start	Flow stop	Test stop
KA3550G01:2[(1)]	5.20–7.30	X	–[(1)]	–	–	–	–	–
KA3552G01:2	4.35–6.05	X	4:1	2004-08-11	17:00:00	17:20:00	19:20:00	22:30:00
KA3554G01:2	22.60–24.15	X	4:2a	2004-08-17	08:00:00	08:50:00	10:50:00	13:10:00
KA3554G01:2	22.60–24.15	X	4:2b	2004-08-17	13:10:00	13:10:00	15:10:00	16:10:00
KA3554G01:2	22.60–24.15	X	4:2c	2004-08-17	16:10:00	16:10:00	18:10:00	20:30:00
KA3554G02:4	10.50–12.20	X	4:3a	2004-08-12	12:30:00	14:10:00	16:10:00	17:10:00
KA3554G02:4	10.50–12.20	X	4:3b	2004-08-12	17:10:00	17:10:00	19:10:00	20:10:00
KA3548A01:3	8.80–10.75	X	4:4	2004-08-18	06:00:00	07:35:00	08:35:00	10:00:00
KA3542G01:3	18.60–20.30	X	4:5a	2004-08-16	09:00:00	11:05:00	12:05:00	14:35:00
KA3542G01:3	18.60–20.30	X	4:5b	2004-08-16	14:00:00	14:35:00	15:35:00	17:35:00
KA3542G01:3	18.60–20.30	X	4:5c	2004-08-16	17:00:00	17:35:00	18:35:00	20:00:00
KA3544G01:2[(1)]	8.90–10.65	X	–[(1)]	–	–	–	–	–
KA3542G02:2	25.60–27.20	X	4:7	2004-08-13	06:00:00	06:50:00	09:50:00	13:50:00
KA3546G01:2	6.75–8.30	X	4:9	2004-08-12	08:00:00	09:05:00	12:05:00	15:05:00
KA3539G:2	15.85–17.6	X	4:13a	2004-08-18	09:00:00	10:00:00	11:00:00	12:30:00
KA3539G:2	15.85–17.6	X	4:13b	2004-08-18	12:30:00	12:30:00	13:30:00	15:30:00

[(1)] indicates packer system failure, “X” indicates that section is equipped with HM sensors.

Table A3-6. Single hole tests during the campaign in January 2005.

Borehole	Section (m)	HM section	Single hole test no.	Date of test	Start of test	Flow start	Flow stop	Test stop
KA3550G01:2[(1)]	5.20–7.30	X	–[(1)]	–	–	–	–	–
KA3552G01:2	4.35–6.05	X	5:1	2005-01-23	11:00:00	13:05:00	15:00:00	17:00:00
KA3554G01:2	22.60–24.15	X	5:2a	2005-01-20	10:30:00	12:30:00	14:30:00	16:30:00
KA3554G01:2	22.60–24.15	X	5:2b	2005-01-21	10:00:00	12:00:00	14:00:00	16:00:00
KA3554G01:2	22.60–24.15	X	5:2c	2005-01-22	13:00:00	15:00:00	21:00:00	15:00:00*
KA3554G02:4	10.50–12.20	X	5:3a	2005-01-24	08:00:00	09:00:00	11:00:00	13:00:00
KA3554G02:4	10.50–12.20	X	5:3b	2005-01-25	15:00:00	16:00:00	18:00:00	20:00:00
KA3548A01:3	8.80–10.75	X	5:4a	2005-01-20	06:00:00	07:15:00	08:15:00	10:15:00
KA3548A01:3	8.80–10.75	X	5:4b	2005-01-23	10:00:00	11:00:00	12:00:00	14:00:00
KA3548A01:3	8.80–10.75	X	5:4c	2005-01-24	06:00:00	07:00:00	08:00:00	10:00:00
KA3542G01:3	18.60–20.30	X	5:5a	2005-01-20	08:00:00	09:15:00	10:15:00	12:15:00
KA3542G01:3	18.60–20.30	X	5:5b	2005-01-21	08:00:00	09:00:00	10:00:00	12:00:00
KA3542G01:3	18.60–20.30	X	5:5c	2005-01-22	06:00:00	07:00:00	08:00:00	10:00:00
KA3544G01:2[(1)]	8.90–10.65	X	–[(1)]	–	–	–	–	–
KA3542G02:2	25.60–27.20	X	5:7a	2005-01-22	08:00:00	10:00:00	13:00:00	15:00:00
KA3542G02:2	25.60–27.20	X	5:7b	2005-01-23	06:00:00	07:00:00	10:00:00	12:00:00
KA3563G:4	1.50–3.00	–	5:8	2005-01-24	11:00:00	12:00:00	13:00:00	15:00:00
KA3546G01:2	6.75–8.30	X	5:9	2005-01-25	10:00:00	11:00:00	14:00:00	16:00:00
KA3566G01:2	20.00–21.50	–	5:10	2005-01-25	06:00:00	07:00:00	07:58:00	10:00:00
KA3572G01:2	2.70–5.30	–	5:11	2005-01-21	06:00:00	07:00:00	08:00:00	10:00:00
KA3574G01:3	1.80–4.10	–	5:12	2005-01-25	08:00:00	09:00:00	10:00:00	12:00:00
KA3539G:2	15.85–17.60	X	5:13a	2005-01-19	12:00:00	13:30:00	14:30:00	16:30:00
KA3539G:2	15.85–17.60	X	5:13b	2005-01-20	14:30:00	15:30:00	21:30:00	15:30:00*

[(1)] indicates packer system failure, “X” indicates that section is equipped with HM sensors.

Table A3-7. Interference tests during the campaign in January 2005.

Borehole	Section (m)	HM section	Test no.	Date of test	Start of test	Flow start	Flow stop	Test stop (Next day)
KA3539G:2	15.85–17.60	X	5:21	2005-01-20	13:30:00	15:30:00	21:30:00	15:30:00
KA3542G02:5	2.00–8.00	–	5:22	2005-01-24	13:00:00	15:00:00	21:00:00	15:00:00
KA3554G01:2	22.60–24.15	X	5:23	2005-01-22	13:00:00	15:00:00	21:00:00	15:00:00
KA3590G02:1	25.50–30.01	–	5:24	2005-01-21	13:00:00	15:00:00	21:00:00	15:00:00
KG0021A01:3	35.00–36.00	–	5:25	2005-01-19	14:00:00	16:00:00	22:00:00	16:00:00
KG0048A01:3	32.80–33.80	–	5:26	2005-01-23	14:00:00	16:00:00	22:00:00	16:00:00
KA3573A:4	10.50–12.50	–	5:27	2005-01-25	17:00:00	19:00:00	15:00:00*	19:00:00**

* = 2005-01-26,
** = 2005-01-28.

Table A3-8. Single hole tests during the campaign in November–December 2005.

Borehole	Section (m)	HM section	Single hole test no.	Date of test	Start of test	Flow start	Flow stop	Test stop
KA3550G01:2[(1)]	5.20–7.30	X	–[(1)]	–	–	–	–	–
KA3552G01:2	4.35–6.05	X	6:1	2005-11-30	12:00:00	13:00:00	15:00:00	16:00:00
KA3554G01:2	22.60–24.15	X	6:2a	2005-11-28	18:00:00	19:00:00	21:00:00	22:00:00
KA3554G01:2	22.60–24.15	X	6:2b	2005-11-29	17:00:00	18:00:00	20:00:00	21:00:00
KA3554G01:2	22.60–24.15	X	6:2c	2005-11-30	17:00:00	18:00:00	20:00:00	21:00:00
KA3554G02:4	10.50–12.20	X	6:3a	2005-11-29	07:00:00	08:00:00	10:00:00	11:00:00
KA3554G02:4	10.50–12.20	X	6:3b	2005-12-01	12:00:00	13:00:00	15:00:00	16:00:00
KA3548A01:3	8.80–10.75	X	6:4a	2005-11-29	15:00:00	16:00:00	17:00:00	18:00:00
KA3548A01:3	8.80–10.75	X	6:4b	2005-11-30	15:00:00	16:00:00	17:00:00	18:00:00
KA3548A01:3	8.80–10.75	X	6:4c	2005-12-01	15:10:00	16:10:00	17:10:00	18:10:00
KA3542G01:3	18.60–20.30	X	6:5c	2005-11-28	13:40:00	14:00:00	15:00:00	17:00:00
KA3542G01:3	18.60–20.30	X	6:5a	2005-11-29	10:00:00	11:00:00	12:00:00	14:00:00
KA3542G01:3	18.60–20.30	X	6:5b	2005-12-01	17:15:00	18:15:00	19:15:00	21:15:00
KA3544G01:2[(1)]	8.90–10.65	X	–[(1)]	–	–	–	–	–
KA3542G02:2	25.60–27.20	X	6:7a	2005-12-01	07:00:00	08:00:00	11:00:00	13:00:00
KA3542G02:2	25.60–27.20	X	6:7b	2005-12-02	06:30:00	07:30:00	10:30:00	12:30:00
KA3563G:4	1.50–3.00	–	–[(2)]	–	–	–	–	–
KA3546G01:2	6.75–8.30	X	6:9	2005-11-30	07:00:00	08:00:00	11:00:00	13:00:00
KA3566G01:2	20.00–21.50	–	–[(2)]	–	–	–	–	–
KA3572G01:2	2.70–5.30	–	–[(2)]	–	–	–	–	–
KA3574G01:3	1.80–4.10	–	–[(2)]	–	–	–	–	–
KA3539G:2	15.85–17.60	X	6:13a	2005-11-28	16:00:00	17:00:00	18:00:00	19:00:00
KA3539G:2	15.85–17.60	X	6:13b	2005-11-29	13:00:00	14:00:00	16:00:00	16:00:00

[(1)] indicates packer system failure, “X” indicates that section is equipped with HM sensors.
[(2)] indicates no test is done in this campaign.

Table A3-9. Single hole tests during the campaign in September 2006.

Borehole	Section (m)	HM section	Single hole test no.	Date of test	Start of test	Flow start	Flow stop	Test stop
KA3550G01:2[(1)]	5.20–7.30	X	–[(1)]	–	–	–	–	–
KA3552G01:2	4.35–6.05	X	7:1	2006-09-28	08:00:00	09:00:00	11:00:00	12:00:00
KA3554G01:2	22.60–24.15	X	7:2a	2006-09-25	12:00:00	13:00:00	15:00:00	17:00:00
KA3554G01:2	22.60–24.15	X	7:2b	2006-09-26	09:00:00	10:00:00	12:00:00	13:00:00
KA3554G01:2	22.60–24.15	X	7:2c	2006-09-27	08:00:00	09:00:00	11:00:00	12:00:00
KA3554G02:4	10.50–12.20	X	7:3a	2006-09-26	06:00:00	07:00:00	09:00:00	10:00:00
KA3554G02:4	10.50–12.20	X	7:3b	2006-09-28	11:00:00	12:00:00	14:00:00	15:00:00
KA3548A01:3	8.80–10.75	X	7:4a	2006-09-26	14:00:00	15:00:00	16:00:00	17:00:00
KA3548A01:3	8.80–10.75	X	7:4b	2006-09-27	06:00:00	07:00:00	08:00:00	09:00:00
KA3548A01:3	8.80–10.75	X	7:4c	2006-09-28	06:00:00	07:00:00	08:00:00	09:00:00
KA3542G01:3	18.60–20.30	X	7:5a	2006-09-25	17:00:00	18:00:00	19:00:00	21:00:00
KA3542G01:3	18.60–20.30	X	7:5b	2006-09-26	16:00:00	17:00:00	18:00:00	20:00:00
KA3542G01:3	18.60–20.30	X	7:5c	2006-09-27	16:00:00	17:00:00	18:00:00	20:00:00
KA3544G01:2[(1)]	8.90–10.65	X	–[(1)]	–	–	–	–	–
KA3542G02:2	25.60–27.20	X	7:7a	2006-09-28	14:00:00	15:00:00	18:00:00	20:00:00
KA3542G02:2	25.60–27.20	X	7:7b	2006-09-29	04:30:00	05:30:00	08:30:00	10:30:00
KA3563G:4	1.50–3.00	–	–[(2)]	–	–	–	–	–
KA3546G01:2	6.75–8.30	X	7:9	2006-09-27	11:00:00	12:00:00	15:00:00	17:00:00
KA3566G01:2	20.00–21.50	–	–[(2)]	–	–	–	–	–
KA3572G01:2	2.70–5.30	–	–[(2)]	–	–	–	–	–
KA3574G01:3	1.80–4.10	–	–[(2)]	–	–	–	–	–
KA3539G:2	15.85–17.60	X	7:13a	2006-09-25	15:00:00	16:00:00	17:00:00	18:00:00
KA3539G:2	15.85–17.60	X	7:13b	2006-09-26	12:00:00	13:00:00	14:00:00	15:00:00

[(1)] indicates packer system failure, “X” indicates that section is equipped with HM sensors.
[(2)] indicates no test is done in this campaign.

Table A3-10. Single hole tests during the campaign in October 2007.

Borehole	Section (m)	HM section	Single hole test no.	Date of test	Start of test	Flow start	Flow stop	Test stop
KA3550G01:2[1]	5.20–7.30	X	–[1]	–	–	–	–	–
KA3552G01:2	4.35–6.05	X	8:1	2007-10-18	07:30:00	08:30:30	10:30:00	11:30:00
KA3554G01:2	22.60–24.15	X	8:2a	2007-10-15	14:40:00	15:41:00	17:40:00	18:40:00
KA3554G01:2	22.60–24.15	X	8:2b	2007-10-16	09:00:00	10:00:00	12:00:00	13:00:00
KA3554G01:2	22.60–24.15	X	8:2c	2007-10-17	07:30:00	08:30:00	10:30:00	11:30:00
KA3554G02:4	10.50–12.20	X	8:3a	2007-10-16	06:00:00	07:00:00	09:00:00	10:00:00
KA3554G02:4	10.50–12.20	X	8:3b	2007-10-17	10:30:00	11:30:00	13:30:00	14:30:00
KA3548A01:3	8.80–10.75	X	8:4a	2007-10-16	14:20:00	15:20:00	16:20:00	17:20:00
KA3548A01:3	8.80–10.75	X	8:4b	2007-10-17	05:30:00	06:30:00	07:30:00	08:30:00
KA3548A01:3	8.80–10.75	X	8:4c	2007-10-18	05:30:00	06:30:00	07:30:00	08:30:00
KA3542G01:3	18.60–20.30	X	8:5a	2007-10-15	19:40:00	20:40:00	21:40:00	23:40:00
KA3542G01:3	18.60–20.30	X	8:5b	2007-10-16	19:20:00	20:20:00	21:20:00	23:20:00
KA3542G01:3	18.60–20.30	X	8:5c	2007-10-17	15:35:00	16:35:00	17:35:00	19:35:00
KA3544G01:2[1]	8.90–10.65	X	–[1]	–	–	–	–	–
KA3542G02:2	25.60–27.20	X	8:7a	2007-10-18	13:30:00	14:30:00	17:30:00	19:00:00
KA3542G02:2	25.60–27.20	X	8:7b	2007-10-19	04:50:00	05:50:00	08:50:00	10:20:00
KA3563G:4	1.50–3.00	–	–[2]	–	–	–	–	–
KA3546G01:2	6.75–8.30	X	8:9	2007-10-17	10:35:00	11:35:00	14:35:05	16:05:00
KA3566G01:2	20.00–21.50	–	–[2]	–	–	–	–	–
KA3572G01:2	2.70–5.30	–	–[2]	–	–	–	–	–
KA3574G01:3	1.80–4.10	–	–[2]	–	–	–	–	–
KA3539G:2	15.85–17.60	X	8:13a	2007-10-15	17:40:00	18:40:00	19:40:00	20:40:00
KA3539G:2	15.85–17.60	X	8:13b	2007-10-16	12:00:00	13:00:00	14:00:00	15:00:00

[1] indicates packer system failure, “X” indicates that section is equipped with HM sensors.
[2] indicates no test is done in this campaign.

Table A3-11. Single hole tests during the campaign in October 2008. (HMS time).

Borehole	Section (m)	HM section	Single hole test no.	Date of test	Start of test	Flow start	Flow stop	Test stop
KA3550G01:2[1]	5.20–7.30	X	–[1]	–	–	–	–	–
KA3552G01:2	4.35–6.05	X	9:1	2008-10-23	09:00:00	10:00:00	–[3]	–
KA3554G01:2	22.60–24.15	X	9:2a	2008-10-20	13:25:00	14:25:00	16:25:00	17:25:00
KA3554G01:2	22.60–24.15	X	9:2b	2008-10-21	10:00:00	11:00:00	13:00:00	14:00:00
KA3554G01:2	22.60–24.15	X	9:2c	2008-10-22	08:40:00	09:40:00	11:40:00	12:40:00
KA3554G02:4	10.50–12.20	X	9:3a	2008-10-21	07:00:00	08:00:00	10:00:00	11:00:00
KA3554G02:4	10.50–12.20	X	9:3b	2008-10-23	12:00:00	13:00:00	15:00:00	16:00:00
KA3548A01:3	8.80–10.75	X	9:4a	2008-10-21	15:00:00	16:00:00	17:00:00	18:00:00
KA3548A01:3	8.80–10.75	X	9:4b	2008-10-22	06:40:00	07:40:00	08:40:00	09:40:00
KA3548A01:3	8.80–10.75	X	9:4c	2008-10-23	06:40:00	07:40:00	08:40:00	09:40:00
KA3542G01:3	18.60–20.30	X	9:5a	2008-10-20	18:30:00	19:30:00	20:30:00	22:30:00
KA3542G01:3	18.60–20.30	X	9:5b	2008-10-21	17:00:00	18:00:00	19:00:00	21:00:00
KA3542G01:3	18.60–20.30	X	9:5c	2008-10-22	16:40:00	17:40:00	18:40:00	20:40:00
KA3544G01:2[1]	8.90–10.65	X	–[1]	–	–	–	–	–
KA3542G02:2	25.60–27.20	X	9:7a	2008-10-23	15:20:00	16:20:00	19:20:00	21:20:00
KA3542G02:2	25.60–27.20	X	9:7b	2008-10-24	05:30:00	06:30:00	09:30:00	11:30:00
KA3563G:4	1.50–3.00	–	–[2]	–	–	–	–	–
KA3546G01:2	6.75–8.30	X	9:9	2008-10-22	11:40:00	12:40:00	15:40:00	17:40:00
KA3566G01:2	20.00–21.50	–	–[2]	–	–	–	–	–
KA3572G01:2	2.70–5.30	–	–[2]	–	–	–	–	–
KA3574G01:3	1.80–4.10	–	–[2]	–	–	–	–	–
KA3539G:2	15.85–17.60	X	9:13a	2008-10-20	16:30:00	17:30:00	18:30:00	19:30:00
KA3539G:2	15.85–17.60	X	9:13b	2008-10-21	13:00:00	14:00:00	15:00:00	16:00:00

[1] indicates packer system failure, “X” indicates that section is equipped with HM sensors.
[2] indicates no test is done in this campaign.
[3] A probable packer failure.

Table A3-12. Interference tests during the campaign in November 2009.

Borehole	Section (m)	HM section	Test no.	Date of test	Start of test	Flow start	Flow stop	Test stop (Next day)
KA3539G:2	15.85–17.60	X	10:21	2009-11-10	07:30:00	08:00:00	14:00:00	08:00:00
KA3542G02:5	2.00–8.00	–	10:22	2009-11-12	07:30:00	08:00:00	14:00:00	08:00:00
KA3554G01:2	22.60–24.15	X	10:23	2009-11-17	07:30:00	08:00:00	14:00:00	08:00:00
KA3590G02:1	25.50–30.01	–	10:24	2009-11-19	07:30:00	08:10:00	14:10:00	08:10:00
KG0021A01:3	35.00–36.00	–	10:25	2009-11-18	07:30:00	08:00:00	14:00:00	08:00:00
KG0048A01:3	32.80–33.80	–	10:26	2009-11-11	07:30:00	08:00:00	14:00:00	08:00:00

Overview of monitoring boreholes

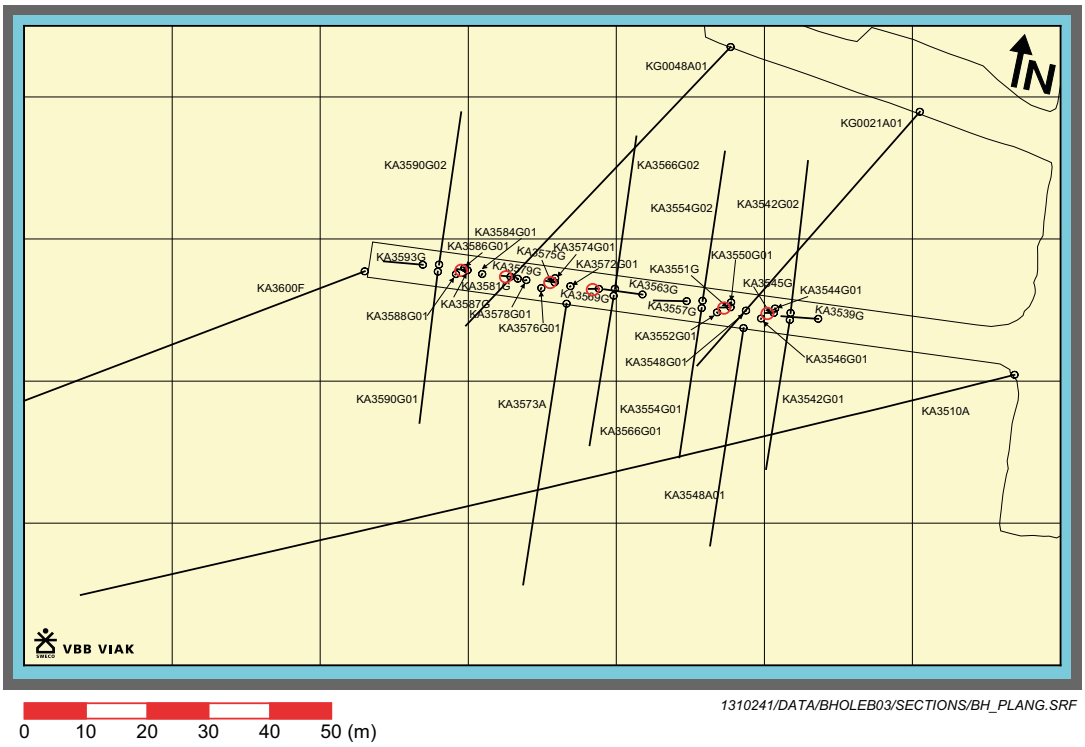

Figure A4-1. *Horizontal view of boreholes along the Prototype tunnel.*

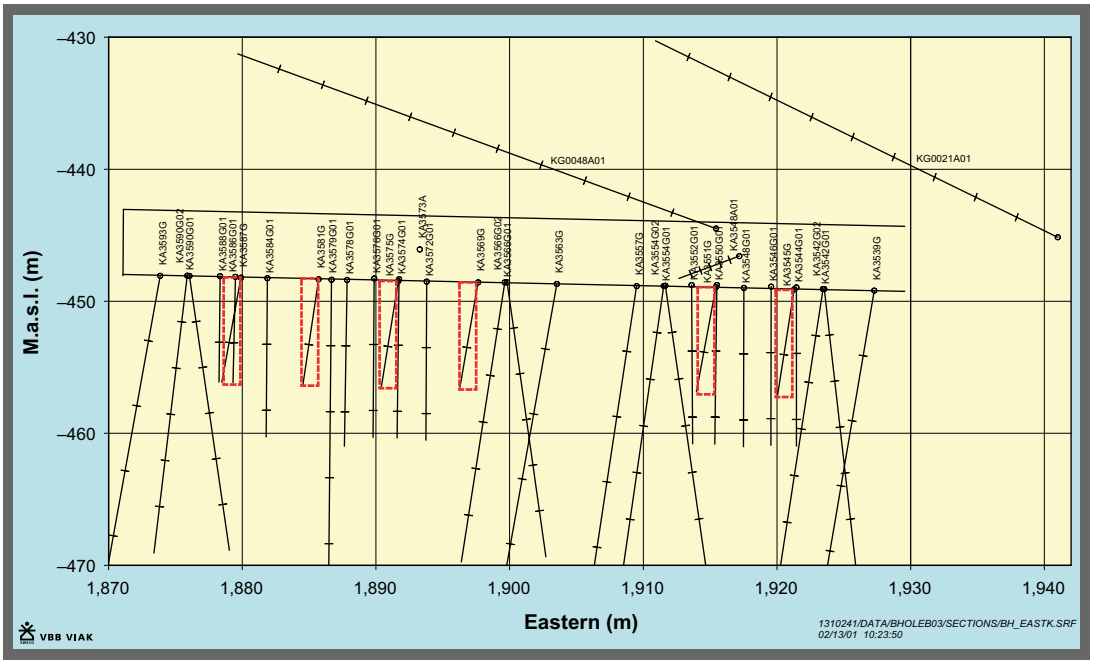

Figure A4-2. *Vertical section along the Prototype tunnel.*

Appendix 5

Geology of borehole test sections

A5.1 KG0010B01 (2.80–4.35 m)

In Figure A5-1 the BIPS image of the section is shown.

A5.2 KA3539G (15.85–17.60 m)

In Figure A5-2 the BIPS image of the section is shown. The fractures that are monitored are at sections 16.86 and 16.87 m.

Table A5-1. Fractures in KA3539G, 15.85–17.60 m. (Aperture: Estimated from BIPS and should not be interpreted as hydraulic aperture but rather as an indication of difference of openness between observed (interpreted) open fracture.)

Borehole	Section (m)	Strike (°)	Dip (°)	Aperture (mm)	Mineral	Comments
KA3539G	16.86	195	59	2	Calcite	Monitored
KA3539G	16.87	53	27	2	Calcite	Monitored

A5.3 KA3542G01 (18.60–20.35 m)

In Figure A5-3 the BIPS image of the section is shown. The fracture that is monitored is at section 19.21 m.

Table A5-2. Fractures in KA3542G01, 18.60–20.35 m.

Borehole	Section (m)	Strike (°)	Dip (°)	Aperture (mm)	Mineral	Comments
KA3542G01	18.74	230	43	1	Chlorite	
KA3542G01	19.21	136	87	2	Calcite	Monitored

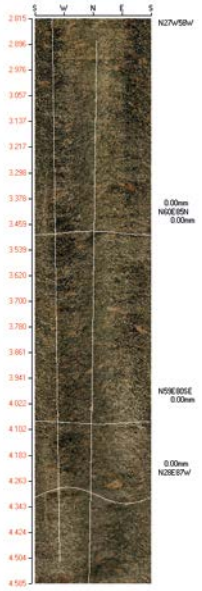

The rocktype of the section is granodiorite. There are veins of pegmatite between 19.16–19.18, 19.48–19.51 and 20.04–20.57 meters.

Figure A5-1. *BIPS image of KG0010B01 (2.80–4.35 m).*

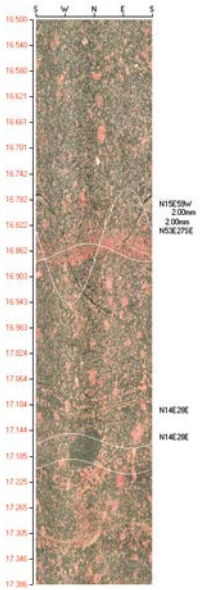

The rocktype of the section is granodiorite. There are xenoliths of mafic igneous rock between 16.15–16.20 m and 17.16–17.20 m.

Figure A5-2. *BIPS image of KA3539G (16.5–17.4 m).*

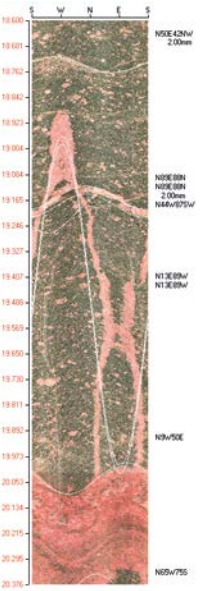

The rocktype of the section is granodiorite. There are veins of pegmatite between 19.16–19.18, 19.48–19.51 and 20.04–20.57 meters.

Figure A5-3. *BIPS image of KA3542G01 (18.60–20.35 m).*

A5.4 KA3542G02 (25.60–27.20 m)

In Figure A5-4 the BIPS image of the section is shown. The fracture that is monitored is at section 26.60 m.

Table A5-3. Fractures in KA3542G02, 25.60–27.20 m.

Borehole	Section (m)	Strike (°)	Dip (°)	Aperture (mm)	Mineral	Comments
KA3542G02	26.56	137	87	1	Pyrite	
KA3542G02	26.60	136	82	1	Pyrite	Monitored
KA3542G02	26.63	138	90	1	Pyrite	
KA3542G02	27.06	47	35	1	Chlorite	

A5.5 KA3544G01 (8.90–12.65 m)

In Figure A5-5 the BIPS image of the section is shown. The fracture that is monitored is at section 9.89 m.

Table A5-4. Fractures in KA3544G01, 8.90–12.65 m.

Borehole	Section (m)	Strike (°)	Dip (°)	Aperture (mm)	Mineral	Comments
KA3544G01	8.98	201	58	4	Pyrite	
KA3544G01	9.89	115	25	1	Pyrite	Monitored
KA3544G01	10.69	174	14	2	Pyrite	
KA3544G01	11.30	59	45	1	Chlorite	

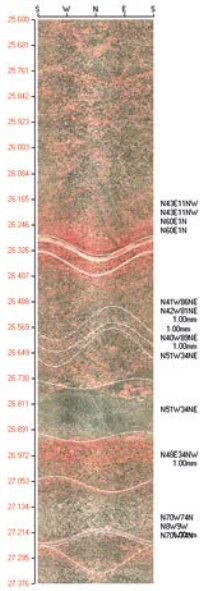

The rocktype of the section is granodiorite. There is a vein of pegmatite between 26.31–26.33 m and a vein of aplite at 26.36 m. There are xenoliths of mafic igneous rock within the section.

Figure A5-4. *BIPS image of KA3542G02 (25.60–27.20 m).*

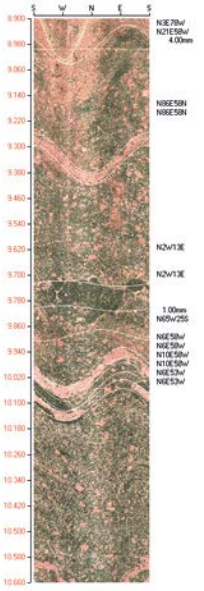

The rocktype of the section is granodiorite. There are veins of pegmatite between 9.32–9.36, 9.99–10.02 and 10.08–10.11 meters. There are xenoliths of mafic igneous rock within the section.

Figure A5-5. *BIPS image of KA3544G01 (8.90–12.65 m).*

A5.6 KA3546G01 (6.75–8.30 m)

In Figure A5-6 the BIPS image of the section is shown. The fracture that is monitored is at section 7.76 m.

Table A5-5. Fractures in KA3546G01, 6.75–8.30 m.

Borehole	Section (m)	Strike (°)	Dip (°)	Aperture (mm)	Mineral	Comments
KA3546G01	7.47	172	77	1	Chlorite	
KA3546G01	7.68	291	29	2	Calcite	
KA3546G01	7.76	278	24	3	Calcite	Monitored

A5.7 KA3548A01 (8.80–10.75 m)

In Figure A5-7 the BIPS image of the section is shown. The fractures that are monitored is at section 9.80 and 9.87 m.

Table A5-6. Fractures in KA3548A01, 8.80–10.75 m.

Hole	Section	Strike	Dip	Aperture (mm)	Mineral	Comments
KA3548A01	9.80	303	76	2	Calcite	Monitored
KA3548A01	9.87	108	82	1	Calcite	Monitored
KA3548A01	9.92	29	63	1	Chlorite	
KA3548A01	9.93	234	81	1	Chlorite	
KA3548A01	10.03	37	67	2	Chlorite	
KA3548A01	10.69	267	50	1	Chlorite	

A5.8 KA3550G01 (5.20–7.30 m)

In Figure A5-8 the BIPS image of the section is shown. Nine fractures are monitored within the section.

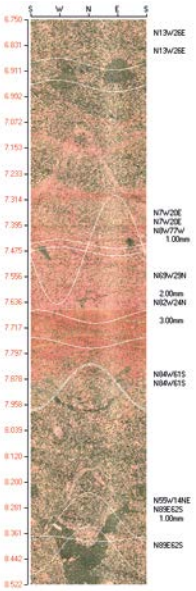

The rocktype of the section is granodiorite. There are xenoliths of mafic igneous rock within the section.

Figure A5-6. *BIPS image of KA3546G01 (6.75–8.30 m).*

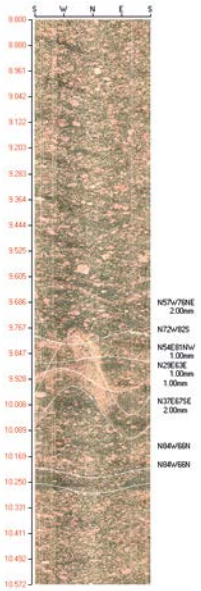

The rocktype of the section is granodiorite. There is a xenolith (10.22–10.27 m) of mafic igneous rock within the section.

Figure A5-7. *BIPS image of KA3548A01 (8.80–10.75 m).*

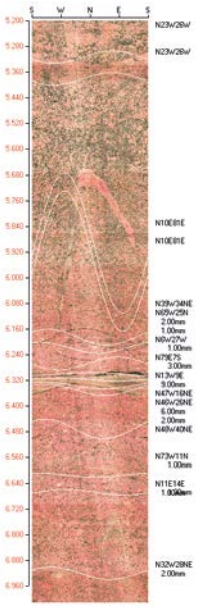

The rocktype of the section is granodiorite. There is a vein of aplite between 5.31–5.38 m and another vein of pegmatite between 5.89–5.95 m within the section.

Figure A5-8. *BIPS image of KA3550G01 (5.20–7.30 m).*

Table A5-7. Fractures in KA3550G01, 5.20–7.30 m.

Borehole	Section (m)	Strike (°)	Dip (°)	Aperture (mm)	Mineral	Comments
KA3550G01	6.19	321	34	2	Chlorite	Monitored
KA3550G01	6.22	295	25	1	Chlorite	Monitored
KA3550G01	6.27	174	27	1	Calcite	Monitored
KA3550G01	6.30	79	7	3	Chlorite	Monitored
KA3550G01	6.32	347	9	9	Chlorite	Monitored
KA3550G01	6.34	313	16	6	Chlorite	Monitored
KA3550G01	6.35	314	26	2	Chlorite	Monitored
KA3550G01	6.47	312	40	1	Chlorite	Monitored
KA3550G01	6.62	287	11	1	Chlorite	Monitored
KA3550G01	6.67	11	14	1	Chlorite	Monitored
KA3550G01	6.92	328	28	2	Chlorite	

A5.9 KA3552G01 (4.35–6.05 m)

In Figure A5-9 the BIPS image of the section is shown. The fractures that are monitored is at section 5.04 m.

Table A5-8. Fractures in KA3552G01, 4.35–6.05 m.

Borehole	Section (m)	Strike (°)	Dip (°)	Aperture (mm)	Mineral	Comments
KA3552G01	5.04	193	44			Monitored

A5.10 KA3554G01 (22.60–24.15 m)

In Figure A5-10 the BIPS image of the section is shown. The fractures that are monitored is at section 23.64 and 23.76 m.

Table A5-9. Fractures in KA3554G01, 22.60–24.15 m.

Borehole	Section (m)	Strike (°)	Dip (°)	Aperture (mm)	Mineral	Comments
KA3554G01	22.86	204	30	1	Calcite	
KA3554G01	23.29	251	27	2	Epidote	
KA3554G01	23.34	40	75	1	Calcite	
KA3554G01	23.64	313	90	2	Calcite	Monitored
KA3554G01	23.76	308	86	1	Calcite	Monitored

A5.11 KA3554G02 (10.50–12.20 m)

In Figure A5-11 the BIPS image of the section is shown. The fracture that is monitored is at section 11.20 m.

Table A5-10. Fractures in KA3554G02, 10.50–12.20 m.

Borehole	Section (m)	Strike (°)	Dip (°)	Aperture (mm)	Mineral	Comments
KA3554G02	11.20	145	85	2	Calcite	Monitored

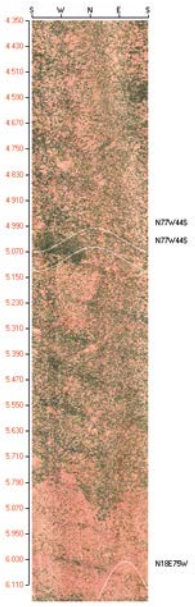

The rocktype of the section is granodiorite. There is a xenolith (5.03–5.09 m) of mafic igneous rock within the section.

Figure A5-9. *BIPS image of KA3552G01 (4.35–6.05 m).*

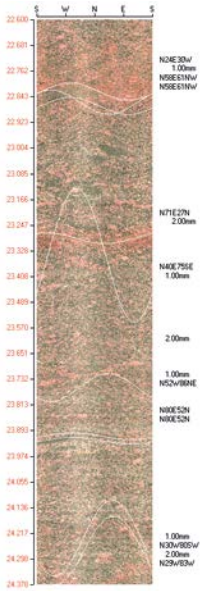

The rocktype of the section is granodiorite. There are a xenoliths between 22.83–22.87 m and 23.91–23.93 m of mafic igneous rock within the section.

Figure A5-10. *BIPS image of KA3554G01 (22.60–24.15 m).*

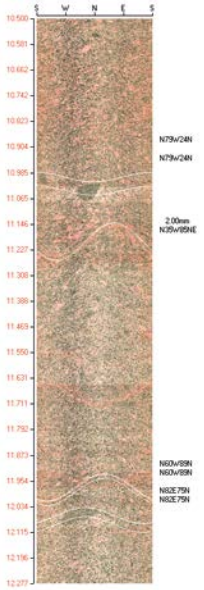

The rocktype of the section is granodiorite. There is a xenolith of mafic igneous rock between 11.00–11.04 m and 12.06–12.09 metres and a vein of aplite between 11.97–11.99 metres.

Figure A5-11. *BIPS image of KA3554G02 (10.50–12.20 m).*